Local Orthogonal Rectification: A New Tool for Geometric Phase Space Analysis

by

Benjamin G. Letson

BA in Mathematics and Physics, Ohio Wesleyan University, 2014

Submitted to the Graduate Faculty of

the Dietrich School of Arts and Sciences in partial fulfillment

of the requirements for the degree of

Doctor of Philosophy

University of Pittsburgh

2019

UNIVERSITY OF PITTSBURGH

DIETRICH SCHOOL OF ARTS AND SCIENCES

This dissertation was presented

by

Benjamin G. Letson

It was defended on

November 18, 2019

and approved by

Jonathan E. Rubin, Dept. of Math., Univ. of Pittsburgh

Jason DeBlois, Dept. of Math., Univ. of Pittsburgh

G. Bard Ermentrout, Dept. of Math., Univ. of Pittsburgh

Jaun Manfredi, Dept. of Math., Univ. of Pittsburgh

Theodore Vo, School of Math., Monash Univ.

Dissertation Director: Jonathan E. Rubin, Dept. of Math., Univ. of Pittsburgh

Local Orthogonal Rectification: A New Tool for Geometric Phase Space Analysis

Benjamin G. Letson, PhD

University of Pittsburgh, 2019

Local orthogonal rectification (LOR) provides a natural and useful geometric frame for analyzing dynamics relative to manifolds embedded in flows. LOR can be applied to any embedded base manifold in a system of ODEs of arbitrary dimension to establish a corresponding system of LOR equations for analyzing dynamics within the LOR frame. The LOR equations encode geometric properties of the underlying flow and remain valid, in general, beyond a local neighborhood of the embedded manifold. Additionally, we illustrate the utility of LOR by showing a wide range of application domains. In the plane, we use the LOR approach to derive a novel definition for rivers, long-recognized but poorly understood trajectories that locally attract other orbits yet need not be related to invariant manifolds or other familiar phase space structures, and to identify rivers within several example systems. In higher dimensions, we apply LOR to identify periodic orbits and study the transient dynamics nearby. In the LOR method, the standard approach of finding periodic orbits by solving for fixed points of a Poincaré return map is replaced by the solution of a boundary value problem with fixed endpoints, and the computation provides information about the stability of the identified orbit. We detail the general method and derive theory to show that once a periodic orbit has been identified with LOR, the LOR coordinate system allows us to characterize the stability of the periodic orbit, to continue the orbit with respect to system parameters, to identify invariant manifolds attendant to the periodic orbit, and to compute the asymptotic phase associated with points in a neighborhood of the periodic orbit in a novel way. Finally, we generalize the definition of rivers beyond planar systems, and demonstrate a fundamental connection between canard solutions in two-timescale systems and generalized rivers. We will again use a blow-up transformation on the LOR equations, which provides a useful decomposition for studying trajectories' behavior relative to the embedded base curve.

Table of Contents

List of Tables

List of Figures

1.0 Introduction

Often the dynamics of an ordinary differential equation (ODE) defies rectangular coordinate schemes; that is, the geometry induced by a flow may be difficult to represent in Cartesian coordinates. In fact, a common early step in analysis is to exchange Cartesian coordinates for a geometry better suited for the problem [56, 9, 49, 67, 69, 59, 70]. In this thesis, we present a technique that allows us to use any embedded manifold (not necessarily invariant) to generate a natural coordinate frame for a dynamical system. We call this technique *Local Orthogonal Rectification (LOR)*.

We will be interested in ordinary differential equations (ODEs) of the form

$$\dot{x} = f(x;\lambda) \qquad\qquad x(0) = x_0 \in \Omega \tag{1.1}$$

where $\dot{x} := dx/dt$, $f : \Omega \times \Lambda \to \Omega$ is a sufficiently smooth (usually $\mathscr{C}^1$) vector field which may depend on a vector of parameters $\lambda \in \Lambda$, and $\Omega \subseteq \mathbb{R}^n, \Lambda \subseteq \mathbb{R}^\ell$ are open subsets. We say that (1.1) is a system of n ODEs, or an n-dimensional system with ℓ parameters. It is well known [54, 63], that initial value problems (IVPs) like (1.1) can be reformulated as a *dynamical system* or a *flow*, which is a smooth map $\Phi_\lambda : \Omega \times \mathbb{R} \to \Omega$ which satisfies

$$\Phi_\lambda(x, 0) = x$$
$$\Phi_\lambda(\Phi_\lambda(x, t_1), t_2) = \Phi_\lambda(x, t_1 + t_2)$$

for all $x \in \Omega, t_1, t_2 \in \mathbb{R}, \lambda \in \Lambda$ [63]. We say that Φ_λ is the flow *induced* by (1.1) if

$$\frac{d}{dt}\Phi_\lambda(x, t) = f\left(\Phi_\lambda(x, t), \lambda\right)$$

for all $x \in \Omega, t \in \mathbb{R}$; it is well known that every smooth ODE uniquely induces a smooth flow, and vice versa [63]. Using the flow induced by an ODE, we can analyze differential equations *geometrically*; that is we can consider the trajectories of a flow $\phi(t; x_0) = \Phi_\lambda(x_0, t)$, for $x_0 \in \Omega$, as geometric objects in space. Many of the most elegant theorems in dynamical systems rely on this geometric view of systems of ODEs.

In broad strokes, local orthogonal rectification is a tool which allows us to exploit analytical coordinate changes while preserving geometric intuition. Oftentimes necessary coordinate changes can squash geometric clarity, for example, when working with Floquet coordinates near a periodic trajectory it is easy to lose track of where solutions to the linearized system lie relative to the original periodic orbit. Or when we rectify a system about a given manifold, the rectified system may have strange angles-of-approach, due to the non-conformal nature of a standard rectification. LOR is designed to address these types of issues by leveraging the orthogonality of the tangent and normal bundles of an embedded manifold and decomposing our flow into these bundles. In a sense, LOR is a more Lagrangian reference frame than the standard Eulerian viewpoint; using the LOR frame, we view the flow from the perspective of an embedded manifold using an intrinsic coordinate, which we denote by η, and an extrinsic coordinate, denoted ξ, which lies in the normal bundle. By tailoring our reference frame to the problem at hand, we can quantify phase-plane contraction, study trapping regions to understand asymptotic dynamics, identify periodic orbits and novel invariant manifolds attendant to those periodic orbits, compute the asymptotic phase of a stable periodic orbit in a natural way, and demonstrate that canard type solutions must lie very near weak river solutions.

The rest of this chapter serves to lay out some background material for the problems we will consider in the following four chapters. The four main chapters of this thesis are based on four papers; the material in chapters 2-4 have been published, accepted, or submitted for publication in [45],[47], [46], respectively, and chapter 5 is based on a paper which will be submitted in short order. The remainder of this thesis is organized thusly: chapter 2 is devoted to deriving the LOR frame in total generality with full geometric rigor. In this chapter we build the geometric machinery we require for understanding manifolds embedded in $\mathbb{R}^n$; our goal in this construction is not to further the field of differential geometry, but rather to establish the notation and operators we will need in our derivation of the LOR frame. In chapters 3-5 we apply the LOR frame to solve problems that are fundamentally important in the study of dynamical systems.

Chapter 3 is devoted to identifying hitherto unexplained regions of phase-plane contraction which we term *rivers*; we provide a novel, general, and rigorous definition for rivers

using the zero-curvature set of a flow combined with a quantitative measure for the near-invariance of a curve. In chapter 4 we show that the LOR frame can be used to identify and analyze periodic trajectories in arbitrary dimensions. We transform the standard Poincaré map identification technique into a boundary value problem (BVP) with fixed endpoints; this approach also allows us to identify novel invariant manifolds attendant to periodic orbits using a novel angular reference frame. Chapter 5 generalizes the planar river definition to a system arbitrary dimension and demonstrates that rivers and canard solutions are fundamentally equivalent; additionally we demonstrate that the LOR frame can be used to analyze the dynamics near canard solutions and compute the way-in way-out function.

1.1 The Frenet Reference Frame and the Differential Geometry of Surfaces

We begin our background material with a brief explanation of the Frenet frame, which is a moving normal form for a curve embedded in $\mathbb{R}^n$. Suppose that $\gamma : I \to \mathbb{R}^n$ is a $\mathscr{C}^{n-1}$ curve defined on some interval $I \subseteq \mathbb{R}$. We say that γ is a Frenet curve if the first $n-1$ derivatives of γ are linearly independent, that is, if

$$\text{dimspan}\left\{\gamma'(\eta), \gamma''(\eta), \cdots, \gamma^{(n-1)}(\eta)\right\} = n-1 \tag{1.2}$$

for all $\eta \in I$, where $\gamma'(\eta) = d\gamma/d\eta$ [40],[7]. Note that this condition is fairly generic, for any fixed η we would expect (1.2) to hold, as $n-1$ vectors in $\mathbb{R}^n$ are generically linearly independent. Indeed, we would expect (1.2) to hold everywhere but a set of measure zero. The construction which follows in this section can be performed on any sub-interval $I' \subseteq I$ on which γ is Frenet, however we will suppose in the sequel that γ is a Frenet curve.

We wish to construct an orthonormal moving frame for γ using the derivatives of γ. We define the obvious tangent vector $T\gamma(\eta) = \gamma'(\eta)/\left\|\gamma'(\eta)\right\|$ where $\|\cdot\|$ is the norm induced by the standard Euclidean inner product, which we denote by $\langle\cdot,\cdot\rangle$. Knowing that $\gamma''(\eta)$ is linearly independent of $\gamma'(\eta)$, we define

$$N_1\gamma(\eta) = \frac{\gamma''(\eta) - \langle\gamma''(\eta), T\gamma(\eta)\rangle}{\|\gamma''(\eta) - \langle\gamma''(\eta), T\gamma(\eta)\rangle\|}$$

i.e. we perform Gram-Schmidt orthonomalization on $\gamma'(\eta), \gamma''(\eta)$ [44]. We continue in this fashion to define $N_2\gamma(\eta), \cdots, N_{n-2}\gamma(\eta)$, at which point we have used the first $n-1$ derivatives of γ (note that the index of $N_j\gamma$ is offset by one, reflecting the fact that we have a single tangent vector). Given a set of $n-1$ orthonormal vectors in $\mathbb{R}^n$, there are exactly two unit vectors which complete the set to an orthonormal basis [44], we use the wedge product to choose $N_{n-1}\gamma(\eta)$ in accordance with the right-hand rule

$$N_{n-1}\gamma(\eta) = T\gamma(\eta) \wedge N_1\gamma(\eta) \wedge \cdots \wedge N_{n-2}\gamma(\eta)$$

where $x_1 \wedge \cdots \wedge x_{n-1}$ is the standard wedge product in $\mathbb{R}^n$ [40]. We call the set of vector valued maps, defined on the domain of γ, $\{T\gamma(\eta), N_1\gamma(\eta), \cdots, N_{n-1}\gamma(\eta)\}$ the Frenet frame relative to γ. For notational convenience, we define $k = n-1$ and call k the co-dimension of γ.

The Frenet-Serret equations, which describe the derivatives of the moving frame in terms of the frame itself, are central to the analysis of curves [40]. In matrix form, they are given by

$$\frac{d}{d\eta}\begin{pmatrix} T\gamma(\eta) \\ N_1\gamma(\eta) \\ N_2\gamma(\eta) \\ \vdots \end{pmatrix} = \|\gamma'(\eta)\| \begin{pmatrix} 0 & \kappa_1(\eta) & 0 & \cdots \\ -\kappa_1(\eta) & 0 & \kappa_2(\eta) & \cdots \\ 0 & -\kappa_2(\eta) & 0 & \ddots \\ \vdots & \vdots & \ddots & \ddots \end{pmatrix} \begin{pmatrix} T\gamma(\eta) \\ N_1\gamma(\eta) \\ N_2\gamma(\eta) \\ \vdots \end{pmatrix} \tag{1.3}$$

where the mappings $\kappa_1(\eta), \cdots, \kappa_k(\eta)$ are called the Frenet curvatures of γ [40, 7]. The matrix in (1.3) is a tri-diagonal, anti-symmetric matrix with a zero diagonal, and we have

$$\kappa_i(\eta) = \frac{\langle N_{i-1}\gamma'(\eta), N_i\gamma(\eta)\rangle}{\|\gamma'(\eta)\|}$$

where we define $N_0\gamma(\eta) := T\gamma(\eta)$ for notational convenience. The first $k-1$ curvature terms are positive definite for $\eta \in I$, while the last curvature $\kappa_k(\eta)$ can take either sign, and can be computed

$$\kappa_k(\eta) = \frac{\gamma'(\eta) \wedge \cdots \wedge \gamma^{(n)}(\eta)}{\alpha(\gamma'(\eta), \cdots, \gamma^{(n)}(\eta))}$$

where $\alpha(x_1, \cdots, x_n) > 0$, provided that γ is $\mathscr{C}^n$ [40]. Being able to describe the change in the Frenet frame in terms of itself is fundamentally important in the derivation of the

LOR frame in the plane; indeed we generalize the Frenet-Serret equations to what we call differential-algebraic closures in our general conception of the LOR frame.

We will also draw on the theory of surfaces embedded in $\mathbb{R}^3$. We say that $\sigma : \mathcal{U} \subseteq \mathbb{R}^2 \to \mathbb{R}^3$ is the chart of a regular, differentiable manifold if $\mathcal{U}$ is open, σ is a diffeomorphism on its range and if

$$\text{dimspan}\left\{\frac{\partial\sigma}{\partial\eta_1}(\eta_1,\eta_2), \frac{\partial\sigma}{\partial\eta_2}(\eta_1,\eta_2)\right\} = 2$$

for all $(\eta_1, \eta_2) \in \mathcal{U}$. We will denote $\partial_i = \partial/\partial\eta_i$ for compactness. This final condition, reminiscent of the definition of a Frenet curve, is called regularity. A collection of charts with overlapping domains $\{(\mathcal{U}_\alpha, \sigma_\alpha)\}_{\alpha\in A}$ is called an atlas, and the set $\mathcal{M} = \cup_{\alpha\in A}\sigma_\alpha(\mathcal{U}_\alpha)$ is called a 2-manifold embedded in $\mathbb{R}^3$ [40]. We provide a rigorous definition of what "overlapping charts" means in chapter 2 when such technicalities are relevant.

As we did before, we are interested in a reference frame which is well-suited to a patch of $\mathcal{M}$. Indeed we can follow the same procedure as above, let

$$N\sigma(\eta) = \frac{\partial_1\sigma(\eta) \times \partial_2\sigma(\eta)}{\|\partial_1\sigma(\eta) \times \partial_2\sigma(\eta)\|}$$

then $\{\partial_1\sigma(\eta), \partial_2\sigma(\eta), N\sigma(\eta)\}$ will form a basis of $\mathbb{R}^3$ for any $\eta \in \mathcal{U}$, which is generically not orthonormal. As with the Frenet frame, we will be interested in expressing the derivatives of $\partial_1\sigma, \partial_2\sigma, N\sigma$ as linear combinations of $\partial_1\sigma, \partial_2\sigma, N\sigma$, and we will do so in Chapter 2.

1.2 Periodic Trajectories and Relevant Coordinate Transformations

Oscillatory dynamics arise in a variety of physical and societal settings, emerging naturally from intrinsic nonlinearities in some cases, such as in neuronal rhythm generating circuits, circadian rhythms, and various chemical reactions, and resulting from periodic forcing in other scenarios, such as in seasonality and the delivery of alternating current to certain targets (e.g., [27, 42, 18, 32, 23]). Correspondingly, the problems of identifying and analyzing periodic solutions are central in dynamical systems. Although periodic behavior in dynamical systems has been extensively studied, a unified framework for analysis of oscillations is lacking.

A wide variety of methods have been applied to prove the existence of periodic solutions to systems of ODEs or to generate numerical approximations to such orbits [28, 63, 8]. A special case arises when periodic orbits bifurcate from a curve of equilibria, and another set of tools allows for the identification of these bifurcations as well as others that involve periodic orbits such as period-doubling [17, 43]. Bifurcation analysis may also provide information about orbit stability sufficiently close to the bifurcation point; for an arbitrary given periodic orbit, however, a separate Floquet analysis based on linearization is generally required for assessment of stability. Given a stable periodic orbit, phase response curves provide a tool to analyze responses to sufficiently small perturbations off of the orbit, or equivalently to determine the asymptotic phases of points in a sufficiently small neighborhood of the orbit, based on linearization and consideration of an adjoint equation [19, 30, 20].

For reference, we will establish standard notation for periodic trajectories. We say a solution $\phi(t; x_0)$ to (1.1) is periodic with period $T > 0$ if T is the smallest number such that $\phi(t + T; x_0) = \phi(t; x_0)$ for all $t > 0$. The textbook approach for identifying periodic orbits employs Poincaré sections and return maps: let Σ be a manifold which is transverse to the flow at $x_0 \in \Sigma$, if x_0 eventually returns to Σ after time t then there exists $\delta > 0$ and a smooth map $T : B(x_0, \delta) \cap \Sigma \to \mathbb{R}$ such that $T(x_0) = t$ and $\Phi_\lambda(x, T(x)) \in \Sigma$ for all $x \in B(x_0, \delta) \cap \Sigma$. The map $H(x) := \Phi(x, T(x))$ is called a return map, and the trajectory $\phi(t; x_1)$ with $x_1 \in \Sigma$ is periodic if and only if $H(x_1) = x_1$ [54, 28, 63]. The map H can also be interrogated to determine the stability of $\phi(t; x_1)$ which gives rise to Floquet theory, which we will not describe in detail here but rather refer the curious reader to [54, 63] for a full explanation.

The transient dynamics near periodic trajectories is of great interest in many theoretical and applied problems. For example, circadian rhythms have long been modeled as periodic trajectories with nearby dynamics dictating responses to changes in light exposure or melatonin levels [64, 33]. Along these lines, when viewed in the context of dynamical systems, jet lag can be thought of as a perturbation from a stable circadian oscillation and the resultant discomfort is caused by the transient return to a stable rhythm [14]. A major effort in theoretical neuroscience concerns the use of dynamics near stable periodic orbits to analyze neuronal responses to inputs [20, 57]. Understanding the transient dynamics near periodic orbits provides information about how trajectories behave as they approach a periodic limit,

how the oscillator will respond to perturbations, and how to build dimensional reductions that capture key features of system behavior.

Previous work has introduced new coordinate systems based on decomposing dynamics into phase and amplitude components [9, 67, 59]. We define the asymptotic phase of a limit cycle thusly: suppose that x_0 is in the basin of attraction of the limit cycle Γ, then there will be a value of $\theta \in [0, T)$ such that

$$\lim_{t\to\infty} \|\phi(t; x_0) - \Gamma(t + \theta)\| = 0$$

and we call $\theta(x_0)$ the asymptotic phase map [20, 28]. In a sense, the trajectory $\phi(t; x_0)$ will approach Γ at phase θ. We call the level sets of θ, denoted $I_\theta = \{x|\theta(x) = \theta\}$, the isochrons of the system. Isochrons and asymptotic phase are crucial in understanding how coupled oscillators can phase lock [20, 19, 30, 20], and the computation of asymptotic phase is often done using a brute-force sampling approach.

Recent work has been focused on using isostable coordinates, which are defined using the Poincare return map $H(x)$. Suppose that $H(x_0) = x_0$, expanding near x_0 we have $H(x) = x_0 + J(x - x_0) + \mathcal{O}(\|x - x_0\|^2)$, where $J = D_x H(x_0)$. If J is diagonalized by V and has eigenvalues $\lambda_1, \cdots, \lambda_n$ then we define

$$\psi_i(x) = \left\langle V^{-1}(P(x) - x_0) \exp\left(-\log(\lambda_i)\frac{T(x)}{T(x_0)}\right), e_i \right\rangle$$

where e_i is the i^{th} fundamental basis vector [69, 70]. Intuitively, $\psi_i(x)$ measures how quickly $P(x)$ is converging to x_0 along the i^{th} eigenvector of J. Note that this definition only holds on the Poincaré section Σ, however it is simple to extend it to the basin of Γ by flowing each initial condition to Σ. The level-sets of ψ_i are called isostables [69, 49].

As the eigenvalues λ_i are the Floquet multipliers of Γ, $\lambda_1 = 1$ (without loss of generality) [28, 63], hence the first isostable map $\psi_1(x)$ is uninteresting. The remaining $n - 1$ isostable maps, paired with the asymptotic phase $\theta(x)$ will form a coordinate scheme, which are called isochron-isostable coordinates [69]. Using adjoint methods [20, 19, 69], we can derive linearized dynamics governing θ, ψ_i and use these to understand the approximate transient dynamics near the limit cycle. In Chapter 4 we will use the LOR frame to study the transient dynamics near a limit cycle and demonstrate that the LOR frame serves as a geometric reformulation of isochron-isostable coordinates.

1.3 Fast-Slow Systems and Fenichel's Theory

Physical and bio-physical systems often have dynamics which vary on vastly different timescales. For example, consider the interaction of fast, weather variables and slow, climate variables; clearly climate level dynamics will slowly affect weather patterns, and weather patterns can affect climate dynamics over a long period of time (through desertification or deforestation). Similarly, multi-reagent chemical reactions can happen on different timescales [55]; indeed multi-timescale dynamics seem to be central in the ion dynamics governing neurons [3, 29, 10, 60, 52, 37] and across a wide range of multi-mode oscillatory dynamics [36, 31, 58].

We say a system of ODEs is a two timescale system or a fast-slow system if it can be expressed as

$$\begin{aligned} \dot{x} &= F(x, y) \\ \dot{y} &= \varepsilon G(x, y) \end{aligned} \tag{1.4}$$

where $x \in \mathbb{R}^{n_f}, y \in \mathbb{R}^{n_s}$ such that $n_f + n_s = n$, and $0 < \varepsilon \ll 1$ [2]. The x variables are called the fast variables, and the y variables are called the slow variables, as ε controls the size of their derivative. If we consider (1.4) on the slow timescale, $\tau := \varepsilon t$ we find

$$\begin{aligned} \varepsilon x' &= F(x, y) \\ y' &= G(x, y) \end{aligned} \tag{1.5}$$

where $x' = dx/d\tau$. We call (1.5) the slow subsystem of (1.4). Note that, in the singular limit $\varepsilon \to 0$ these two formulations give very different perspectives on the system; the fast subsystem becomes

$$\begin{aligned} \dot{x} &= F(x, y) \\ \dot{y} &= 0 \end{aligned} \tag{1.6}$$

hence is a system of n_f ODEs with n_s parameters. The set of fixed points of (1.6), $\mathcal{M} = \{(x, y)|F(x, y) = 0\}$, is called the critical manifold of (1.4). Turning our attention to the slow subsystem we find

$$\begin{aligned} 0 &= F(x, y) \\ y' &= G(x, y) \end{aligned} \tag{1.7}$$

which is a differo-algebraic system which is only defined on $\mathcal{M}$. To analyze a fast-slow system, we typically employ Geometric Singular Perturbation Theory (GSPT) which is also called Fenichel Theory [21]. GSPT allows us to piece together the dynamics of (1.4) for $\varepsilon > 0$ using (1.6) and (1.7).

In order to discuss Fenichel's Theorem, we first must define the concept of a normally hyperbolic invariant manifold. A manifold $\mathcal{N}$ with boundary $\partial\mathcal{N}$ is locally-invariant in the flow Φ_λ if for all $x \in \mathcal{N}$ there is an open interval $0 \in (t_1, t_2) \subseteq \mathbb{R}$ such that

$$\Phi_\lambda(x, t) \in \mathcal{N} \qquad\qquad t \in (t_1, t_2)$$

and $\Phi_\lambda(x, t_i) \in \partial\mathcal{N}$ for $i \in \{1, 2\}$ [34]. Intuitively, $\mathcal{N}$ is locally invariant if points on $\mathcal{N}$ remain in $\mathcal{N}$ with the exception of points which leave through the boundary $\partial\mathcal{N}$. Supposing that $\mathcal{N}$ is an m-dimensional, locally invariant manifold, we say that $\mathcal{N}$ is normally hyperbolic if there are $n - m$ eigenvalues of the linearized vector field along $\mathcal{N}$, $S(D_x f(x; \lambda))$ for $x \in \mathcal{N}$ where S denotes the spectrum, with nonzero real part; that is

$$\#[S\left(D_x f(x; \lambda)\right) \setminus \{\mathrm{Re}(z) = 0\}] = n - m \qquad\qquad x \in \mathcal{N}.$$

A normally hyperbolic invariant manifold will have the same types of stability as fixed points, for example if $\mathcal{N}$ has $n - m$ eigenvalues with negative real parts, then initial conditions near $\mathcal{N}$ will approach $\mathcal{N}$ and we say that $\mathcal{N}$ is stable [68]. We can now state Fenichel's theorem which guarantees the persistence of the slow manifold for $\varepsilon > 0$, we follow the statement from [34]

Theorem 1.3.1 (Fenichel's First Manifold Theorem and Stable Manifold Theorem)**.** *Suppose that* $\mathcal{M} = \{(x, y)|F(x, y) = 0\}$ *is a locally invariant, normally hyperbolic manifold, then for* $\varepsilon > 0$ *sufficiently small there exists a manifold* $\mathcal{M}_\varepsilon$ *which is diffeomorphic to* $\mathcal{M}$*, is* $\mathcal{O}(\varepsilon)$ *close to* $\mathcal{M}$ *and is locally invariant under* (1.4)*. Furthermore,* $\mathcal{M}_\varepsilon$ *will have the same stability type as* $\mathcal{M}$*, and the dynamics of the flow restricted to* $\mathcal{M}_\varepsilon$ *will be an* $\mathcal{O}(\varepsilon)$ *perturbation of the slow subsystem* (1.7)*.*

In broad strokes, there will be an n_f-dimensional invariant manifold in (1.4) with the same stability type as $\mathcal{M}$ and the dynamics along that manifold are effectively given by the slow dynamics. In order to unpack the slow dynamics, we usually suppose that the critical manifold can be expressed as the graph of a function, i.e. we can write $x = h(y)$ for some h. Note that this can always be done locally for a normally hyperbolic manifold, as we supposed $D_x f(x, y)$ is invertible on $\mathcal{M}$ [34, 68]. Using this graph expression we can simplify the slow dynamics to $y' = G(h(y), y)$.

The condition that $\mathcal{M}$ is normally hyperbolic is fairly mild, and is generically true; however Fenichel's theorem will fail to hold if $\mathcal{M}$ is not normally hyperbolic. Indeed, some of the most interesting examples in GSPT are cases in which parts of $\mathcal{M}$ are not normally hyperbolic. The critical manifold can lose normal hyperbolicity through a fold, which is a set of points such that our graph $x = h(y)$ would have an infinite derivative. Oftentimes, the stability of the critical manifold will change across folds; one of the eigenvalues of $S(D_x f(x; \lambda))$ will cross the $\mathrm{Re}(z) = 0$ axis at a fold, and $\mathcal{N}$ will fail to be normally hyperbolic.

One of the most interesting, and counterintuitive, features of dynamics nead folded critical manifolds is the *canard* solution. The origin of the name canard solution is foggy, but each of the etymological explanations sheds light on the canard phenomenon; the first example of a canard solution was found in the van der Pol system [38] and the trajectory of interest is somewhat duck-shaped, and in British slang "canard" refers to a joke or a prank. A canard solution is a trajectory with an initial condition near a stable branch of the critical manifold, which we will denote by $\mathcal{N}_S$, which will evolve along $\mathcal{N}_S$, reach a fold in the critical manifold, and spend a "long time" near the unstable branch of the critical manifold $\mathcal{N}_U$. We would expect, given that $\mathcal{N}_U$ is linearly unstable, that trajectories near $\mathcal{N}_U$ should leave $\mathcal{N}_U$ in logarithmic time, as the fast variables will grow exponentially. However, a canard solution

will linger near the unstable critical manifold for an *algebraic* amount of time [38]. We will show that this characteristic delay can be explained using curvature techniques paired with the LOR blow-up coordinates.

2.0 Local Orthogonal Rectification

The material in this chapter has been conditionally accepted for publication in DCDS as "Local Orthogonal Rectification: Deriving Natural Coordinates to Study Flows Relative to Manifolds" and was co-authored by Jonathan E. Rubin.

2.1 Motivation

Consider an ODE and initial condition

$$\dot{x} = f(x), \qquad x(0) = x_0 \in \Omega, \tag{2.1}$$

where $f \in \mathscr{C}^r(\Omega, \mathbb{R}^n)$ for $n, r \geq 1$ and Ω is an open subset of $\mathbb{R}^n$, which induces a flow $\Phi : \Omega \times \mathbb{R} \to \Omega$. For simplicity, we introduce the notation $\partial_i = \partial/\partial\eta_i$. Suppose that $\mathcal{M}$ is a codimension-k $\mathscr{C}^s$-regular manifold embedded in Ω. Specifically, suppose there exist an indexing set A and an atlas of charts $\{(\mathcal{U}_\alpha, \sigma_\alpha)\}_{\alpha\in A}$ where $\mathcal{M} = \cup_{\alpha\in A}\sigma_\alpha(\mathcal{U}_\alpha)$, such that for all $\alpha, \beta \in A$:

1. each $\mathcal{U}_\alpha \subseteq \mathbb{R}^{n-k}$ is open with corresponding $\sigma_\alpha \in \mathscr{C}^s(\mathcal{U}_\alpha, \Omega)$ a homeomorphism on its image;
2. if $\sigma_\alpha(\mathcal{U}_\alpha) \cap \sigma_\beta(\mathcal{U}_\beta) \neq \emptyset$ then the map $\kappa_{\alpha,\beta} : U_\alpha \cap \sigma_\alpha^{-1} \circ \sigma_\beta(\mathcal{U}_\beta) \to \mathcal{U}_\beta \cap \sigma_\beta^{-1} \circ \sigma_\alpha(\mathcal{U}_\alpha)$ defined by $\kappa_{\alpha,\beta} = \sigma_\beta^{-1} \circ \sigma_\alpha$ is a diffeomorphism;
3. for all $\eta \in \mathcal{U}_\alpha$,
$$\text{dimspan}\,\{\partial_1\sigma_\alpha, \ldots, \partial_{n-k}\sigma_\alpha\} = n - k;$$
4. $\mathcal{M}$ can be equipped with a local normal frame; that is, there are mappings $N_j\sigma_\alpha \in \mathscr{C}^1(\mathcal{U}_\alpha, \mathbb{R}^n)$ such that

$$\langle N_{j_1}\sigma_\alpha(\eta), v\rangle = 0,\ \langle N_{j_1}\sigma_\alpha(\eta), N_{j_2}\sigma_\alpha(\eta)\rangle = \delta_{j_1,j_2}\ \ \forall\eta \in \mathcal{U}_\alpha,\ \forall v \in T_{\sigma_\alpha(\eta)}\mathcal{M},$$

where $\langle \cdot, \cdot \rangle$ denotes the standard Euclidean inner product, $j_1, j_2 \in \{1, \ldots, k\}$, and δ_{j_1,j_2} is the Kronecker delta.

We call these four conditions the *LOR assumptions*. These assumptions guarantee that the tangent space to $\mathcal{M}$ at any point $p \in \mathcal{M}$, denoted by $T_p\mathcal{M}$, is an $n-k$ dimensional space.

To simplify indexing, we will use the convention that any index related to tangential objects will be denoted by i, or when necessary by $i_1, i_2, \ldots$, and any index related to normal objects will be denoted by j or by $j_1, j_2, \ldots$. Stated simply, $\{N_j\sigma_\alpha(\eta)\}_{j=1}^k$ forms an orthonormal basis of $(T_{\sigma_\alpha(\eta)}\mathcal{M})^\perp$ on $\mathcal{U}_\alpha$. The existence of such a basis is straightforward to establish locally, and by refining our domains $\mathcal{U}_\alpha$ we can guarantee that such mappings exist.

With our notation and assumptions in hand, we now motivate the underlying geometric idea for constructing the LOR frame. Suppose that we are interested in studying the dynamics near a point $x_0 \in \Omega$ that lies close to our embedded manifold. Furthermore, suppose that x_0 can be written in the form

$$x_0 = \sigma_\alpha(\eta_0) + \sum_{j=1}^{k} \xi_{0,j} N_j \sigma_\alpha(\eta_0), \qquad \eta_0 \in \mathcal{U}_\alpha, (\xi_{0,1}, \xi_{0,2}, \ldots, \xi_{0,k}) \in \mathbb{R}^k. \tag{2.2}$$

To write equation (2.2), we have assumed that x_0 can be decomposed into a point on $\mathcal{M}$, namely $\sigma_\alpha(\eta_0)$, and a vector in the orthogonal complement of $T_{\sigma_\alpha(\eta_0)}\mathcal{M}$. We will establish that such a decomposition is generic, sufficiently close to $\mathcal{M}$. We define $\Psi_\alpha : \mathcal{U}_\alpha \times \mathbb{R}^k \to \mathbb{R}^n$ by

$$\Psi(\eta, (\xi_1, \cdots, \xi_k)) = \sigma_\alpha(\eta) + \sum_{j=1}^{k} \xi_j N_j \sigma_\alpha(\eta)$$

and denote $\xi = (\xi_1, \cdots, \xi_k)$, so that (2.2) can be more succinctly expressed as $x_0 = \Psi(\eta_0, \xi_0)$.

Now, denote by $\phi(t)$ the trajectory of (2.1) such that $\phi(0) = x_0$. We want to continue tracking $\phi(t)$ in our decomposition. To do so, we seek smooth $\eta : (-\delta, \delta) \to \mathcal{U}_\alpha$, $\xi : (-\delta, \delta) \to \mathbb{R}^k$ such that $\phi(t) = \Psi(\eta(t), \xi(t))$ for $t \in (-\delta, \delta)$. We will establish that this continuation can be achieved, providing a convenient new set of coordinates (η, ξ), which we will call the *LOR frame*. We will also derive a system of ODEs that govern the evolution of $\eta(t), \xi(t)$, the *LOR equations*, by using the ODE satisfied by $\phi(t)$.

We call (η, ξ) the *LOR coordinates* for the base manifold $\mathcal{M}$. By choosing $\mathcal{M}$ to be dynamically relevant (i.e., a structure that can be observed to play a role in organizing the flow), we will be able to study the dynamics near $\mathcal{M}$ using the corresponding LOR frame. The geometric nature of the LOR frame can offer striking insights into the local behavior of the flow, representing a powerful approach for the theoretical study of dynamical systems.

The remainder of the chapter is organized as follows. In Section 2.2, we state our main result, which stipulates the existence of the LOR frame and the form of the LOR equations. Next, in Section 2.3, we set up the notation and definitions needed to prove this result, while the proof itself appears in Section 2.4. In Section 2.5, we consider LOR in a variety of settings. We treat the special cases where $\mathcal{M}$ is codimension-1 or codimension-$(n-1)$, present an algorithm for constructing a particularly useful normal frame assuming that $\mathcal{M}$ is equipped with a Frenet-type atlas, and introduce a blow-up approach to studying how trajectories in Ω evolve relative to $\mathcal{M}$. We conclude in Section 2.6 with a computational example to explicitly illustrate the implementation of LOR, in this case to easily identify trajectories organizing canard behavior near a fold of a critical manifold in a two-timescale system.

2.2 Statement of the Main Result

In what follows, we will pick a specific chart of $\mathcal{M}$ and drop our indexing subscript; that is, we will study the LOR frame on the chart $(\mathcal{U}, \sigma)$ of $\mathcal{M}$. Once our theory is established locally, we will prove that transfer across charts is well-defined, a result that is critical to the utility of LOR.

To state our main result, we define $Tf : \mathcal{U} \times \mathbb{R}^k \to \mathbb{R}^{n-k}$, $Nf : \mathcal{U} \times \mathbb{R}^k \to \mathbb{R}^k$ by

$$Tf(\eta,\xi) = \begin{pmatrix} \langle f \circ \Psi(\eta,\xi), \partial_1 \sigma(\eta) \rangle \\ \vdots \\ \langle f \circ \Psi(\eta,\xi), \partial_{n-k} \sigma(\eta) \rangle \end{pmatrix}, \quad Nf(\eta,\xi) = \begin{pmatrix} \langle f \circ \Psi(\eta,\xi), N_1 \sigma(\eta) \rangle \\ \vdots \\ \langle f \circ \Psi(\eta,\xi), N_k \sigma(\eta). \rangle \end{pmatrix}. \quad (2.3)$$

Note that $Tf(\eta,\xi)$ projects the vector field at $\Psi(\eta,\xi)$ into the tangent space of $\mathcal{M}$ and $Nf(\eta,\xi)$ projects the vector field at $\Psi(\eta,\xi)$ into the normal space of $\mathcal{M}$. With this additional notation, we can state our main result.

Main Result (LOR Equations Lemma). *Suppose that $x_0 \in \Omega$ can be expressed as $x_0 = \Psi(\eta_0,\xi_0)$ for $\eta_0 \in \mathcal{U}$ and $\xi_0 \in \mathbb{R}^k$. If $\|\xi_0\|$ is sufficiently small, then there exist $\delta > 0$, $\eta \in \mathscr{C}^1((-\delta,\delta),\mathcal{U}), \xi \in \mathscr{C}^1((-\delta,\delta),\mathbb{R}^k)$ such that $\Phi(x_0,t) = \Psi(\eta(t),\xi(t))$. Furthermore, $\eta(t),\xi(t)$ satisfy the initial value problem*

$$\begin{aligned} \dot{\eta} &= S_\sigma(\eta,\xi)^{-1} Tf(\eta,\xi) && \eta(0) = \eta_0, \\ \dot{\xi} &= Nf(\eta,\xi) - K_\sigma(\eta,\xi) S_\sigma(\eta,\xi)^{-1} Tf(\eta,\xi) && \xi(0) = \xi_0, \end{aligned} \tag{2.4}$$

where $S_\sigma(\eta,\xi) \in \mathbb{R}^{n-k\times n-k}, K_\sigma(\eta,\xi) \in \mathbb{R}^{k\times n-k}$ are defined in Section 2.3.2.

The following section will supply the explicit forms of $S_\sigma(\eta,\xi)$ and $K_\sigma(\eta,\xi)$ and will establish some key results that underlie the LOR Equations Lemma. We call $S_\sigma(\eta,\xi)$ and $K_\sigma(\eta,\xi)$ the *tangent* and *normal exchange operator*, respectively, for reasons that will become apparent in subsection 2.3.2 and in Section 2.4, where we give the proof of the LOR Equations Lemma.

2.3 Constructing the LOR Frame

To start the construction, we will present a set of tools for the local analysis of embedded manifolds and some of their properties, establish our notation and review relevant concepts for readers. Subsequently, in subsection 2.3.3, we establish an important tracking result.

2.3.1 First and Second Fundamental Forms

When studying surfaces embedded in $\mathbb{R}^3$, the first and second fundamental forms, often denoted I, II respectively, play a crucial role in representing local properties or shape. We will review the generalization of these concepts to an $(n-k)$-manifold embedded in $\mathbb{R}^n$.

Remark 1. There is a substantial body of work regarding the differential geometry of embedded manifolds including generalization of the concept of a second fundamental form [40]. While there may be a more elegant presentation of the following material, we set up just what we need for the problem at hand.

Definition 2.3.1. Given a chart $(\mathcal{U}, \sigma)$ of the $\mathscr{C}^r$ codimension-k manifold $\mathcal{M}$ with $r \geq 2$ and a $\mathscr{C}^s$ normal frame $\{N_j\sigma(\eta)\}_{j=1}^k$ with $s \geq 1$, define the mappings $\mathrm{I}, \mathrm{II}_j : \mathcal{U} \to \mathbb{R}^{n-k \times n-k}$ entrywise by

$$\begin{aligned}(\mathrm{I}(\eta))_{i_1,i_2} &= \langle \partial_{i_1}\sigma(\eta), \partial_{i_2}\sigma(\eta)\rangle \\ (\mathrm{II}_j(\eta))_{i_1,i_2} &= \langle \partial_{i_1}\sigma(\eta), \partial_{i_2}N_j\sigma(\eta)\rangle \end{aligned} \tag{2.5}$$

where $i_1, i_2 \in \{1, \cdots, n-k\}, j \in \{1, \cdots, k\}$. We call $\mathrm{I}(\eta), \{\mathrm{II}_j(\eta)\}_{j=1}^k$ the first and second fundamental forms of σ, respectively.

In the instance where $n = 3$ and $k = 1$, such that $\mathcal{M}$ is a surface embedded in $\mathbb{R}^3$, our representations of the first and second fundamental forms reduce to the standard definition. For any manifold embedded in $\mathbb{R}^n$, the arclength of a curve along the manifold is defined using the first fundamental form; given a $\mathscr{C}^1$ curve $\gamma : [0,1] \to \mathcal{M}$, there is a parametrized curve $\bar{\gamma} : [0,1] \to \mathcal{U}$ such that $\gamma(t) = \sigma \circ \bar{\gamma}(t)$, with $\langle \gamma'(t), \gamma'(t)\rangle = \langle [D\sigma \circ \bar{\gamma}(t)]\bar{\gamma}'(t), [D\sigma \circ \bar{\gamma}(t)]\bar{\gamma}'(t)\rangle = \langle [\mathrm{I} \circ \bar{\gamma}(t)]\bar{\gamma}(t), \bar{\gamma}(t)\rangle$, where the final equality follows from transposition. Therefore, the arclength functional may be expressed as

$$\mathcal{L}(\gamma) = \int_0^1 \sqrt{\langle [\mathrm{I} \circ \bar{\gamma}(t)]\bar{\gamma}'(t), \bar{\gamma}'(t)\rangle}\mathrm{d}t.$$

Note that the second fundamental forms depend on the choice of normal frame and hence are not (generically) intrinsic features of $\mathcal{M}$. However, $\mathrm{I}(\eta)$ is preserved under diffeomorphic reparameterization. The following result presents the properties of these matrices that are relevant for our analysis.

Lemma 2.3.2. *The maps* $\mathrm{I}(\eta), \{\mathrm{II}_j(\eta)\}_{j=1}^k$ *are self-adjoint,* $\mathrm{I}(\eta)$ *is positive definite,*

$$(\mathrm{II}_j(\eta))_{i_1,i_2} = -\langle \partial_{i_1}\partial_{i_2}\sigma(\eta), N_j\sigma(\eta)\rangle,$$

and

$$\mathrm{I}(\eta) = D_\eta\sigma(\eta)^T D_\eta\sigma(\eta), \qquad \mathrm{II}_j(\eta) = D_\eta\sigma(\eta)^T D_\eta N_j\sigma(\eta). \tag{2.6}$$

Proof. For notational convenience we will suppress η-dependence. From the symmetry of the inner product, we note that I is self-adjoint. Furthermore, the regularity of $\mathcal{M}$ (LOR assumption 3) implies that $\{\partial_i \sigma\}_{i=1}^{n-k}$ forms a linearly independent set. Thus, I is a Gram matrix and hence is positive definite.

Now consider

$$0 = \partial_{i_2} 0 = \partial_{i_2} \langle \partial_{i_1} \sigma, N_j \sigma \rangle = \langle \partial_{i_1} \partial_{i_2} \sigma, N_j \rangle + (\mathrm{II}_j)_{i_1, i_2}. \tag{2.7}$$

Equation (2.7) implies that $(\mathrm{II}_j)_{i_1,j_2} = -\langle \partial_{i_1} \partial_{i_2} \sigma, N_j \rangle$ and, as second derivatives commute, II_j is self-adjoint. The equalities in (2.6) follow immediately from matrix multiplication. □

2.3.2 The Tangent and Normal Exchange Operators

We will use the first and second forms to define a linear operator that is fundamental to the LOR frame. We call this operator the *tangent exchange operator* because it takes tangent vectors in $T_{\sigma(\eta)}\mathcal{U}$ and exchanges them for other tangent vectors in $T_{\sigma(\eta)}\mathcal{M}$, as will become clear later, in Section 2.4.

Definition 2.3.3. Given a chart $(\mathcal{U}, \sigma)$ of the $\mathscr{C}^r$ codimension-k manifold $\mathcal{M}$ with $r \geq 2$ and a $\mathscr{C}^s$ normal frame $\{N_j \sigma(\eta)\}_{j=1}^k$ with $s \geq 1$, define the mapping $S_\sigma : \mathcal{U} \times \mathbb{R}^k \to \mathbb{R}^{n-k \times n-k}$ by

$$S_\sigma(\eta, \xi) = \mathrm{I}(\eta) + \sum_{j=1}^{k} \xi_j \mathrm{II}_j(\eta). \tag{2.8}$$

As noted in Section 2.2, we call $S_\sigma(\eta, \xi)$ the tangent exchange operator of σ.

For our analysis, we will require the following result, which shows that given an embedding into $\mathbb{R}^n$, S_σ is invariant under change of normal frame (i.e., S_σ is extrinsically invariant).

Lemma 2.3.4. *For any $\eta \in \mathcal{U}$ and $\xi \in \mathbb{R}^k$ sufficiently small in norm, $S_\sigma(\eta, \xi)$ is invertible. Suppose that $\{N_j \sigma(\eta)\}_{j=1}^k, \{\hat{N}_j \sigma(\eta)\}_{j=1}^k$ are distinct normal frames to $\sigma(\eta)$. If*

$$\sigma(\eta) + \sum_{j=1}^{k} \xi_j N_j \sigma(\eta) = \sigma(\eta) + \sum_{j=1}^{k} \hat{\xi}_j \hat{N}_j \sigma(\eta), \tag{2.9}$$

then $S_\sigma(\eta, \xi) = \hat{S}_\sigma(\eta, \hat{\xi})$ where S_σ is the tangent exchange operator calculated from normal basis $\{N_j \sigma(\eta)\}$ and $\hat{S}_\sigma$ is the tangent exchange operator calculated from $\{\hat{N}_j \sigma\}$.

Proof. Note that $S_\sigma(\eta, 0) = \mathrm{I}(\eta)$, which is a positive matrix, and hence there is a $\delta > 0$ such that $\det S_\sigma(\eta, \xi) > 0$ for $\xi \in B_\delta(0)$, from the continuity of S_σ. Suppose that $\{N_j\sigma(\eta)\}_{j=1}^k, \{\hat{N}_j\sigma(\eta)\}_{j=1}^k$ are distinct normal frames to $\sigma(\eta)$, with corresponding second fundamental forms $(\mathrm{I\!I}_j(\eta))_{i_1,i_2}, (\hat{\mathrm{I\!I}}_j(\eta))_{i_1,i_2}$. As each $\{N_j\sigma(\eta)\}, \{\hat{N}_j\sigma(\eta)\}$ forms an orthonormal basis,

$$N_{j_1}\sigma(\eta) = \sum_{j_2=1}^k \left\langle N_{j_1}\sigma(\eta), \hat{N}_{j_2}\sigma(\eta) \right\rangle \hat{N}_{j_2}\sigma(\eta).$$

Let $B_{j_1,j_2}(\eta) = \left\langle N_{j_1}\sigma(\eta), \hat{N}_{j_2}\sigma(\eta) \right\rangle$. Subtracting $\sigma(\eta)$ from both sides of (2.9) and projecting onto $N_{j_1}\sigma(\eta)$ yields

$$\xi_{j_1} = \sum_{j_2=1}^k \hat{\xi}_{j_2} \left\langle N_{j_1}\sigma(\eta), \hat{N}_{j_2}\sigma(\eta) \right\rangle = \sum_{j_2=1}^k B_{j_1,j_2}(\eta)\hat{\xi}_{j_2}.$$

Therefore, for fixed $i_1, i_2 \in \{1, \cdots, n-k\}$,

$$\begin{aligned}
(S_\sigma(\eta,\xi))_{i_1,i_2} &= (\mathrm{I}(\eta))_{i_1,i_2} + \sum_{j_1=1}^k \xi_{j_1}(\mathrm{I\!I}_{j_1}(\eta))_{i_1,i_2} \\
&= (\mathrm{I}(\eta))_{i_1,i_2} - \sum_{j_1=1}^k \left(\sum_{j_2=1}^k B_{j_1,j_2}(\eta)\hat{\xi}_{j_2} \right) \left\langle \partial^2_{i_1,i_2}\sigma(\eta), N_{j_1}\sigma(\eta) \right\rangle \\
&= (\mathrm{I}(\eta))_{i_1,i_2} - \sum_{j_1=1}^k \sum_{j_2=1}^k \hat{\xi}_{j_2} B_{j_1,j_2}(\eta) \left\langle \partial^2_{i_1,i_2}\sigma(\eta), \sum_{j_3=1}^k B_{j_1,j_3}(\eta)\hat{N}_{j_3}\sigma(\eta) \right\rangle \\
&= (\mathrm{I}(\eta))_{i_1,i_2} - \sum_{j_1=1}^k \sum_{j_2=1}^k \sum_{j_3=1}^k \hat{\xi}_{j_2} B_{j_1,j_2}(\eta) B_{j_1,j_3}(\eta) \left\langle \partial^2_{i_1,i_2}\sigma(\eta), \hat{N}_{j_3}\sigma(\eta) \right\rangle \\
&= (\mathrm{I}(\eta))_{i_1,i_2} + \sum_{j_1=1}^k \sum_{j_2=1}^k \sum_{j_3=1}^k \hat{\xi}_{j_2} B_{j_1,j_2}(\eta) B_{j_1,j_3}(\eta) (\hat{\mathrm{I\!I}}_{j_3}(\eta))_{i_1,i_2}. \qquad (2.10)
\end{aligned}$$

Next we derive a simple identity to simplify this flurry of indices. Note that

$$\begin{aligned}
\hat{N}_{j_1}\sigma(\eta) &= \sum_{j_2=1}^k B_{j_2,j_1}(\eta) N_{j_2}\sigma(\eta) \\
&= \sum_{j_2=1}^k B_{j_2,j_1}(\eta) \left(\sum_{j_3=1}^k B_{j_2,j_3}(\eta)\hat{N}_{j_3}\sigma(\eta) \right) \\
&= \sum_{j_2=1}^k \sum_{j_3=1}^k B_{j_2,j_1}(\eta) B_{j_2,j_3}(\eta) \hat{N}_{j_3}(\eta). \qquad (2.11)
\end{aligned}$$

Projecting both sides of (2.11) onto $\hat{N}_{j_4}\sigma(\eta)$ yields

$$\begin{aligned}\delta_{j_1,j_4} &= \sum_{j_2=1}^{k}\sum_{j_3=1}^{k} B_{j_2,j_1}(\eta)B_{j_2,j_3}(\eta)\delta_{j_3,j_4} \\ &= \sum_{j_2=1}^{k} B_{j_2,j_1}(\eta)B_{j_2,j_4}(\eta). \end{aligned} \tag{2.12}$$

Applying (2.12) to (2.10) yields

$$\begin{aligned}(S_\sigma(\eta,\xi))_{i_1,i_2} &= (\mathrm{I}(\eta))_{i_1,i_2} + \sum_{j_2=1}^{k}\sum_{j_3=1}^{k} \hat{\xi}_{j_2}(\hat{\mathrm{II}}_{j_2}(\eta))_{i_1,i_2}\,(\delta_{j_2,j_3}) \\ &= (\mathrm{I}(\eta))_{i_1,i_2} + \sum_{j_2=1}^{k} \hat{\xi}_{j_2}(\hat{\mathrm{II}}_{j_2}(\eta))_{i_1,i_2} \\ &= (\hat{S}_\sigma(\eta,\hat{\xi}))_{i_1,i_2}. \end{aligned} \tag{2.13}$$

Since i_1, i_2 were arbitrary, the result follows. □

Corollary 1. *If* $\{N_j\sigma(\eta)\}_{j=1}^k, \{\hat{N}_j\sigma(\eta)\}_{j=1}^k$ *are normal frames and* $\Psi(\eta,\xi) = \hat{\Psi}(\eta,\hat{\xi})$ *then* $(B(\eta))_{j_1,j_2} = \left\langle N_{j_1}\sigma(\eta), \hat{N}_{j_2}\sigma(\eta)\right\rangle$ *is a unitary matrix, and* $\xi = B(\eta)\hat{\xi}$.

To conclude this subsection, we present a definition for another linear map, which has no obvious analogue in the theory of surfaces.

Definition 2.3.5. Given a chart $(\mathcal{U},\sigma)$ of the $\mathscr{C}^r$ codimension-k manifold $\mathcal{M}$ with $r \geq 2$ and a $\mathscr{C}^s$ normal frame $\{N_j\sigma(\eta)\}_{j=1}^k$ with $s \geq 1$, define the mapping $K_\sigma : \mathcal{U}\times\mathbb{R}^k \to \mathbb{R}^{k\times n-k}$ by

$$K_\sigma(\eta,\xi) = \sum_{j=1}^{k} \xi_j [N\sigma(\eta)][D_\eta N_j\sigma(\eta)], \tag{2.14}$$

where

$$N\sigma(\eta) := (N_1\sigma(\eta),\ldots,N_k\sigma(\eta))^T. \tag{2.15}$$

As noted in Section 2.4, we call K_σ the normal exchange operator.

2.3.3 LOR Tracking Lemma

The following lemma provides the backbone of our main result.

Lemma (LOR Tracking Lemma). *Suppose that $x_0 \in \Omega$ can be expressed as $\Psi(\eta_0, \xi_0)$ for $\eta_0 \in \mathcal{U}$, $\xi_0 \in \mathbb{R}^k$ and that $\gamma : I \to \mathbb{R}^n$ is a $\mathscr{C}^1$ curve defined on an interval I containing zero with $\gamma(0) = x_0$. If $\|\xi_0\|$ is sufficiently small, then there exist $\delta > 0$ such that $(-\delta, \delta) \subseteq I$ and functions $\eta \in \mathscr{C}^1((-\delta, \delta), \mathcal{U}), \xi \in \mathscr{C}^1((-\delta, \delta), \mathbb{R}^k)$ with $\eta(0) = \eta_0, \xi(0) = \xi_0$ such that $\gamma(t) = \Psi(\eta(t), \xi(t))$ for $t \in (-\delta, \delta)$.*

Proof. We will apply the Implicit Function Theorem (IFT). Define $F : \mathcal{U} \times \mathbb{R}^k \times I \to \mathbb{R}^n$ by

$$F(\eta, \xi, t) = \Psi(\eta, \xi) - \gamma(t).$$

Note that F is $\mathscr{C}^1$ and $F(\eta_0, \xi_0, 0) = 0$. Hence we need only show that $D_{(\eta,\xi)}\ F(\eta_0, \xi_0, 0)$ is invertible. We compute

$$\begin{aligned} \partial_i \Psi(\eta, \xi) &= \partial_i \sigma(\eta) + \sum_{j=1}^{k} \xi_j \partial_i N_j \sigma(\eta) \\ \frac{\partial \Psi}{\partial \xi_j}(\eta, \xi) &= N_j \sigma(\eta) \end{aligned} \tag{2.16}$$

for $i \in \{1, \cdots, n-k\}, j \in \{1, \cdots, k\}$. It suffices to prove that the n vectors described in (2.16) are linearly independent. By way of contradiction suppose that there are non-zero scalars $\{\alpha_i\}_{i=1}^{n-k}, \{\beta_j\}_{j=1}^{k} \subseteq \mathbb{R}$ such that

$$\sum_{i=1}^{n-k} \alpha_i \partial_i \Psi(\eta, \xi) + \sum_{j=1}^{k} \beta_j \frac{\partial \Psi}{\partial \xi_j}(\eta, \xi) = 0.$$

Projecting both sides of this relation into $\partial_{i_2}\sigma(\eta)$ and simplifying yields

$$\sum_{i_1=1}^{n-k} \left(\langle \partial_{i_1}\sigma(\eta), \partial_{i_2}\sigma(\eta) \rangle + \sum_{j=1}^{k} \xi_j \langle \partial_{i_1} N_j \sigma(\eta), \partial_{i_2}\sigma(\eta) \rangle \right) \alpha_{i_1} = 0$$

or, when vectorized, $S_\sigma(\eta, \xi)\alpha = 0$ for $i_2 \in \{1, \cdots, n-k\}$. We can guarantee that there is a $\delta > 0$ such that $S_\sigma(\eta, \xi)$ is invertible for all $\xi_0 \in B_\delta(0)$, by Lemma 2.3.4, hence $\alpha = 0$. Furthermore, $\{N_j\sigma(\eta)\}_{j=1}^{k}$ is an orthonormal set and thus $\beta_j = 0$ follows for all j. Thus, we obtain the desired contradiction and conclude that $D_{(\eta,\xi)}F(\eta_0, \xi_0, 0)$ is invertible, such that our claim follows from the IFT. □

The non-constructive wording "for ξ_0 sufficiently small in norm" in the LOR Tracking Lemma can actually be made exact.

Definition 2.3.6. Given a chart $(\mathcal{U}, \sigma)$ of the $\mathscr{C}^r$ codimension-k manifold $\mathcal{M}$ with $r \geq 2$ and a $\mathscr{C}^s$ normal frame $\{N_j\sigma(\eta)\}_{j=1}^k$ with $s \geq 1$, for each $\eta \in \mathcal{U}$, let $\mathcal{P}_\eta$ be the maximal, by inclusion, path-connected subset of $\mathbb{R}^k$ containing the origin such that

$$\det S_\sigma(\eta, \xi) > 0 \qquad \forall \xi \in \mathcal{P}_\eta.$$

Define the maximal parameter domain $\mathcal{P}$ by

$$\mathcal{P} = \bigcup_{\eta \in \mathcal{U}} \{\eta\} \times \mathcal{P}_\eta.$$

The definition of the maximal parameter domain provides the following rewording of the LOR Tracking Lemma.

Corollary 2. *Suppose that $x_0 \in \Omega$ can be expressed $\Psi(\eta_0, \xi_0)$ for $\eta_0 \in \mathcal{U}$, $\xi_0 \in \mathbb{R}^k$, and that $\gamma : I \to \mathbb{R}^n$ is a $\mathscr{C}^1$ curve defined on an interval I containing zero with $\gamma(0) = x_0$. If $(\eta_0, \xi_0) \in \mathcal{P}$, then there exist $\delta > 0$ such that $(-\delta, \delta) \subseteq I$ and functions $\eta \in \mathscr{C}^1((-\delta, \delta), \mathcal{U}), \xi \in \mathscr{C}^1((-\delta, \delta), \mathbb{R}^k)$ such that $\gamma(t) = \Psi(\eta(t), \xi(t))$ for $t \in (-\delta, \delta)$.*

With this result, the continuation of the LOR frame for curve tracking is guaranteed up to but not across $\mathcal{P}_0 := \mathrm{cl}(\mathcal{P}) \cap \{\det S_\sigma(\eta, \xi) = 0\}$. The reader may be worried that $\mathcal{P}$ depends on our choice of normal frame and thus $\Psi(\mathcal{P}), \Psi(\mathcal{P}_0) \subseteq \mathbb{R}^n$ may be dependent on the choice of normal frame.Thankfully, we find that Lemma 2.3.4 can be used to eliminate any such uneasiness.

Corollary 3. *$\Psi(\mathcal{P})$ and $\Psi(\mathcal{P}_0)$ are invariant to choice of normal frame.*

Proof. Pick any two normal frames $\{N_j\sigma(\eta)\}_{j=1}^k, \{\hat{N}_j\sigma(\eta)\}_{j=1}^k$ and define corresponding maximal parameter domains $\mathcal{P}, \hat{\mathcal{P}}$. For any $x \in \Psi(\mathcal{P})$, there exist $(\eta, \xi) \in \mathcal{P}$ such that $\Psi(\eta, \xi) = x$. Now, fix $\eta \in \mathcal{U}$. Denote by $\gamma : [0, 1] \to \mathcal{P}_\eta$ any path connecting 0 to ξ, let $\Gamma(s) = (\eta, \gamma(s))$ for all $s \in [0, 1]$, and note that $\det S_\sigma \circ \Gamma(s) > 0$.

From Lemma 2.3.4 we know that there is a unitary change of basis matrix, U, between $\{N_j\sigma(\eta)\}_{j=1}^k$ and $\{\hat{N}_j\sigma(\eta)\}_{j=1}^k$. Therefore the curve Γ will lift to $\hat{\Gamma}(s) = (\eta, U\gamma(s))$. By

Lemma 2.3.4, $\det \hat{S}_\sigma \circ \hat{\Gamma}(s) = \det S_\sigma \circ \Gamma(s) > 0$, and hence $(\eta, U\xi) \in \hat{\mathcal{P}}$ by maximality. Thus $x \in \hat{\Psi}(\hat{\mathcal{P}})$ and $\Psi(\mathcal{P}) \subseteq \hat{\Psi}(\hat{\mathcal{P}})$.

Reversing the proof gives the opposite inclusion. Note that Ψ is defined on an approriate domain of (η, ξ) independent of LOR tracking, so $\Psi(\mathcal{P})$ is uniquely defined as desired, and the claim regarding $\Psi(\mathcal{P}_\prime)$ follows analogously. □

2.4 Proof of the Main Result

With our definitions and preliminary results laid out, we can prove our main result.

Proof of the LOR Equations Lemma. Suppose that $x_0 \in \Omega$ can be expressed as $\Psi(\eta_0, \xi_0) = x_0$ for $\eta_0 \in \mathcal{U}, \xi_0 \in \mathbb{R}^k$. Denote $\phi(t) = \Phi(x_0, t)$ and note that $\phi \in \mathscr{C}^1$. If $\|\xi_0\|$ is sufficiently small, then there exist $\delta > 0$, $\eta \in \mathscr{C}^1((-\delta, \delta), \mathcal{U}), \xi \in \mathscr{C}^1((-\delta, \delta), \mathbb{R}^k)$ such that $\phi(t) = \Psi(\eta(t), \xi(t))$ for $t \in (-\delta, \delta)$, by the LOR Tracking Lemma.

Suppressing time dependence, we compute

$$\dot{\phi} = \frac{d}{dt}\Psi(\eta, \xi) = \left(D_\eta \sigma(\eta) + \sum_{j=1}^{k} \xi_j D_\eta N_j \sigma(\eta) \right) \dot{\eta} + \sum_{j=1}^{k} \dot{\xi}_j N_j \sigma(\eta). \tag{2.17}$$

Note that $\dot{\phi} = f \circ \phi = f \circ \Psi(\eta, \xi)$. Acting on the left by $D_\eta \sigma(\eta)^T$ yields

$$\left(D_\eta \sigma(\eta)^T D_\eta \sigma(\eta) + \sum_{j=1}^{k} \xi_j D_\eta \sigma(\eta)^T D_\eta N_j \sigma(\eta) \right) \dot{\eta} = D_\eta \sigma(\eta)^T f \circ \Psi(\eta, \xi),$$

which reduces to

$$S_\sigma(\eta, \xi)\dot{\eta} = Tf(\eta, \xi). \tag{2.18}$$

Thus $\dot{\eta} = S_\sigma(\eta, \xi)^{-1} T f(\eta, \xi)$, as S_σ is invertible near (η_0, ξ_0). The equation governing $\dot{\xi}$ follows analogously by left acting on equation (2.17) by the expression given in (2.15). □

Remark 2. Equation (2.18) highlights the exchange of tangent vectors via the action of S_σ that motivates our choice to name this the exchange operator. Note that the standard shape operator from differential geometry also exchanges tangent vectors, but these operators are not identical.

We have once again used non-constructiive language to constrain ξ_0. We can strengthen this language by using $\mathcal{P}$ and "reverse" the statement of the main result.

Corollary 4. *Suppose that $\eta(t), \xi(t)$ solve system (2.4) for $(\eta_0, \xi_0) \in \mathcal{P}$ for $t \in (-\delta, \delta)$. Then $\Psi(\eta(t), \xi(t)) = \Phi(\Psi(\eta_0, \xi_0), t)$ for $t \in (-\delta, \delta)$.*

Given a vector field f and a chart $(\mathcal{U}, \sigma)$ of a smooth, regular, codimension-k manifold, we denote the *LOR vector field* by

$$\mathscr{L}_\sigma f(\eta, \xi) = \begin{pmatrix} S_\sigma(\eta, \xi)^{-1} T f(\eta, \xi) \\ N f(\eta, \xi) - K_\sigma(\eta, \xi) S_\sigma(\eta, \xi)^{-1} T f(\eta, \xi) \end{pmatrix}.$$

Interestingly, the operator $\mathscr{L}_\sigma$ is linear; that is,

$$\mathscr{L}_\sigma(\alpha g + \beta f)(\eta, \xi) = \alpha \mathscr{L}_\sigma g(\eta, \xi) + \beta \mathscr{L}_\sigma f(\eta, \xi)$$

as f, g only appear in Tf, Tg, Nf, Ng, which are vectors of inner products. Therefore the LOR dynamics respects additive perturbations. We hope to take advantage of this fact in future work.

It is natural to wonder whether the LOR flow is topologically conjugate to the flow induced by (2.1). It can be computationally difficult to find a codomain on which Ψ is a homeomorphism. However, the flow induced by (2.1) is a *submersion* of the LOR flow via Ψ.

Definition 2.4.1. Suppose that Φ_X, Φ_Y are both continuous flows on X, Y respectively, with Φ_X defined on $\{(x, t) : x \in X, t \in I_x\}$ for time intervals $I_x \subset \mathbb{R}$. The flow Φ_Y is a submersion of Φ_X via H if there is a continuous, surjective map $H : X \to Y$ such that

$$H \circ \Phi_X(x, t) = \Phi_Y(H(x), t) \qquad \forall x \in X, t \in I_x.$$

This is simply the definition of topological conjugacy of flows with the injectivity of the homeomorphism relaxed.

Corollary 5. *The flow induced by f is a submersion of the flow induced by $\mathscr{L}_\sigma f$ via Ψ.*

2.5 Extensions and Applications

In this section, we highlight several scenarios where the computations involving LOR simplify in useful ways. We also discuss certain auxiliary ideas, namely a measure of near-invariance for a surface in a flow that can be defined based on LOR and a blow-up transformation that can be applied to the LOR equations, that enhance the utility of LOR. The near-invariance measure plays a useful role in Section 2.6.

2.5.1 Hypersurfaces and Frenet Curves

In the cases where $k = 1$ and $k = n - 1$, which correspond to $\mathcal{M}$ being a curve and a hypersurface, respectively, there is a canonical choice of normal frame that allows us to simplify the LOR dynamics. First, suppose that $k = n - 1$ and $\mathcal{M}$ is a codimension-1 manifold. In this case, $T_p\mathcal{M}$ is a $n-1$ dimensional space, with a one-dimensional orthogonal complement in $\mathbb{R}^n$. Therefore there are exactly 2 unit vectors that could serve as a normal frame. We choose the normal vector is accordance with the right hand rule; specifically, we define

$$N\sigma(\eta) = \frac{\partial_1\sigma(\eta) \wedge \cdots \wedge \partial_{n-1}\sigma(\eta)}{\|\partial_1\sigma(\eta) \wedge \cdots \wedge \partial_{n-1}\sigma(\eta)\|} \tag{2.19}$$

where $x_1 \wedge \cdots \wedge x_{n-1}$ is the outer product of $n-1$ vectors, which is a generalization of the cross product. We easily attain the following result.

Proposition 1. *For $N\sigma(\eta)$ given in (2.19), $K_\sigma(\eta, \xi) = 0$.*

Proof. Note that $\langle N\sigma(\eta), N\sigma(\eta)\rangle = 1$ and hence

$$0 = \partial_i \langle N\sigma(\eta), N\sigma(\eta)\rangle = 2 \langle \partial_i N\sigma(\eta), N\sigma(\eta)\rangle .$$

Therefore, $K_\sigma(\eta, \xi) = 0$. □

Thus, with this choice of $N\sigma(\eta)$, the $\dot{\xi}$ equation in (2.4) simplifies significantly.

The study of curves is more interesting. Suppose that σ parameterizes a curve in $\mathbb{R}^n$. By imposing additional structure on σ we can generate a natural normal frame, namely we will assume that σ is a Frenet curve.

Using the Frenet frame allows us to greatly simplify the LOR equations; we find that,

$$\begin{aligned}\mathrm{I}(\eta) &= \|\sigma'(\eta)\|^2 \\ \mathrm{II}_j(\eta) &= -\|\sigma'(\eta)\|^2 \delta_{1,j}\kappa_1(\eta)\end{aligned}$$

hence $S_\sigma(\eta) = \|\sigma'(\eta)\|^2 (1 - \xi_1\kappa_1(\eta))$. With significantly more index wrangling, we find that

$$K_\sigma(\eta, \xi) = \|\sigma'(\eta)\| \hat{C}(\eta)\xi$$

where $\hat{C}(\eta)$ is the $(1,1)$-principal minor of $C(\eta)$. Therefore (2.4) simplifies to

$$\begin{aligned}\dot{\eta} &= \frac{\langle f \circ \Psi(\eta, \xi), T\sigma(\eta)\rangle}{\|\sigma'(\eta)\| (1 - \xi_1\kappa_1(\eta))} \\ \dot{\xi} &= Nf(\eta, \xi) - \frac{\langle f \circ \Psi(\eta, \xi), T\sigma(\eta)\rangle}{1 - \xi_1\kappa_1(\eta)} \hat{C}(\eta)\xi. \end{aligned} \tag{2.20}$$

We call system (2.20) the Frenet LOR equations. This example illustrates that when σ is a Frenet curve, K_σ reduces to the matrix of curvatures. If we take $\sigma(\eta)$ to be a trajectory of (2.1), then $Nf(\eta, \xi) = 0$ and $\dot{\eta}|_{\xi=0} = 1$.

By dividing through by $\dot{\eta}$ to eliminate time from system (2.20), we find

$$\frac{d\xi}{d\eta} = \|\sigma'(\eta)\| (1 - \xi_1\kappa_1(\eta)) \frac{Nf(\eta, \xi)}{\langle f \circ \Psi(\eta, \xi), T\sigma(\eta)\rangle} - \|\sigma'(\eta)\| \hat{C}(\eta)\xi. \tag{2.21}$$

This set of equations (2.21) is well-suited to study transition maps: suppose we choose σ to be a dynamically relevant trajectory, and we want to study how the normal space of σ at $\eta = 0$ is mapped to the normal space at $\eta = 1$. Usually, one has to deal with approximating the time it takes for trajectories to travel from one section Σ_1 to another section Σ_2, defined to represent this mapping. In (2.21), however, we have eliminated time dependence; thus, we can simply integrate trajectories from $\eta = 0$ to $\eta = 1$. Therefore it is very natural to represent Poincaré maps in the LOR frame.

2.5.2 A Measure for Near-Invariance

In this section, we present a natural generalization of a technique used for curves in planar systems in [45]; namely, we construct a quantitative measure that quantifies how close a surface is to being invariant under a flow. We will focus on the simplest case $k = 1$, when $\mathcal{M}$ is a hypersurface embedded in Ω. Recall, from the preceding section that the ξ dynamics in the LOR frame for a codimension-one chart is given by $\dot{\xi} = Nf(\eta, \xi)$. Note that $\sigma(\mathcal{U})$ is locally invariant if and only if $\dot{\xi}|_{\xi=0} = 0$; that is, $Nf(\eta, 0) = 0$ for all $\eta \in \mathcal{U}$. Geometrically, $Nf(\eta, 0) = 0$ if and only if $f \circ \sigma(\eta) \in T_{\sigma(\eta)}\mathcal{M}$; thus, the normal vector $N\sigma(\eta)$ is orthogonal to our vector field along σ. Heuristically, we note that $\sigma(\mathcal{U})$ is closer to being invariant if $|Nf(\eta, 0)|$ is small, as LOR trajectories cannot rapidly escape $\mathcal{U} \times \{0\}$.

There are several natural candidates for constructing a measure of this "near-invariance" property. We choose one that we find particularly informative.

Definition 2.5.1. Given a chart $(\mathcal{U}, \sigma)$ of the $\mathscr{C}^r$ codimension-1 manifold $\mathcal{M}$ with $r \geq 2$ and a $\mathscr{C}^s$ normal vector $N\sigma(\eta)$ with $s \geq 1$, we define $\mu_\sigma : \mathcal{U} \to \mathbb{R}^+$ by

$$\mu_\sigma(\eta) = \inf_{\xi \in \mathcal{P}_\eta} \{|\xi| : Nf(\eta, \xi) = 0\}. \tag{2.22}$$

with the convention that $\inf \emptyset = -\infty$. We call μ_σ the near-invariance measure of σ. Furthermore, define $\Xi_\sigma : \mathcal{U} \to \mathbb{R}$ by

$$\Xi_\sigma(\eta) = \arg \inf_{\xi \in \mathcal{P}_\eta} \{|\xi| : Nf(\eta, \xi) = 0\}.$$

We call Ξ_σ the correction to σ.

Intuitively, $\mu_\sigma(\eta)$ represents the closest point $(\eta, \xi) \in \{\eta\} \times \mathcal{P}_\eta$ such that $Nf(\eta, \xi) = 0$; it measures how far off the manifold we must travel to reach the ξ-nullsurface. Note that $\Xi_\sigma(\eta)$, when defined, is the smallest ξ, in norm, such that $Nf(\eta, \xi) = 0$.

Initially, these definitions seem cumbersome; however, μ_σ, Ξ_σ have interesting properties. For example, $\mu_\sigma(\eta) \equiv 0$ if and only if $\sigma(\mathcal{U})$ is locally invariant. The correction Ξ_σ allows us to study how non-invariant manifolds can create trapping regions. If $Nf(\eta, 0) > 0$ and $\Xi_\sigma(\eta) > 0$ for $\eta \in \mathcal{U}$, then the set $W = \{(\eta, \xi) : \eta \in \mathcal{U}, 0 \leq \xi \leq \Xi_\sigma(\eta)$ is positively locally invariant if $\langle \nabla \Xi_\sigma(\eta), f \circ \Xi_\sigma(\eta) \rangle > 0$ for $\eta \in \mathcal{U}$. This type of trapping region can help to

explain how non-invariant manfiolds can play an organizing role in dynamics. Indeed, the use of the near-invariance measure plays a key role in the precise definition and identification of rivers in planar systems [45].

Furthermore, we can utilize the function Ξ_σ to obtain useful nearly invariant manifolds. If Ξ_σ is well-defined and $\mathscr{C}^1$ on $\hat{\mathcal{U}} \subseteq \mathcal{U}$, then consider the function $\hat{\sigma} : \hat{\mathcal{U}} \to \Omega$ defined by

$$\hat{\sigma}(\eta) = \sigma(\eta) + \Xi_\sigma(\eta) N\sigma(\eta).$$

Generically, $\hat{\sigma}$ is a regular chart itself; that is, it parametrizes a codimension-1 manifold $\hat{\mathcal{M}}$, in which case we call $\hat{\sigma}$ the corrected chart of σ. Interestingly, the corrected chart is often more nearly-invariant than the original chart, with $\mu_{\hat{\sigma}}(\eta) < \mu_\sigma(\eta)$ for $\eta \in \hat{\mathcal{U}}$. We make use of this property in our computational example 2.6 to identify canard behavior in the normal form system for a folded-saddle node bifurcation [39, 66].

2.5.3 Constructing a Normal Frame to a Manifold à la Frenet

In the theory presented thus far, we have simply assumed that the user can provide a normal frame. In this section, we present a rigorous algorithm for constructing these frames.

In the construction of the Frenet frame for the $k = 1$ case, we used higher derivatives of the curve to "fill-up" $T_pM^\perp$ and then applied the Gram-Schmidt process to orthonormalize these derivatives and thus construct our moving frame. Here, we apply the same ideas, albeit with more notation, to generalize this construction to higher codimensions.

Suppose that $f \in \mathscr{C}^r(\mathbb{R}^m, \mathbb{R}^n)$. Given an index $\alpha = (\alpha_1, \cdots, \alpha_m) \in \mathbb{N}^m$ such that $\sum_{i=1}^m \alpha_i := |\alpha| \leq r$, we use ∂_α to denote the indicial derivative:

$$\partial_\alpha f(x) = \frac{\partial^{|\alpha|} f}{\partial_{x_1}^{\alpha_1} \partial_{x_2}^{\alpha_2} \cdots \partial_{x_m}^{\alpha_m}}(x).$$

Note that, when represented indicially, $\partial_i := \partial/\partial x_i = \partial_{e_i}$ where e_i is the i^{th} canonical basis vector.

Definition 2.5.2. A chart $(\mathcal{U}, \sigma)$ of a regular, $\mathscr{C}^{r\geq 2}$, m-manifold M embedded in $\Omega \subseteq \mathbb{R}^n$ for $n > m$ is a Frenet chart if there are indices $\{\alpha_j\}_{j=m+1}^n$ such that $\alpha_j \in \mathbb{N}^m$, $2 \leq |\alpha_j| \leq r-1$ for $m+1 \leq j \leq n$, and

$$\dim \operatorname{span} \left\{ \partial_{e_1}\sigma(\eta), \cdots, \partial_{e_m}\sigma(\eta), \partial_{\alpha_{m+1}}\sigma(\eta), \cdots, \partial_{\alpha_n}\sigma(\eta) \right\} = n \qquad \forall \eta \in \mathcal{U}. \tag{2.23}$$

In this case, $\{\alpha_j\}_{j=m+1}^n$ is a Frenet index set.

When considering curves, the $m = 1$ case, taking $\alpha_j = j$ for $m+1 = 2 \leq j \leq n$, the above condition is equivalent to the curve in question being Frenet. Definition 2.5.2 allows for the use of more complicated configurations of derivatives to build a basis for $\mathbb{R}^n$.

To simplify notation, given a Frenet index set $\{\alpha_j\}_{j=m+1}^n$, we define $\alpha_j = e_j$ for $1 \leq j \leq m$, after which condition (2.23) simplifies to

$$\dim \operatorname{span} \left\{ \partial_{\alpha_j}\sigma(\eta) \right\}_{j=1}^n = n \qquad \forall \eta \in \mathcal{U}.$$

Clearly we can perform the Gram-Schmidt process on $\{\partial_{\alpha_j}\sigma\}$ to construct an orthonormal basis. The first m vectors will be linear combinations of $\{\partial_{e_j}\sigma\}$ and hence form an orthonormal basis for $T_{\sigma(\eta)}M$; thus, we denote them $T_i\sigma(\eta), i = 1, \ldots, m$. The final $n-m$ orthonormal vectors produced will be orthogonal to $T_{\sigma(\eta)}M$ and can be denoted $N_j\sigma(\eta)$ without any abuse of notation; they form a normal frame per LOR assumption 4. Therefore, we can produce normal frames to manifolds in an algorithmic way, provided that we make a fairly generic assumption about the manifolds' higher derivatives.

One advantage of the Frenet frame in the preceding section is that it allows us to easily compute $\mathrm{I\!I}_i, K_\sigma$ using inherent properties of the LOR base curve. We shall next establish that we can compute $\mathrm{I\!I}_i, K_\sigma$ from the properties of our generalized Frenet frame as well.

The Gram-Schmidt process, being linear, can be represented as a matrix multiplication. That is, there is an $n \times n$ matrix $G : \mathcal{U} \to \mathbb{R}^{n\times n}$ such that

$$G(\eta) \begin{pmatrix} \partial_{\alpha_1}\sigma(\eta) \\ \vdots \\ \partial_{\alpha_n}\sigma(\eta) \end{pmatrix} = \begin{pmatrix} T_1\sigma(\eta) \\ \vdots \\ N_k\sigma(\eta) \end{pmatrix},$$

and G is $\mathscr{C}^1$, everywhere invertible, and lower triangular. Note that G is of the form

$$G(\eta) = \left(\begin{array}{c|c} G_1(\eta) & 0 \\ \hline G_2(\eta) & G_3(\eta) \end{array}\right) \tag{2.24}$$

where $G_1(\eta), G_3(\eta)$ are $\mathscr{C}^1$, invertible, $m \times m, k \times k$ (respectively), lower triangular matrices, and $G_2(\eta)$ is a $\mathscr{C}^1$ $k \times m$ matrix. Define

$$\hat{G}(\eta) = \left(\begin{array}{c|c} I & 0 \\ \hline G_2(\eta) & G_3(\eta) \end{array}\right) \tag{2.25}$$

where I is the $m \times m$ identity matrix, then by definition

$$\hat{G}(\eta) \begin{pmatrix} \partial_{e_1}\sigma(\eta) \\ \vdots \\ \partial_{e_m}\sigma(\eta) \\ \partial_{\alpha_{m+1}}\sigma(\eta) \\ \vdots \\ \partial_{\alpha_n}\sigma(\eta) \end{pmatrix} = \begin{pmatrix} \partial_{e_1}\sigma(\eta) \\ \vdots \\ \partial_{e_m}\sigma(\eta) \\ N_1\sigma(\eta) \\ \vdots \\ N_k\sigma(\eta) \end{pmatrix}. \tag{2.26}$$

To finish our generalization of the Frenet frame, we need to understand how the derivatives of $T_i\sigma, N_j\sigma$ can be expressed as linear combinations of $T_i\sigma, N_j\sigma$, as in the Frenet-Serret equations. To this end, we define the following.

Definition 2.5.3. Suppose that $(\mathcal{U}, \sigma)$ is a Frenet chart with index set $\{\alpha_j\}_{j=1}^n$. Then $\{\partial_{\alpha_j}\sigma(\eta)\}_{j=1}^n$ forms a basis for $\mathbb{R}^n$ and therefore there are matrices $A_i : \mathcal{U} \to \mathbb{R}^{n\times n}$ such that

$$\partial_{e_i} \begin{pmatrix} \partial_{\alpha_1}\sigma(\eta) \\ \vdots \\ \partial_{\alpha_n}\sigma(\eta) \end{pmatrix} = \begin{pmatrix} \partial_{\alpha_1+e_i}\sigma(\eta) \\ \vdots \\ \partial_{\alpha_n+e_i}\sigma(\eta) \end{pmatrix} =: A_i(\eta) \begin{pmatrix} \partial_{\alpha_1}\sigma(\eta) \\ \vdots \\ \partial_{\alpha_n}\sigma(\eta) \end{pmatrix}.$$

We call these matrices the differo-algebraic closures of the index set.

Remark 3. At first glance, the entries of $A_i(\eta)$ appear to be arbitrary and thus could be difficult to compute. However, by filling out our normal frame with higher derivatives of σ, we can greatly simplify A_i. Note that $\partial_{e_i}\partial_{\alpha_s}\sigma(\eta) = \partial_{\alpha_s+e_i}\sigma(\eta)$, and therefore if $\alpha_s+e_i \in \{\alpha_j\}_{j=1}^n$, then the s^{th} row of $A_i(\eta)$ is a canonical basis vector; that is, if $\alpha_s + e_i = \alpha_j$ then $A_i(\eta)_s = e_j$, hence A_i can be fairly sparse. In fact, the remarkable simplicity of the Frenet-Serret equation is caused by the sparseness of the relevant differo-algebraic closure.

Proposition 2. *If $(\mathcal{U}, \sigma)$ is a Frenet chart with index set $\{\alpha_j\}_{j=1}^n$ and differo-algebraic closures $\{A_j(\eta)\}_{j=1}^n$, then for $i = 1, \ldots, m$,*

$$\partial_{e_i} v(\eta) = \left[(\partial_{e_i}\hat{G}(\eta) + \hat{G}(\eta)A_i(\eta))\hat{G}^{-1}(\eta)\right] v(\eta), \tag{2.27}$$

where $\hat{G}$ is given in equation (2.25), and

$$v(\eta) = (\partial_{e_1}\sigma(\eta), \cdots, \partial_{e_m}\sigma(\eta), N_1\sigma(\eta), \cdots, N_k\sigma(\eta))^T \tag{2.28}$$

Proof. Taking derivatives of both sides of (2.26), using the definition of the differo-algebraic closures, and applying (2.26) yields the result. □

Proposition 2 allows us to compute $\mathrm{I\!I}_i, K_\sigma$ from first principles, after we define the following operators.

Definition 2.5.4. Given a chart $(\mathcal{U}, \sigma)$ of the $\mathscr{C}^r$ codimension-k manifold $\mathcal{M}$ with $r \geq 2$ and a $\mathscr{C}^s$ normal frame $\{N_j\sigma(\eta)\}_{j=1}^k$ with $s \geq 1$, we define mappings $\mathrm{I\!I\!I}_{j_1} : \mathcal{U} \to \mathbb{R}^{k\times n-k}$ entry wise by

$$(\mathrm{I\!I\!I}_{j_1}(\eta))_{j_2,i} = \langle \partial_i N_{j_1}\sigma(\eta), N_{j_2}\sigma(\eta)\rangle,$$

where $j_1, j_2 \in \{1, \cdots, k\}, i \in \{1, \cdots, n-k\}$. We call $\{\mathrm{I\!I\!I}_i(\eta)\}_{i=1}^{n-k}$ the third fundamental forms of σ.

These operators have no clear analogue in the theory of surfaces; however, they bear some resemblance to the Christoffel symbols. The third fundamental forms are useful insofar as they determine K_σ.

Lemma 2.5.5. *Given a chart $(\mathcal{U}, \sigma)$ of the $\mathscr{C}^r$ codimension-k manifold $\mathcal{M}$ with $r \geq 2$ and a $\mathscr{C}^s$ normal frame $\{N_j\sigma(\eta)\}_{j=1}^k$ with $s \geq 1$,*

$$K_\sigma(\eta) = \sum_{j=1}^{k} \xi_j \mathbb{III}_j(\eta).$$

Now we can derive formulae for $\mathbb{I}_j, \mathbb{III}_j$ using properties of our Frenet-type frame. Let

$$A_i(\eta) = \left(\begin{array}{c|c} A_{i,1}(\eta) & A_{i,2}(\eta) \\ \hline A_{i,3}(\eta) & A_{i,4}(\eta) \end{array}\right)$$

where $A_{i,1}(\eta)$ is $m \times m$, $A_{i,2}(\eta), A_{i,3}(\eta)^T$ are $m \times k$ and $A_{i,4}(\eta)$ is $k \times k$. Let

$$B_1(\eta) = \begin{pmatrix} \mathbb{I}_1(\eta)_{i,1} & \cdots & \mathbb{I}_k(\eta)_{i,1} \\ \vdots & \cdots & \vdots \\ \mathbb{I}_1(\eta)_{i,m} & \cdots & \mathbb{I}_k(\eta)_{i,m} \end{pmatrix} \qquad B_2(\eta) = \begin{pmatrix} \mathbb{III}_1(\eta)_{i,1} & \cdots & \mathbb{III}_1(\eta)_{i,k} \\ \vdots & \cdots & \vdots \\ \mathbb{III}_k(\eta)_{i,1} & \cdots & \mathbb{III}_k(\eta)_{i,k} \end{pmatrix}$$

Corollary 6. *If $(\mathcal{U}, \sigma)$ is a Frenet chart with index set $\{\alpha_j\}_{j=1}^n$, then*

$$\begin{aligned} B_1(\eta) &= -A_{i,2}(\eta) G_3(\eta)^{-1} \\ B_2(\eta) &= \partial_{e_i} G_3(\eta) G_3(\eta)^{-1} + G_3(\eta) A_{i,4}(\eta) G_3(\eta)^{-1}. \end{aligned} \tag{2.29}$$

Proof. From the definition of $\mathbb{I}_i, \mathbb{III}_i$ and Lemma 2.3.2 we can compute

$$\partial_{e_i} v(\eta) = \left(\begin{array}{c|c} & -B_1(\eta) \\ \hline B_1(\eta)^T & B_2(\eta) \end{array}\right) v(\eta)$$

where the blank $m \times m$ matrix block is irrelevant, and $v(\eta)$ is defined in (2.28) Comparing this expression to (2.27) and using the definitions (2.24), (2.25) yields the result, after some simple block matrix computation. □

2.5.4 Blowing Up an Invariant Manifold to Study Local Transient Dynamics

Suppose that $(\mathcal{U}, \sigma)$ is a chart of a locally invariant codimension-k manifold $\mathcal{M}$ that satisfies our LOR assumptions. We will study the LOR flow generated by (2.4) to determine the dynamics near $\sigma(\mathcal{U})$ and will introduce what we term *LOR blow-up coordinates* to serve in this process.

First we let $\xi = r\bar{\xi}$ where $\left\|\bar{\xi}\right\| = 1$ such that $r^2 = \langle \xi, \xi \rangle$. Intuitively, r represents the Hausdorff distance of $\Psi(\eta, \xi)$ from the manifold $\mathcal{M}$ and $\bar{\xi}$ represents the "angle" of ξ relative to the manifold.

It is straightforward, using the fact that $\left\langle \bar{\xi}, \bar{\xi} \right\rangle = 1$ and hence $\left\langle \dot{\bar{\xi}}, \bar{\xi} \right\rangle = 0$, to compute that for $r > 0$,

$$\begin{aligned} \dot{r} &= \left\langle \dot{\xi}, \bar{\xi} \right\rangle, \\ r\dot{\bar{\xi}} &= \dot{\xi} - \left\langle \dot{\xi}, \bar{\xi} \right\rangle \bar{\xi}. \end{aligned} \tag{2.30}$$

System (2.30) becomes potentially problematic in the $r \to 0^+$ limit, which is precisely what we are interested in, in order to study dynamics local to $\mathcal{M}$. Note that if $\lim_{r \to 0^+} \dot{\xi}/r$ is well-defined then we can continuously extend the dynamics of (2.30) to $r = 0$. In our new coordinate scheme, the LOR equations (2.4) give us

$$\dot{\xi} = Nf(\eta, r\bar{\xi}) - K_\sigma(\eta, r\bar{\xi}) S_\sigma(\eta, r\bar{\xi})^{-1} Tf(\eta, r\bar{\xi}). \tag{2.31}$$

By definition, $K_\sigma(\eta, r\bar{\xi}) = rK_\sigma(\eta, \bar{\xi})$; hence, as $r \to 0^+$, the right hand side of (2.31) limits to 0. Therefore, we can compute the L'Hôpital type limit

$$\lim_{r \to 0^+} \frac{\dot{\xi}}{r} = \frac{d}{dr} \dot{\xi} \bigg|_{r=0} = D_\xi Nf(\eta, 0)\bar{\xi} - K_\sigma(\eta, \bar{\xi}) S_\sigma(\eta, 0)^{-1} Tf(\eta, 0) =: g(\eta, \bar{\xi}) \tag{2.32}$$

so that from (2.31), (2.32), and $\xi = r\bar{\xi}$, we have

$$\begin{aligned} \dot{\eta} &= S_\sigma(\eta, 0)^{-1} Tf(\eta, 0) + \mathcal{O}(r) \\ \dot{\bar{\xi}} &= g(\eta, \bar{\xi}) - \left\langle g(\eta, \bar{\xi}), \bar{\xi} \right\rangle \bar{\xi} + \mathcal{O}(r) \\ \dot{r} &= \left\langle g(\eta, \bar{\xi}), \bar{\xi} \right\rangle r + \mathcal{O}(r^2). \end{aligned} \tag{2.33}$$

Note that in the above representation, at leading order, the $\dot{\eta}$ equation depends only upon η and the $\dot{\bar{\xi}}$ equation depends only on $\eta, \bar{\xi}$. Therefore, we have decoupled the dynamics along the manifold (the η dynamics) from the angular dynamics relative to the manifold (the $\bar{\xi}$ dynamics) from the contraction/expansion dynamics (the r dynamics) for r sufficiently small. This non-trivial decoupling is possible because we have chosen to represent our dynamics in their natural frame.

We call the $(\eta, \bar{\xi}, r)$ coordinates the *LOR blow-up coordinates*, as the corresponding phase space has the form $\mathcal{U} \times S^{k-1} \times [0, \varepsilon)$, where $S^{k-1} = \{x \in \mathbb{R}^k | \, \|x\| = 1\}$ is the k-sphere and $0 < \varepsilon \ll 1$. This coordinate representation is effectively equivalent to performing geometric desingularization on the entirety of $\mathcal{M}$ [12].

The stability of $\mathcal{M}$ depends only on the sign of $\left\langle g(\eta, \bar{\xi}), \bar{\xi} \right\rangle$; $\mathcal{M}$ is stable in regions where $\left\langle g(\eta, \bar{\xi}), \bar{\xi} \right\rangle < 0$ and unstable where $\left\langle g(\eta, \bar{\xi}), \bar{\xi} \right\rangle > 0$.

To study the dynamics near the manifold, we first consider the η dynamics on $r = 0$, denoting by Φ_η the flow induced by $\dot{\eta} = S_\sigma(\eta, 0)^{-1} T f(\eta, 0)$. Next, we consider the $\bar{\xi}$ dynamics on $r = 0$, treating η as a non-autonomous forcing term. Denote the corresponding flow by $\Phi_{\bar{\xi}}$. Finally, we can approximate the r solution by

$$r(t) \approx r_0 \exp\left(\int_0^t \left\langle g(\eta(s), \bar{\xi}(s)), \bar{\xi}(s) \right\rangle \mathrm{d}s \right).$$

We will use these blow-up coordinates to aid our analysis in Chapters 4 and 5.

2.5.5 Fast-Slow Analysis

Consider now the $\mathscr{C}^r$ fast-slow system

$$\begin{aligned} \dot{x}_1 &= f_1(x_1, x_2; \varepsilon) \\ \dot{x}_2 &= \varepsilon f_2(x_1, x_2; \varepsilon) \end{aligned} \tag{2.34}$$

with $x_1 \in \mathbb{R}^k, x_2 \in \mathbb{R}^{n-k}$ and critical manifold $\mathcal{M}_0 := \{f_1(x_1, x_2; 0) = 0\}$. When $\varepsilon = 0$, $\mathcal{M}_0$ is a set of equilibria and hence is trivially invariant. Using the rescaled slow time variable

$\tau = \varepsilon t$, equation (2.34) becomes

$$\begin{aligned} \varepsilon x_1' &= f_1(x_1, x_2; \varepsilon) \\ x_2' &= f_2(x_1, x_2; \varepsilon) \end{aligned} \tag{2.35}$$

where $' = d/d\tau$. The $\varepsilon \to 0^+$ limit of system (2.35) specifies the slow timescale dynamics on $\mathcal{M}_0$. Suppose that $(\mathcal{U}, \sigma)$ parameterizes a chart of $\mathcal{M}_0$. If $\sigma(\mathcal{U})$ is normally hyperbolic, then Fenichel's Theorem [22] guarantees the existence of $\varepsilon^+ > 0$ for which there exists a chart $\tilde{\sigma} : \mathcal{U} \times [0, \varepsilon^+) \to \mathbb{R}^n$ such that: $\tilde{\sigma}$ parameterizes a locally-invariant, regular, codimension-k manifold $\mathcal{M}_\varepsilon$ for each $\varepsilon \in [0, \varepsilon^+)$, $\tilde{\sigma}(\eta; 0) = \sigma(\eta)$, and $\tilde{\sigma}(\eta; \varepsilon)$ is $\mathscr{C}^r$ $\mathcal{O}(\varepsilon)$-close to σ.

As long as our chosen normal frame is continuous in ε, we can perform the LOR transformation, treating ε as a parameter, which will yield dynamics of the form

$$\begin{aligned} \dot{\eta} &= \varepsilon S_{\hat{\sigma}}(\eta, \xi; \varepsilon)^{-1} \hat{T} f(\eta, \xi; \varepsilon), \\ \dot{\xi} &= N f(\eta, \xi; \varepsilon) - \varepsilon K_{\hat{\sigma}}(\eta, \xi; \varepsilon) S_{\hat{\sigma}}(\eta, \xi; \varepsilon)^{-1} \hat{T} f(\eta, \xi; \varepsilon) \end{aligned} \tag{2.36}$$

where $\varepsilon \hat{T} f(\eta, \xi; \varepsilon) = T f(\eta, \xi; \varepsilon)$, which remains well-defined as $T f(\eta, \xi; \varepsilon) = \mathcal{O}(\varepsilon)$. Hence the LOR equations are also fast-slow. Tranforming to LOR blow-up coordinates and expanding in ε yields, from equations (2.33) and (2.32),

$$\begin{aligned} \dot{\eta} &= \varepsilon S_{\hat{\sigma}}(\eta, 0; 0)^{-1} \hat{T} f(\eta, 0; 0) + \mathcal{O}(r, \varepsilon^2) \\ \dot{\bar{\xi}} &= B(\eta)\bar{\xi} - \left\langle B(\eta)\bar{\xi}, \bar{\xi} \right\rangle \bar{\xi} + \mathcal{O}(r, \varepsilon) \\ \dot{r} &= \left\langle B(\eta)\bar{\xi}, \bar{\xi} \right\rangle r + \mathcal{O}(r^2, \varepsilon) \end{aligned} \tag{2.37}$$

where $B(\eta) = D_\xi N f(\eta, 0; 0)$. Note that since $S_{\hat{\sigma}}, T f, N f$ are being evaluated on $\varepsilon = 0$, we use the *existence* of $\hat{\sigma}$ only to justify our derivation; the equations in (2.37) that we have obtained depend only on the critical manifold $\mathcal{M}_0$. Thus, system (2.37) gives a natural framework to study dynamics relative to a slow manifold $\mathcal{M}_\varepsilon$ that relates the dynamics relative to $\mathcal{M}_\varepsilon$ to the dynamics relative to $\mathcal{M}_0$.

Equation (2.37) is similar to the Fenichel Normal Form presented in [34]; the η coordinate plays the role of the slow dynamics defined on the rectified critical manifold, while the $(\bar{\xi}, r)$ coordinates track the fast variables as they approach or depart from the critical manifold.

The $\bar{\xi}$ coordinate allows us to anticipate the "angle" at which fast trajectories will approach $\mathcal{M}$; i.e. they are playing the role of the *fast fibration*, which is critical in technical Fenichel analysis [34, 68]. We conclude this computation by noting that it is unclear how, if at all, the ideas of fast-fibrations may be applied to general dynamical systems; the LOR blow-up coordinates are a natural contender for generalizing fast-slow type analysis to arbitrary invariant manifolds.

2.6 A Computational Example

In this final section, we present a long-form computational example of the LOR frame in action. We choose a well-known, fast-slow system for our analysis, the normal form for a folded-saddle node canard [61], which is given by

$$\begin{pmatrix} \dot{x} \\ \dot{y} \\ \dot{z} \end{pmatrix} = \begin{pmatrix} \varepsilon(by + cz) \\ \varepsilon a \\ x + z^2 \end{pmatrix} =: f(x, y, z; \varepsilon) \tag{2.38}$$

for parameters a, b, c as well as $0 < \varepsilon \ll 1$. In the $\varepsilon \to 0^+$ limit, the critical manifold $\mathcal{M}_0$, parameterized by $\sigma(\eta_1, \eta_2) = (-\eta_2^2, \eta_1, \eta_2)$, becomes a surface of critical points. Let $\mathcal{U}_L = \{(\eta_1, \eta_2) | \eta_2 < 0\}, \mathcal{U}_R = \{(\eta_1, \eta_2) | \eta_2 > 0\}, \mathcal{U}_F = \{(\eta_1, \eta_2) | \eta_2 = 0\}$, then $\sigma(\mathcal{U}_L)$ is a sheet of normally hyperbolic, stable fixed points in the $\varepsilon = 0$ system, while $\sigma(\mathcal{U}_R)$ is a sheet of normally hyperbolic, unstable fixed points. The set $\sigma(\mathcal{U}_F)$, called the fold, is a line of nilpotent fixed points.

Fenichel theory guarantees, for $\varepsilon > 0$ but sufficiently small, the existence of charts $\sigma_{L,\varepsilon}, \sigma_{R,\varepsilon}$ such that $\sigma_{i,\varepsilon}(\mathcal{U}_i)$ is a locally-invariant manifold, $\|\sigma(\eta) - \sigma_{i,\varepsilon}(\eta)\| = \mathcal{O}(\varepsilon)$ for $\eta \in \mathcal{U}_i$, and $\sigma_{i,\varepsilon}(\mathcal{U}_i)$ has the same stability properties as $\sigma(U_i)$ for $i \in \{L, R\}$.

The most intriguing feature of (2.38) is the existence of trajectories beginning in $\sigma_{L,\varepsilon}(\mathcal{U}_L)$ that cross into $\sigma_{R,\varepsilon}(\mathcal{U}_R)$; these trajectories are referred to as canards and play an organizing role in various forms of fast-slow dynamics including mixed-mode oscillations.

The standard technique for identifying canards is to perform geometric desingularization in a neighborhood of the origin of system (2.38) and track carefully chosen trajectories across the multiple "charts" of the desingularized variables. Here, we present an approach based on LOR techniques.

To begin, we note that

$$\partial_1 \sigma(\eta_1, \eta_2) = (0, 1, 0)$$
$$\partial_2 \sigma(\eta_1, \eta_2) = (-2\eta_2, 0, 1)$$

hence

$$N\sigma(\eta) = \frac{(2\eta_1, 0, 1)}{\sqrt{4\eta_1^2 + 1}}$$

forms a normal frame to σ. We compute

$$\mathrm{I}(\eta) = \begin{pmatrix} 4\eta_1^2 + 1 & 0 \\ 0 & 1 \end{pmatrix}, \qquad \mathrm{II}(\eta) = \begin{pmatrix} \frac{2}{\sqrt{4\eta_1^2+1}} & 0 \\ 0 & 0 \end{pmatrix},$$

and therefore

$$S_\sigma(\eta, \xi) = \begin{pmatrix} \alpha(\eta)^2 + \frac{2\xi}{\alpha(\eta)} & 0 \\ 0 & 1 \end{pmatrix}$$

where $\alpha(\eta) = \sqrt{4\eta_1^2 + 1}$. Note that $S_\sigma(\eta, \xi)$ is invertible as long as $\xi \neq -\alpha(\eta)^3/2$. Thus,

$$P_\eta = \left\{ \xi \in \mathbb{R} \,\middle|\, \xi > -\frac{\alpha(\eta)^3}{2} \right\}.$$

Note that the normal exchange operator is zero, as demonstrated in Proposition 1.

We find the LOR dynamics have the form

$$\dot{\eta}_1 = \sum_{i=0}^{2} p_i(\eta)\xi^i \tag{2.39}$$

$$\dot{\eta}_2 = \varepsilon a \tag{2.40}$$

$$\dot{\xi} = \sum_{i=0}^{2} q_i(\eta)\xi^i \tag{2.41}$$

where p_i, q_i are rational functions of η_1, η_2. Interestingly, it turns out that $q_0(\eta) = \mathcal{O}(\varepsilon)$, so that $\dot{\xi} = \mathcal{O}(\varepsilon, \|\xi\|)$.

We can solve $\dot{\xi} = 0$ explicitly to obtain two solution manifolds $\xi = \Xi_{\pm}(\eta)$. We find that $\Xi_{+}(\eta)$ is $\mathcal{O}(\eta_1^{-3})$ near $\eta_1 = 0$ while $\Xi_{-}(\eta)$ takes the form

$$\Xi_{-}(\eta) = -\frac{b}{c}\eta_2 + \frac{2b}{c^2\varepsilon}\eta_1\eta_2 + \mathcal{O}(\eta_1^2).$$

Thus, for η_1 sufficiently small, the correction $\Xi(\eta)$ is given by $\Xi(\eta) = \Xi_{-}(\eta)$.

In this system, the correction plays a central role in organizing the dynamics near $\{\xi = 0\}$ and we can use it to easily build a simple trapping region and demonstrate the existence of a perturbed slow manifold. The trajectories of interest in this system begin in $\{\eta_1 < 0, \eta_2 < 0\}$ and evolve towards the fold $\{\eta_2 = 0\}$. We find that

$$\dot{\xi}|_{\xi=0} = \varepsilon\frac{\mu\eta_1 - 2(\mu+1)\eta_2}{2\alpha(\eta)}$$

and note that if

$$\eta_2 < 0 \text{ and } \frac{\eta_1}{\eta_2} < \frac{2(\mu+1)}{\mu}$$

then $\dot{\xi}|_{\xi=0} > 0$, for this reason, we define a first "funnel"

$$\mathcal{F}_1 = \left\{ \eta \in \mathbb{R}^2 \,\middle|\, \eta_2 < 0, \frac{\eta_1}{\eta_2} < \frac{2(\mu+1)}{\mu} \right\}.$$

If $(\eta_0, \xi_0) \in \mathcal{F}_1 \times \mathbb{R}^+$ then $\xi(t) > 0$ for as long as $\eta(t) \in \mathcal{F}_1$. By refining $\mathcal{F}_1$ we can also bound $\xi(t)$ from above.

Proposition 3. *Let*

$$\mathcal{F} = \{(\eta_1, \eta_2) \in \mathcal{F}_1 \,|s(\eta) < 0\}$$

where $s(\eta)$ is defined by

$$s(\eta) = \frac{\left(-16\eta_2^4 - \mu^2\left(2\eta_2 - \eta_1\right)\left(8\eta_2^2\left(-\eta_2 + \eta_1\right) + \eta_1\right) - 2\left(12\alpha^4 + 1\right)\eta_2\mu\left(-2\eta_2 + \eta_1\right)\right)}{16\eta_2^3\left(4\eta_2^2 + 1\right)^{3/2}} + \mathcal{O}(\varepsilon). \tag{2.42}$$

If $\eta(t) \in \mathcal{F}$ then $0 < \xi(t) < \Xi_{-} \circ \eta(t)$ for $\varepsilon > 0$ sufficiently small. Furthermore, if $\eta_0 \in \mathcal{F}$ and there exists a $T > 0$ such that $\eta(T) \notin \mathcal{F}$ then there exists $0 < t_F < T$ such that $\eta_2(t_F) = 0$.

Proof. If $\xi_0 < \Xi_-(\eta_0)$ and $\eta_0 \in \mathcal{F}$ then we need only satisfy $\dot{\xi}(t) < \left\langle \nabla \Xi_- \circ \eta(t), \dot{\eta(t)} \right\rangle$ for $\eta(t) \in \mathcal{F}$ and $\varepsilon > 0$ sufficiently small. An order expansion of $\dot{\xi}|_{\xi=\Xi_-(\eta)} - \left\langle \nabla \Xi_-(\eta), \dot{\eta}|_{\xi=\Xi_-(\eta)} \right\rangle$ at $\varepsilon = 0$ yields the expression on the right hand side of equation (2.42), which we require to be negative, yielding the region $\mathcal{F}$. We find that $\Xi_- \circ \eta(t)$ is a supersolution of $\dot{\xi}$ exactly when $\eta(t) \in \mathcal{F}$. Hence the first part of the result follows.

The second claim follows from similar subsolution arguments. For $\varepsilon > 0$ sufficiently small, the boundary of $\mathcal{F}_1$, given by $\eta_1 + 8\eta_1\eta_2^2 - 8\eta_2^3 = 0$, is impassible when $\eta_2 < 0$. Thus any trajectories that escape $\mathcal{F} \times \mathbb{R}^+$ must cross the fold curve $\{\eta_2 = 0\}$. □

Two features of this result bear mentioning. First, we have demonstrated that any trajectories that escape from a neighborhood of the stable critical manifold must do so through the fold. Second, recalling that $\Xi_-(\eta) = \mathcal{O}(\varepsilon)$, we have verified a weak version Fenichel's Theorem for system (2.38). The organizational role of the correction is demonstated in the left half of Fig. 1.

By performing an additional transformation of our system, we can extract canard-type solutions, which pass across the fold $\{\eta_2 = 0\}$, in a very natural way. We have demonstrated that the correction manifold plays a strong role in organizing the flow near the critical manifold, so it is natural to use the correction as a base manifold for another LOR transformation. That is, we define

$$\hat{\sigma}(\hat{\eta}) = \sigma(\hat{\eta}) + \Xi_-(\hat{\eta}) N\sigma(\hat{\eta}),$$

which is a manifold embedded in our original space that satisfies all of our LOR assumptions, such that we can compute the LOR dynamics relative to $\hat{\sigma}$. We suppress the computations for brevity; however, they follow exactly along the lines of the previous computations, and can be executed extremely quickly by symbolic computation software (e.g., Mathematica, Maple, Julia). Note that in this trasformation, $\hat{\eta}$ is geometrically equivalent to η; that is, $\hat{\eta_1}$ still corresponds to x in the original system, just as $\hat{\eta}_2$ corresponds to y, but we need the $\hat{\eta}$ notation to represent the change from ξ to $\hat{\xi}$. We could iterate this process to better approximate the canard solution, however only the ε terms in the remainder term will improve.

The lowest order terms of the resultant system are given by

$$\dot{\hat{\eta}}_1 = \varepsilon + \mathcal{O}(\varepsilon^2, \xi) \tag{2.43}$$

$$\dot{\hat{\eta}}_2 = \frac{\varepsilon}{4}\left(2 + \left(2 - \frac{\hat{\eta}_1}{\hat{\eta}_2}\right)\mu\right) + \mathcal{O}(\varepsilon^2, \xi) \tag{2.44}$$

$$\dot{\hat{\xi}} = 2\hat{\eta}_2\hat{\xi} + \mathcal{O}(\varepsilon\hat{\xi}, \varepsilon^2). \tag{2.45}$$

Note that $\{\hat{\xi} = 0\}$ is invariant to $\mathcal{O}(\varepsilon^2)$, which is an improvement to the previous system; trajectories starting on $\{\hat{\xi} = 0\}$ must spend an $\mathcal{O}(\varepsilon^{-2})$ amount of time near $\{\hat{\xi} = 0\}$ before escaping.

We remain interested in trajectories beginning in $\{\hat{\eta}_2 < 0\}$ that cross the fold curve. If we numerically plot the $\hat{\eta}$ dynamics on $\{\hat{\xi} = 0\}$, we notice that there is a single trajectory that plays an outsized role in organizing the $\hat{\eta}$ phase plane.

It is easily verified that $\gamma(t) = (\varepsilon t, \varepsilon\mu t/2, 0)$ solves (2.43) to $\mathcal{O}(\varepsilon^2)$, and this is, in fact, the "central" trajectory of the approximate dynamics. We also note that γ is the only trajectory that remains well-defined as it crosses the fold, through a L'Hopital type limit. Finally, we note that $\gamma(t)$ approximate solution is constrained to lie in a plane, as its trace in $\hat{\eta}$ is a line; stated equivalently, $\gamma(t)$ has everywhere vanishing curvature.

Previous work has established the zero curvature set plays an organizational role in planar systems [1, 24, 25], we use the LOR frame to study where the zero curvature set is invariant. One advantage of this definition, is that it generalizes easily to arbirary dimension. In $\mathbb{R}^n$ we define a river to be a Frenet trajectory $\Gamma(t)$ whose Frenet curvature $\kappa_{n-2}(t)$ vanishes to second order; that is, if there exists t^* such that

$$\kappa_{n-2}(t^*) = \dot{\kappa}_{n-2}(t^*) = 0$$

then $\Gamma(t)$ is a river, and we call $\Gamma(t^*)$ a confluence [45].

Our analysis suggests that $\gamma(t)$ is an organizing trajectory that lies in a plane and thus has identically zero Frenet curvature. This result suggests a strong connection between canards and rivers. In fact, if we study the zero curvature locus of the original system (2.38), we find that there are seven trajectories that have identically zero curvature and hence are rivers by

our definition. The most interesting of these, in terms of apparent correspondence to $\gamma(t)$, can be given by

$$\Gamma(z) = \left(-z^2 + \frac{\varepsilon\mu}{2}, \frac{2z}{\mu}, z \right)$$

and is invariant, such that it can be reparameterized as a solution. For $z < 0$, Γ lies near the stable branch of the critical manifold, at $z = 0$ it passes near the fold, and for $z > 0$ it remains $\mathcal{O}(\varepsilon)$ close to the unstable critical manifold. We examine this surprising connection in Chapter 5.

2.7 Figures and Tables

Notation	Name	Short Description
$\mathcal{M}$	LOR base-manifold	m-manifold (co-dimension k) embedded in $\mathbb{R}^n$ of dynamical interest
$(\mathcal{U}, \sigma)$	chart	$\sigma : \mathcal{U} \subseteq \mathbb{R}^m \to \mathbb{R}^n$ parameterizes a patch of $\mathcal{M}$
$\partial_1\sigma(\eta), \cdots, \partial_m\sigma(\eta)$	tangent basis	basis of the tangent space at $\sigma(\eta)$
$N_1\sigma(\eta), \cdots, N_k\sigma(\eta)$	normal basis	orthonormal basis of the normal space at $\sigma(\eta)$
$\mathrm{I}(\eta)$	first fundamental form	defined in (2.5), defines the Riemann metric
$\mathrm{I\!I}_1(\eta), \cdots, \mathrm{I\!I}_k(\eta)$	second fundamental forms	defined in (2.7), measures deformation of the tangent space in the normal directions
$S_\sigma(\eta, \xi)$	tangent exchange operator	defined in (2.8), pulls vectors into $T_\eta\mathcal{U}$.
$K_\sigma(\eta, \xi)$	normal exchange operator	defined in (2.14), pulls vectors into $T_\eta\mathcal{U}^\perp$
$Tf(\eta, \xi)$	tangential dynamics	defined in (2.3), the vector field f projected into the tangent space
$Nf(\eta, \xi)$	normal dynamics	defined in (2.3), the vector field f projected into the normal space

Table 1: A Cheat Sheet of LOR Terminology

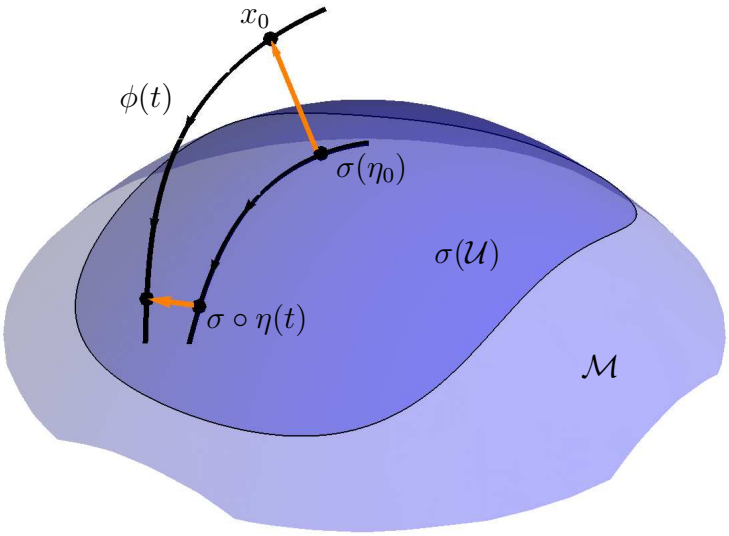

Figure 1: The geometric setup for Local Orthogonal Rectification: We consider an inital condition x_0 near a given manifold, and decompose the trajectory through x_0, denoted by ϕ, into a curve on the manifold and a curve in the normal bundle to the manifold.

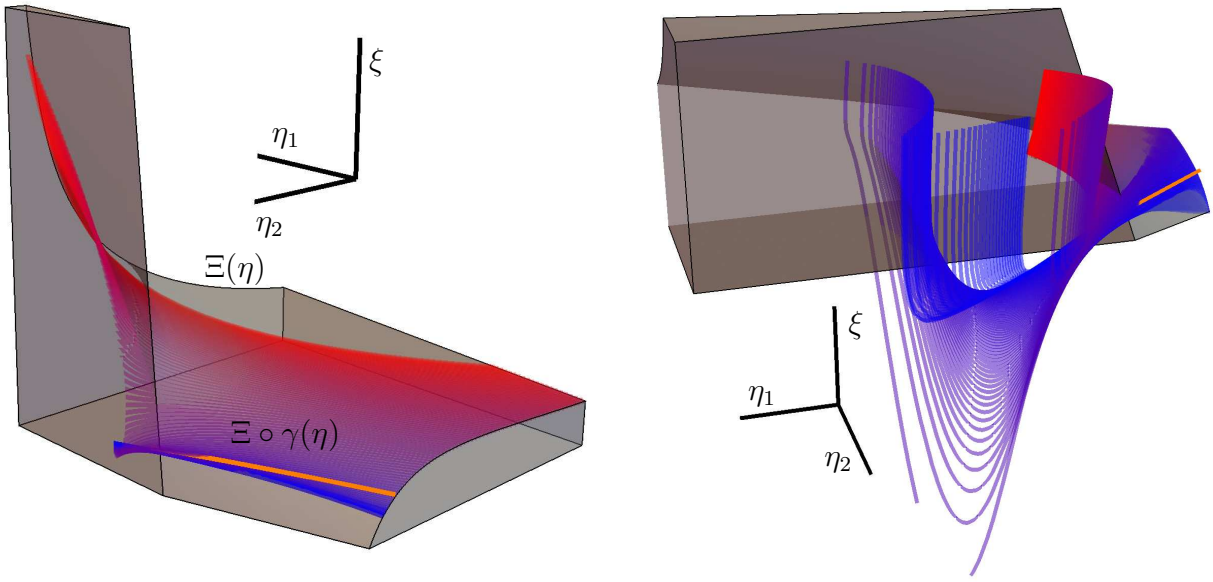

Figure 2: The dynamics near the critical manifold. (Left) The trapping region detailed in Prop. 3, between $\{\xi = 0\}$ and the correction Ξ. Note how trajectories with $\eta(t) \in \mathcal{F}$ cannot escape, as they are bounded above by Ξ. Our approximate canard solution $\Xi \circ \gamma(\eta)$ is shown in orange. The blue and red curves are trajectories, red curves have initial conditions further from the fold. (Right) The full trapping region, where the $\mathcal{O}(\varepsilon^2)$ term of (2.42) is negative. Note the twisting of orbits as they escape from the influence of the correction.

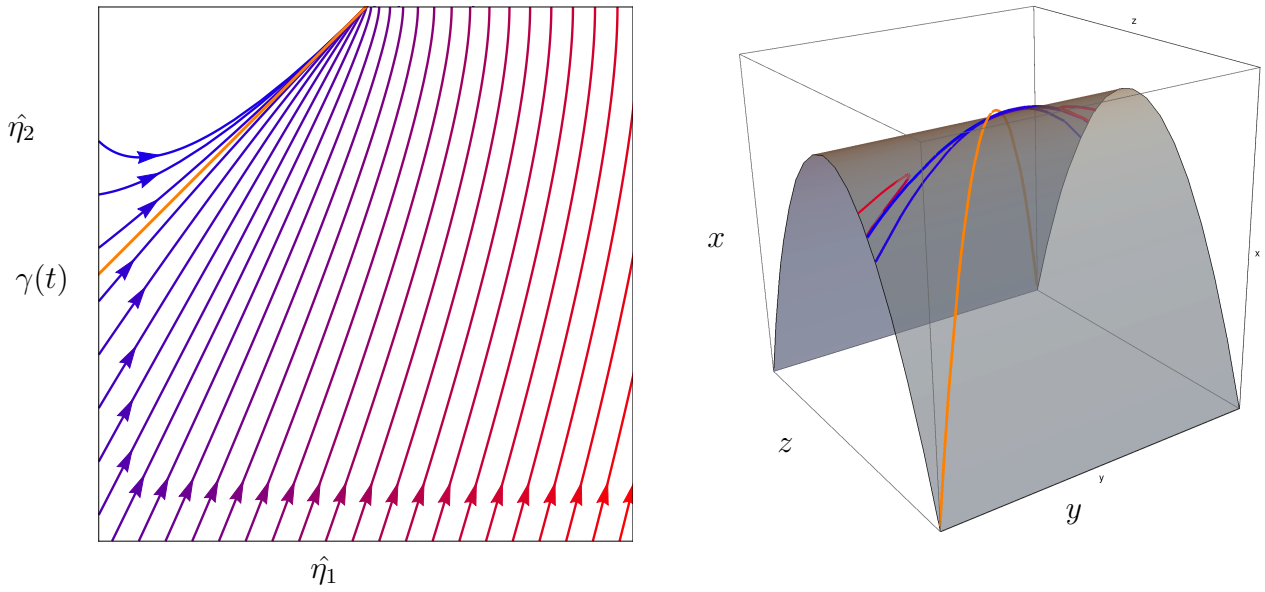

Figure 3: Dynamics near the canard solution. (Left) The dynamics on $\{\hat{\xi} = 0\}$ of system (2.43). Note how the approximate trajectories organize around the orange curve, called γ in the text. (Right) A plot of the rivers of (2.38), three of which cross the fold of the critical manifold. The orange curve, $\gamma(z)$, is indistinguishable from the identified approximate canard solution $\Psi_2(\gamma(t), 0)$.

3.0 Rivers in the Plane

The material in this chapter has been published in SIADS as "A New Frame for an Old (Phase) Portrait: Finding Rivers and Other Flow Features in the Plane" and was co-authored by Jonathan E. Rubin.

3.1 Motivation

A fundamental problem in dynamical systems is to identify the structures in phase space that organize the trajectories generated by a flow. Methods to achieve this identification often focus on attractors defined asymptotically in time, as well as on separatrices between attractor basins formed by stable manifolds of saddle points, which are themselves defined in terms of their asymptotic properties. In multiple-timescale systems, classical methods due to Fenichel [34] provide a link from normally hyperbolic critical manifolds that act as attractors for fast dynamics to nearby invariant structures, or slow manifolds, that exist for and organize trajectories of the full flow when the separation between timescales is sufficiently strong. These methods ensure a closeness between slow manifolds and critical manifolds but do not otherwise guide the process of precisely identifying the locations of slow manifolds, and they do not indicate how strong of a timescale separation qualifies as "sufficiently strong" for any particular system. Other analytical methods or frameworks to characterize structures that may exert a finite-time organizing influence or even an asymptotic time influence in the absence of a strong timescale separation [13] are rather limited, particularly in terms of pinpointing the locations of these structures. Such structures may include periodic orbits, for example, or rivers, which are orbits that attract nearby trajectories over some finite time window. Rivers have been identified by inspection in various systems [6, 62], but have never been methodically analyzed or precisely defined outside of polynomial vector fields on $\mathbb{R}^2$ that satisfy a particular algebraic homogeneity condition [16, 15].

In this chapter, we introduce a general approach to locating trajectories with particu-

lar properties within a given flow generated by a system of ordinary differential equations (ODEs). The idea of this approach is to start with a curve in phase space as an initial guess for such a trajectory and then use a coordinate transformation that we call a *local orthogonal rectification* (LOR), based on the well-known Frenet frame [41, 7], to generate a frame in which a correction to the guess can easily be derived. Importantly, the initial guess need not be particularly close to the sought-after trajectory. It should simply be tailored somewhat to the property of interest; for example, the guess should consist of a simple closed curve if the goal is to find a periodic orbit.

The LOR provides a new system of ODEs that can be analyzed to supply the desired correction and thus locate an actual trajectory of the original flow with the property of interest. We apply the LOR approach to define rivers in a way that relates attractiveness, invariance, and the curvature of trajectories, and to locate them, as well as periodic orbits and extensions of invariant manifolds away from the singular, separated-timescale limit, in planar dynamical systems. Interestingly, the LOR yields a differentiable surjective mapping that provides a submersion of the flow in the LOR frame into the original phase space; in the river case, we therefore observe that it takes a submersion to find a river.

The remainder of this chapter is organized as follows. We define a notion of near-invariance that proves useful for analyzing the flow within the LOR frame, and we extend the LOR frame to the study of asymptotic dynamics defined in the long-time limit. We will present an example of this asymptotic analysis in the context of fast-slow analysis. In Section 3.3, we plunge into *rivers*. We define quantities that are specifically useful for that study, including the *zero-curvature locus* that has been used by some previous authors [1, 26], and provide precise definitions for rivers and their points of origin, which we call *confluences* for reasons that we explain. We argue that the presented definitions are particularly useful and illustrate these ideas in examples. Moreover, we consider bifurcation-like events in which confluences interact as well as asymptotic rivers, which can separate regions of phase space on which trajectories exhibit distinct transient dynamics as they approach a common attractor. The chapter finishes with a summary of our conclusions and a discussion of some natural future directions, of which there are many.

3.2 Nearly Invariant Curves

We will use curves in the plane, $\gamma : (\delta_1, \delta_2) \to \Omega$, as LOR basecurves. We begin by presenting how the near invariance measure, described in section 2.5.2 can be used to study asymptotic approach.

3.2.1 Nearly Invariant Curves

Consider a curve $\gamma : (\delta_1, \delta_2) \to \Omega$, we would like to have a quantitative measure of how close γ is to being an actual solution along its domain. The ξ component of the LOR dynamics in the case of a curve in the plane is given by

$$\dot{\xi} = \langle f \circ \Psi_\gamma(\eta, \xi), N\gamma(\eta) \rangle$$

and consider the ξ nullcline, which we denote by

$$C = \{(\eta, \xi) \in \mathcal{U}_\gamma | \, \langle f \circ \Psi_\gamma(\eta, \xi), N\gamma(\eta) \rangle = 0\}. \tag{3.1}$$

Hence $\mu_\gamma : (\delta_1, \delta_2) \to \mathbb{R}^+$, defined in (2.22) can be used to describe curves which are *nearly* invariant.

Immediately, we note that $\mu_\gamma(\delta_1, \delta_2) = 0$ if and only if $\gamma(\delta_1, \delta_2)$ is invariant. Note also that $\Xi_\gamma(\eta)$ is simply the branch of $\{\dot{\xi} = 0\}$ that is closest to $\{\xi = 0\}$; see Figure 4. With this new measurement in hand, we can define a weak notion of invariance, which we call near invariance.

Definition 3.2.1. Suppose that $\gamma : (\delta_1, \delta_2) \to \Omega$ is a simple, regular $\mathscr{C}^2$ curve and $f : \Omega \to \mathbb{R}^2$ is a $\mathscr{C}^1$ vector field. We say that γ is ε-nearly invariant on $\{\eta_1, \eta_2\} \subseteq (\delta_1, \delta_2)$ if

$$\mu_\gamma(\eta) \leq \varepsilon \qquad \text{for all } \eta \in \{\eta_1, \eta_2\},$$

where $\{\eta_1, \eta_2\}$ represents any type of interval (open, half-closed, etc.).

3.2.2 LOR Asymptotics

The LOR frame extends naturally and usefully for studying asymptotic dynamics. This analysis is based on a fairly general lemma that we prove, using the LOR coordinates, which relies on $\Xi_\gamma(\eta)$ and hence on near invariance. Note that $\Xi_\gamma(\eta)$ may be positive or negatve; we use $[0, \Xi_\gamma(\eta)]$ to refer to both cases in the following statement.

Lemma 3.2.2. *Suppose that $f : \Omega \to \mathbb{R}^2$ is $\mathscr{C}^1$ and $\gamma : [0, \infty) \to \Omega$ is a regular $\mathscr{C}^2$ curve such that*

$$\lim_{\eta\to\infty} \|\gamma(\eta)\| = \infty \text{ and } \lim_{\eta\to\infty} \frac{1}{\kappa_\gamma(\eta)} \neq 0.$$

Additionally, suppose that the correction to γ, $\Xi_\gamma(\eta)$, is $\mathscr{C}^1$ and $\Xi_\gamma(\eta) \to 0$ monotonically as $\eta \to \infty$ with

$$\langle f \circ \Psi_\gamma(\eta, \xi), T\gamma(\eta)\rangle > 0 \qquad \text{for all } \eta \geq 0, \xi \in [0, \Xi_\gamma(\eta)].$$

If $\langle f \circ \Psi(0, 0), N\gamma(0)\rangle$ and $\Xi_\gamma(0)$ have opposite signs, then there is a trajectory $\phi(t) = \Psi_\gamma(\eta(t), \xi(t))$ such that

$$\lim_{t\to\infty} d_H(\phi(t), \gamma) \searrow 0.$$

where d_H is the Hausdorff distance. Furthermore, we can choose ϕ such that $(\eta(0), \xi(0)) = (0, \xi^*)$ for $\xi^* \in [0, \Xi_\gamma(0)]$ and we have that $\xi(t) \in [0, \Xi_\gamma(\eta(t))]$ for $t > 0$.

Proof. As $\Xi_\gamma(\eta) \to 0$ monotonically, either $\Xi_\gamma(\eta) > 0, \Xi'_\gamma(\eta) < 0$ or $\Xi_\gamma(\eta) < 0, \Xi'_\gamma(\eta) > 0$. We will treat the first case here; the second case follows in the same manner. In what follows, we will use (η, ξ) to denote the coordinates in the LOR frame with basecurve γ.

Define the following sets:

$$\begin{aligned} W &= \{(\eta, \xi) | \eta \geq 0, 0 \leq \xi \leq \Xi_\gamma(\eta)\}, \\ W_+ &= \{(\eta, \Xi_\gamma(\eta)) | \eta \geq 0\} \cup \{(\eta, 0) | \eta \geq 0\}, \\ W_0 &= \{(0, \xi) | 0 \leq \xi \leq \Xi_\gamma(0)\}. \end{aligned} \tag{3.2}$$

We will show that there must be some trajectory ϕ with $\phi(0) \in W_0$ such that $\phi(t) \subseteq W$ for all $t \geq 0$. To do so we will use Wazewski's Lemma. Denote the flow induced by $(\dot\eta, \dot\xi) = \mathscr{L}_\gamma f(\eta, \xi)$ by $\Phi(x, t)$. We define $W_i = \{x \in W | \forall t_1 > 0, \exists t_2 \in (0, t_1) : \Phi(x, t_2) \notin W\}, W_e = \{x \in W | \exists t > 0 : \Phi(x, t) \notin W\}$ and we call W_i, W_e the immediate and eventual

exit sets of W, respectively. Then Wazewski's Lemma can be stated as follows; see [11] for a proof of a more general version of this result.

Wazewski's Lemma: If W_i and W are closed, then W_e is a strong deformation retract of W_i.

To clarify, X is a strong deformation retract of $A \subseteq X$ if there exists a homotopy $h : X \times [0,1] \to X$ such that for $x \in X, a \in A, t \in [0,1]$ we have $h(x,0) = x, h(x,1) \in A$, and $h(a,t) = a$. That is, h is a homotopy between X, A that restricts to the identity on $X \times \{0\}$ and on $A \times [0,1]$. For our purposes we will only need the following fact: the number of path connected components of a closed set is preserved under homotopy.

Returning to our problem, we see that $W_i = W_+$ and that W, W_+ are closed sets; therefore, W_i, W_e are homotopic and hence have the same number of path connected components. Suppose that $W = W_e$; that is, all trajectories beginning in W leave W eventually. Then W_e is path connected and hence W_+ is path connected, which is false. Therefore, $W \neq W_e$, and there is at least one trajectory $\phi(t) = (\eta(t), \xi(t))$ that has $\phi(t) \subseteq W$ for all $t \geq 0$. We note that $\dot{\eta} > 0$ on W and hence $\eta(t) \nearrow \infty$ (see Figure 5). Therefore, our assumptions that $\dot{\xi} < 0$ on $W \setminus W_i$, $0 \leq \xi(t) \leq \Xi_\gamma(\eta(t))$, and $\Xi_\gamma(\eta) \to 0$ monotonically as $\eta \to \infty$ imply that $\xi(t) \searrow 0$ as $\eta \to \infty$.

Furthermore, reversing time, we can flow ϕ backwards in time until $\eta(t) = 0$. Hence, we can take $\phi(0) = (0, \xi^*)$ for some $\xi^* \in [0, \Xi_\gamma(0)]$. □

We remark that if we change the parameterization of γ in the above result such that $\gamma : (-\infty, 0) \to \Omega$, then we can reparameterize to meet the conditions of Lemma 3.2.2, hence the parameterization of γ is immaterial.

3.2.3 Tracking Slow Manifolds in the LOR Frame

There is already a substantial body of work dealing with identifying invariant manifolds in multiple timescale systems. The most powerful and most cited result is Fenichel's theorem [34], which states that given a $\mathscr{C}^r, r \geq 1$ system $\dot{x} = f(x,y), \dot{y} = \epsilon g(x,y)$, with a $\mathscr{C}^r$ connected *critical manifold* defined by $\mathcal{M}_0 \subset \{(x,y) : f(x,y) = 0\}$, such that the matrix $D_x f(x,y)$

is normally hyperbolic (i.e., has no eigenvalues of zero real part) for all $(x, y) \in \mathcal{M}_0$, there exists, *for* $\epsilon > 0$ *sufficiently small*, a perturbed $\mathscr{C}^r$ *slow manifold* $\mathcal{M}_\epsilon$ that is invariant, is diffeomorphic to $\mathcal{M}_0$, and lies $\mathscr{C}^1\mathcal{O}(\epsilon)$-close to $\mathcal{M}_0$.

Despite its significant generality and utility, Fenichel's Theorem does not provide any a priori indication of what values of ε qualify as sufficiently small. This constrains the applicability of Fenichel's theorem in concrete settings, as it is difficult to determine whether a particular parameter set fits the bill. Using our concept of near invariance, we will illustrate a way to derive information about the range of ε over which a family of slow manifolds extends and can be tracked.

We will consider the FitzHugh-Nagumo system given by

$$\begin{aligned} \dot{v} &= v - \frac{v^3}{3} - w - I \\ \dot{w} &= \varepsilon(v + a - bw), \end{aligned} \tag{3.3}$$

where a, b, ε, I are positive constants, traditionally we require that $0 < \varepsilon \ll 1$. In the singular limit, $\varepsilon \to 0$, we see that the parameterization of the critical manifold given by $\gamma(\eta) = (\eta, \eta - \eta^3/3 - I)$ is an invariant curve, as it is a curve of fixed points. This curve is normally hyperbolic everywhere except for $\eta = \pm 1$; therefore, Fenichel's theorem tells us that there will be invariant perturbations to γ away from $\eta = \pm 1$ for ε sufficiently small.

If we take our LOR basecurve to be the critical manifold, then

$$\begin{aligned} \|\gamma'(\eta)\| &= \sqrt{1 + (1 - \eta^2)^2} & T\gamma(\eta) &= \frac{(1, 1 - \eta^2)}{\|\gamma'(\eta)\|} \\ N\gamma(\eta) &= \frac{(\eta^2 - 1, 1)}{\|\gamma'(\eta)\|} & \kappa_\gamma(\eta) &= \frac{-2\eta}{\|\gamma'(\eta)\|^3}. \end{aligned} \tag{3.4}$$

We will not display the full details of the LOR equations, but we claim that they are simple to compute and take the form

$$\begin{aligned} \sigma(\eta, \xi)\dot{\eta} &= \sum_{i=0}^{3} \alpha_i(\eta)\xi^i =: f_\eta(\eta, \xi) \\ \dot{\xi} &= \sum_{i=0}^{3} \beta_i(\eta)\xi^i =: f_\xi(\eta, \xi) \end{aligned} \tag{3.5}$$

where $\sigma(\eta,\xi) = \|\gamma'(\eta)\|\,(1-\xi\kappa_\gamma(\eta))$ and

$$\alpha_0(\eta) = -\frac{\varepsilon(\eta^2-1)(3a-3(b-1)\eta+b\eta^3+3bI)}{3\,\|\gamma'(\eta)\|} \qquad \beta_0(\eta) = \frac{\varepsilon(3a-(3b-1)\eta+b\eta^3+3bI)}{3\,\|\gamma'(\eta)\|}$$

$$\alpha_1(\eta) = -1-\varepsilon+\frac{\varepsilon(1+b(\eta^2-1))}{\|\gamma'(\eta)\|^2} \qquad \beta_1(\eta) = 1-\eta^2+\frac{\varepsilon(\eta^2-1-b)}{\|\gamma'(\eta)\|^2}$$

$$\alpha_2(\eta) = -\frac{\eta(\eta^2-1)^2}{\|\gamma'(\eta)\|^3} \qquad \beta_2(\eta) = -\frac{\eta(\eta^2-1)^3}{\|\gamma'(\eta)\|^3}$$

$$\alpha_3(\eta) = -\frac{(\eta^2-1)^3}{3\,\|\gamma'(\eta)\|^4} \qquad \beta_3(\eta) = -\frac{(\eta^2-1)^4}{3\,\|\gamma'(\eta)\|^4}..$$

Figure 6 shows us that the ξ-nullcline plays a strong role in organizing trajectories in the region $\{|\eta|>1\}$. We will focus our analysis on showing how $\{\dot{\xi}=0\}$ informs us about how the critical manifold perturbs on $\{\eta<-1\}$.

Proposition 4. *Given $\varepsilon, b>0$, there is a trajectory $\phi(t)$ of (3.3) such that $d_H(\phi(t),\gamma)\searrow 0$ as $t\to-\infty$.*

Proof. From (3.5), the ξ-nullcline has the form

$$\sum_{i=0}^{3}\beta_i(\eta)\xi^i = 0, \tag{3.6}$$

which has three computable root functions $\xi_j(\eta):\mathbb{R}\to\mathbb{C}$, $j\in\{1,2,3\}$. Furthermore, we can determine the number of real solutions at each value of η by computing the discriminant of the cubic polynomial (3.6), which we will denote $\Delta_\xi(\eta,\varepsilon)$. Employing a symbolic computation program, we find that

$$\Delta_\xi(\eta,\varepsilon) = \frac{(\eta^2-1)^4}{3\,\|\gamma'(\eta)\|^{10}}\left(-\eta^{18}+\varepsilon p(\eta,\varepsilon)\right)$$

where $p(\eta,\varepsilon)$ is a multinomial in (η,ε) that has orders $(16,3)$ respectively, $p(\eta,\varepsilon,a,b,I)$ can be written in the form $p(\eta,\varepsilon,a,b,I)=\sum_{i=0}^{16}p_i(\varepsilon,a,b,I)\eta^i$.

If $\Delta_\xi(\eta,\varepsilon)<0$ then (3.6) has a single real root, if $\Delta_\xi(\eta,\varepsilon)>0$ then there are 3 real solutions, and if $\Delta_\xi(\eta,\varepsilon)=0$ then further analysis is required. Note that, for all ε, as $\eta\to\pm\infty$, $\Delta_\xi(\eta,\varepsilon)\to-\infty$. Therefore there are functions $\eta_-(\varepsilon)\le\eta_+(\varepsilon)$ such that

$$\Delta_\xi(\eta,\varepsilon)<0 \qquad\qquad \varepsilon\in\mathbb{R},\eta\in\mathbb{R}\setminus[\eta_-(\varepsilon),\eta_+(\varepsilon)],$$

as the solutions to $\Delta_\xi(\eta,\varepsilon)=0$ are bounded. Thus, for $\eta<\eta_-(\varepsilon)$, there is exactly one real branch to $\{\dot{\xi}=0\}$, and therefore $\Xi_\gamma(\eta)$ is a smooth function for $\eta<\eta_-(\varepsilon)$.

We will use the following simple asymptotic approximation for $\Xi_\gamma(\eta)$. It can be shown by direct computation, for any $\delta\in\mathbb{R}$ and for f_ξ given in (3.5),

$$f_\xi\left(\eta,\frac{\delta+b\varepsilon}{3\eta}\right)=-\frac{\delta}{3}\eta+\frac{\varepsilon(9-b(3+b\varepsilon))+\delta(3-2b\varepsilon)-\delta^2}{9\eta}+\mathcal{O}\left(\frac{1}{\eta^2}\right)$$

as $\eta\to-\infty$. Therefore, given any $\alpha,\beta>0$ we have

$$\lim_{\eta\to-\infty}f_\xi\left(\eta,\frac{-\alpha+b\varepsilon}{3\eta}\right)=-\infty,\qquad\qquad\lim_{\eta\to-\infty}f_\xi\left(\eta,\frac{\beta+b\varepsilon}{3\eta}\right)=\infty.$$

Hence there exists an $\tilde{H}$ sufficiently negative such that for $\eta<\tilde{H}$,

$$\frac{\beta+b\varepsilon}{3\eta}<\Xi_\gamma(\eta)<\frac{-\alpha+b\varepsilon}{3\eta}.$$

Therefore $\Xi_\gamma(\eta)\to0$ as $\eta\to-\infty$. Note that

$$\Xi_\gamma'(\eta)=-\frac{\partial_\eta f_\xi(\eta,\Xi_\gamma(\eta))}{\partial_\xi f_\xi(\eta,\Xi_\gamma(\eta))}$$

and it can be shown that

$$-\frac{\partial_\eta f_\xi}{\partial_\xi f_\xi}\left(\eta,\frac{\beta+b\varepsilon}{3\eta}\right)=\frac{-2\beta-b\varepsilon}{\eta^2}+\mathcal{O}\left(\frac{1}{\eta^3}\right).$$

Thus, we can choose $\beta>0$ and $H\le\tilde{H}$ such that $\Xi_\gamma'(\eta)<0$ for $\eta<H$, which implies that $\Xi_\gamma(\eta)$ converges to 0 monotonically as $\eta\to-\infty$. We can compute that $1/\kappa_\gamma(\eta)$ blows up as $\eta\to-\infty$ and hence $\lim_{\eta\to-\infty}1/\kappa_\gamma(\eta)\neq0$. Additionally, using the same asymptotic approach employed above, $\langle f\circ\Psi_\gamma(\eta,\xi),T\gamma(\eta)\rangle<0$ for η sufficiently negative and $\xi\in[0,\Xi_\gamma(\eta)]$. Finally we note that $\langle f\circ\Psi_\gamma(\eta,0),N\gamma(\eta)\rangle<0$ for η sufficiently small (in fact, $\lim_{\eta\to-\infty}\langle f\circ\Psi_\gamma(\eta,0),N\gamma(\eta)\rangle=-\infty$). Therefore, for η sufficiently negative,
$\langle f\circ\Psi_\gamma(\eta,0),N\gamma(\eta)\rangle$ and $\Xi_\gamma(\eta)$ have the same sign.

Hence, in backwards time, our system satisfies all of the hypothesis of Lemma 3.2.2, therefore there is a trajectory $\phi(t)$ of (3.3) such that $d_H(\phi(t),\gamma)\searrow0$ as $t\to-\infty$. □

Corollary 7. *Given $\varepsilon,b>0$ and η sufficiently negative, $(\eta,0)$ is a super-solution of (3.5) and $(\eta,\Xi_\gamma(\eta))$ is a sub-solution of (3.5).*

Proof. Choose $H < -1$ so that $\Xi'_\gamma(\eta) < 0$, $f_\eta(\eta, \Xi_\gamma(\eta)) > 0$ (so that $f_\eta(\eta, \Xi_\gamma(\eta)) > 0$ in backwards time) and $f_\xi(\eta, 0) < 0$ for all $\eta < H$, which was shown to exist in the proof of Proposition 4 in the supplementary materials. Clearly $(\eta, 0)$ is a super-solution. We note that $f_\xi(\eta, \Xi_\gamma(\eta)) = 0$ by construction, hence $\Xi_\gamma(\eta)$ is a sub-solution.

Furthermore, we can compute H. Let $A_1 = \{\eta | \partial_\eta f_\xi(\eta, \Xi_\gamma(\eta)) = 0\}$, $A_2 = \{\eta | f_\eta(\eta, \Xi_\gamma(\eta)) = 0\}$, and $A_3 = \{\eta | f_\xi(\eta, 0) = 0\}$. Taking $H = \min(A_1 \cup A_2 \cup A_3 \cup \{-1\})$ will suffice. □

This result allows us to track ϕ along γ. Denote by $H(\varepsilon)$ the value of H in the previous proof as a function of ε.

Therefore, for $\eta < H(\varepsilon)$ our "slow manifold" is trapped in between $(\eta, 0)$ and $(\eta, \Xi_\gamma(\eta))$ in the LOR frame. When we map back to (x, y) space, our identified trajectory ϕ must satisfy $d_H(\phi(t), \gamma) < \mu_\gamma(\eta(t))$ as long as $\eta(t) < H(\varepsilon)$. Furthermore, we note that $\Xi'_\gamma(\eta) < 0, \Xi_\gamma(\eta) < 0$ for $\eta < H(\varepsilon)$ hence $\mu_\gamma(\eta(t)) \leq \mu_\gamma(H(\varepsilon))$ for $\eta(t) < H(\varepsilon)$. Thus we have the uniform estimate $d_H(\phi(t), \gamma) \leq \mu_\gamma(H(\varepsilon))$ as long as $\eta(t) < H(\varepsilon)$.

We chose to parameterize γ by the x coordinate, so $\eta = x$. If we employ the asymptotic estimate from the proof of Prop. 4 (supplementary materials) we see that

$$d_H(\phi(t), \gamma) < \mu_\gamma(x(t)) \leq \frac{b\varepsilon}{3|x(t)|}$$

as long as $x(t)$ is sufficiently negative. This proves that $d_H(\phi(t), \gamma) = \mathcal{O}(\varepsilon)$ as $\varepsilon \to 0$, thus we have recovered a Fenichel-type tracking estimate. Yet our method also demonstrates that the existence of "perturbed critical manifolds" is a *geometric* feature of the flow that is not necessarily dependent on timescale separation.

While we chose to study $\eta < -1$, one can just an easily study $\eta > 1$ and attain analogous results. In Figure 7, we display the family of perturbed critical manifolds as ε varies and a plot of $H(\varepsilon)$ against ε. One seemingly counterintuitive feature of this figure is the positive jump in $H(\varepsilon)$. That is, as ε increases, we can track the perturbation of the critical manifold closer to where normal hyperbolicity is lost, which would correspond to $H = -1$, although with an increase in distance from the critical manifold corresponding to larger $\mu_\gamma(H)$. In other words, our technique performs *better* as ε becomes larger, which is contrary to standard Fenichel Theory. This outcome is possible due to the asymptotic nature of this approach.

3.3 Curvature of a Flow and Rivers

In the second main section of this chapter, we study how the curvature of a flow can be used to understand certain phase space structures. We will continue to make use of the LOR frame and the associated invariance measure, and we will turn our focus to understanding "rivers". Recent work has demonstrated that the curvature of trajectories can relate to interesting dynamical effects [26, 13, 1]. We will argue that rivers, the attractiveness of which has hitherto remained insoluble, are caused by curvature phenomena.

3.3.1 Curvature of Trajectories

We wish to characterize the curvature of trajectories of the flow induced by $\dot{x} = f(x)$. As we rarely, if ever, can express a trajectory $\phi : (t_1, t_2) \to \Omega$ explicitly, we will use properties of $f(x)$ to compute the curvature of $\phi(t)$. For $\dot{\phi}(t) = f(\phi(t))$, taking a time derivative yields

$$\ddot{\phi}(t) = [D_x f(\phi(t))]\dot{\phi}(t) = [D_x f(\phi(t))]f(\phi(t))$$

where $[D_x f(x)]$ is the Jacobian of $f(x)$. Define $f^{(2)} : \Omega \to \mathbb{R}^2$ by $f^{(2)}(x) = [D_x f(x)]f(x)$ such that by definition $\ddot{\phi}(t) = f^{(2)}(\phi(t))$. Similarly, taking an additional time derivative, we find

$$\dddot{\phi}(t) = \left[D_x f^{(2)}(\phi(t))\right] f(\phi(t));$$

thus, we define $f^{(3)}(x) = D_x f^{(2)}(x) f(x)$ so that $\dddot{\phi}(t) = f^{(3)}(\phi(t))$. Clearly we can inductively define $f^{(i)}(x)$ for $i \geq 1$ as long as f is smooth enough. Recall that the curvature of $\phi(t)$ is given by

$$\kappa_\phi(t) = \frac{\dot{\phi}(t) \wedge \ddot{\phi}(t)}{\left\|\dot{\phi}(t)\right\|^3} \tag{3.7}$$

where $x \wedge y = \det(x, y)$. All of the quantities on the right hand side of (3.7) can be computed from $f(x)$; that is,

$$\kappa_\phi(t) = \frac{f(\phi(t)) \wedge f^{(2)}(\phi(t))}{\|f(\phi(t))\|^3}, \tag{3.8}$$

which leads us to the following definition.

Definition 3.3.1. Suppose that $f : \Omega \to \mathbb{R}^2$, where $\Omega \subseteq \mathbb{R}^2$ is open, is a $\mathscr{C}^2$ vector field. Denote

$$\Omega_0 = f^{-1}(\{0\}).$$

We call the function $\kappa : \Omega \setminus \Omega_0 \to \mathbb{R}$ defined by

$$\kappa(x) = \frac{f(x) \wedge f^{(2)}(x)}{\|f(x)\|^3} \tag{3.9}$$

the curvature of the flow induced by $f(x)$. Additionally we denote

$$\Delta_{i,j}(x) = f^{(i)}(x) \wedge f^{(j)}(x) \tag{3.10}$$

for i, j such that $f^{(i)}(x), f^{(j)}(x)$ are well-defined.

The following smoothness estimate follows directly from the definition of $\kappa(x)$.

Proposition 5. *If $f \in \mathscr{C}^\alpha(\Omega, \mathbb{R}^2)$ with $\alpha \geq 2$, then $\kappa \in \mathscr{C}^{\alpha-1}(\Omega \setminus \Omega_0, \mathbb{R})$. If $\phi : (t_1, t_2) \to \Omega$ is a trajectory of the flow induced by $f(x)$, then $\kappa_\phi(t) = \kappa(\phi(t))$.*

Proof. The smoothness conditions come from noticing that $f^{(i)}(x)$ is $\mathscr{C}^{\alpha+1-i}$ (where $f^1(x) := f(x)$). The second condition follows from Definition 3.3.1. □

3.3.2 Confluences and Rivers

Define the set

$$Z_\kappa = \{x \in \Omega \setminus \Omega_0 | \kappa(x) = 0\},$$

which we call the *zero-curvature locus* (ZCL). We remark that Z_κ has been studied in previous papers [26, 13, 1]; however, our use of the LOR frame in the current chapter to identify special flow-organizing trajectories will be novel. Let $\gamma_z : (-\delta, \delta) \to \Omega$ be a regular parameterization of Z_κ so that $\kappa(\gamma_z(\eta)) = 0$ for $\eta \in (-\delta, \delta)$. Before plumbing the role of Z_κ, we use our invariance measure to identify a phenomenon that we call a river.

Definition 3.3.2. We say that $\eta^* \in (-\delta, \delta)$ is confluent if $\mu_{\gamma_z}(\eta^*) = 0$. Additionally we call the point $\gamma_z(\eta^*)$ a confluence. We say that a trajectory $\rho(t)$ of $\dot{x} = f(x)$ is a river if $\rho(0)$ is a confluence.

Remark 4. 1. While there is no general, precise definition of a river, except for the definition of Diener and Diener [16, 15] that applies only to polynomial flows, there are two key features of trajectories that are typically dubbed rivers: other trajectories experience a strong contraction/repulsion towards them, and there is a lack of a clear cause for this contraction. That is, the definition of river shold apply to a trajectory that is not a stable manifold, limit cycle or some other clearly distinguished solution yet locally organizes the flow nonetheless. Although it is not particularly apparent at this point, we shall see that Definition 3.3.2 provides the former property without requiring that a river is any sort of otherwise distinguished curve.

2. It has been noted in the literature [1] that there are curves where $\kappa = 0$ that have no clear effect on the flow. Such branches of Z_κ are called ghosts. By studying how Z_κ aligns with the flow (via μ_{γ_z}), we not only identify points where Z_κ is instantaneously invariant, but we also eliminate ghosts.

3. Finally we justify our use of the word "confluence". Typically a confluence is where two rivers come together. We use the term because there are special manifolds that do cross at our confluences, discussed below in Theorem 3.3.3, and it is exactly these crossings that give birth to rivers. Since the term "source" already has other meaning, we decided to name these points based on the crossing property rather than selecting a more obscure term for birthplace of a river.

3.3.3 Rivers in the FitzHugh-Nagumo System

We return to the FitzHugh-Nagumo system (3.3) for a brief example of how we can fish for rivers. In our study of "slow manifolds" in Interlude 2, by focusing on $\{|\eta| > 1\}$, we completely omitted any mention of the middle, unstable branch of the critical manifold for the FHN system. We address this omission here in the context of rivers.

We can explicitly compute the ZCL for the FitzHugh-Nagumo system. The curvature of the flow has the form

$$\kappa(v, w) = \frac{\sum_{i=0}^{2} \varepsilon \alpha_i(v) w^i}{\|f(v, w)\|^3}$$

where $\alpha_i(v)$ are computable polynomials in v. For each $v \in \mathbb{R}$ there are up to two branches

to Z_κ. Let $w_\pm(v)$ denote the solutions to $\sum_{i=0}^{2} \alpha_i(v) w^i = 0$. Consider Figure 8(a), which shows $w_+(v), w_-(v)$ in red and blue, respectively, in the flow. The outer branches of $w_+(v)$ and the central branch of $w_-(v)$ seem to be nearly invariant. For now, we will search for confluences along the central branch of $w_-(v)$ by taking $\gamma_-(v) := (v, w_-(v))$ for this branch of $w_-(v)$ as a LOR basecurve.

Computing the LOR dynamics using this basecurve yields Figure 8(b) for small ξ, with the correction $\Xi_{\gamma_-}(\eta)$ shown in blue. We see that $\Xi_{\gamma_-}(0) = 0$, which is caused by symmetries of the FHN system. Therefore, the point $\gamma_-(0) = (0, w_-(0))$ is a confluence, and hence, the trajectory through $(0, w_-(0))$ is a river, which we will denote ρ_-. Examining the LOR dynamics, it appears that this river is unstable, as nearby trajectories seem to be pushed away, which is consistent with the appearance of the original flow.

We confirm this intuition by studying the river more carefully in (v, w) space, shown in Figure 8(c). The submersion of the river ρ_- is shown in orange; this trajectory evolves counter-clockwise and asymptotically approaches the periodic orbit. We take a sequence of initial conditions from a transverse section to ρ_- and integrate them backward in time, and we note that ρ_- is highly unstable in forward time. This observation raises the important point that rivers, as we have defined them, may attract trajectories in forward time or in backward time; in the latter case, they repel trajectories in forward time.

We also see that ρ_- lies fairly close to the middle branch of the v-nullcline, so we suggest that this river may be playing the role of an unstable slow manifold. As we have taken $\varepsilon = 0.3$, however, we are far from the singular limit; nontheless, our curvature analysis has apparently located a remnant of the fast-slow structure in the FHN system. This observation is consistent with the previous literature; in [1], the authors note that the ZCL does a good job of identifying fast-slow behavior.

The final panel in Figure 8 shows a more efficient method of identifying confluences, which is stated in Theorem 3.3.3. We also note that there is a second river in the FHN system, outside of the periodic orbit.

3.3.4 A Basic Theory of Confluences

The FHN example in Interlude 3 illustrates how the definition of rivers based on confluences aligns with desirable properties of the flow (possibly in backward time) but also can be tedious to apply. To locate rivers using these ideas, the ZCL must be parameterized and the LOR frame must be computed with a basecurve derived from the ZCL. Here we provide a list of equivalent conditions that may simplify the divining process.

Theorem 3.3.3. *Suppose that $\rho(t)$ is a trajectory of $\dot{x} = f(x)$ such that $\rho(0) = \rho_0$. The following are equivalent:*

1. *$\rho(t)$ is a river,*
2. *$\Delta_{1,2}(\rho_0) = \Delta_{1,3}(\rho_0) = 0$,*
3. *$\kappa_\rho(0) = \dot{\kappa}_\rho(0) = 0$,*
4. *dim span$\{f(\rho_0), f^{(2)}(\rho_0), f^{(3)}(\rho_0)\} = 1$.*

Proof. To show that $1 \Leftrightarrow 2$, it suffices to show that $\mu_{\gamma_z}(\eta^*) = 0$ if and only if $\Delta_{1,3}(\gamma_z(\eta^*)) = 0$. Recall that $\kappa(\gamma_z(\eta)) \equiv 0$ for the parameterization $\gamma_z(\eta)$ of the ZCL defined on $(-\delta, \delta)$. Differentiating both sides of this equation yields $\langle D_x\kappa(\gamma_z(\eta)), \gamma_z'(\eta)\rangle = 0$. Therefore, $D_x\kappa(\gamma_z(\eta))$ is collinear with $N\gamma_z(\eta)$ for all $\eta \in (-\delta, \delta)$. Thus

$$\langle f(\gamma_z(\eta)), N\gamma_z(\eta)\rangle = 0 \text{ if and only if } \langle D_x\kappa(\gamma_z(\eta)), f(\gamma_z(\eta))\rangle = 0,$$

where $D_x\kappa(\gamma_z(\eta)) \neq 0$ is assured by our assumption that γ_z has a regular parameterization. To conclude, fix $\eta \in (-\delta, \delta)$ and note that for the trajectory $\phi(t)$ such that $\phi(0) = \gamma_z(\eta)$,

$$\langle D_x\kappa(\gamma_z(\eta)), f(\gamma_z(\eta))\rangle = \frac{d}{dt}\kappa(\phi(t))\bigg|_{t=0}$$

and

$$\frac{d}{dt}\kappa(\phi(t)) = \frac{d}{dt}\kappa_\phi(t) = \frac{\det(f(\phi(t)), f^{(3)}(\phi(t)))}{\|f(\phi(t))\|^3} - 3\kappa_\phi(t)\frac{\langle f^{(2)}(\phi(t)), f(\phi(t))\rangle}{\|f(\phi(t))\|^2}.$$

As $\kappa_\phi(0) = \kappa(\gamma_z(\eta)) = 0$, definition (3.10) for $\Delta_{i,j}$ implies that $\mu_{\gamma_z}(\eta^*) = 0$ if and only if $\Delta_{1,3}(\gamma_z(\eta^*)) = 0$. The above computation clearly shows that $2 \Leftrightarrow 3$, and $2 \Leftrightarrow 4$ by definition. □

Remark 5. Theorem 3.3.3 helps justify the choice to refer to the birthplace of a river as a confluence. Conditions (2) and (3) in the theorem both show that a confluence, as we have defined it, corresponds to a point where the sets satisfying two different conditions come together.

Theorem 3.3.3 provides simple conditions for identifying rivers. We would also like to have a simple condition for differentiating between attracting and repelling rivers. Express the dynamics in a neighborhood of a confluence in the LOR frame, using our parameterization γ_z of $Z\kappa$ as our base curve. We suppose without loss of generality that the confluence occurs at $\gamma_z(0) =: \rho_0$. A simple Taylor expansion reveals that

$$\begin{aligned} \dot{\eta} &= \pm \frac{\|f(\rho_0)\|}{\|\gamma_z'(0)\|} + \mathcal{O}(\eta, \xi), \\ \dot{\xi} &= \langle [D_x f(\rho_0)] N\gamma_z(0), N\gamma_z(0) \rangle \, \xi + \mathcal{O}(\eta, \xi^2). \end{aligned} \tag{3.11}$$

Hence the attractivity of γ_z is determined by the sign of $\langle [D_x f(\rho_0)] N\gamma_z(0), N\gamma_z(0) \rangle$. To simplify matters, we note that $N\gamma_z(0) = \pm N\rho(0)$ where $\rho(t)$ is the river. Hence

$$\langle [D_x f(\rho_0)] N\gamma_z(0), N\gamma_z(0) \rangle = \langle [D_x f(\rho_0)] N\rho(0), N\rho(0) \rangle ,$$

which allows the following simple classification of rivers.

Definition 3.3.4. A river ρ is hyperbolic if $\langle [D_x f(\rho_0)] N\rho(0), N\rho(0) \rangle \neq 0$. If

$$\langle [D_x f(\rho_0)] N\rho(0), N\rho(0) \rangle > 0$$

then ρ is attracting, if

$$\langle [D_x f(\rho_0)] N\rho(0), N\rho(0) \rangle < 0$$

then ρ is repelling.

3.3.5 Some Limnology and Fluvial Cartography

Since we have already inundated the reader with results about the FHN oscillator, we will now study another well known system: a pair of coupled oscillators of the form

$$\begin{aligned}\dot{\theta} &= 1 - \cos(\theta) + (1 + \cos(\theta))(I_1 + P(\theta) - g_1 P(\phi)),\\ \dot{\phi} &= 1 - \cos(\phi) + (1 + \cos(\phi))(I_2 + P(\phi) - g_2 P(\theta))\end{aligned} \tag{3.12}$$

where $P(\alpha) = (1 - \cos(\alpha))/2\pi$ and $g_1, g_2, I_1, I_2 > 0$. These are basic self-excitatory theta model [5] oscillators with asymmetric coupling representing the effects of inhibitory synapses, which have been studied for example in [48]. For the sake of concreteness, we take $I_1 = 1, I_2 = 2, g_1 = 1, g_2 = 3$ for our phase portrait, shown in Figure 9. Note that our vector field is invariant under the transformation $(\theta, \phi) \mapsto (-\theta, -\phi)$, thus its flow is symmetric about the origin.

With our equivalent formulations in hand, we set out in search of rivers. We find the most promising dowser to be condition 2 of Theorem 3.3.3. Using this condition, we can find all of the rivers in our domain simultaneously without having to worry about parameterizing each branch of Z_κ and computing its correction. Our algorithm for identifying rivers is as follows: compute the zero-level sets of $\Delta_{1,2}(x), \Delta_{1,3}(x)$ on the domain of interest $x \in \Omega$, look for regions where the two level sets are close, and then use Newton's Method to approximate the location of the river to arbitrary accuracy.

We find that there are four crossings of $\{\Delta_{1,2}(x) = 0\}, \{\Delta_{1,3}(x) = 0\}$ in $[-\pi, \pi]^2$, the coordinates of which we label C_1 through C_4, and therefore our system has four rivers. From the aforementioned symmetry in the system (which induces symmetry in $\{\Delta_{1,2}(x) = 0\}, \{\Delta_{1,3}(x) = 0\}$), $C_4 = -C_1, C_3 = -C_2$. We designate the four rivers of the system as $\{R_i\}_{i=1}^4$ in the natural way. A simple computation reveals that all four confluences yield hyperbolic rivers, R_1, R_2 are attracting and R_3, R_4 are repelling. Figure 10 shows the four rivers and how they interact.

We see that R_1 and R_2 rapidly contract towards one another, but R_2 seems to exert more "influence" on the flow, similarly with their antipodes. So in a sense, R_2, R_3 are the dominant rivers in the system; we will comment on this in more detail in the following section.

Note that all four confluences lie near the identity line, which is more than a passing curiosity. If $g_1 = g_2$ and $I_1 = I_2$, then it is easy to verify that $\{\theta = \phi\}$ is an invariant subset of the flow. We see that this set has everywhere vanishing curvature, as all lines do. Furthermore, the set $\{\theta = \phi\}$ has everywhere vanishing torsion, as its curvature is constant. Thus, by Theorem 3.3.3 every point in $\{\theta = \phi\}$ is a confluence, with corresponding flow shown in Figure 11(a).

As we vary our parameters away from the symmetric case, it is unsurprising that this continuum of confluences breaks apart. However, some of the crossings of $\{\Delta_{1,2}(x) = 0\}, \{\Delta_{1,3}(x) = 0\}$ persist, as shown in Figure 11(b). Hence, the proximity of the confluences to the identity line in Figure 10 can be viewed as an artifact of the symmetry of system (3.12).

Hopefully, this quick dip into the rivers of the theta model is enough to whet the appetite of our readers for a deeper look at the interactions of confluences, which we present in the next subsection.

3.3.6 Confluence Bifurcations

We have seen that the theta model (3.12) has four rivers, two attracting and two repelling, for the parameter values that we initially studied. For small g_2 close to g_1, however, the system has just two rivers. Hence, we are led to float some interesting questions: Are confluences robust under parameter perturbation? Can confluences undergo "bifurcations"? If so, is there a numerical condition to identify bifurcation values? In this section we will provide answers to these questions, and demonstrate that confluences (and therefore rivers) are generically robust in parameter space. At the end of the section we will consider parameter dependence of rivers in system (3.12).

First, we compute a sufficient condition for confluences to persist in parameter space.

Proposition 6. *Suppose that $f(x, \lambda)$ is $\mathscr{C}^3$ in x on Ω and $\mathscr{C}^1$ in λ on some open parameter set $\Lambda \subseteq \mathbb{R}^n$. Suppose $M_1 = \{\Delta_{1,2}(x, \lambda) = 0\}, M_2 = \{\Delta_{1,3}(x, \lambda) = 0\}$ are smooth, codimension-1 (in $\Omega \times \Lambda$) manifolds such that $(x_0, \lambda_0) \in M_1 \cap M_2$. If*

$$\Delta_{1,4}(x_0, \lambda_0) \neq 0$$

then there is there is a submanifold $\tilde{M} \subseteq (M_1 \cap M_2) \cap B((x_0, \lambda_0), \delta)$. *Additionally, if* $\partial_{\lambda_i} \Delta_{1,3}(x_0, \lambda_0) \neq 0$ *for any* $i \in \{1, \cdots, n\}$, *then* $\tilde{M} \not\subseteq \{\lambda = \lambda_0\}$.

Proof. Suppose that $\sigma_1 : U_1 \subseteq \mathbb{R}^{n-1} \to \Omega \times \Lambda$ is a chart of M_1 at (x_0, λ_0), that is $\Delta_{1,2} \circ \sigma_1(y) = 0$ for all $y \in U_1$. Hence for each $1 \leq i \leq n+2$,

$$0 = \partial_i(\Delta_{1,2} \circ \sigma_1(y)) = \langle D_x \Delta_{1,2} \circ \sigma_1(y), \partial_i \sigma_1(y) \rangle .$$

Therefore, $T_{(x_0,\lambda_0)} M_1 \perp D_x \Delta_{1,2}(x_0, \lambda_0)$ and analogously $T_{(x_0,\lambda_0)} M_2 \perp D_x \Delta_{1,3}(x_0, \lambda_0)$. We note that

$$0 = \Delta_{1,3}(x_0, \lambda_0) = \langle D_x \Delta_{1,2}(x_0, \lambda_0), (f(x_0, \lambda_0), 0, \cdots, 0) \rangle ;$$

hence, $(f(x_0, \lambda_0), 0, \cdots, 0) \in T_{(x_0,\lambda_0)} M_1$. Therefore, if

$$\langle D_x \Delta_{1,3}(x_0, \lambda_0), (f(x_0, \lambda_0), 0, \cdots, 0) \rangle \neq 0,$$

then $(f(x_0, \lambda_0), 0, \cdots, 0) \notin T_{(x_0,\lambda_0)} M_2$, hence $\mathbb{R}^n = (f(x_0, \lambda_0), 0, \cdots, 0) \oplus T_{(x_0,\lambda_0)} M_2 \subseteq T_{(x_0,\lambda_0)} M_1 \oplus T_{(x_0,\lambda_0)} M_2$, and thus M_1, M_2 intersect transversely at (x_0, λ_0). To conclude we note that

$$\langle D_x \Delta_{1,3}(x_0, \lambda_0), (f(x_0, \lambda_0), 0, \cdots, 0) \rangle = \Delta_{1,4}(x_0, \lambda_0) + \Delta_{2,3}(x_0, \lambda_0)$$

yet $\Delta_{2,3}(x_0, \lambda_0) = 0$ by condition 4 of Theorem 3.3.3. Hence,

$$\langle D_x \Delta_{1,3}(x_0, \lambda_0), (f(x_0, \lambda_0), 0, \cdots, 0) \rangle = \Delta_{1,4}(x_0, \lambda_0).$$

Thus, the transverse manifold theorem gives the existence of $\tilde{M}$. The last remark in the proposition statement holds as $T_{(x_0,\lambda_0)} \tilde{M} \subseteq T_{(x_0,\lambda_0)} M_2$ and $T_{(x_0,\lambda_0)} M_2 \not\subseteq \{\lambda = \lambda_0\}$. □

Thus we have shown that generic confluences are robust in parameter space. Additionally, applying the contrapositive of the above proposition, if two (or more) confluences come together, then we must have a loss of transversality. Thus, we have an analytic condition for "bifurcations" of confluences: a confluence bifurcation is a point in phase space that satisfies

$$\Delta_{1,2}(x,\lambda) = \Delta_{1,3}(x,\lambda) = \Delta_{1,4}(x,\lambda) = 0. \tag{3.13}$$

Now, we will discuss why we refer to the events identified by condition (3.13) are "bifurcations" and not bifurcations. We note that curvature (and therefore, the curvature of a flow) is not a topological invariant. That is, if we consider a diffeomorphism $F : \mathbb{R}^2 \to \mathbb{R}^2$ and a curve $\gamma : [0,1] \to \mathbb{R}^2$, the curvatures of γ and $F \circ \gamma$ will generally differ. For example, if we stretch a circle of radius one to a circle of radius two, the curvature of the circle changes from 1 to 1/2. Therefore, the zero-curvature locus is not necessarily a topological invariant of the flow.

As an example, we consider the parameter dependence of rivers of (3.12). Note that we can express $\Delta_{1,2}, \Delta_{1,3}$ for (3.12) as

$$\begin{aligned}\Delta_{1,2}(\theta,\phi) &= \sum_{i,j,k,l} a_{i,j,k,l}(I_1,I_2,g_1,g_2)\sin^i(\theta)\cos^j(\theta)\sin^k(\phi)\cos^l(\phi)\\ \Delta_{1,3}(\theta,\phi) &= \sum_{i,j,k,l} b_{i,j,k,l}(I_1,I_2,g_1,g_2)\sin^i(\theta)\cos^j(\theta)\sin^k(\phi)\cos^l(\phi)\end{aligned} \tag{3.14}$$

where $a_{i,j,k,l}(I_1,I_2,g_1,g_2), b_{i,j,k,l}(I_1,I_2,g_1,g_2)$ are known functions. We define

$$(x,y,u,v) = (\sin(\theta),\cos(\theta),\sin(\phi),\cos(\phi))$$

which transforms (3.14) into a multinomial equation, which is additionally subject to $x^2 + y^2 = 1, u^2 + v^2 = 1$. We employ a numerical root solver to identify all real roots of $\Delta_{1,2}(x,y,u,v) = \Delta_{1,3}(x,y,u,v) = 0, x^2+y^2 = u^2+v^2 = 1$ as one parameter is varied away from our base parameter value $(I_1,I_2,g_1,g_2) = (1,2,1,3)$. These solutions are transformed back into (θ,ϕ) confluences via $(\theta,\phi) = (\arctan(y/x)\arctan(v/u)$.

We present two one-parameter bifurcation diagrams, varying g_1 and I_1, respectively. Figure 12 shows plots of the θ coordinate of the confluences of (3.12) versus the parameter being varied; the color of each branch denotes the stability of the confluence, with blue for

stable and red for unstable. The dotted vertical lines denote parameter values at which confluence bifurcations occur (including two that occur at the same g_1 value).

As we vary $g_1 \in [0, 1.3]$ we find that there are four confluence bifurcations that fall into three phenomenological categories, which we term $(+,+)$ confluence bifurcations, $(-,-)$ confluence bifurcations, $(+,-)$ confluence bifurcations. In the $(+,-)$ bifurcations, a stable confluence meets an unstable confluence and the pair annihilate; we see both subcritical and supercritical variations of this bifurcation. The $(+,+)$ and $(-,-)$ bifurcations, in which confluences with the same stability type collide, only occur in Fig 12(a) , but they demonstrate that confluences do not behave like fixed points, as we can have two attracting or repelling rivers arbitrarily near one another. Two $(+,-)$ confluence bifurcations occur as we vary $I_1 \in [0, 6.4]$ (Figure 12(b)).

3.3.7 Asymptotic Rivers

Note that, in Figure 8(d), the ZCL (shown in red) and $\{\Delta_{1,3}(x) = 0\}$ (shown in blue) cross exactly twice. Additionally, in the upper left and lower right corners of the figure, these two sets seem asymptotically approach one another. To study this type of behavior, we extend our definition of rivers to an asymptotic setting.

Having already defined rivers, we note that a river is born when the ZCL is (momentarily) invariant in the flow. We generalize this formulation to allow for asymptotic invariance of the ZCL as it escapes to infinity.

Definition 3.3.5. Let $\gamma_z : (0, \infty) \to \Omega$ be a parameterization of the ZCL such that $\lim_{\eta\to\infty} \|\gamma_z(\eta)\| = \infty$; that is, γ_z escapes to infinity. We say that γ_z has an asymptotic confluence if

$$\lim_{\eta\to\infty} \mu_{\gamma_z}(\eta) = 0.$$

A trajectory $\phi(t)$ is an asymptotic river if

$$\lim_{t\to\pm\infty} d_H(\phi(t), \gamma_z) = 0$$

and γ_z has an asymptotic confluence.

We note that the first condition ($\mu_{\gamma_z} \to 0$) gives rise to a "confluence at infinity", and the second condition is analogous to Definition 3.3.2, where a river is a trajectory that passes through a confluence; here, an asymptotic river is a trajectory that limits to a confluence at infinity along the ZCL.

If we take γ_z to be a LOR basecurve, we can use Lemma 3.2.2 to derive a sufficient condition for an asymptotic river to exist.

Lemma 3.3.6. *Suppose that $f : \Omega \to \mathbb{R}^2$ is $\mathscr{C}^1$ and $\gamma_z : [0, \infty) \to \Omega$ is a regular $\mathscr{C}^2$ parameterization of the ZCL such that*

$$\lim_{\eta \to \infty} \|\gamma_z(\eta)\| = \infty \text{ and } \lim_{\eta \to \infty} \frac{1}{\kappa_{\gamma_z}(\eta)} \neq 0.$$

Additionally, suppose that the correction to γ_z, $\Xi_{\gamma_z}(\eta)$, is $\mathscr{C}^1$ and $\Xi_{\gamma_z}(\eta) \to 0$ monotonically as $\eta \to \infty$ with

$$\langle f \circ \Psi_{\gamma_z}(\eta, \xi), T\gamma_z(\eta) \rangle > 0 \qquad \text{for all } \eta \geq 0, \xi \in [0, \Xi_{\gamma_z}(\eta)].$$

If $\langle f \circ \Psi_{\gamma_z}(0,0), N\gamma_z(0) \rangle$ and $\Xi_{\gamma_z}(0)$ have opposite signs, then there is a trajectory $\phi(t)$ such that

$$\lim_{t \to \infty} d_H(\phi(t), \gamma_z) \searrow 0;$$

that is, ϕ is an asymptotic river.

Proof. We note that $\mu_{\gamma_z}(\eta) = |\Xi_{\gamma_z}(\eta)|$ hence γ_z has an asymptotic confluence by assumption. The existence of ϕ follows from Lemma 3.2.2. □

Finally, we remark that the necessary conditions derived in Theorem 3.3.3 do not necessarily generalize to the asymptotic case, due to possibly ill-behaved limits at infinity.

3.3.8 A Deluge of Rivers in a Hodgkin-Huxley Type Neuron Model

To conclude our study of rivers, we will consider a neural oscillator with more complicated dynamics than the FitzHugh-Nagumo system. We take from [62] a Hodgkin-Huxley type neuron with dynamics given by

$$\begin{aligned} C\dot{v} &= -I_{Na}(v,n) - I_K(v,n) - I_L(v), \\ \dot{n} &= \phi\left(\frac{n_\infty(v) - n}{\tau_n(v)}\right), \end{aligned} \tag{3.15}$$

where $I_{Na}, I_K, I_L, n_\infty, \tau_n$ are of a form that is standard within this class of models; We consider three ion currents

$$\begin{aligned} I_{Na}(v,n) &= g_{Na} m_\infty^3(v)(1-n)(v - v_{Na}) \\ I_K(v,n) &= g_K n^4 (v - v_k) \\ I_L(v) &= g_L(v - v_L) \end{aligned}$$

where

$$\begin{aligned} m_\infty(v) &= \left(1 + \exp\left(-\frac{(v-\theta_m)}{\sigma_m}\right)\right) \\ n_\infty(v) &= \left(1 + \exp\left(-\frac{(v-\theta_n)}{\sigma_n}\right)\right) \\ \tau_\infty(v) &= \tau_0 + \tau_1\left(1 + \exp\left(-\frac{(v-\theta_\tau)}{\sigma_\tau}\right)\right) \end{aligned}$$

and parameter values given by Table 2.

Over a broad range of parameter values the model (3.15) supports a stable periodic oscillation, which flows counter-clockwise. Denote this limit cycle by $\Gamma(t)$ and its period by T. In their antediluvian but prescient analysis, the authors of [62] show that two intrinsically oscillatory neurons governed by (3.15) that are coupled by mutual synaptic inhibition can display irregular dynamics that is robust to parameter changes. Specifically, they construct a return map from the coupled neuron dynamics that exhibits hallmarks of chaos. The authors also suggest that part of the mechanism underlying the observed irregular dynamics is a contraction of trajectories to a river-like structure not obviously associated with any particular phase plane structure. We will show that, in the absence of coupling, the system

(3.15) already has a rich river structure, and its rivers can be useful in classifying the transient manner by which trajectories approach the periodic solution.

First, we remark that this system has four rivers (see black dots in Figure 13(a)), three asymptotic rivers, and one additional structure that we term a weak river. We will study each of these in turn.

One interesting river lies inside $\Gamma(t)$, shown in Figure 13(b) in orange and labeled ρ_2. This river is hyperbolic and repelling. We note that ρ_2 passes very close to the v-nullcline and hence can be thought of as a relic of the fast-slow structure in the system even though ϕ is not particularly small. This river plays a very similar role to the river shown in Figure 8(a), in that it seems to demonstrate extreme sensitivity to asymptotic phase. For the sake of brevity, we omit a figure demonstrating this. A connection between rivers and phase separatrices clearly exists, and a rigorous study of this relationship is underway.

There is another river of note outside the limit cycle, labeled by ρ_1 in Fig. 13(b). This river captures the rapid contraction in the neighborhood of its confluence. In [62], the authors note that the contraction in this region, combined with the local instability of the limit cycle (which we also relate to river activity in this section) cause extreme sensitivity to initial conditions. Additionally, ρ_1 informs the shape of the limit cycle and how trajectories must approach the limit cycle.

Next, we catalogue and consider the asymptotic rivers of (3.15). The three asymptotic rivers, labeled as $\rho_{\infty,i}$ for $i \in \{1, 2, 3\}$ in Figure 13(b), are drawn to three different branches of the ZCL (i.e., of $\{\Delta_{1,2}(x) = 0\}$), specifically the branches labeled A, B, D in Figure 13(a). These asymptotic rivers meet the conditions laid out in Lemma 3.2.2 in backwards time. We note that all three of these trajectories also asymptotically approach the nullclines of the system in backwards time; $\rho_{\infty,1}$ limits to the v-nullcline and $\rho_{\infty,2}, \rho_{\infty,3}$ limit to the n-nullcline.

System (3.15) is a fast-slow system for ϕ sufficiently small. In the analysis of [62] and here as well, the parameter $\phi = 0.2$, which is not so small, yet we still see dynamical effects related to the critical manifold. Thus, the existence and behavior of the asymptotic river $\rho_{\infty,1}$, which limits to the v-nullcline, is not surprising; it is, in the sense of Interlude 2, a slow manifold. However, framing the system as fast-slow makes the existence and behavior of $\rho_{\infty,2}, \rho_{\infty,3}$ all the more perplexing, as these are trajectories that limit to the "wrong" nullcline! Hence

these asymptotic rivers are novel phenomena, outside of usual multiple-timescale theory.

The asymptotic rivers $\rho_{\infty,1}, \rho_{\infty,2}$ have an additional interesting dynamical effect: they serve to funnel trajectories towards the limit cycle (black dashed curve in Figure 13(b) and in Figure 14(a)). One of the outstanding features of this system is the geometry of the limit cycle; the left portion of the curve (as n plunges from $\approx .9$ to $\approx .2$) is nearly vertical, after which the limit cycle develops a peninsular shape. In their analysis, the authors of [62] note that, near this vertical plunge on the exterior of the limit cycle, trajectories are repelled away from the limit cycle, yet rapidly converge to some structure below the limit cycle. We claim that the asymptotic rivers $\rho_{\infty,1}, \rho_{\infty,2}$ can be used to explain this effect.

We can study the local attractivity of a trajectory ϕ by studying the quantity $H_\phi(t) := \langle [D_x f(\phi(t))] N\phi(t), N\phi(t) \rangle$. Specifically, if $H_\phi(t) < 0$ then the Hausdorff distance between ϕ and nearby trajectories is decreasing, with the opposite true if $H_\phi(t) > 0$; this relation arises through linearization in the LOR frame, given in (3.11). In the phase plane, similar to our earlier analysis, we can define a map $H : \Omega \to \mathbb{R}$ by

$$H(x) = \frac{\langle [D_x f(x)] Rf(x), Rf(x) \rangle}{\|f(x)\|^2},$$

where R is rotation by $\pi/2$ such that $N\phi(t) = Rf(\phi(t))/\|f(\phi(t))\|$, with $H_\phi(t) = H(\phi(t))$. The function $H(x)$ quantifies the attracting qualities of the trajectory with respect to x.

As the the limit cycle $\Gamma(t)$ of (3.15) traces its course, it makes four intersections with $\{H(\Gamma(t)) = 0\}$ (see Fig. 14(a), where the shaded blue region is $\{H(x) \leq 0\}$), corresponding to four changes in local stability. As mentioned earlier, the loss of stability in the upper left sector of the plane is more dynamically interesting. Here, the limit cycle becomes locally unstable for about 10% of it's period (and about 25% of its arc length).

Note from Fig.14(a) that there is a narrow portion of the region $\{H(x) \leq 0\}$, near the rectangle, which extends all the way to $n = 1$; this region is also evident in the zoomed view in panel (b). We note that $\rho_{\infty,1}$ lies in this region, and as trajectories are repelled by Γ, they pass into $\{H(x) \leq 0\}$ and are pulled towards $\rho_{\infty,1}$. Subsequently, Γ itself reenters $\{H(x) \leq 0\}$ and all trajectories near Γ contract together. This sequence may contribute to the expansion, orientation reversal, and subsequent contraction yielding chaos in the coupled version of this system [62].

The structure that we call a weak river, denoted by ρ_w in Figure 13(b), is neither a river nor an asymptotic river. If we examine the branch of the ZCL near C, which we denote by $\gamma_{z,C}$, we find that there are no points such that $\mu_{\gamma_{z,C}}(\eta) = 0$. However, we can compute that there is a maximally nearly-invariant point on $\gamma_{z,C}$; that is, there is an η^* such that

$$\mu_{\gamma_{z,C}}(\eta^*) = \inf_{\eta \in I} \mu_{\gamma_{z,C}}(\eta)$$

where I is the domain of this branch of γ_z. We compute that $\gamma_{z,C}(\eta^*) \approx (14.1, -1.1)$ and $\mu_{\gamma_{z,C}}(\eta^*) \approx 0.00041$. The trajectory ρ_w satisfies $\rho_w(0) = \gamma_{z,C}(\eta^*)$, which is outside of our meaningful phase region; however, in forward time ρ_w flows into $0 \leq n \leq 1$ as shown in Figure 13(b). We also see that this trajectory evolves along the v-nullcline for a non-trivial amount of time, hence ρ_w can be seen as a form of slow manifold.

To conclude this section, we show how $\rho_{\infty,1}, \rho_{\infty,2}, \rho_w$ serve as transient attraction modes to Γ. Although we do not provide a rigorous definition, we say that a trajectory ϕ is a transient attraction mode to a limit cycle Γ if initial conditions near ϕ converge to ϕ more quickly than they converge to Γ. The idea we seek to study is how the phase plane feeds into the attracting periodic orbit Γ. In a standard relaxation oscillation, we note that there should be two transient attraction modes, the attracting slow manifolds corresponding to the attracting branches of the critical manifold.

In system (3.15), we seem to have three transient attraction modes. To study this observation in more detail, we fix a rectangular region of space, here $[-120, 120] \times [-0.1, 1.1]$, we pick 1000 uniformly spaced initial conditions on the boundary, and we integrate these initial conditions forward in time. Then we color code the resultant trajectories. The trajectory emanating from the upper left corner is colored red and trajectories uniformly blend to blue as we move clockwise along the boundary. The results are shown in Figure 15, with the rivers $\rho_{\infty,1}, \rho_{\infty,2}, \rho_w$ shown in black. We see that some trajectories are rapidly drawn towards these three modes before eventually feeding into Γ.

While we have left the concept of transient attraction modes, which we hope to study more rigorously in the future, rather vague, we hope that we have demonstrated that rivers serve as easily identifiable trajectories that have interesting transient dynamical effects in

this complicated system and that could naturally be important in many other planar systems as well.

3.3.9 A Theta Model with Adaptation and the Liouville System

The following one-variable phase reduction with adaptation is presented in [6]:

$$\begin{aligned} \dot{\theta} &= 1 - \cos\theta + J(1+\cos\theta) - \frac{2}{3}(I_E - J)\sin\theta \\ \tau_I \dot{J} &= I_E - J \end{aligned} \tag{3.16}$$

where θ represents the phase of an oscillator and J is an adaptive current. The authors of [6] note the existence of two rivers that completely organize the phase plane; we will demonstrate that these structures are asymptotic rivers. Performing a change of variables, system (3.16) is equivalent to system (27.11) presented in [4]. Furthermore, equation (3.16) is structurally similar to the Liouville system, given by

$$\begin{aligned} \dot{x} &= y - x^2 \\ \dot{y} &= 1. \end{aligned} \tag{3.17}$$

This system plays an important role in Fenichel theory; in a system with one fast variable and one slow variable $(\dot{x}_1, \dot{x}_2) = (f_1(x_1, x_2), \varepsilon f_2(x_1, x_2))$ in which the critical manifold loses normal hyperbolicity via a generic fold, blow-up analysis reveals that (3.17) represents the flow near the fold [38]. Additionally, Diener et al. remark in [16, 15] that (3.17) contains two fleuves, by their definition. We will show that these are asymptotic rivers by our definitions.

Trajectories of (3.16) are shown in Fig. 16(b) along with several organizing rivers and asymptotic rivers. The two asymptotic rivers, shown in black, actually correspond to the rivers that Börgers et al. identify. There are also three rivers in this system; the set $\{J = 1\}$ is an invariant line hence is a river, and there are two additional crossings of $\{\Delta_{1,2} = 0\}, \{\Delta_{1,3} = 0\}$, shown in Fig. 16(a). The asymptotic river limiting in the direction B has a clear attracting influence. The other asymptotic river initially repels trajectories. Interestingly, in forward time, all of the river structures come together, along with the other system trajectories, as flow progresses in the direction of increasing θ near $\{J = 1\}$, although they collect into two separate groupings along the way.

3.3.10 A Templator System

In [1], the authors present a two variable chemical templator system which has dynamics

$$\begin{aligned}\dot{X} &= a_1 - a_2X^2 - a_3X^2T \\ \dot{T} &= a_2X^2 + a_3X^2T - \frac{a_4T}{a_5+T}.\end{aligned} \tag{3.18}$$

where we take $a_1 = 0.9, a_2 = .01, a_3 = a_4 = 1, a_5 = 0.02$, as do Benoit et al.

The authors note that this system displays dynamics which are very similar to fast-slow behavior, however there is no temporal separation. Benoit et al. demonstrate that this behavior is linked to low-curvature phenomena, and claim that the set $\{\Delta_{1,2} = 0\}$ organizes the phase but remark that there are regions where $\{\Delta_{1,2} = 0\}$ seems completely unrelated to the flow; they call these curves "ghosts". With our invariance measure and asymptotic rivers we can eliminate these "ghosts" and show that this phase plane can be organized around two asymptotic rivers.

To make these dynamics more apparent, we perform a logarithmic change of variables $(x, y) = (X, \log T)$ to study the region where T is small. Figure 17 displays the rapid contraction towards the asymptotic rivers we identify in the transformed system. Note that the shape of the limit cycle can also be predicted from the structure of these asymptotic rivers.

3.3.11 A River in a Changing World

Diener et al. [16] defined a *fleuve* as a trajectory in a planar polynomial system that satisfies a certain algebraic homogeneity condition. In [16], they remark that the ODE given by

$$\begin{aligned}\dot{x} &= 1 \\ \dot{y} &= x(y-x) + 1\end{aligned} \tag{3.19}$$

exhibits a fleuve given by $\{y = x\}$. Specifically, $\{y = x\}$ is an invariant set that is *une fleuve de rank* $(1, 1)$. This set, being an invariant line, has zero curvature hence is a river by our definition as well. This river serves as a separatrix for asymptotic behavior (Figure 18).

This is a fragile river, however. We note that the sets $\{\Delta_{1,2} = 0\}, \{\Delta_{1,3} = 0\}$ are given by $\{y = x\}$ and $\{y = x\} \cup \{x = 0\}$ respectively; therefore, $\{y = x\}$ is a continuum of non-transverse intersections of $\{\Delta_{1,2} = 0\}, \{\Delta_{1.3} = 0\}$.

To study this fragility we apply a diffeomorphism that alters the curvature of the flow, namely let $\varepsilon > 0$ and define $(\alpha, \beta) = (x, y - \varepsilon x^2)$. We note that this transformation bends the plane in a way that does not preserve the curvature of trajectories. Futhermore, we can continuously control the extent of this distortion by tuning ε.

We compute the new flow

$$\begin{aligned} \dot{\alpha} &= 1 \\ \dot{\beta} &= \alpha(\beta - \alpha) + 1 + \varepsilon\alpha(\alpha^2 - 2), \end{aligned} \tag{3.20}$$

which is obviously equivalent to (3.19) when $\varepsilon = 0$. The river in this system with $\varepsilon = 0$ ($\{y = x\}$) is degenerate with regard to our persistence result, Proposition 6. Even with $\varepsilon > 0$, however, a river persists through the point $(0, 2\varepsilon)$ and there is a doubly asymptotic river that serves as a separatrix between trajectories that blow up to $-\infty$ in β and those that blow up to $+\infty$, just as $\{y = x\}$ does in system (3.19). By doubly asymptotic river, we mean that this trajectory is an asymptotic river as $t \to \pm\infty$ (Figure 19).

The true river in our perturbed system no longer serves as a separatrix, but rather attracts trajectories in a local region near its confluence. As α gets larger, the curvature deformation introduced by our diffeomorphism becomes more extreme, as does the deviation of the asymptotic river from the identity line. Nonetheless, the separating role of the asymptotic river remains clear.

3.4 Figures and Tables

Conductances (nS)	Potentials (mV)	Activations (mV)	Slopes	Rates (1/ms)	Other
$g_{Na} = 100.0$	$v_{Na} = 55.0$	$\theta_m = -37.0$	$\sigma_m = 10.0$	$\phi = 0.2$	$C = 1.0$ pF
$g_K = 10.0$	$v_K = -80.0$	$\theta_n = -50.0$	$\sigma_n = 14.0$	$\alpha = 5.0$	$\tau_0 = 0.05$ ms
$g_L = 0.02$	$v_L = -30.0$	$\theta_\tau = -40.0$	$\sigma_\tau = -12.0$	$\beta = 1.0$	$\tau_1 = 0.27$ ms

Table 2: Parameter Values for System (3.15)

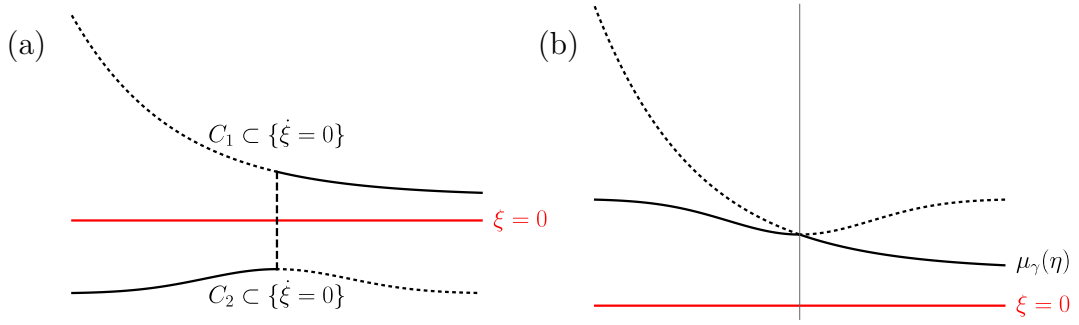

Figure 4: A pictorial representation of the correction and invariance measure. (a) Two branches of the nullcline $\{\dot{\xi} = 0\}$, denoted C_1, C_2, plotted in black (dotted and solid), as η varies. Note that the solid black curve is $\Xi_\gamma(\eta)$, formed from the branches closest to $\xi = 0$ (red). (b) C_1, C_2 from (a) are both reflected to one side (without loss of generality, the positive side) of $\xi = 0$ and the solid black parts of these curves form the graph of the actual invariance measure $\mu_\gamma(\eta)$ over the plotted range. That is, $\mu_\gamma(\eta) = |\Xi_\gamma(\eta)|$.

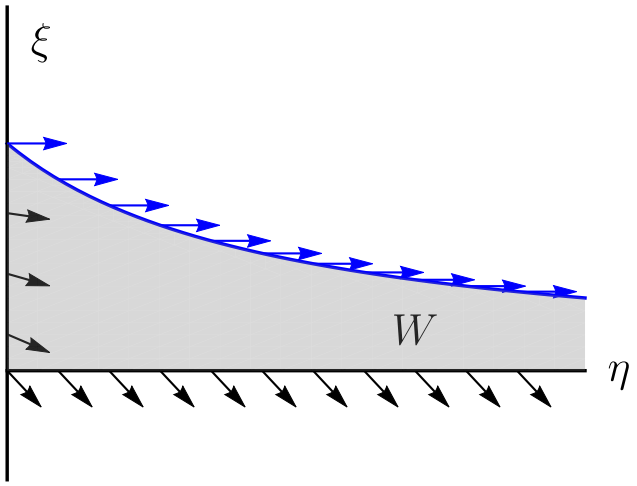

Figure 5: A sketch of the geometric consequences of the assumptions of Lemma 2.9. In blue is $\Xi_\gamma(\eta)$. Arrows designate the direction of the flow along $\Xi_\gamma(\eta), \xi = 0$, and $\eta = 0$. These three curves are used to construct the boundary of a Wazewski set.

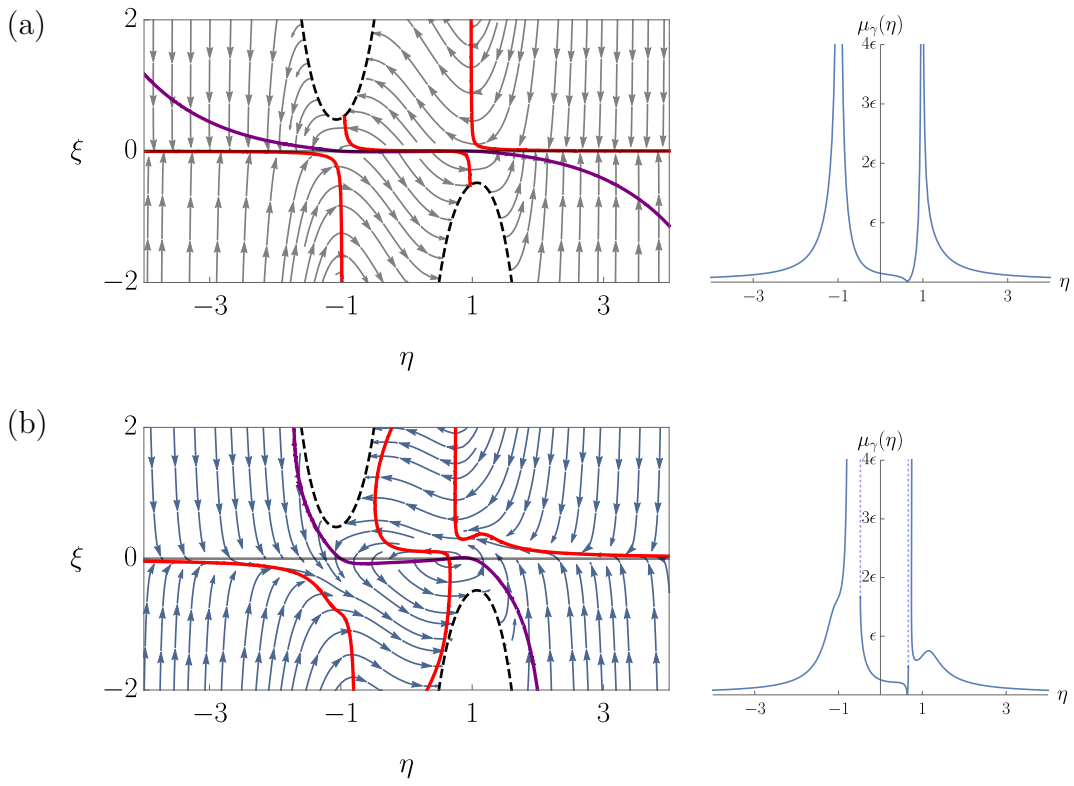

Figure 6: Streamplots of the (η, ξ) dynamics. (a) For $\varepsilon = 0.05$, the η-nullcline is shown in purple, the ξ-nullcline is shown in red, and the boundary of the maximal parameter set is shown in dashed black. Recall that the correction is defined by selecting branches of the ξ-nullcline near $\xi = 0$; its magnitude $\mu_\gamma(\eta)$ is shown to the right. Note that trajectories rapidly converge to the ξ-nullcline for $|\eta| > 1$, where the nullcline is very close to $\xi = 0$. (b) For a much larger choice, $\varepsilon = 0.5$, using the same color assignations, we see that the ξ-nullcline has moved away from $\xi = 0$, yet trajectories in $\{\eta < -1\} \cup \{\eta > 1\}$ still rapidly converge to the correction set. In both (a) and (b), in $\{-1 < \eta < 1\}$, we see the opposite effect: trajectories seem indifferent to the correction set.

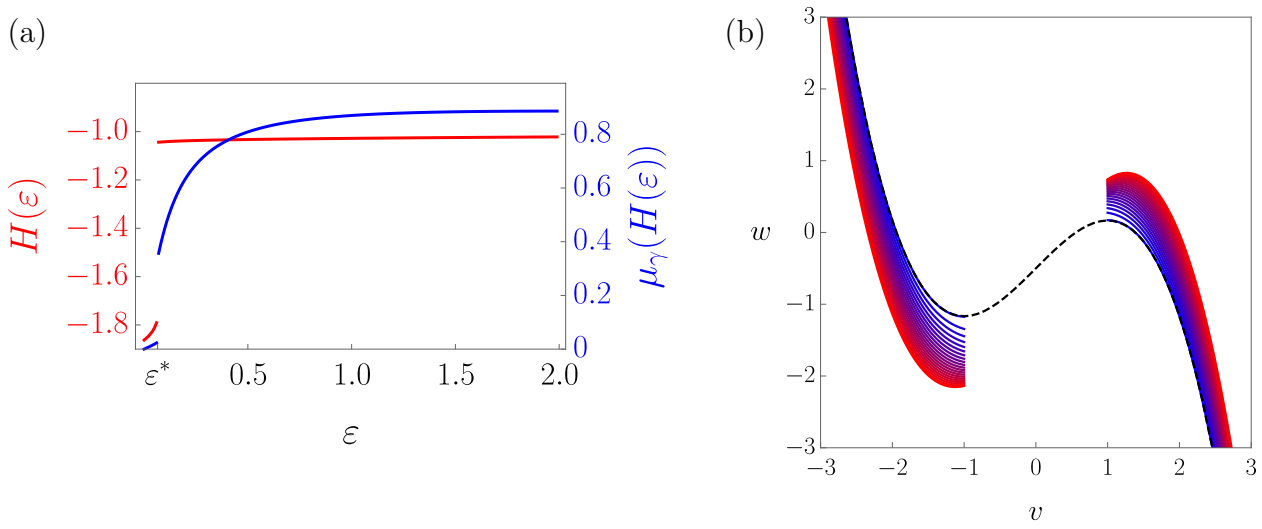

Figure 7: Tracking slow manifolds for arbitrary ε. (a) $H(\varepsilon)$ is the value of η to which we can track our perturbed slow manifolds, and $\mu_\gamma(H(\varepsilon))$ is an upper bound on the distance to the critical manifold. (b) A sampling of the asymptotic trajectories for various values of ε with coloring going from blue to red as ε increases from 0.0001 to 2.

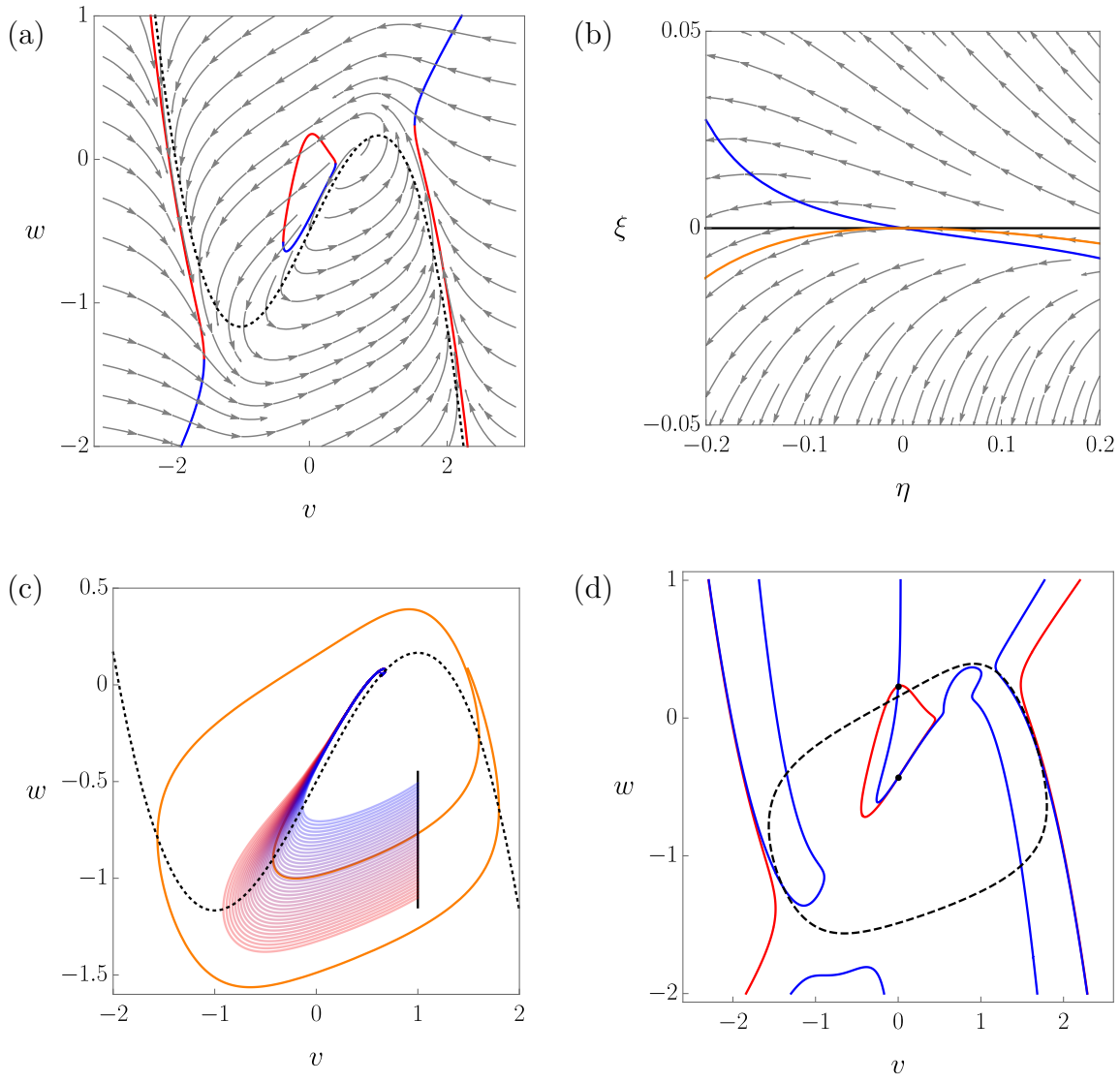

Figure 8: The river structure of the FHN system. (a) The ZCL (red and blue branches) and the v-nullcline (black dashed) presented together with a field of representative trajectories. (b) The LOR dynamics derived by taking the central blue portion of the ZCL as a basecurve. The correction is shown in blue, and the river identified in the frame is shown in orange. (c) The river (orange) and nearby trajectories (shaded from red to blue). We see that the river is highly unstable. (d) The ZCL in red and the set $\{\Delta_{1,3}(x) = 0\}$ in blue. In Theorem 3.3.3 we show that the two crossings of these curves, indicated by points, are confluences; the lower of these corresponds to the river show in (b) and (c).

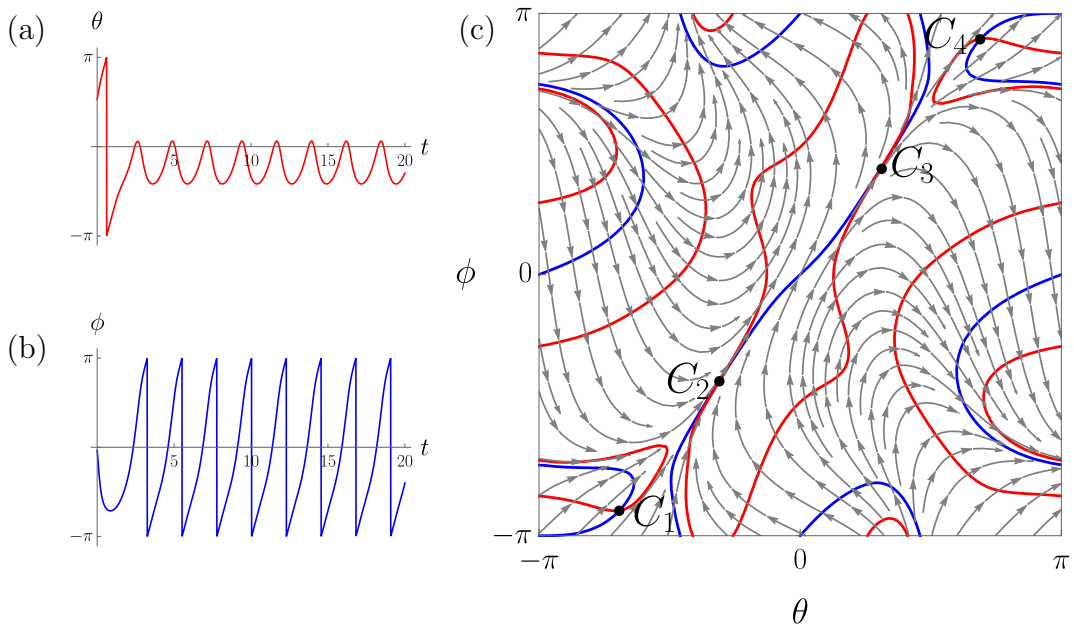

Figure 9: Dynamics of the theta model (3.12) with $I_1 = 1, I_2 = 2, g_1 = 1, g_2 = 3$. (a) A time plot of a representative solution of (3.12), with $\theta(t)$ in red and $\phi(t)$ in blue. Note that, after some initial transient dynamics, the system settles into regular oscillations. (b) The level sets $\Delta_{1,2}(x) = 0, \Delta_{1,3}(x) = 0$ in red and blue, respectively, along with a stream plot of the system. We see that these contours cross four times on $[-\pi, \pi]^2$, at points with coordinates $C_1, \ldots, C_4$ depicted here in black, and therefore we have four rivers.

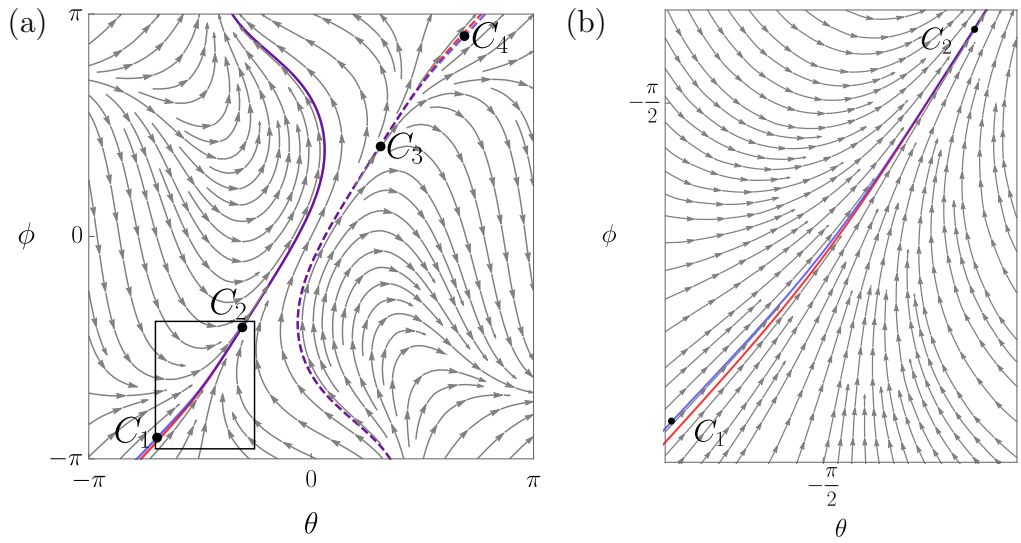

Figure 10: Rivers in the theta model (3.12) with $I_1 = 1, I_2 = 2, g_1 = 1, g_2 = 3$. (a) The four rivers of the system, issuing forth from $\{C_i\}$. In solid blue and red we have R_1, R_2, respectively, which are attracting rivers, and in dashed blue and dashed red we have R_3, R_4, respectively, which are repelling rivers. (b) A zoom of the rectangle shown in (a). Note the strong local contraction in the region near R_1 and R_2.

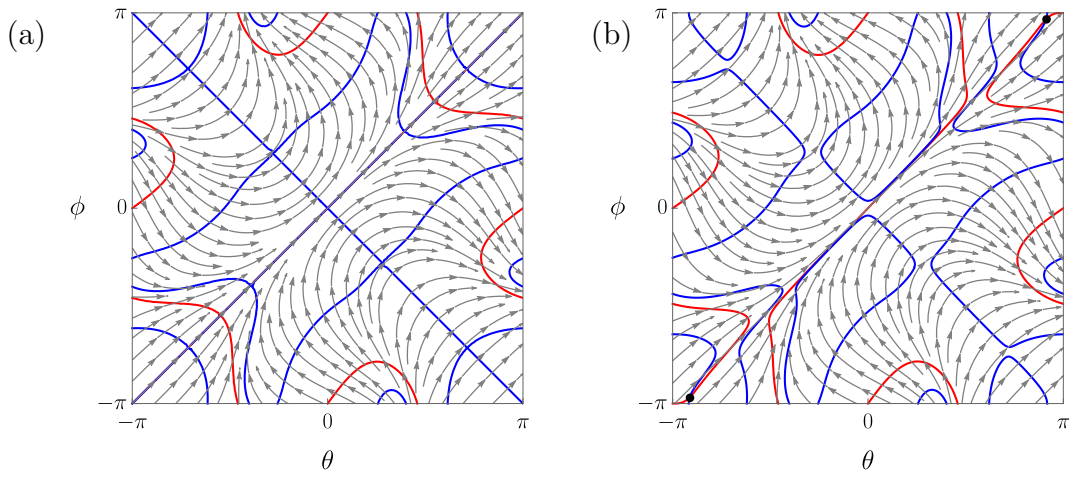

Figure 11: Theta model (3.12) with symmetry and after symmetry breaking. Parameter values common to both panels are $I_1 = 1, I_2 = 1, g_1 = 1$. (a) In the symmetric case with $g_2 = 1$, (3.12) has an invariant set $\{\theta = \phi\}$ that is a continuum of confluences. (b) In the case that $g_2 = 1.1$, with the parameter symmetry broken, the system has only two confluences (shown as black points), which lie close to the identity line.

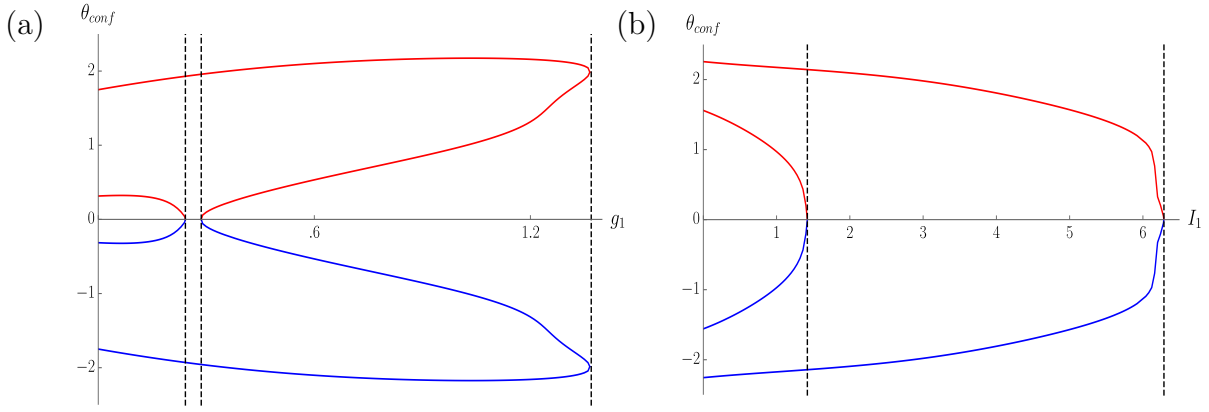

Figure 12: Confluence bifurcations in the theta model (3.12). We plot the branches of confluences as we vary a single parameter, with stable confluences in blue and unstable confluences in red. (a) Varying $g_1 \in [0, 1.3]$ yields four confluence bifurcations, including two at the same g_1 value. (b) Varying $I_1 \in [0, 6.4]$ yields two confluence bifurcations.

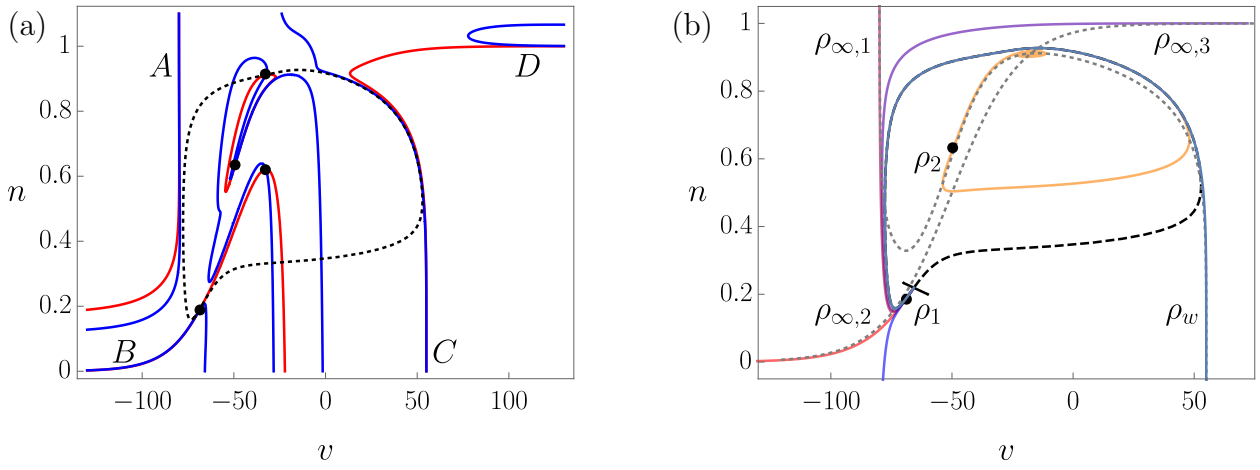

Figure 13: Analysis of rivers of (3.15) in the vicinity of an attracting periodic orbit (black dashed). (a) The sets $\{\Delta_{1,2}(x) = 0\}, \{\Delta_{1,3}(x) = 0\}$ appear in red and blue, respectively. We find that these sets cross to form confluences 4 times, shown here as black points, giving birth to 4 rivers. Letters A, B, C, D label curves along which $\{\Delta_{1,2}(x) = 0\}, \{\Delta_{1,3}(x) = 0\}$ come together asymptotically. (b) A phase plane view for system (3.15), including nullclines (grey dashed). We identify two dynamically relevant rivers $\rho_{1,2}$, three asymptotic rivers $\rho_{\infty,1,2,3}$, and one weak river.

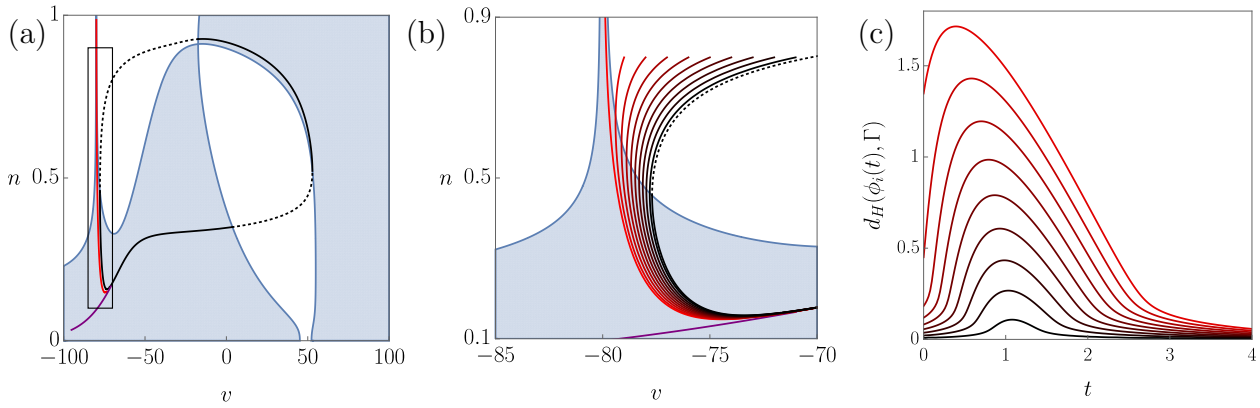

Figure 14: Studying the local stability of the limit cycle of (3.15). (a) The shaded blue regions depict the set $\{H(x) \leq 0\}$ ($H(x)$ is defined in the text) whose boundary, in darker blue, is $\{H(x) = 0\}$. The black curve is the limit cycle of (3.15), shown in solid where it belongs to $\{H(x) = 0\}$ and hence is locally attracting and dashed where locally repelling. In red and purple (lower left) are $\rho_{\infty,1}, \rho_{\infty,2}$ respectively. Where the limit cycle is locally unstable, the collective effects of $\rho_{\infty,1}, \rho_{\infty,2}$ serve to trap nearby trajectories near the limit cycle. (b) Zoomed view of the rectangle shown in (a). The additional curves are trajectories of (3.15). (c) The Hausdorff distance between the trajectories shown in (b) and the limit cycle Γ, which are color coordinated. Note that these distances initially increase, yet are well controlled by $d_H(\rho_{\infty,1}(t), \Gamma)$ (outermost red curve)

.

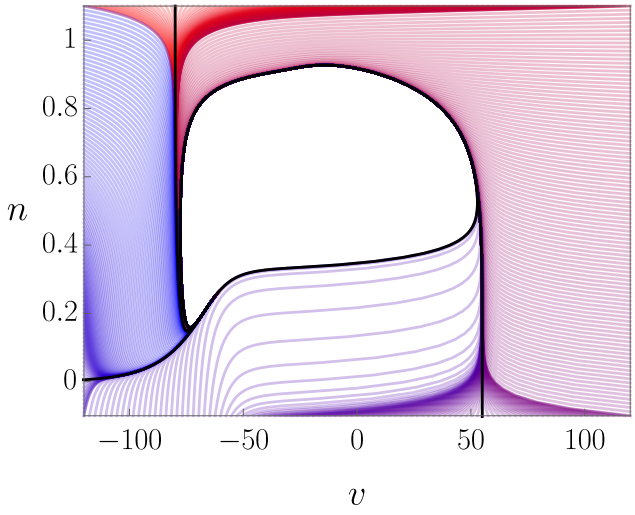

Figure 15: The dynamical effects of $\rho_{\infty,1}, \rho_{\infty,2}, \rho_w$. A plot of 1000 trajectories with initial conditions chosen uniformly along the rectangular boundary. More detail is provided in the text. We see that trajectories are drawn towards the three river features as they approach the limit cycle. Rivers allow us to identify transient features of the flow.

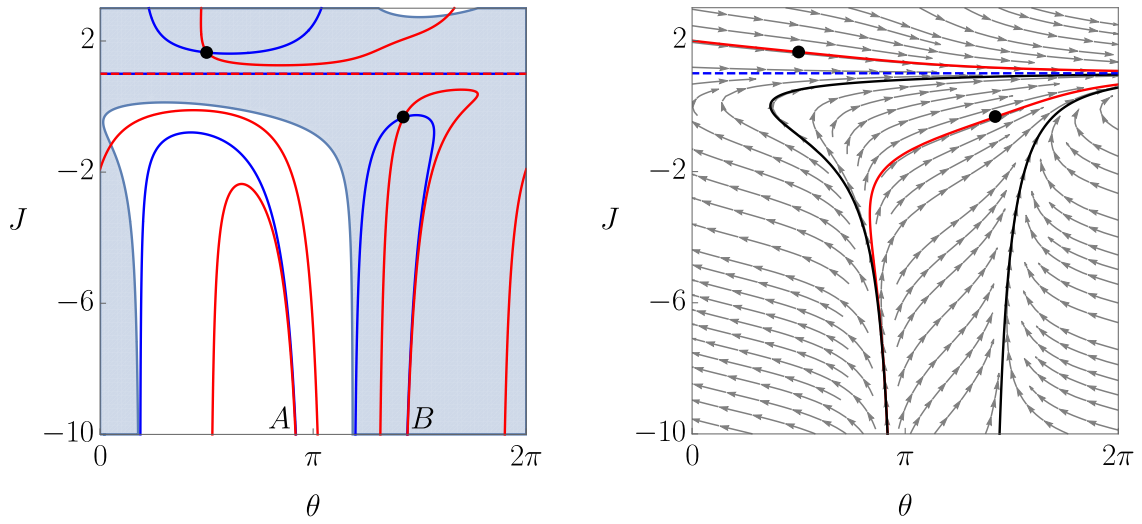

Figure 16: Rivers in system (3.16) with $I_E = \tau_I = 1$. In (a), the sets $\{\Delta_{1,2} = 0\}, \{\Delta_{1,3} = 0\}$, shown in blue and red respectively, cross transversely twice at the black points and intersect non-transversely along $\{J = 1\}$. The blue shaded region represents $\{H(x) \leq 0\}$, which is described in Section 3.6 of the main text. In (b), the rivers through the transverse crossings are shown in red and the to asymptotic rivers, which limit to the $\{\Delta_{1,2} = 0\}$ along the branches of $\{\Delta_{1,2} = 0\}$ and $\{\Delta_{1,3} = 0\}$ near A, B in (a), are shown in black.

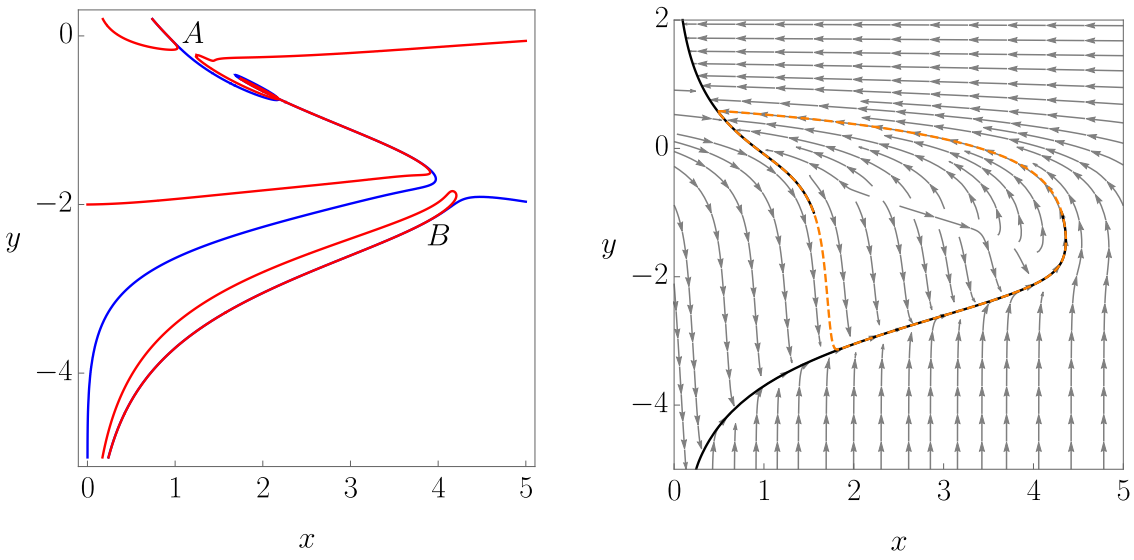

Figure 17: Rivers in system (3.18). (a) The sets $\{\Delta_{1,2} = 0\}, \{\Delta_{1,3} = 0\}$, shown in blue and red respectively, approach one another along the branches near A, B. These give rise to asymptotic rivers. While these sets lie near each other, they do not cross. (b) The asymptotic rivers, which limit to the $\{\Delta_{1,2} = 0\}$ along the branches near A, B, are shown in black. Shown in dashed orange is the limit cycle of the system.

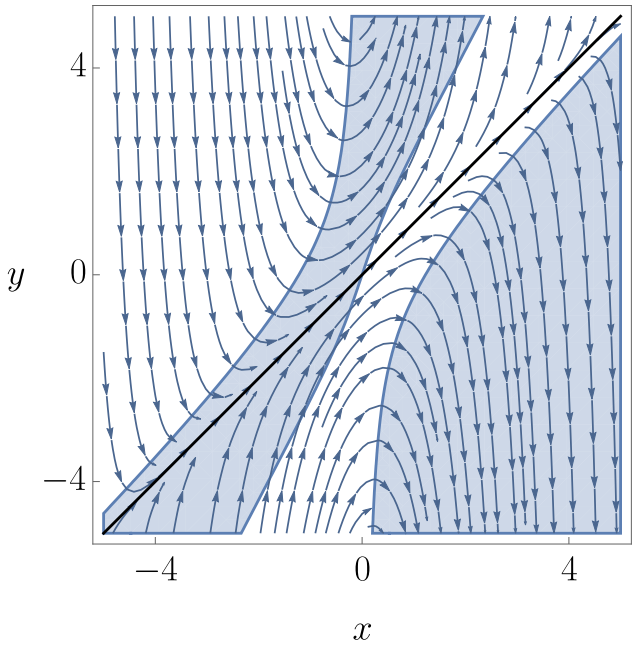

Figure 18: The river in system (3.19) along with representative trajectories. The blue region corresponds to $\{H(x) \leq 0\}$ (see Section 3.6 of the main text).

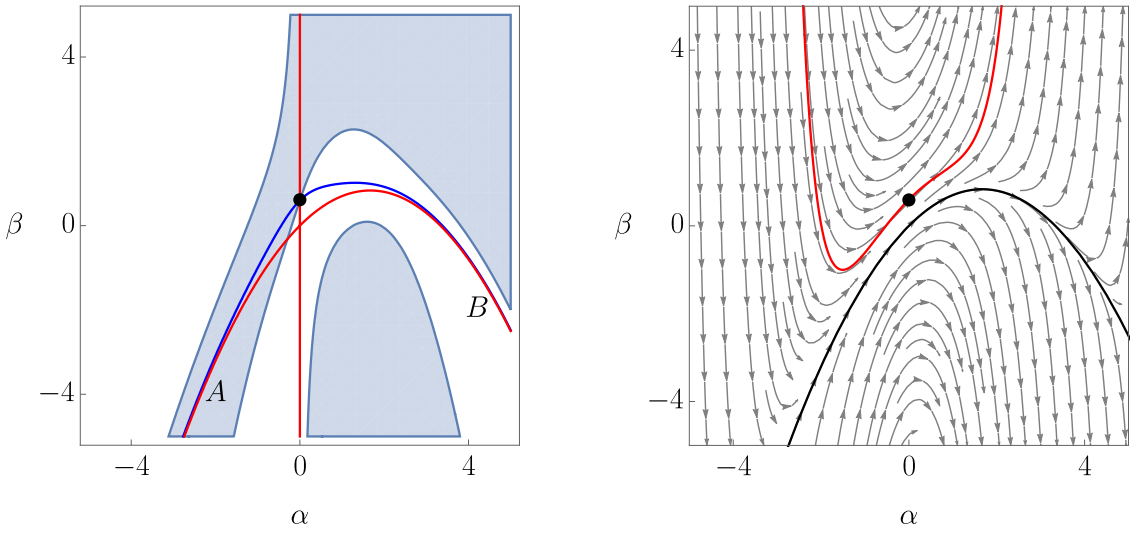

Figure 19: The rivers in the perturbed system (3.20) for $\varepsilon = 0.3$. (a) The sets $\{\Delta_{1,2} = 0\}, \{\Delta_{1,3} = 0\}$, shown in blue and red respectively, approach one another along the branches near A, B. These give rise to a double asymptotic river. The blue shaded region is $\{H(x) \leq 0\}$. (b) The doubly asymptotic river, which limits to the set $\{\Delta_{1,2} = 0\}$ along the branches near A, B, is shown in black. The red curve is the (non-asymptotic) river of the system.

4.0 Periodic Orbits and Transient Dynamics

The material in this chapter has been accepted for publication in SIADS as "LOR Analysis for Periodic Orbits: A One-stop Shop Approach" and was co-authored by Jonathan E. Rubin.

4.1 Identification of Periodic Orbits

In this section, we will use the LOR frame to reformulate the identification of a periodic trajectory into a boundary value problem (BVP) in a simplified geometry. To begin, we will assume that our LOR basecurve γ lies near a suspected periodic trajectory. Furthermore, we will suppose that γ is a simple closed curve. Without loss of generality, we parameterize γ to have period 2π (i.e., $\gamma(\eta + 2\pi) = \gamma(\eta)$).

4.1.1 From Basecurve to Periodic Orbit

Suppose that we are looking for periodic trajectories of the system

$$\dot{x} = f(x) \qquad\qquad x(0) = x_0 \tag{4.1}$$

where f is sufficiently smooth (continuosly differentiable will suffice) on an open set Ω. Suppose also that we suspect that our periodic trajectory lies near the curve $\gamma : \mathbb{R} \to \Omega$ which is a simple closed curve with period 2π. We will seek this periodic solution in the following way: we will choose a parameter value, say $\eta = 0$, and search the normal hyperplane of γ at $\eta = 0$ for an initial condition that returns to itself after some amount of time. In this respect, our technique is similar to studying Poincaré maps; however, the LOR frame allows us to use *geometric time* and hence to avoid computing the first return times associated with initial conditions.

In the LOR frame, with flow Φ_γ, we are looking for an initial condition $\eta = 0, \xi = \xi_0$ such that there exists a time $T > 0$ that satisfies $\Phi_\gamma((0, \xi_0), T) = (2\pi, \xi_0)$; recall that γ

is 2π-periodic, such that $\Psi(2\pi, \xi_0) = \Psi(0, \xi_0)$ and thus the initial condition with normal coordinates ξ_0 will be a T-periodic trajectory. Hence we have exchanged our initial value problem for a BVP of the form

$$\begin{pmatrix} \dot{\eta} \\ \dot{\xi} \end{pmatrix} = \mathcal{L}_\gamma f(\eta, \xi), \qquad \eta(0) = 0,\ \eta(T) = 2\pi,\ \xi(0) = \xi(T). \tag{4.2}$$

To eliminate the computation of the first return time T, we need a definition that we call *compatibility*. Intuitively, a parameterized curve is compatible with a vector field if the parameterization of the curve advances in the same direction as time along the flow.

Definition 4.1.1. A smooth curve $\gamma : I \to \Omega$ is compatible with a vector field $f : \Omega \to \mathbb{R}^n$ if

$$\langle T\gamma(\eta), f \circ \gamma(\eta) \rangle \neq 0 \qquad \forall \eta \in I.$$

Definition 4.1.1 allows us eliminate time from our LOR equations, as stated in the following result.

Lemma 4.1.2. *Given a compatible, Frenet, 2π-periodic curve γ, there exists $\delta > 0$ such that*

$$\frac{d\xi}{d\eta} = \frac{\dot{\xi}}{\dot{\eta}} =: g(\eta, \xi)$$

is well-defined and equivalent to the LOR dynamics for $(\eta, \xi) \in [0, 2\pi] \times B(0, \delta)$.

Proof. Compatibility guarantees that $\dot{\eta}|_{\xi=0}$ does not change signs. Hence by continuity there is a tube around $\{\xi = 0\}$ such that $\dot{\eta}$ is not zero. The claim of equivalence follows from standard ODE theory. □

Now that we can safely eliminate time from our ODE, we can restate our BVP as follows:

$$\frac{d\xi}{d\eta} = g(\eta, \xi), \qquad \xi(\eta = 0) = \xi(\eta = 2\pi). \tag{4.3}$$

Therefore, we have exchanged our autonomous, n-dimensional BVP with a variable endpoint for a non-autonomous, $(n-1)$-dimensional, periodic BVP. The key insight in this procedure is to use η as a time variable; in the LOR frame, η quantifies how trajectories advance along γ and hence serves as a natural geometric substitute for time, as long as γ is a compatible curve. To summarize, we have shown the following result.

Theorem 4.1.3. *Suppose that $\gamma : \mathbb{R} \to \Omega$ is a compatible, Frenet, 2π-periodic curve and $f : \Omega \to \mathbb{R}^n$ is a smooth vector field. There exists $\delta > 0$ such that*

$$\frac{d\xi}{d\eta} = g(\eta, \xi) \tag{4.4}$$

is well-defined and equivalent to the LOR dynamics for $(\eta, \xi) \in [0, 2\pi] \times B(0, \delta)$. If $\xi(\eta)$ solves the above ODE subject to $\xi(0) = \xi(2\pi)$, i.e., system (4.3), then there is a reparameterization of the curve $\Psi(\eta, \xi(\eta))$ that is a periodic solution to (4.1).

Thus, LOR provides an approach to identifiying periodic orbits via the solution of a single BVP, without a need to solve for the period itself.

Remark 6. In the statement of Theorem 4.1.3, we start from a basecuve γ and use the LOR equations to check for corresponding periodic orbits. This approach may suggest the question of whether every periodic orbit can be found this way. In fact, it is obvious that every periodic orbit Γ will solve a corresponding LOR BVP as given in Theorem 4.1.3, derived trivially by using Γ itself as the basecurve. On the other hand, there is no reason to expect that a single such BVP could be used to identify all periodic orbits of a system if more than one is present.

We also note that this technique will identify periodic trajectories regardless of their stability type. If a periodic solution is not attracting, then the numerical implementation of the technique may become more complicated, but the theory does not change.

4.1.2 An Example of Identifying a Periodic Orbit with LOR

In this section, we use our LOR approach to identify a periodic orbit in a four-dimensional, competitive Lotka-Volterra type ecosystem model and describe a generic technique for constructing LOR basecurves computationally that we find useful in practice. We consider the system

$$\dot{x}_i = r_i x_i \left(1 - \sum_{j=1}^{4} \alpha_{i,j} x_j\right) \qquad i \in \{1, 2, 3, 4\} \tag{4.5}$$

where $r_i, \alpha_{i,j}$ are positive parameters. The quantities x_i represent the relative populations of four competing species, the parameter r_i quantifies the rate at which x_i would grow in

the absence of competitors, and the parameter $\alpha_{i,j}$ represents the effect of population x_j on population x_i for each i, j; we require that $\alpha_{i,i} = 1$ to impose a logistic-type carrying capacity on each species.

We choose values of $r_i, \alpha_{i,j}$ near those used in [65] to demonstrate that system (4.5) displays chaotic behavior, but we decrease $\alpha_{1,2}, \alpha_{1,3}$ slightly to avoid entering a regime of period-doubling bifurcations. Specifically, we use

$$r = \begin{pmatrix} 1 \\ 0.72 \\ 1.53 \\ 1.27 \end{pmatrix} \qquad \alpha = \begin{pmatrix} 1 & 0.7 & 1.2 & 0 \\ 0 & 1 & 0.44 & 1.36 \\ 2.33 & 0 & 1 & 0.47 \\ 1.21 & 0.51 & 0.35 & 1 \end{pmatrix}$$

where we have vectorized the parameter sets $\{r_i\}, \{\alpha_{i,j}\}$ in the obvious way.

To begin the process of locating a periodic orbit for system (4.5), we choose a sample trajectory of the system, say the trajectory ϕ such that $\phi(0) = (.5, .5, .5, .5)$. After some initial transient dynamics, we note that ϕ is "nearly-recurrent"; that is, it passes near itself, specifically in the time window $[47, 100]$, which is shown in Fig. 20. We will use this nearly-recurrent trajectory to construct an admissible, simple closed curve which will serve as the basecurve for LOR, which we will apply to identify the periodic orbit of the system.

Recall that a curve γ is admissible if it satisfies $\langle f \circ \gamma(\eta), T\gamma(\eta) \rangle > 0$ for η in the domain of γ; if γ is a trajectory, then we have $\langle f \circ \gamma(\eta), T\gamma(\eta) \rangle = \|\gamma'(t)\| > 0$ and thus all trajectories are admissible curves. To construct a simple closed curve which is likely to be admissible, we compute the truncated Fourier series for each coordinate of ϕ; as ϕ is admissible and nearly-recurrent, our hope is that the Fourier approximation of ϕ, call it $\bar{\phi}$, will also be admissible. Note that $\bar{\phi}$ will be simple and closed by construction, with period 2π.

In general, we recommend constructing a basecurve as follows: first identify a trajectory ϕ which is nearly-recurrent, which is to say there is are times t_1, t_2 such that $\|\phi(t_1) - \phi(t_2)\| < \delta$, where δ is a tolerance parameter. Second, for each vector component of ϕ we compute the truncated Fourier series, considering terms up to some maximum frequency F. Third, we check to see if our computed basecurve is admissible; if the computed curve is not admissible, we can increase F and allow more terms in our approximation. If allowing more terms does

not yield an admissible curve, then we decrease the initial tolerance δ and reselect our trajectory ϕ.

For system (4.5) and trajectory ϕ we find that a Fourier approximation with three terms suffices; the approximation $\bar{\phi}$ is an admissible curve that can be used to identify the periodic orbit of (4.5). We proceed with the exact process described in the preceding section: we compute the Frenet frame for $\bar{\phi}$, compute the LOR equations of system (4.5) with basecurve $\bar{\phi}$, and then solve the $d\xi/d\eta$ BVP (4.3) to identify the periodic orbit.

We remark that there is an efficient way to implement the computation of the Frenet frame and the LOR equations with basecurve $\bar{\phi}$. Note that the derivatives of Fourier approximations are themselves Fourier approximations. Thus the vectors of the Frenet frame can be expressed as rational functions (perhaps with square roots) of trigonometric functions and the LOR equations can be similarly represented. The formulation allows us to perform computations on the sequences of Fourier coefficients, as opposed to operating on large combinations of trigonometric functions.

The results of this analysis are summarized in Fig. 20. Standard techniques for identifying a periodic orbit would require searching a three-dimensional transverse section of the flow for a fixed point of the Poincaré map, which would involve the computation of many trajectories. The LOR approach completely eschews the need to estimate the period of the cycle and only requires computing a single trajectory, producing a Fourier approximation of this trajectory, and solving a three-dimensional fixed-endpoint BVP.

4.2 Identifying Periodic Orbits in the Plane

4.2.1 Planar LOR Stability

We begin by presenting the LOR BVP technique, described in the preceding section, in the planar case. Given the simplicity of the LOR dynamics in two-dimensional systems, we will also derive a quantity for testing the stability of planar periodic trajectories. We generalize this stability quantity in the following section and show it is functionally equivalent

to the Floquet stability test.

Corollary 8. *Suppose that $f : \Omega \to \mathbb{R}^2$ is a $\mathscr{C}^1$ vector field, and $\gamma : [0, 2\pi] \to \Omega$ is a simple, regular, $\mathscr{C}^2$ curve such that $\gamma(0) = \gamma(2\pi)$. Then (4.3) becomes*

$$g(\eta, \xi) = \frac{\mathscr{L}_{\gamma,2}(\eta, \xi)}{\mathscr{L}_{\gamma,1}(\eta, \xi)} = \|\gamma'(\eta)\| \, (1 - \xi\kappa_\gamma(\eta)) \frac{\langle f \circ \Psi_\gamma(\eta, \xi), N\gamma(\eta)\rangle}{\langle f \circ \Psi_\gamma(\eta, \xi), T\gamma(\eta)\rangle}$$

on the domain where $\langle f \circ \Psi_\gamma(\eta, \xi), T\gamma(\eta)\rangle \neq 0$.

Furthermore, the periodic orbit ϕ, the periodic trajectory through $x_0 = \Psi_\gamma(\eta_0, \xi_0)$, is stable if and only if $\lambda < 0$, where

$$\lambda := \int_0^{2\pi} \frac{\partial}{\partial \xi} g(\eta, \xi^*(\eta)) \, d\eta. \tag{4.6}$$

Proof. The first claim follows directly from Theorem 4.1.3 after simplifying the LOR dynamics. To study the stability of $\xi^*(\eta)$ we will exploit the geometry of the LOR frame with a closed basecurve. Now, note that $(0, \xi^*(0)) \in \{\langle f \circ \Psi_\gamma(\eta, \xi), T\gamma(\eta)\rangle \neq 0\}$ by assumption, and therefore $f \circ \Psi_\gamma(0, \xi^*(0))$ is transverse to $N\gamma(0)$. Thus, given $\delta > 0$ we can define

$$\Sigma_\delta = \{\gamma(0) + \xi N\gamma(0) | \xi^*(0) - \delta < \xi < \xi^*(0) + \delta\},$$

for δ sufficiently small such that Σ_δ is a transverse section to ϕ at $\phi(0)$. We can choose $\delta, \bar{\delta} > 0$ such that there exists a Poincaré return map $P : \Sigma_\delta \to \Sigma_{\bar{\delta}}$ with $P(\phi(0)) = \phi(0)$. Given any $x \in \Sigma_\delta$, there is a unique ξ_x such that $x = \gamma(0) + \xi_x N\gamma(0)$, provided that x is sufficiently close to $\gamma(0)$. Therefore there is a mapping $\hat{P} : (\xi^*(0) - \delta, \xi^*(0) + \delta) \to (\xi^*(0) - \delta, \xi^*(0) + \delta)$ such that

$$P(x) = P(\gamma(0) + \xi_x N\gamma(0)) = \gamma(0) + \hat{P}(\xi_x) N\gamma(0).$$

Note that, given $x, y \in \Sigma_\delta$, $\|P(x) - P(y)\| = \left|\hat{P}(\xi_x) - \hat{P}(\xi_y)\right|$; thus, $\phi(0)$ is a stable fixed point of $P(x)$ if and only if $\xi^*(0)$ is a stable fixed point of $\hat{P}(\xi)$. Given $x \in \Sigma_\delta$ denote the first return time function by $t(x)$. Then $P(x) = \Phi(x, t(x))$ where $\Phi(x, t)$ denotes the flow induced by $\dot{x} = f(x)$, and by construction $\Phi(x, t) = \Psi_\gamma \circ \hat{\Phi}(\Psi_\gamma^{-1}(x), t)$ where $\hat{\Phi}$ denotes the LOR flow. Therefore $\hat{P}(\xi) = \pi_2 \hat{\Phi}((0, \xi), t(\Psi_\gamma((0, \xi)))$, where π_2 is projection onto $(0, 1)$.

By shrinking $\delta > 0$ as necessary, we can assume that $g(\eta, \xi)$ remains bounded for all trajectories with initial conditions in $B \cap \{\eta = 0\}$ for

$$B := \{(\eta, \xi^*(\eta)) + (0, \xi) | -\delta < \xi < \delta, 0 \leq \eta \leq 2\pi\}.$$

Solving equation (4.4) with $\xi(0) \in B \cap \{\eta = 0\}$ defines $\hat{P}(\xi)$, and the expression (4.6) defines the corresponding eigenvalue, which determines stability of fixed points of $\hat{P}(\xi)$ and hence of the periodic orbit $\phi(t)$, as desired. □

Corollary 9. *Suppose that $f : \Omega \to \mathbb{R}^2$ is a $\mathscr{C}^1$ vector field and that $\Gamma(t)$ is a T-periodic trajectory of $\dot{x} = f(x)$. Γ is asymptotically stable if and only if $\lambda < 0$ where*

$$\lambda = \int_0^T \langle [D_x f \circ \Gamma(t)] N\Gamma(t), N\Gamma(t) \rangle \, dt.$$

Proof. Taking Γ as a LOR basecurve, our BVP (4.4) has $\xi \equiv 0$ as a solution. The result follows from the previous stability analysis and computing $\partial_\xi g(\eta, 0)$. □

With a slight modification to this technique, we can track a periodic trajectory as we vary parameters, which may be present in our flow. Suppose that our original vector field is of the form $f : \mathbb{R}^2 \times \Lambda \to \mathbb{R}^2$, where $\Lambda \subseteq \mathbb{R}^m$ is a set of parameter values. Then, given a basecurve γ, it is simple to see that equation (4.4) will become

$$\frac{d\xi}{d\eta} = g(\eta, \xi(\eta); \lambda) \qquad \xi(0) = \xi(2\pi)$$

where $\lambda \in \Lambda$ is a parameter value. Suppose that we can solve the above for $\lambda_0 \in \Lambda$, that is, we have a solution $\xi(\eta; \lambda_0)$.

4.2.2 Periodic orbits in the FitzHugh-Nagumo Equations

We will now illustrate the utility of the LOR approach by considering the stable limit cycle of the FitzHugh-Nagumo (FHN) equations. Of course, we could proceed in the standard fashion: by identifying a positively invariant compact region, invoking Poincaré-Bendixson, identifying an appropriate Poincaré section, computing a return map and studying the stability of its fixed point. None of these steps is difficult on its own, but by computing a single LOR transformation, we can essentially achieve a complete analysis in one fell swoop.

Specifically, we will find the periodic solution of the system

$$\begin{aligned} \dot{v} &= v - \frac{v^3}{3} - w - I \\ \dot{w} &= \varepsilon(v + a - bw), \end{aligned} \tag{4.7}$$

initally taking the parameter values $a = -0.6, b = 0.8, I = 0.5, \varepsilon = 0.3$. The choices of a, b, I eliminate any symmetries that make the periodic orbit easier to find, and our choice of ε of a similar magnitude to the other parameters eliminates any strong fast-slow structure.

To start, we face the question of how to choose a basecurve to find a periodic orbit. In fact, nothing special is needed; we choose γ to be the simplest closed curve: a circle. We take the center and the radius of the circle so that γ lies inside the region where a quick check of the direction field hints at rotation. Specifically, we let

$$\gamma(\eta) = \left(\frac{3}{5}\cos(\eta), \frac{3}{5}\sin(\eta) - \frac{3}{5}\right) \tag{4.8}$$

as shown in Figure 21 and compute $\|\gamma'(\eta)\| = 1/\kappa_\gamma(\eta) = 3/5$, $T\gamma(\eta) = (-\sin(\eta), \cos(\eta))$ and $N\gamma(\eta) = (-\cos(\eta), -\sin(\eta))$. Therefore $\mathcal{U}_\gamma = (-\infty, \infty) \times (-\infty, 5/3)$ and $\Psi_\gamma(\mathcal{U}_\gamma) = \mathbb{R}^2 \setminus \{(0, -3/5)\}$. Our LOR equations take the form

$$\begin{aligned} (5 - 3\xi)\dot{\eta} &= \sum_{j=0}^{2} \alpha_{1,j}(\xi)\cos(j\eta) + \sum_{j=1}^{4} \alpha_{2,j}(\xi)\sin(j\eta) \\ \dot{\xi} &= \sum_{j=0}^{4} \beta_{1,j}(\xi)\cos(j\eta) + \sum_{j=1}^{2} \beta_{2,j}(\xi)\sin(j\eta) \end{aligned} \tag{4.9}$$

where

$$\alpha_{1,0}(\xi) = \frac{1+\varepsilon}{2} \qquad \beta_{1,0}(\xi) = -\frac{(3-5\xi)(100b\varepsilon + (7+5\xi)(5\xi-13))}{1000}$$
$$\alpha_{1,1}(\xi) = \frac{\varepsilon(5a+3b)}{3-5\xi} \qquad \beta_{1,1}(\xi) = \frac{5I-3}{500}$$
$$\alpha_{1,2}(\xi) = \frac{\varepsilon-1}{2} \qquad \beta_{1,2}(\xi) = -\frac{(3-5\xi)(66+75b\varepsilon+5(6-5\xi)\xi)}{750}$$
$$\alpha_{2,1}(\xi) = \frac{5I-3}{3-5\xi} \qquad \beta_{1,3}(\xi) = 0$$
$$\alpha_{2,2}(\xi) = -\frac{141+150b\varepsilon+5(6-5\xi)\xi}{300} \qquad \beta_{1,4}(\xi) = \frac{(3-5\xi)^2}{3000}$$
$$\alpha_{2,3}(\xi) = 0 \qquad \beta_{1,1}(\xi) = -\frac{\varepsilon(5a+3b)}{500}$$
$$\alpha_{2,4}(\xi) = \frac{(3-5\xi)^2}{600} \qquad \beta_{1,2}(\xi) = \frac{(1-\varepsilon)(3-5\xi)}{10}.$$

.

A quick glance at system (4.9) might suggest that we have made our problem much more difficult; indeed, we find that the LOR dynamics can be analytically intractable.

Note that in (4.9), η only appears in the arguments of trigonometric functions. Therefore, our LOR equations are 2π-periodic in η; this property is inherited from the 2π-periodicity of γ. In other words, we have separated the rotational properties of our flow from its contractive properties.

First, we will demonstrate that a periodic orbit does, in fact, exist for these parameter values. There is exactly one fixed point in (v, w) space, which is unstable. Note that, in Figure 21(b), the ξ-nullcline does not cross the line $\xi = -6$; hence, $\dot{\xi}$ does not change signs along $\xi = -6$. Specifically, we can compute analytically that $\langle f \circ \Psi_\gamma(\eta, -6), N\gamma(\eta)\rangle > 0$ for $\eta \in [0, 2\pi]$. Interpreting this condition geometrically, the flow along the circle defined by $\Psi_\gamma(\eta, -6)$ (which is the circle of radius $6+3/5$ centered at $(0, 3/5)$ in (x, y) space) must have only inward flux, as $N\gamma(\eta)$ points inwards. That is, we have shown that the circle $\Psi_\gamma(\eta, -6)$ is positively invariant, which we observe is more straightforward than finding an explicit trapping region from (4.7) directly. The Poincaré-Bendixson Theorem gives us a periodic orbit inside $\Psi_\gamma([0, 2\pi], -6)$.

With existence established, we next use the LOR frame to compute the actual periodic orbit. We consider the non-autonomous boundary value problem (BVP) given in (4.4) with

basecurve γ specified by (4.8), on a region where $1/\dot{\eta}$ is well-defined. We implement a standard shooting algorithm in Mathematica to find a solution to (4.4), which we denote $\xi_p(\eta)$, on this region. That is, $\xi_p(\eta)$ is a solution to a temporal re-scaling of (4.9), and hence $\Psi_\gamma(\eta, \xi_p(\eta))$ is a temporal rescaling of a trajectory, which in turn is a periodic orbit, from Theorem 4.1.3. The relevant orbit is shown in the LOR frame and in the original phase plane in Figure 21.

Note that, if we were to try this BVP approach in (v, w) space, by solving $dw/dv = \dot{w}/\dot{v}$, we could not find the periodic solution, as any periodic orbit must cross each of the v, w nullclines at least twice and hence $dw/dv, dv/dw$ must each blow up twice along any such cycle. Thus, we would be faced with solving at least four separate BVPs with a chain of boundary conditions. By pulling our flow back onto γ, we reduce the complexity of our task.

There are several additional advantages of this approach. First, solving first order non-autonomous boundary value problems with periodic forcing is a fairly standard capability of most numerical integrators and the existence/uniqueness of such solutions is fairly well understood. Second, we have eliminated all temporal dependence in finding a limit cycle; we are computing an invariant 1-manifold that is diffeomorphic to S^1, our basecurve, hence in this formulation there is no need to guess the period of the underlying solution. Third, this method is robust to changes in parameters and can be used to study periodic orbit parameter dependence as demonstrated in Figure 22. This technique also becomes more powerful in higher dimensions, where we can use analogous ideas to identify invariant manifolds that are diffeomorphic to tori and n-spheres.

To generate each panel of Figure 22, we vary one parameter over an mesh of values within an interval and, for each value, we numerically solve the LOR BVP (4.4) with basecurve from (4.8) to find the periodic orbit. The coloration is added to emphasize the progression of each parameter. In (a), for example, we vary $\varepsilon \in [0.01, 0.7414]$; the blue curve corresponds to the computed periodic orbit for $\varepsilon = 0.01$, the red curve corresponds to the computed periodic orbit for $\varepsilon = 0.7414$, and the remaining curves are also periodic orbits colored uniformly as ε increases.

To conclude, we note that we can also assess the stability of a periodic trajectory computed via (4.4) by direct integration, as specified in (4.6) in Theorem 4.1.3. For the FHN

limit cycle we have identified, we find $\lambda \approx -9.1$, and thus the periodic orbit identified by our method is stable.

4.3 Analysis near Periodic Orbits

In this section, we will demonstrate that the LOR frame can be used to decouple the temporal and normal dynamics near a periodic orbit. Using this decoupling, we can study the stability of the underlying orbit and, in $\mathbb{R}^3$, construct novel invariant manifolds that organize the local phase space and identify regions of phase advance and retreat relative to an attracting periodic orbit.

Suppose that Γ is a T-periodic solution to (4.1). For convenience, although we may very well have found Γ using a first LOR transformation, we will now use Γ as a basecurve for LOR, and we denote the flow for the new LOR system by Φ_Γ. Note that when we use Γ as a basecurve, we define LOR on $[0, T)$ rather than on $[0, 2\pi)$, since the period T is now a known quantity. The stability of Γ can be computed from the original LOR equations that are used to find it (see the preceding section for the planar case). Alternatively, deriving new LOR equations based on Γ requires just one additional step, with the advantage that the LOR equations simplify somewhat if the basecurve is a trajectory of the flow being studied. Specifically, we will use the Frenet Frame based along the trajectory in question as a normal frame and analyze the LOR blow-up coordinates.

4.3.1 Radial Dynamics: Stability

Note that Γ is compatible, and hence there is a tube around $\{\xi = 0\}$ on which $d\xi/d\eta$ is well-defined. To better understand the LOR dynamics, we will change coordinates by decomposing ξ into radial and angular components. Specifically, we define $r = \|\xi\|, u = \xi/r$. Intuitively, r measures the Hausdorff distance from the periodic orbit and u represents the bearing in the normal hyperplane within the LOR frame. We can derive dynamics on r, u

from Theorem 4.1.3:

$$\begin{pmatrix} r' \\ u' \end{pmatrix} = \begin{pmatrix} \langle g(\eta, ru), u \rangle \\ \dfrac{g(\eta, ru) - \langle g(\eta, ru), u \rangle u}{r} \end{pmatrix} \tag{4.10}$$

for $r > 0$, where $' = d/d\eta$. System (4.10) appears to be ill-defined at $r = 0$; however, the dynamics actually extends continuously to $r = 0$. To establish this property, note that $g(\eta, 0) = 0$ and that the limit

$$\lim_{r \to 0^+} \frac{g(\eta, ru) - \langle g(\eta, ru), u \rangle u}{r} = [D_\xi g(\eta, 0)]u - \langle [D_\xi g(\eta, 0)]u, u \rangle u$$

is a well-defined L'Hopital type limit.

In fact, since we are interested in the $r \ll 1$ regime, we will consider the Taylor expansion of the r, u dynamics from (4.10), given by

$$\begin{aligned} r' &= \langle [D_\xi g(\eta, 0)]u, u \rangle r + \mathcal{O}(r^2) \\ u' &= [D_\xi g(\eta, 0)]u - \langle [D_\xi g(\eta, 0)]u, u \rangle u + \mathcal{O}(r). \end{aligned} \tag{4.11}$$

We compute that $D_\xi g(\eta, 0) = D_\xi N f(\eta, 0) - C(\eta)$. Interestingly, as $C(\eta)$ is anti-symmetric, $\langle C(\eta)u, u \rangle = 0$. Hence, the curvature matrix does not directly influence the r dynamics yet can affect the evolution of u.

Note that the set $\{r = 0\}$, which corresponds to $\{\xi = 0\}$ in our original LOR coordinates, is invariant, as expected. Furthermore we have uncovered nontrivial angular dynamics on $\{r = 0\}$; intuitively, this dynamics captures how trajectories rotate around Γ for $r \ll 1$. This approach is similar in spirit to geometric desingularization, or blow-up, techniques, and the LOR frame allows us to perform these computations in a tractable way.

We can use the order expansion (4.11) to study both the stability of Γ and the transient angular dynamics governing trajectories in a neighborhood of Γ. Our plan of attack is as follows. For small r, we note that the $r = 0$ terms will dominate the u dynamics in (4.11), which decouples from r in the $r \to 0$ limit. Thus, we will approximate u by a solution $\tilde{u}$ that solves the second equation from (4.11) with $r = 0$, and then we will use this approximation to estimate the behavior of r.

Theorem 4.3.1. *Suppose that* $(r(\eta), u(\eta))$ *solve* (4.10) *subject to initial conditions* $(r(0), u(0)) = (r_0, u_0)$ *and that* $\tilde{u}(\eta)$ *solves*

$$\tilde{u}' = [D_\xi g(\eta, 0)]\tilde{u} - \langle [D_\xi g(\eta, 0)]\tilde{u}, \tilde{u}\rangle\, \tilde{u}, \qquad \tilde{u}(0) = u_0. \tag{4.12}$$

Let $\tilde{r}(\eta)$ *be defined by*

$$\tilde{r}(\eta) = r_0 \exp\left(\int_0^\eta \langle [D_\xi N f(s, 0)]\tilde{u}(s), \tilde{u}(s)\rangle\, ds\right)$$

There exist constants $C_1, C_2, L_1, L_2 > 0$ *such that*

$$\begin{aligned} \|u(\eta) - \tilde{u}(\eta)\| &\leq C_1 r_0 \exp(L_1 t) \\ |r(\eta) - \tilde{r}(\eta)| &\leq C_2 r_0^2 \exp(L_2 t) \end{aligned} \tag{4.13}$$

for $t \geq 0$.

Proof. We approximate the solution $(r(\eta), u(\eta))$ to (4.10) where $r(0) \ll 1$; namely we let $\varepsilon = r(0)$ and expand

$$\begin{aligned} r(\eta) &= \varepsilon r_1(\eta) + \mathcal{O}(\varepsilon^2) \\ u(\eta) &= u_0(\eta) + \mathcal{O}(\varepsilon). \end{aligned}$$

The ε^0 term of $r(\eta)$ vanishes, as $\{r = 0\}$ is invariant under (4.10). Expanding the derivatives of r, u we find

$$\begin{aligned} r_1' &= \langle [D_\xi g(\eta, 0)]u_0(\eta), u_0(\eta)\rangle\, r_1 \\ u_0' &= [D_\xi g(\eta, 0)]u_0 - \langle [D_\xi g(\eta, 0)]u_0, u_0\rangle\, u_0 \end{aligned}$$

where $r_1(0) = \varepsilon, u_0(0) = u_0^*$. Note that these are the dynamics of $\bar{r}, \bar{u}$; standard perturbation theory yields our exponential bounds. □

Therefore, we can study the stability of Γ by considering integrals of a quadratic form. Denote by $\Phi_\Gamma^a : S^{n-2} \times \mathbb{R} \to S^{n-2}$ the flow induced by the angular equation (4.12), and define the mapping $L : S^{n-2} \to \mathbb{R}$ by

$$L(u_0) = \int_0^T \langle D_\xi N f(\eta, 0) \Phi_\Gamma^a(u_0, s), \Phi_\Gamma^a(u_0, s) \rangle \, \mathrm{d}s.$$

We can use this function to completely characterize the stability of Γ.

Corollary 10. *If $L(u_0) < 0$ for all $u_0 \in S^{n-2}$, then Γ is a stable periodic orbit. If Γ is an unstable periodic orbit, then there exists a $u_0^* \in S^{n-2}$ such that $L(u_0^*) \geq 0$.*

Proof. If $L(u_0) < 0$ for a point $u_0 \in S^{n-2}$, then for any initial condition (r_0, u_0) the solution to (4.10) has

$$r(T) = |r(T) - \tilde{r}(T) + \tilde{r}(T)| \leq r_0 \exp(L(u_0)) + C_2 r_0^2 \exp(L_2 T) \tag{4.14}$$

for each u_0. Since $L(u_0) < 0$ and T is fixed, we can choose $r_0 > 0$ sufficiently small to guarantee from (4.14) that $r(T) < r_0$. Therefore, since $r = \|\xi\|$, we have shown that trajectories sufficiently close to Γ become closer to Γ after one period and thus Γ is stable. The second claim follows analogously. □

We have derived a novel approach to studying the stability of a periodic orbit that is more geometric in spirit than the standard linearization technique; the two methods are related though, as

$$D_\xi N f(\eta, 0) = \begin{pmatrix} \langle [J(\eta)] N_1\Gamma(\eta), N_1\Gamma(\eta) \rangle & \cdots & \langle [J(\eta)] N_k\Gamma(\eta), N_1\Gamma(\eta) \rangle \\ \langle [J(\eta)] N_1\Gamma(\eta), N_2\Gamma(\eta) \rangle & \cdots & \langle [J(\eta)] N_k\Gamma(\eta), N_2\Gamma(\eta) \rangle \\ \vdots & \ddots & \vdots \\ \langle [J(\eta)] N_1\Gamma(\eta), N_k\Gamma(\eta) \rangle & \cdots & \langle [J(\eta)] N_k\Gamma(\eta), N_k\Gamma(\eta) \rangle \end{pmatrix} \tag{4.15}$$

where $J(\eta) = D_x f \circ \Gamma(\eta)$ is the Jacobian of the vector field of (4.1) evaluated along its periodic solution Γ. If we define the $k \times n$ matrix $N\Gamma(\eta) = (N_1\Gamma(\eta), N_2\Gamma(\eta), \cdots, N_k\Gamma(\eta))^T$ then the above simplifies to $D_\xi N f(\eta, 0) = N\Gamma(\eta) J(\eta) N\Gamma(\eta)^T$, which is the projection of the linearized dynamics of (4.1) into the normal space of the curve Γ. This quantity appears

as $H(x)$ in Section 3.6 of [45], in the study of regions of flow contraction in a Hodgkin-Huxley type planar system, and also arises in [51], where Nave and Ross use it to identify coherent Lagrangian structures. Next, we show that by separating the rotational and radial components of the normal flow, we can easily identify regions of contraction and expansion of trajectories in the neighborhood of Γ.

4.3.2 Angular Dynamics: Organizing Transient Behavior

In this section we will study the angular dynamics of the (r, u) system (4.11) and show that we can use T-periodic solutions of the $r = 0$ subsystem to construct invariant manifolds that organize the transient dynamics near a Γ.

Recall from (4.11) that the $r = 0$ subsystem has the form

$$\frac{du}{d\eta} = [D_\xi g(\eta, 0)]u - \langle [D_\xi g(\eta, 0)]u, u\rangle\, u$$

and hence is a non-autonomous ODE on the hypersphere S^{n-2}, with flow that we denote Φ^a_Γ. As the vector field is cubic, and therefore odd, the angular flow Φ^a_Γ is antipode-preserving; that is, $\Phi^a_\Gamma(-u, \eta) = -\Phi^a_\Gamma(u, \eta)$, so we need only study the dynamics on half of the sphere. In the planar case, with $n = 2$, our angular dynamics is trivial as ξ would be a scalar, i.e. $r = |\xi|$ and $u = 1$. For the analysis of three-dimensional systems, it is helpful to write $u = (\cos\theta, \sin\theta) =: z(\theta)$ and derive dynamics on the angle θ. This dynamics takes the form

$$\frac{d\theta}{d\eta} = \kappa_2(\eta) - [D_\xi N f(\eta, 0)]z(\theta) \wedge z(\theta), \tag{4.16}$$

which suggests that the torsion $\kappa_2(\eta)$ of a periodic orbit in $\mathbb{R}^3$ greatly influences how nearby trajectories rotate azimuthally. In higher dimensions, one could use hyperspherical coordinates and derive dynamics on the associated set of angles; however, we will not present such computations here.

The key point for our analysis is that the T-periodic solutions to system (4.12) can naturally be used to construct invariant manifolds attendant to our periodic trajectory, which correspond to analogous structures in the LOR equations and in the original system (4.1). Suppose that $u^* \in S^{n-2}$ satisfies $\Phi^a_\Gamma(u^*, T) = u^*$ and hence u^* is a fixed point of the map

$P(x) := \Phi^a_\Gamma(x, T)$. Using standard discrete dynamical systems theory, if u^* is a hyperbolic fixed point of P, then we can construct stable and unstable manifolds $W^s(u^*, 0), W^u(u^*, 0)$ in $S^{n-2} \times \mathbb{R}$, defined by

$$W^s(u^*, 0) = \{x \in \mathcal{P} | P^k(x) \to u^* \text{ as } k \to \infty\}$$
$$W^u(u^*, 0) = \{x \in \mathcal{P} | P^k(x) \to u^* \text{ as } k \to -\infty\}. \tag{4.17}$$

We call these the *invariant angular manifolds* attendant to Γ. With the aforementioned odd-ness of (4.12), we have the following result.

Theorem 4.3.2. *Suppose that $u^* \in S^{n-2}$ satisfies $\Phi^a_\Gamma(u^*, T) = u^*$. If u^* is a hyperbolic fixed point of P with n_s negative real part eigenvalues and n_u positive real part eigenvalues, then there exist invariant n_s-dimensional stable and n_u-dimensional unstable manifolds attendant to $(u^*, 0)$ in $S^{n-2} \times \mathbb{R}$. Furthermore, $-u^*$ is also a hyperbolic fixed point of P with the same stability properties as u^*.*

Remark 7. The requirement of hyperbolicity is not necessary. Since the examples we will consider do not have invariant angular center manifolds, we have simply assumed hyperbolicity for notational convenience.

Next, we return to the full cylindrical dynamics (4.11). The set $\{r = 0\}$ is an invariant, $(n-1)$-dimensional set in our n-dimensional (r, u, η) phase space (i.e., in the relevant subspace of $\mathbb{R}^+ \times S^{n-2} \times \mathbb{R}$). Thus, as long as $\langle [D_\xi g(\eta, 0)]u, u\rangle \neq 0$, the manifolds W^s, W^u extend in this phase space to $(n_s + 1)$- and $(n_u + 1)$-dimensional invariant manifolds in $\{r \geq 0\}$, respectively, and these manifolds will organize the local transient dynamics. Note that even if Γ is stable, it can still have both stable and unstable invariant angular manifolds. Trajectories will contract in the r direction to $\{r = 0\}$, and their angular behavior will be organized by the invariant angular manifolds. An example of the organizational power of these manifolds in $\mathbb{R}^3$ is presented in the next section.

We conclude this section with a result on the existence of the T-periodic angular solutions, which form the basis for our invariant angular manifolds. The following statement demonstrates that such solutions are a topological necessity in even dimension.

Theorem 4.3.3. *If n is even, then there exists $u^* \in S^{n-2}$ such that $\Phi^a_\Gamma(u^*, T) = u^*$.*

Proof. We will use a standard result from algebraic topology, namely the hairy coconut theorem: if $F : S^m \to S^m$ is homotopic to the identity map and m is even, then F must have at least one fixed point. The map $P : S^{n-2} \to S^{n-2}$ defined by $P(x) = \Phi^a_\Gamma(x, T)$ is naturally homotopic to the identity, via $H(x, s) = \Phi^a_\Gamma(x, sT)$ for $s \in [0, 1]$. Hence when n is even, P must have a fixed point [50]. □

Thus we find that T-periodic angular trajectories and their attendant invariant angular manifolds are always present in even dimension. Interestingly, the smallest dimension of interest, $n = 3$, is not guaranteed to have invariant angular dynamics. Indeed, for $n = 3$, our flow map P will map from S^1 to S^1 and thus may be characterized by Denjoy's Theorem: either $P^m(x)$ has a fixed point for some m or P is topologically transitive. Interestingly, we shall see in the next section that fixed points of P can give rise to angular manifolds with complicated twisting geometries in the LOR frame.

4.3.3 Asymptotic Phase

The asymptotic phase of a point x_0 in the basin of a stable limit cycle Γ is the value $\Theta(x_0)$ such that [20]

$$\lim_{t\to\infty} \|\Gamma(t + \Theta(x_0)) - \Phi(x_0, t)\| = 0.$$

That is, there is a one-to-one mapping between points on Γ and phase values between 0 and the period of Γ. Each point x_0 in the basin of Γ is effectively linked to a corresponding base point on Γ, such that in the long-time limit, as x_0 converges to Γ, $\Phi(x_0, t)$ becomes arbitrarily close in Euclidean distance to the trajectory of the base point. Thus, we can uniquely assign the phase of the base point to x_0. This phase is what we have denoted as $\Theta(x_0)$, and the isochron of Γ associated with $\Theta(x_0)$ is defined as the collection of all basin points with $\Theta(x_0)$ as their asymptotic phase.

Thus far in our analysis, we have largely disregarded the η dynamics, opting instead to use η as a convenient parameterization representing geometric time. In this section, we study the η dynamics and demonstrate that, in the $t \to \infty$ limit, η is intimately related to the asymptotic phase.

Theorem 4.3.4. *Suppose that $x_0 = \Psi(\eta_0, \xi_0)$ is in the basin of the stable, Frenet limit cycle Γ. Then*

$$\Theta(x_0) = \lim_{t\to\infty} \eta(t) - t.$$

Proof. Note that by construction, $\Phi(x_0, t) = \Psi \circ \Phi_\Gamma((\eta_0, \xi_0), t)$. Therefore, for any phase θ,

$$\begin{aligned}\|\Gamma(t+\theta) - \Phi(x_0, t)\| &= \left\| \Gamma(t+\theta) - \Gamma\circ\eta(t) - \sum_{j=1}^{k} \xi_j(t) N_j \Gamma \circ \eta(t) \right\| \\ &\leq \|\Gamma(t+\theta) - \Gamma\circ\eta(t)\| + \|\xi(t)\|. \end{aligned} \tag{4.18}$$

As Γ is Frenet, it is $\mathscr{C}^1[0,T]$ and hence is Lipschitz. Thus, (4.18) implies that there exists $L > 0$ for which

$$\|\Gamma(t+\theta) - \Phi(x_0, t)\| \leq L|t + \theta - \eta(t)| + \|\xi(t)\|. \tag{4.19}$$

Since $\|\xi(t)\| \to 0$ as $t \to \infty$, it follows that if we can demonstrate that $\lim_{t\to\infty} \eta(t) - t$ exists, then by choosing $\theta = \lim_{t\to\infty} \eta(t) - t$ and taking the limit $t \to \infty$ in inequality (4.19), we will obtain the desired result.

Let $\{t_n\}_{n=1}^{\infty}$ be any positive sequence such that $t_n \to \infty$. We will first show that $\phi_n := \eta(t_n) - t_n$ is a Cauchy sequence. We note that when $\xi = 0$, $\dot\eta = 1$, and hence we can write $\dot\eta = 1 + \mathcal{O}(\xi)$. Thus, there exist constants $C, M > 0$ such that

$$\begin{aligned}|\phi_n - \phi_m| &= \left| \int_{t_m}^{t_n} (\dot\eta(s) - 1)\, \mathrm{d}s \right| \\ &\leq M \int_{t_m}^{t_n} \|\xi(s)\|\, \mathrm{d}s \\ &\leq CM \int_{t_m}^{t_n} \exp(-\alpha s) \mathrm{d}s \end{aligned} \tag{4.20}$$

where $\|\xi(s)\| \leq C\exp(-\alpha s)$ follows from the stability of Γ, with $-\alpha$ is the smallest (in norm) Floquet exponent of Γ. Taking t_m, t_n sufficiently large, we find that ϕ_n is Cauchy and hence is convergent. Finally, note that although t_n was arbitrary, any other sequence $\tilde t_n \to \infty$ will result in a sequence $\tilde\phi_n$ with the same limit as ϕ_n. Indeed, if $\tilde\phi_n \to \tilde\phi$, then for any $\varepsilon > 0$ there exists an N such that

$$|\phi - \tilde\phi| \leq |\phi - \phi_{n_1}| + |\phi_{n_1} - \tilde\phi_{n_2}| + |\tilde\phi_{n_2} - \tilde\phi| < \varepsilon$$

for $n_1, n_2 > N$, where the middle term is bounded using the integral calculation in (4.20). □

Thus, we can use the LOR dynamics to extract the asymptotic phase for initial conditions in the basin of attraction of a stable periodic orbit. Furthermore, it is quite natural to study the phase dynamics in the LOR frame. For x_0 in the basin of attraction of Γ, denote the corresponding LOR coordinates as (η_0, ξ_0) and let $\Theta(\eta_0, \xi_0)$ denote the asymptotic phase in the LOR frame. Clearly, we have that

$$\Theta(\eta_0, 0) = \eta_0$$

as $\Psi(\eta_0, 0) \in \Gamma$. This equality corresponds to our earlier observation that η provides a reasonable approximation of phase.

Furthermore, the LOR representation of the phase dynamics allows us to easily consider *phase sensitivity* for points in a neighborhood of Γ. If we perturb the point $(\eta_0, 0) \in \Gamma$ by ξ_0 (a small vector in the ξ direction as represented in LOR coordinates), then the new asymptotic phase will have a value $\Theta(\eta_0, \xi_0)$ and thus the change in the phase value is given by $\Delta\Theta(\eta_0, \xi_0) := \Theta(\eta_0, \xi_0) - \eta_0$. If $|\Delta\Theta(\eta_0, \xi_0)|$ is large, then the oscillation is sensitive to perturbations at η_0. If the orbit has saddle-type invariant angular manifolds, i.e. both stable and unstable T-periodic angular manfiolds, then we would expect that perturbations in the direction of the unstable angular manifold should elicit the largest phase response. The unstable angular trajectory will serve as an angular separatrix, and initial conditions on opposite sides of the angular manifold will have long, potential asymmetric excursions as they approach any stable angular manifolds. In the next section, we demonstrate how this effect sculpts the phase sensitivity of the Goodwin oscillator.

4.4 The Goodwin Oscillator

4.4.1 Identification of the Periodic Orbit

In this section we will demonstrate our LOR techniques in action, using the well-known Goodwin oscillator [27, 32] as a proving ground. The Goodwin system is a model for an

oscillatory genetic circuit that has been considered in the study of circadian rhythms. The model is given by three ODEs, which have the form

$$\begin{aligned} \dot{x} &= \frac{a}{k^n + z^n} - bx \\ \dot{y} &= \alpha x - \beta y \\ \dot{z} &= \gamma y - \delta z \end{aligned} \tag{4.21}$$

where $a, k, n, b, \alpha, \beta, \gamma, \delta$ are positive parameters. Here we use $a = 360, k = 1.368, n = 12, b = \alpha = \gamma = 1, \beta = .6, \delta - .8$ for our numerical simulations. It is known that this system has a globally stable periodic trajectory across a wide range of parameter values, provided that $n > 8$ (e.g., [32]). We will use the LOR technique to identify this limit cycle.

The first step in our analysis is to choose a reasonable LOR basecurve. If we have a sense of the region in which a periodic orbit might lie, based for example on the direction field or nullsurface structure, then we can choose any simple closed curve in this region (e.g., see [45]). For the example at hand, we will use the flow itself to do most of the work in specifying this curve.

That is, we somewhat arbitrarily pick the initial point $(1, 1, 1)$, which seems to be near the core of rotation in the vector field of (4.21), and we denote by $\psi(t)$ the trajectory of (4.21) with initial condition $\psi(0) = (1, 1, 1)$. Integrating forward, we note that the segment $\psi([5, 10])$ exhibits a looping structure (see Fig. 23A, red curve), so we will build a simple closed curve from this portion of the trajectory. To do so, we will sample this trajectory segment at regular time intervals $\{\psi(5 + i\delta t)\}_{i=1}^{50}$, where $\delta t = .1$, and fit a planar ellipse to this data, for example using a least squares calculation, which we take as our basecurve γ (also shown in Fig. 23A, blue curve).

It is important to note that while this is a fairly ad hoc procedure for producing a LOR basecurve, we have found that it is successful in multiple examples. The basecurve need not be a close match to the periodic trajectory, just a reasonable first guess, and generating the basecurve need not involve any integration, as we find that an arbitrary simple closed curve in an appropriate region of the phase space will generally work as well.

With our best-fit planar ellipse γ in hand, we next verify that it is a compatible curve by checking that $\dot{\eta}$ remains nonzero along γ, or equivalently along $\{\xi = 0\}$; see Fig. 23B. Once

this property is established, we are prepared to solve the BVP (4.3) and identify the periodic trajectory. We use Mathematica for this process, but any software package with a numerical integrator and a symbolic computation engine would suffice. The solver provides a unique solution to our LOR BVP, as shown in Fig. 23C; the orbit maps back to the corresponding periodic solution in the original coordinates shown in Fig. 23A (purple curve).

To conclude this first part of the example, we briefly discuss the strengths and weaknesses of this approach to periodic orbit identification. Computationally, we have eliminated the need to compute the first return time to a fixed Poincaré section, which can be a nontrivial task in higher dimensions or, alternatively, to solve a two-point BVP with a phase condition and with period as a free parameter. Furthermore, we remark that numerical BVP solvers subject to fixed endpoint, periodic boundary conditions are fast and stable. The tradeoff is that for complicated flows, identifying a compatible basecurve that approximates the shape of the desired periodic orbit can become a nontrivial task, and the normal frame computations required for the LOR approach can also become involved. We use the Mathematica symbolic computation software to execute the LOR method, and we plan to make our code available on GitHub.

While the normal frames and LOR dynamics may be expensive to compute, there is an added bonus of the approach to capturing a periodic orbit: if one is interested in continuing periodic trajectories across an interval of parameter values, a single LOR transformation can often be used multiple times. If our original dynamics depends on parameters – that is, our vector field is of the form $f(x;\lambda)$ – then the right-hand side of the LOR BVP will also depend on the parameter vector λ; however, the λ-dependence will only appear in the $Tf(\eta,\xi;\lambda), Nf(\eta,\xi;\lambda)$ terms, while the underlying curve γ and the Frenet frame will not depend on λ. Each computationally expensive LOR transformation can therefore be used for multiple inexpensive iterations of BVP solution, one for each parameter set. We display projected solutions to the LOR BVP for the Goodwin oscillator (4.21) as the parameter a ranges from 330 to 390 in Fig. 23D, all produced using a single LOR transformation.

4.4.2 Analysis of Transient Dynamics near the Periodic Orbit

We continue our analysis of the Goodwin oscillator to demonstrate the ideas of section 4.3. We use the periodic orbit identified in subsection 4.4.1 as our LOR basecurve Γ. Recall that in the LOR frame, the basecurve corresponds to $\{\xi = 0\}$. The rectified limit cycle together with nearby trajectories of the resulting LOR dynamics are shown in Fig. 24. Note how the trajectories emanating from a circle of initial conditions seem to collapse onto a 2-manifold as they contract towards $\{\xi = 0\}$.

To identify the manifold to which these trajectories are contracting, we will consider the angular $\{r = 0\}$ dynamics, given by (4.16). As the angular flow is antipode-preserving, we note that the dynamics on θ is invariant under a π shift, and as θ only appears in trigonometric functions in (4.16), the most natural domain for the dynamics in (η, θ) is the torus $S^1 \times S^1$. We find that there are two T-periodic angular trajectories that (with their π-shifted counterparts) organize the phase space; these periodic angular solutions are shown with a sweep of initial conditions in Fig. 25A. Note that in the interval $\eta \in [0, T)$, one of these periodic angular solutions, which we denote as $\theta_{s,0}$, is stable and attracts almost all initial conditions, while the other periodic angular solution, say $\theta_{u,0}$, is unstable and plays the role of an angular separatrix.

Next, we will construct the invariant angular manifolds to Γ. In (η, θ, r) space, which includes the radial direction, $\{r = 0\}$ is invariant and is partitioned between the trajectories $\theta_{s,0}, \theta_{u,0}$ and their translates, which we will henceforth collectively refer to as θ_s, θ_u. We have $\langle [D_\xi g(\eta, 0)]u, u\rangle\, r < 0$, such that the radial dynamics given in (4.11) is contracting toward $\{r = 0\}$. Hence there are 2-dimensional invariant angular manifolds of system (4.11) attendant to each of θ_s, θ_u in $\{(\eta, \theta, r) : r > 0\}$, which we denote by $W^s(\theta_s), W^s(\theta_u)$, respectively. This structure is shown in Fig. 26. Note that the saddle behavior of $W^s(\theta_u)$ is interesting, as initial conditions near $W^s(\theta_u)$ yield trajectories that are pushed away from the manifold in the angular direction yet have decreasing r values. Therefore, $W^s(\theta_u)$ serves as a separatrix in the 3-d flow. We also see that the hidden 2-manifold in Fig. 24 is, in fact, the stable invariant angular manifold $W^s(\theta_s)$, which is stable in the angular and radial directions.

Finally, we can transform back to our original coordinates (x, y, z) via Ψ, which also

preserves invariance and stability, and note that our manifolds become topological annuli that intersect transversely along the periodic orbit Γ. As trajectories converge toward Γ, they will quickly approach the stable angular manifold, hence the flow on $\Psi(W^s(\theta_s))$ can be used to provide a natural dimensional reduction for the full dynamics of (4.21). The saddle type manifold $\Psi(W^s(\theta_u))$, being an angular separatrix, will display high sensitivity to initial conditions, and thus represents a region of high asymptotic phase uncertainty. The LOR frame allows us to study the local dynamics near the periodic solution of the Goodwin oscillator model in greater detail than is afforded by standard linearization techniques while maintaining a clear geometric perspective.

To conclude this section, we will show that the invariant angular manifolds do in fact play a major role in determining phase sensitivity. We will use the approach laid out in subsection 4.3.3, based on the observation that the phase of an initial condition can be computed directly from $\lim_{t\to\infty} \eta(t) - t$. We study a 64×64 mesh of initial conditions (η_0, ξ_0) on a cylinder $\|\xi\| = 0.1$. These initial conditions are integrated forward until a time $t = t_{end}$ such that $\|\xi(t)\|$ is sufficiently small (i.e., we have converged sufficiently close to the limit cycle), and then we compute $\eta(t_{end}) - t_{end}$ to extract an approximation to the asymptotic phase $\Theta(\eta_0, \xi_0)$. Note that t_{end} may be different for different initial conditions.

We show the results of these computations in Fig. 28A. As expected, the asymptotic phase values correlate strongly with η_0, as we are in a regime where $\|\xi_0\|$ is fairly small.

In Fig. 28B, we show the phase sensitivity $\Delta\Theta(\eta_0, \xi_0) = \Theta(\eta_0, \xi_0) - \eta_0$ sampled at various (η, ξ) values. The multiple data points (blue) for each value of η all have different initial ξ values. The dependence of $\Delta\Theta$ on ξ can also be appreciated from the contour plot in Fig. 28C; note that for moderate η values, different ξ values lead to very different $\Delta\Theta$. To relate this phase sensitivity to the invariant angular manifolds, we consider the quantity $1/|\theta_s(\eta) - \theta_u(\eta)| =: 1/Z(\eta_0)$, which grows as the invariant angular manifolds come closer together. The red curve in Fig. 28B displays an appropriately rescaled rendering of $Z(\eta)$. We note that the magnitude of this quantity correlates strongly, albeit with a phase shift, with the spread in the phase sensitivity. When $Z(\eta)$ is small, then small changes in the angular variable $\xi/\|\xi\|$ can push trajectories to the opposite side of θ_u, which causes a large angular excursion. Therefore, it is reasonable to use $1/Z(\eta)$ to approximate the relative

phase sensitivity.

The final panel in 28 provides our attempt to portray the full geometry of phase sensitivity in the Goodwin oscillator. The data are arranged as follows: we take an initial condition on the cylinder $\{\|\xi\| = .1\}$, say with coordinates $(\eta_0, \xi_{1,0}, \xi_{2,0})$, and compute the phase sensitivity $\delta := \Delta\Theta(\eta_0, \xi_{1,0}, \xi_{2,0})$, then we add a point to the mesh of panel D at the value

$$(\eta_0, \xi_{1,0}, \xi_{2,0}) + |\delta|(0, \xi_{1,0}, \xi_{2,0}),$$

with the idea being that the further that a point is from $\{\|\xi\| = .1\}$, the more sensitivity of asymptotic phase to initial angle occurs at that point.

4.4.3 Numerical Computations

We conclude this lengthy example with some additional information about our computational methods. To create the figures in this section, we needed to approximate LOR trajectories in both the (η, ξ) and (η, u, r) representations, which may seem daunting. However, we note that we can perform these computations in highly synergistic ways.

When we searched for periodic angular trajectories, we generated 80 trajectories of (4.16), and from these we computed the map from $\eta = 0$ to $\eta = T$. We used these same trajectories to compute the radial stability function $L(u_0)$. Hence, we were able to establish the existence of invariant angular manifolds and study the stability of the underlying periodic orbit simultaneously.

Similarly, when approximating the invariant angular manifolds, which we implemented numerically using the standard BVP continuation technique laid out in [35], we computed a large number of trajectories that lie along our manifolds. We were able to use these trajectories again to compute asymptotic phase values. Thus, we could approximate invariant angular manifolds and study phase sensitivity simultaneously as well. Furthermore, it is easy to imagine how knowledge of stable angular manifolds could be used to optimize the computation of asymptotic phase values, although we have not implemented this technique in these computations: following the computation of the stable angular manifold $W^s(\theta_s)$, the asymptotic phase on $W^s(\theta_s)$ could be obtained using the BVP solutions that were produced

to approximate $W^s(\theta_s)$. Furthermore, we know that almost all trajectories will converge to $W^s(\theta_s)$ as they approach $r = 0$; thus, to estimate the asymptotic phase of an arbitrary trajectory ϕ, we need only track it until it lies near $W^s(\theta_s)$ and then we can use the values of Θ on $W^s(\theta_s)$ to approximate the asymptotic phase of ϕ.

As a benchmark, the computations performed in this section can be executed on a Macbook Air equipped with an Intel i5 processor and sixteen gigabytes of RAM via Wolfram Mathematica in just under three hours; this includes the identification, stability integrals, periodic-angle identification, approximation of invariant angular manifolds, and asymptotic phase computations.

All of these computational shortcuts result from the unified nature of the LOR approach to periodic dynamics. Were we to use standard theory to identify a periodic orbit, analyze its stability, and then compute its invariant manifolds, we would be using computationally unrelated approaches; however, once we have completed the expensive computation of the LOR change of coordinates, we find that computations surrounding the analysis of periodic orbits and their transient dynamics are highly efficient thanks to the LOR frame.

4.5 A Period-Doubling Bifurcation with a Twist

In this section, we examine a polynomial system that exhibits a period-doubling bifurcation and demonstrate that the LOR approach provides an efficient, unified means to identify, analyze, and continue the periodic orbits that arise. The system of interest is given by

$$\begin{aligned} \dot{x} &= y \\ \dot{y} &= z \\ \dot{z} &= \alpha x - x^2 - \beta y - z \end{aligned} \tag{4.22}$$

where $\alpha, \beta > 0$ are parameters [53]. For our initial analysis we will take $\beta = 2$, for which it is known that (4.22) undergoes a period-doubling bifurcation at $\alpha \approx 3.112$. We will begin by identifying the periodic orbit at $\alpha = 3$; as in the Goodwin example, we choose a "nearly recurrent" trajectory, sample over its pseudo-period and fit a planar ellipse to choose

a basecurve. We omit the details of this computation, and show the identified periodic orbit in Fig. 29.

Denote by Γ_0 the periodic orbit identified for $\alpha = 3$, with period T_0. We next compute the LOR vector field $\mathcal{L}_{\Gamma_0} f(x, y, z; \alpha)$, noting that Γ_0 is automatically compatible. As discussed in Section 4.4, this one basecurve can subsequently be used to identify multiple periodic orbits across a range of parameter values. As we have foreknowledge that our system undergoes a period-doubling bifurcation, to find these orbits we amend our BVP approach and, rather than (4.3), we solve the BVP

$$\frac{d\xi}{d\eta} = g_{\Gamma_0}(\eta, \xi; \alpha) \qquad\qquad \xi(0) = \xi(2T_0),$$

where T_0 is the period of Γ_0, for each of a set of α values. That is, we search for 2-periodic points of the flow map. Using this approach, there is no need to piece together parameter domains. The results of these computations are shown in Fig. 29B: we can smoothly continue our BVP solution across the period-doubling bifurcation. Indeed, from the perspective of our modified BVP, there is no bifurcation.

We now turn our attention to the invariant angular manifolds for these periodic orbits. For each of our sampled parameter values, we compute the map $P(\theta; \alpha) = \Phi^a_{\Gamma_0}(\theta, T_\alpha; \alpha)$, where T_α is the period of the periodic trajectory at parameter value α, over a range of initial conditions θ. The fixed points of $P(\theta; \alpha)$ are T_α-periodic angular solutions and, as $P(\theta + \pi; \alpha) = \pi + P(\theta; \alpha)$, we note that $P(P(\theta; \alpha); \alpha) = \theta$ if and only if $P(\theta; \alpha) = \theta$ or $P(\theta; \alpha) = \theta + \pi$. Therefore, we can also identify $2T_\alpha$-periodic angular solutions by studying $P(\theta; \alpha)$.

When $\alpha < \alpha_b$, where α_b denotes the α value at which the period-doubling bifurcation occurs, we find that there are no periodic angular solutions; that is, P fails to have a fixed point. Intuitively, this means that the angular flow is unconstrained, or the trajectories near Γ rotate freely around Γ and do not converge to any angular manifold. For $\alpha > \alpha_b$, we again find that P has no fixed points; however, we find that there are 2 distinct solutions to $P(\theta; \alpha) = \theta + \pi$ and hence we have $2T$-periodic angular solutions. Interestingly, the invariant angular manifolds attendant to these $2T$-periodic solutions are non-orientable, as

our angular flow is antisymmetric. The mapping $P(\theta;\alpha)$ is shown at several values of α in Fig. 30.

The existence of a stable non-orientable manfiold attendant to Γ for $\alpha > \alpha_b$ has already been established [53]. In addition to this stable invariant angular manifold, the LOR technique also reveals an angularly unstable non-orientable manifold, which will play a large role in organizing local phase dynamics. Furthermore, we have shown that as the limit cycle undergoes a period-doubling bifurcation, our periodic angular trajectories (and hence their attendant non-orientable manifolds) undergo a saddle-node bifurcation.

We suspect that the bifurcation of invariant angular manifolds is a common occurrence and could provide a new tool for analyzing bifurcations that affect transient dynamics relative to periodic orbits. For example, if a stable and an unstable angular manifold coincide and then annihilate, then a transition will occur from a scenario in which a 2-manifold organizes trajectories in the neighborhood of the underlying periodic orbit to a scenario in which trajectories exhibit free rotation around the periodic orbit, which will significantly impact the asymptotic phase structure of trajectories within the neighborhood.

4.6 Figures

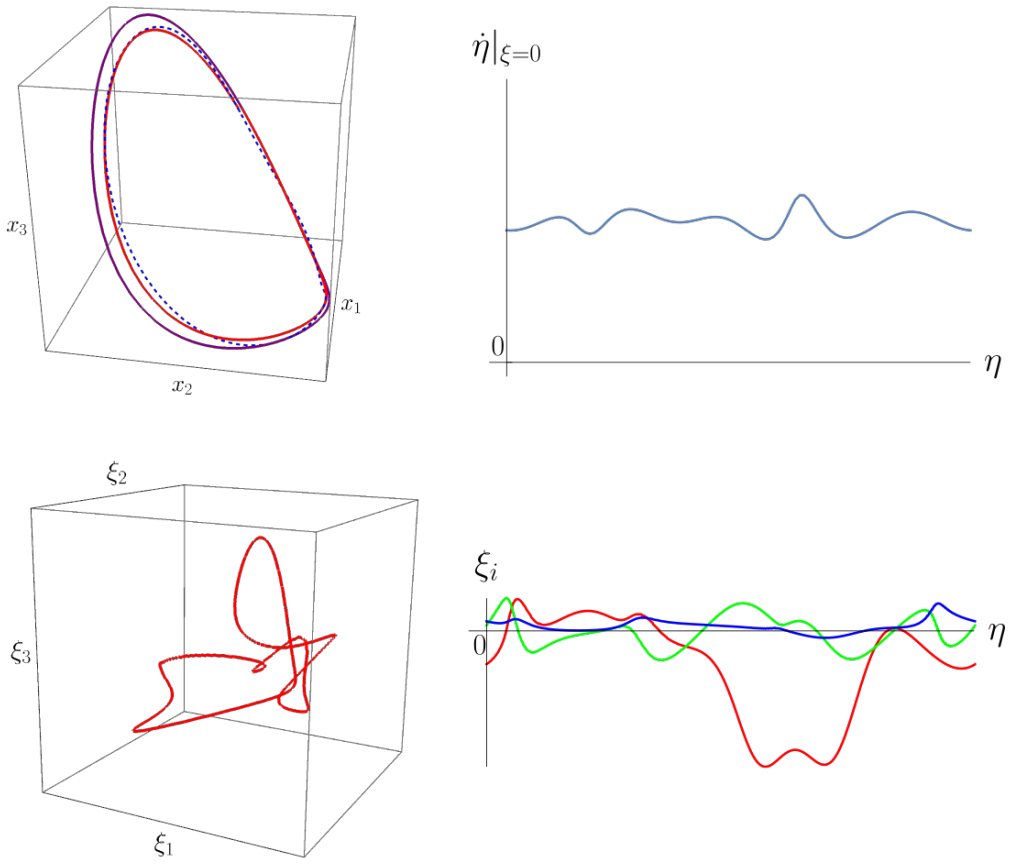

Figure 20: Identifying periodic orbit of (4.5). (Top Left) A three-dimensional projection of the trajectory ϕ described in the text is shown in red, the dashed blue curve is the projected Fourier approximation of ϕ, and the purple curve is a projection of the identified periodic orbit. (Top Right) A plot demonstrating the admissibility of $\bar{\phi}$ as a basecurve. (Bottom Left) The solution to the LOR BVP using $\bar{\phi}$ as a basecurve. (Bottom Right) A component plot of the LOR BVP solution with $\xi_1(\eta)$ in red, $\xi_2(\eta)$ in green, and $\xi_3(\eta)$ in blue.

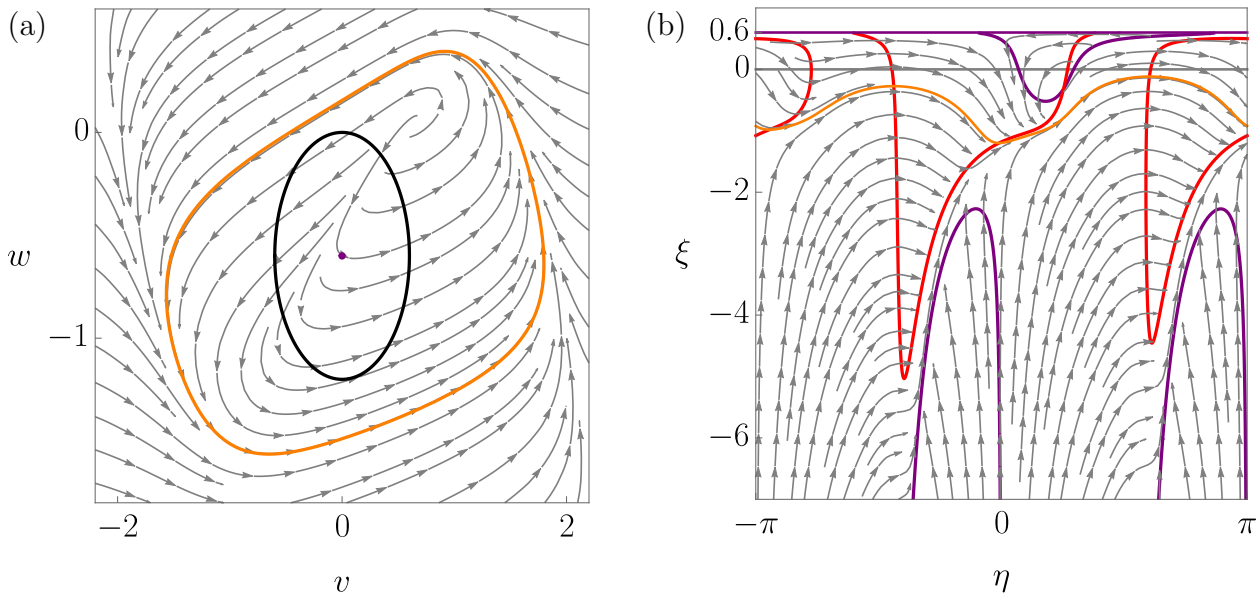

Figure 21: Dynamics for the FitzHugh-Nagumo equations (4.7) and the corresponding LOR equations (4.9). (a) A stream plot in the phase space for (4.7), along with the basecurve γ (black) and the unique periodic orbit of the flow (orange), along which the flow is counter-clockwise. (b) A stream plot in the phase space for (4.9). The grey line is $\xi = 0$, which corresponds to γ in (v, w) space since $\Psi(\eta, 0) = \gamma(\eta)$. Our evolute condition, $\xi \neq 1/\kappa_\gamma(\eta)$, fails to hold at $\xi = .6$. The purple curve is the η nullcline, and the red curve is the ξ nullcline. In orange is the unique limit cycle of the flow, found by solving (4.4) as computed from (4.8).

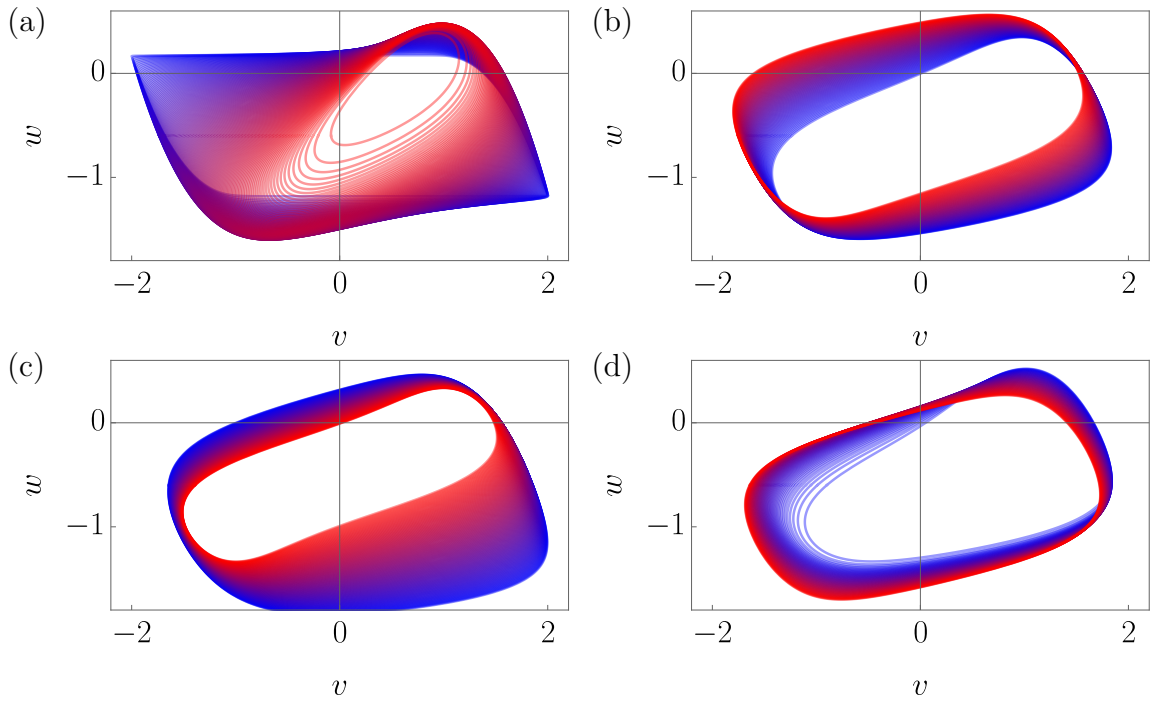

Figure 22: A simple demonstration that the LOR approach for identifying periodic trajectories is robust to parameter variations. In each panel, one of the four parameter values of (4.7) is varied while the other three remain constant. We perturb off of the point $(a, b, \varepsilon, I) = (-0.6, 0.8, 0.5, 0.3)$ in parameter space. In (a) we vary $\varepsilon \in [0.01, 0.7414]$, in (b) we vary $a \in [-0.7, -0.2]$, in (c) we vary $b \in [0.4, 1.2]$ and in (d) we vary $I \in [0.3, 0.7]$. The colors of the obtained orbits transition uniformly from red to blue across each parameter interval.

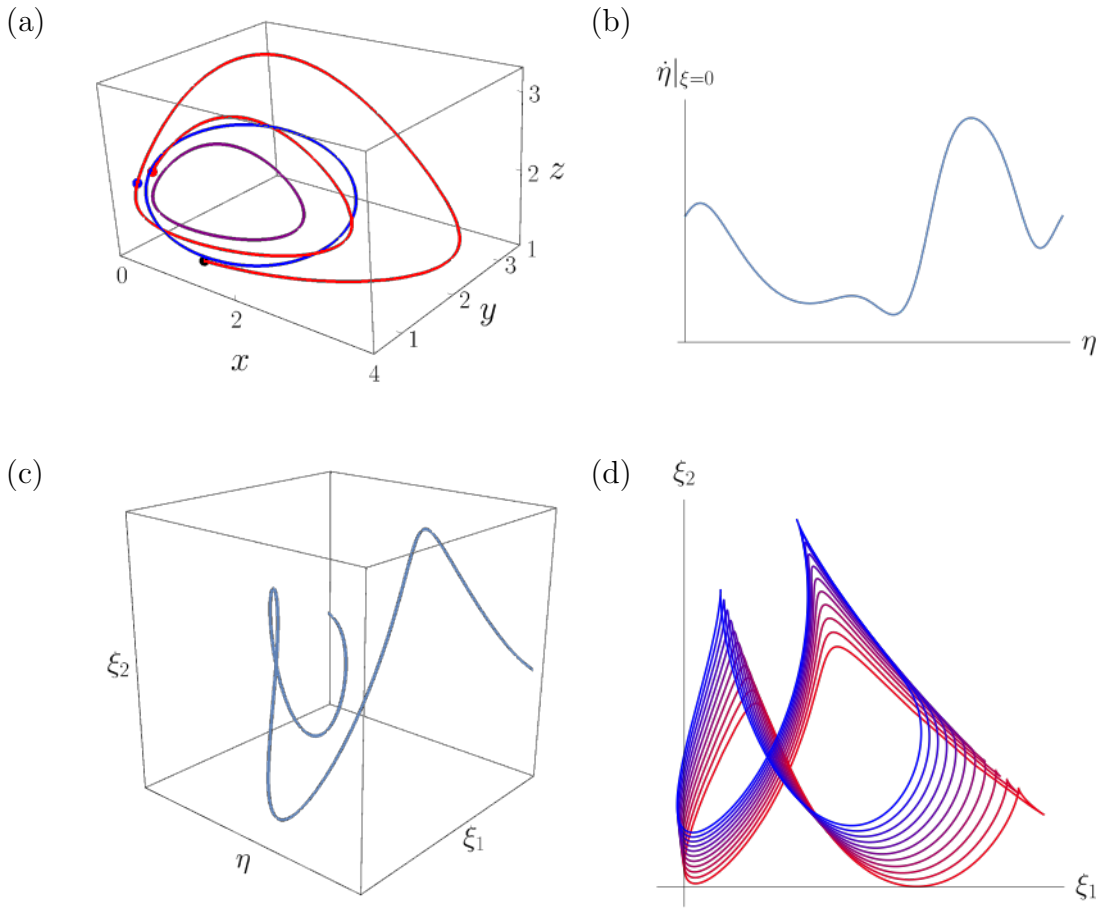

Figure 23: Identifying the Goodwin oscillator. (a) The trajectory segment $\psi([5, 10])$ used to "approximate" the periodic orbit (red), the best fit ellipse γ to that trajectory (blue) and the identified periodic orbit (purple). The black point is the initial condition $(1, 1, 1)$, the blue point is $\phi(5)$ and the red point is $\phi(10)$. (b) A plot of $\langle f \circ \gamma(\eta), T\gamma(\eta)\rangle$, which is positive for $\eta \in [0, 2\pi]$, demonstrating that γ is a compatible curve. need axis labels, at least on vertical axis. (c) The solution to the LOR BVP (4.3), or equivalently to (4.2), based on with basecurve γ, shown in the LOR frame. (d) Projections of solutions for values of the parameter a varying in $[330, 390]$ with a stepsize of 5.

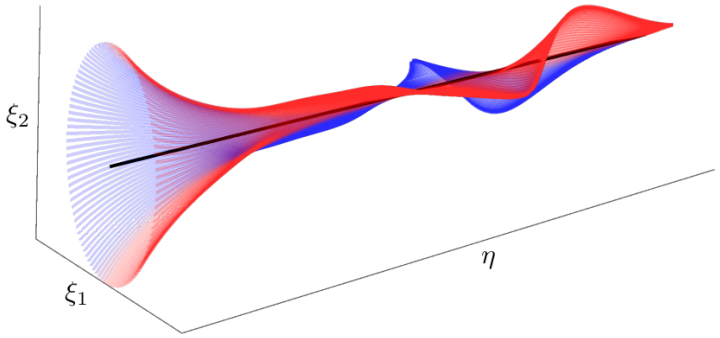

Figure 24: The LOR dynamics near the periodic orbit. Trajectories generated by flowing forward a circle of initial conditions of the LOR equations for system (4.21) from $\{\eta = 0\}$ until $\{\eta = T\}$.

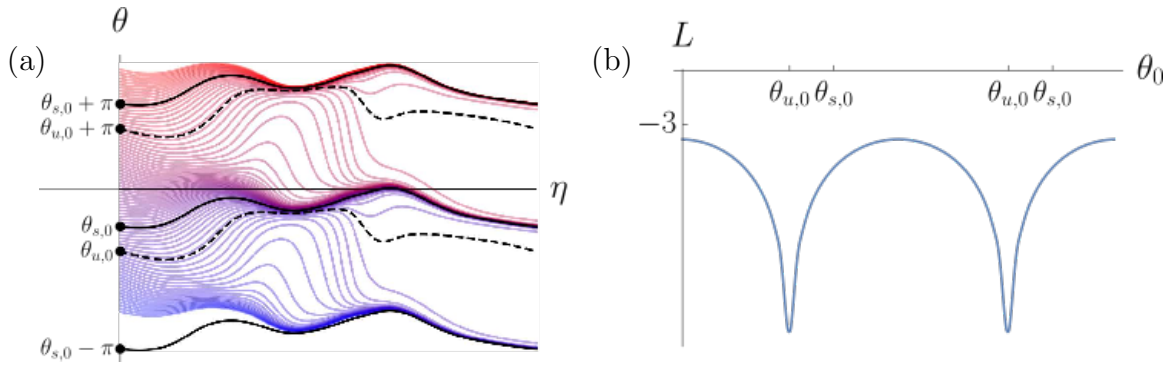

Figure 25: Dynamics of the $r = 0$ angular subsystem (4.12) for the Goodwin Oscillator. (a) The five black curves are T-periodic angular solutions; the solid curves are stable and the dashed curves unstable. The remaining curves are representative trajectories. (b) The function $L(\theta_0)$, which we use to show that Γ is stable.

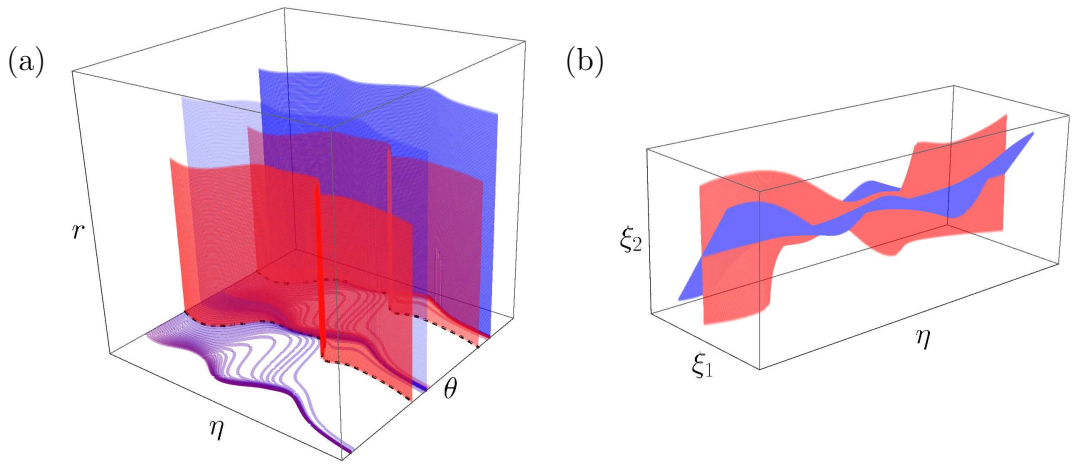

Figure 26: The invariant angular manifolds of the Goodwin oscillator model (4.21) in the LOR frame. (a) The red manifolds are $W^s(\theta^u)$ and the blue manifolds are $W^s(\theta^s)$. Note how these surfaces organize phase space: trajectories are pushed away from the red manifolds towards the blue manifolds as $r \to 0$; furthermore, the red manifold serves as an angular separatrix. (b) The invariant angular manifolds represented in our orignial LOR coordinates. Note that the blue (stable) manifold is the object to which the trajectories in Fig. 24 are drawn.

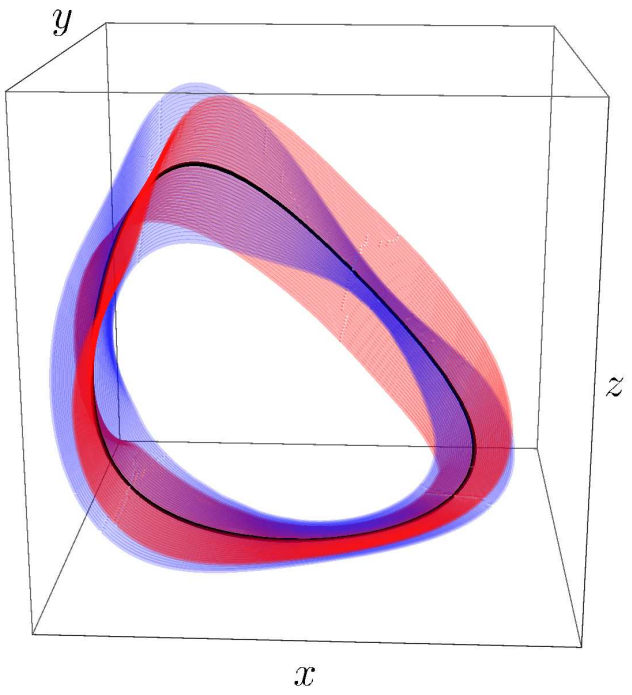

Figure 27: The invariant angular manifolds Goodwin oscillator model (4.21) represented in (x, y, z) space. The blue (stable) manifold the the object to which trajectories are drawn as they approach ϕ. The red (saddle-stable) manifold serves is a separatrix, which displays high sensitivity to initial conditions.

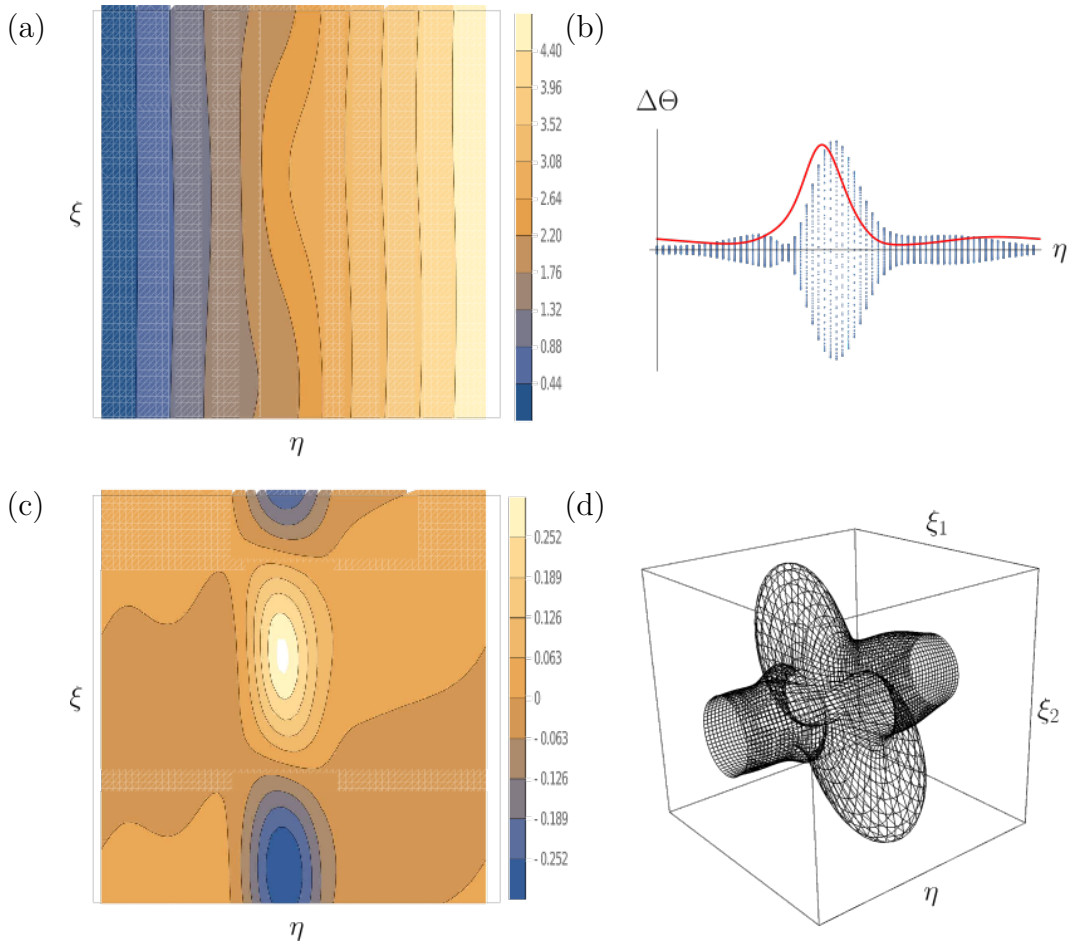

Figure 28: Computing asymptotic phase using the LOR frame. (a) Contour plot of the asymptotic phase $\Theta(\eta_0, \xi_0)$ for initial conditions on the cylinder $\|\xi\| = 0.1$ spaced uniformly in the angular coordinate $\theta := \tan^{-1}(\xi_2/\xi_1)$. (b)Distance between the invariant angular manifolds (red) provides an approximate envelope to the values of phase sensitivity $\Delta\Theta$, computed numerically at initial conditions on the cylinder (blue dots). (c) A contour plot of $\Delta\Theta(\eta_0, \xi_0)$. (d) The same data represented in 3D; details are given in the text.

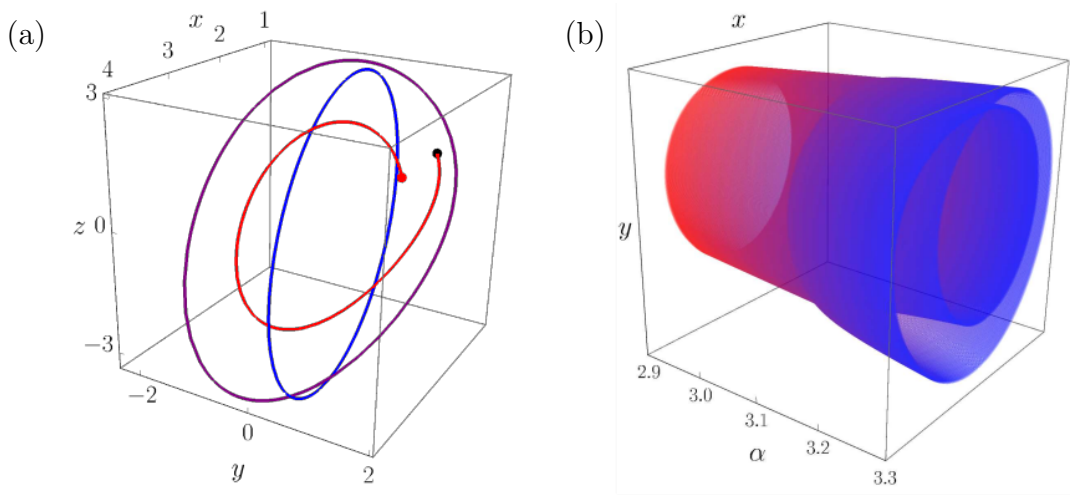

Figure 29: Identifying and continuing the limit cycle across a period-doubling bifurcation. (a) The initial elliptical basecurve (blue) used to identify the periodic orbit at $\alpha = 3$ (purple). To find the basecurve, we find the best-fit planar ellipse to the trajectory of (4.22) with initial condition $(1, 1, 1)$, shown for $t \in [0, 5]$ (red). (b) The continuation of the limit cycle in α, computed using the LOR approach described in the text.

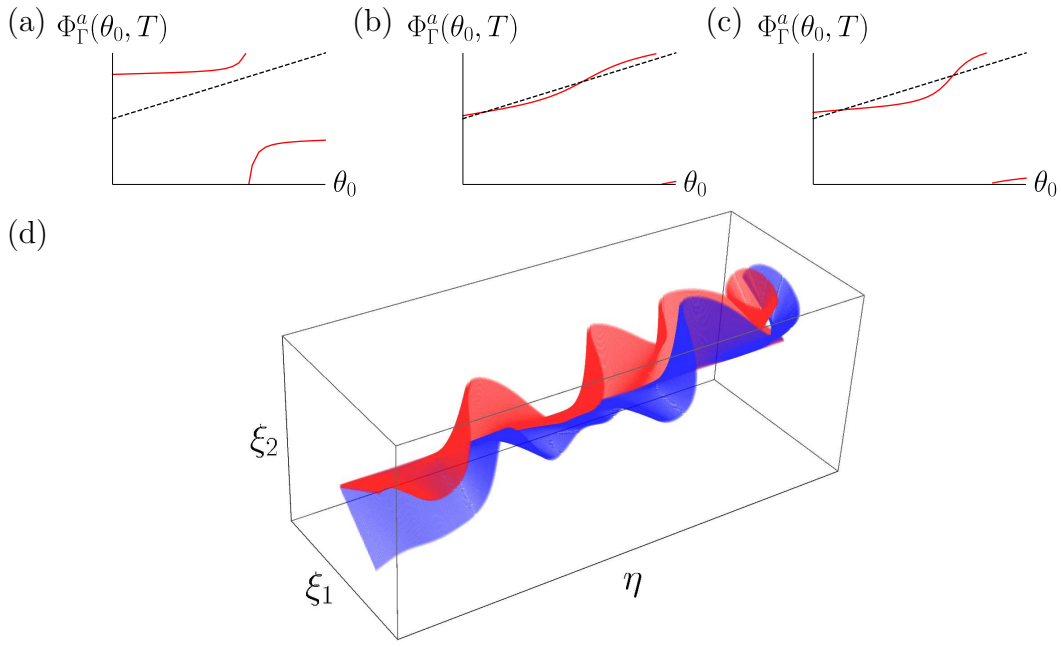

Figure 30: Fixed points in the angular flow map. (a) The angular flow map $P(\theta; 3)$ which has no fixed points nor k-periodic points for $k < 6$. (b) The angular flow map $P(\theta; 3.13)$ which has two 2-periodic points. Note that one crossing of $P(\theta; 3.13)$ and $\theta + \pi$ are nearly tangential, suggesting a saddle-node bifurcation has just occurred. (c) The angular flow map $P(\theta; 3.15)$, which again has two 2-periodic solutions. (d) An approximation of the invariant angular manifolds plotted in LOR coordinates. As $\theta(T) = \pi + \theta(0)$ for the stable and unstable angular trajectories, these manifolds will be diffeomorphic to Möbius strips in (x, y, z)-space.

5.0 Rivers in Space, Identifying Canard Solutions

The material in this chapter is being prepared for publication and is co-authored by Jonathan E. Rubin.

5.1 Motivation

In this chapter, we show that all canards lie in vanishing neighborhoods of rivers. In the process, we observe that the methods involved in this demonstration are also convenient for calculations related to canards. In particular, we can do way-in way-out without complexification of time. Moreover, our approach also reveals some previously unrecognized structure associated with canards, which gives novel insight into the development of small amplitude oscillations during the passage near a critical manifold fold associated with canard dynamics.

5.2 Generalized River Theory

5.2.1 Rivers in Arbitrary Dimensions

Given a curve $\gamma \in \mathscr{C}^{n+2}(I, \mathbb{R}^n)$ for $I \subset \mathbb{R}$, the Frenet curvature of γ is given by

$$\kappa_\gamma(\eta) = \frac{\gamma'(\eta) \wedge \cdots \wedge \gamma^{(n)}(\eta)}{\alpha(\gamma'(\eta), \cdots, \gamma^{(n)}(\eta))}$$

where $\cdot' = d\cdot/d\eta$ and α is a smooth, nonzero function [40]. Therefore, we define the curvature of the vector field f by

$$\kappa(x) := \frac{f(x) \wedge \cdots \wedge f^{(n)}(x)}{\alpha(f(x), \cdots, f^{(n)}(x))},$$

which we can apply directly to compute κ_ϕ.

We will again be most interested in the set of zero-curvature, $\{\kappa(x) = 0\}$, which we call the zero-curvature locus (ZCL). Specifically, we are interested in analyzing how the zero-curvature locus (ZCL) organizes phase space. For convienence and later use, we define

$$\Delta_{(i_1,i_2,\cdots,i_n)}f(x) := f^{(i_1)}(x) \wedge f^{(i_2)}(x) \wedge \cdots \wedge f^{(i_n)}(x) \tag{5.1}$$

for $i_1, i_2, \cdots, i_n \in \{1, \cdots, n+2\}$. Clearly $\kappa(x) = 0$ if and only if $\Delta_{(1,2,\cdots,n)}f(x) = 0$.

Generically, the ZCL will be a codimension-one manifold embedded in Ω, which we denote by $\mathcal{Z}$. To study the effect of the ZCL on the flow Φ, we will parameterize a patch of $\mathcal{Z}$ using a chart $\sigma : \mathcal{U} \subseteq \mathbb{R}^{n-1} \to \Omega$ and we will use LOR to analyze the local dynamics. Note that, because σ provides a parameterization of a level set of the curvature function, we can choose

$$N\sigma(\eta) = \frac{\nabla\kappa \circ \sigma(\eta)}{\|\nabla\kappa \circ \sigma(\eta)\|}$$

as the normal vector to our chart. The LOR dynamics with base manifold σ will have the form

$$\begin{aligned}\dot{\eta} &= [S_\sigma(\eta,\xi)]^{-1} T f(\eta,\xi)\\ \dot{\xi} &= \langle f \circ \Psi(\eta,\xi), N\sigma(\eta)\rangle =: g(\eta,\xi).\end{aligned}$$

Note that in the (η,ξ) LOR frame, σ corresponds to $\{\xi = 0\}$. Correspondingly, the manifold $\mathcal{Z}$ is locally invariant on a sub-patch $\sigma(\mathcal{U}')$ if and only if $g(\eta, 0) = 0$ for $\eta \in \text{int } \mathcal{U}'$, or

$$\langle f \circ \sigma(\eta), N\sigma(\eta)\rangle = 0, \qquad \eta \in \text{int } \mathcal{U}'. \tag{5.2}$$

Thus, the manifold $\mathcal{Z}$ is best-aligned with the flow when $g(\eta, 0) = 0$, and we call the set $C_\sigma = \{\sigma(\eta) | g(\eta, 0) = 0\}$ the *confluence set* corresponding to $(\mathcal{U}, \sigma)$. Note that C_σ need not be invariant, as (5.2) is a only a necesary condition for invariance. Given an atlas (i.e., collection of charts) $\{(\mathcal{U}_\beta, \sigma_\beta)\}_{\beta\in B}$ of $\mathcal{Z}$, we define the full confluence set for $\mathcal{Z}$ by

$$C_{\mathcal{Z}} = \bigcup_{\beta\in B} C_{\sigma_\beta}.$$

We define a *river* as a trajectory ϕ such that $\phi(0) \in C_{\mathcal{Z}}$.

Note that computing an atlas for $\mathcal{Z}$ may be a non-trivial task, so we present a chart-free equivalent condition to membership in the confluence set, which is computationally efficient and also explicitly connects rivers to curvature.

Theorem 5.2.1. *The following are equivalent:*

1. $x \in \Omega$ *is a confluence.*
2. $\Delta_{(1,\cdots,n-1,n)} f(x) = \Delta_{(1,\cdots,n-1,n+1)} f(x) = 0.$
3. *The trajectory* ϕ *such that* $\phi(0) = x$ *satisfies*

$$\kappa_\phi(0) = \frac{d\kappa_\phi}{dt}(0) = 0.$$

Proof. Suppose that $x \in C_{\mathcal{Z}}$. Thus, $\kappa(x) = 0$ and $\langle f(x), \nabla\kappa(x)\rangle = 0$. Now, let ϕ be the trajectory such that $\phi(0) = x$. We have $\kappa_\phi(0) = \kappa \circ \phi(0) = 0$ and

$$0 = \langle f \circ \phi(t), \nabla\kappa \circ \phi(t)\rangle \Big|_{t=0} = \frac{d}{dt}\kappa \circ \phi(t)\Big|_{t=0} = \frac{d\kappa_\phi}{dt}(0)$$

where we have used the chain rule and the definition of $\kappa(x)$, respectively. Thus we have shown that 1 implies 3, and as the relations used are equalities, we have also shown that 3 imples 1.

From the definition of κ_ϕ, differentiation yields

$$\begin{aligned} \frac{d\kappa_\phi}{dt}(t) &= \frac{d}{dt}\left(\frac{\dot\phi(t) \wedge \cdots \wedge \phi^{(n)}(t)}{\alpha(\dot\phi(t), \cdots, \phi^{(n)}(t))}\right) \\ &= \frac{1}{\alpha}\left(\frac{d}{dt}\dot\phi(t) \wedge \cdots \wedge \phi^{(n)}(t) - \frac{\dot\phi(t) \wedge \cdots \wedge \phi^{(n)}(t)}{\alpha(\dot\phi(t), \cdots, \phi^{(n)}(t))}\frac{d}{dt}\alpha(\dot\phi(t), \cdots, \phi^{(n)}(t)).\right) \end{aligned} \tag{5.3}$$

Note that, at $t = 0$, $\dot\phi(0) \wedge \cdots \wedge \phi^{(n)}(0) = 0$ and therefore the $d\alpha/dt$ term in (5.3) will vanish. Hence, we need only compute the derivative of the wedge product. Based on the multi-linearity of the wedge product and the Δ notation from equation (5.1), we can write this expression as

$$\frac{d}{dt}\dot\phi \wedge \cdots \wedge \phi^{(n)} = \sum_{j=1}^{n} \Delta_{(1,\cdots,n)+e_j} f \circ \phi(t) \tag{5.4}$$

where e_j is the j^{th} canonical basis vector. Note that, for $1 \le j \le n-1$, the terms in the above sum have a repeated index, e.g. $(2, 2, 3, \cdots, n), (2, 3, 3, \cdots, n)$, and so on; these wedge

products are zero, as repeated vectors in a determinant are obviously collinear. Hence (5.4) reduces to

$$\frac{d}{dt}\dot{\phi} \wedge \cdots \wedge \phi^{(n)} = \dot{\phi} \wedge \ddot{\phi} \wedge \cdots \wedge \phi^{(n-1)} \wedge \phi^{(n+1)}$$

and hence $\kappa_\phi(0) = d\kappa_\phi/dt(0) = 0$ is equivalent to $\Delta_{1,2,\cdots,n-1,n} f(x) = \Delta_{1,2,\cdots,n-1,n+1} f(x) = 0$. Therefore we have shown that conditions 2 and 3 are equivalent, and hence 1 and 2 are equivalent as well. □

Theorem 5.2.1 provides an obvious corollary that can be used to compute $C_{\mathcal{Z}}$.

Corollary 11.

$$C_{\mathcal{Z}} = \{\Delta_{(1,\cdots,n-1,n)} f(x) = 0\} \cap \{\Delta_{(1,\cdots,n-1,n+1)} f(x) = 0\}.$$

Note that computing $C_{\mathcal{Z}}$ with Corollary 11 is chart-independent and hence is much more efficient than using the condition derived directly from invariance of $\mathcal{Z}$.

As a confluence is a point where the ZCL is well-aligned with the flow, we measure the strength of a river by checking the order of this alignment. Note that for a river ϕ, we can write

$$\kappa_\phi(t) = \frac{d^2\kappa_\phi}{dt^2}(0)t^2 + \mathcal{O}(t^3)$$

for small t. Thus, the strength of ϕ should be inversely proportional to $|d^2\kappa_\phi/dt^2(0)|$. This observation leads us to a classification of rivers.

Definition 5.2.2. A trajectory ϕ is a class k river if

$$\frac{d\kappa_\phi}{dt}(0) = \frac{d^2\kappa_\phi}{dt^2}(0) = \cdots = \frac{d^k\kappa_\phi}{dt^k}(0) = 0.$$

Clearly, every river is at least class 1. We can translate this condition into one involving the Δ notation from equation (5.1) after we establish some combinatorial notation.

Definition 5.2.3. Let $\mathscr{L}_0 = \{(1, \cdots, n)\}$. Using power set notation, define $G : 2^{\mathbb{N}_+^n} \to 2^{\mathbb{N}_+^n}, B : \mathbb{N}_+^n \to \mathbb{N}_+^n$ as follows:

$$G(S) = \bigcup_{\substack{s \in S \\ j \in \{1, \cdots, n\}}} s + e_j$$

$$B(s_1, s_2, \cdots, s_n) = \begin{cases} (s_1, s_2, \cdots, s_n) & s_i \neq s_j \text{ for all } 1 \leq i < j \leq n \\ \emptyset & \text{else} \end{cases} \tag{5.5}$$

and given any subset $S \subseteq 2^{\mathbb{N}_+^n}$ we define $B(S) = \cup_{s \in S} B(s)$.

Finally, define $\mathscr{L}_k = B \circ G(\mathscr{L}_{k-1})$ for $k > 0$. For convenience, we denote $\mathscr{L} = \cup_{k \geq 0} \mathscr{L}_k$.

Intuitively, G adds every canonical basis vector to each element of a set of positive integer vectors and B deletes any entry with a repeated index. With notation established, we provide an efficient way for identifying class k rivers.

Theorem 5.2.4. *A trajectory ϕ is a class k river if and only if $x = \phi(0)$ satisfies*

$$\sum_{\ell \in \mathscr{L}_i} \Delta_\ell f(x) = 0 \qquad \forall i \in \{0, \cdots, k\}.$$

Before proving this theorem, we prove a helpful computational lemma.

Lemma 5.2.5. *Suppressing time dependence,*

$$\frac{d^i}{dt^i} \dot{\phi} \wedge \cdots \wedge \phi^{(n)} = \sum_{\ell \in \mathscr{L}_i} \Delta_\ell f \circ \phi.$$

Proof. Note that $\mathscr{L}_1 = \{(1, \cdots, n-1, n+1)\}$, hence we have already shown the $i = 1$ case within the proof of Theorem 5.2.1. If the desired equality holds at the i^{th} level, then differentiation yields

$$\frac{d^{i+1}}{dt^{i+1}} \dot{\phi} \wedge \cdots \wedge \phi^{(n)} = \frac{d}{dt} \sum_{\ell \in \mathscr{L}_i} \Delta_\ell f \circ \phi.$$

Expanding, we obtain

$$\frac{d}{dt} \sum_{\ell \in \mathscr{L}_i} \Delta_\ell f \circ \phi = \frac{d}{dt} \sum_{\ell \in \mathscr{L}_i} \phi^{(\ell_1)} \wedge \cdots \wedge \phi^{(\ell_n)} = \sum_{\substack{\ell \in \mathscr{L}_i \\ j \in \{1, \cdots, n\}}} \phi^{(\ell_1 + \delta_{1,j})} \wedge \cdots \wedge \phi^{(\ell_n + \delta_{n,j})}$$

where $\delta_{i,j}$ denotes the Kronecker delta function. Collecting terms and using our definition of G gives

$$\sum_{\substack{\ell\in\mathscr{L}_i\\ i\in\{1,\cdots,n\}}} \phi^{(\ell_1+\delta_{1,i})}\wedge\cdots\wedge\phi^{(\ell_n+\delta_{1,i})} = \sum_{\substack{\ell\in\mathscr{L}_i\\ j\in\{1,\cdots,n\}}} \Delta_{\ell+e_j} f\circ\phi = \sum_{\ell\in G(\mathscr{L}_i)} \Delta_\ell f\circ\phi.$$

To conclude, we note that $\Delta_\ell\circ\phi = 0$ whenever ℓ features repeated indices. Hence,

$$\sum_{\ell\in G(\mathscr{L}_i)} \Delta_\ell f\circ\phi = \sum_{\ell\in B\circ G(\mathscr{L}_i)} \Delta_\ell f\circ\phi = \sum_{\ell\in\mathscr{L}_{i+1}} \Delta_\ell f\circ\phi,$$

and we have shown the result. □

Proof of Theorem 5.2.4. Note that we have already proven the $k=1$ case, which we will again use as a base case for induction. Suppose that ϕ is a river of class k.

For simplicity, introduce the notation $p(t) = \alpha(\dot\phi(t),\cdots,\phi^{(n)}(t))^{-1}$ so that, by definition,

$$\kappa_\phi(t) = p(t)(\dot\phi(t)\wedge\cdots\wedge\phi^{(n)}(t)).$$

Suppose that our assertion is true at the k^{th} level and differentiate to progress to the $(k+1)$ term. Suppressing time dependence,

$$\frac{d^{k+1}}{dt^{k+1}}\kappa_\phi = \sum_{i=0}^{k+1}\binom{k+1}{i}\frac{d^{k+1-i}p}{dt^{k+1-i}}\left(\frac{d^i}{dt^i}\dot\phi\wedge\cdots\wedge\phi^{(n)}\right).$$

Application of Lemma 5.2.5 implies that

$$\sum_{i=0}^{k+1}\binom{k+1}{i}\frac{d^{k+1-i}p}{dt^{k+1-i}}\left(\frac{d^i}{dt^i}\dot\phi\wedge\cdots\wedge\phi^{(n)}\right) = \sum_{i=0}^{k+1}\binom{k+1}{i}\frac{d^{k+1-i}p}{dt^{k+1-i}}\sum_{\ell\in\mathscr{L}_i}\Delta_\ell f\circ\phi,$$

which, using our induction hypothesis, simplifies to

$$\frac{d^{k+1}}{dt^{k+1}}\kappa_\phi = p\sum_{\ell\in\mathscr{L}_{k+1}}\Delta_\ell f\circ\phi.$$

Hence, ϕ is a river of class $k+1$ if and only if

$$\sum_{\ell\in\mathscr{L}_i}\Delta_\ell f\circ\phi(0) = 0 \qquad\qquad \forall i\in\{1,\cdots,k+1\},$$

as desired □

With this equivalent condition we can define a confluence of class k.

Definition 5.2.6. The set of class k confluences, denoted $C^k_{\mathcal{Z}}$, is given by

$$C^k_{\mathcal{Z}} = \bigcap_{i=0}^{k} \left\{ \sum_{\ell \in \mathscr{L}_i} \Delta_\ell f(x) = 0 \right\}$$

and a point $x \in \Omega$ is a confluence of class k if $x \in C^k_{\mathcal{Z}}$.

An immediate application of this definition gives the following relationship.

Corollary 12. *A trajectory ϕ is a class k river if and only if $\phi(0)$ is a class k confluence.*

In the generic case, the set of class k confluences will be an $n-k-1$ dimensional manifold. Therefore, the strongest river we can expect (generically) in $\mathbb{R}^n$ is of class $n-1$.

5.3 Normal Form Results

5.3.1 Rivers and Canards

Here we consider the truncated normal form for the flow near a canard point [61],

$$\begin{pmatrix} \dot{x}_1 \\ \dot{x}_2 \\ \dot{x}_3 \end{pmatrix} = \begin{pmatrix} \varepsilon(bx_2 + cx_3) \\ \varepsilon a \\ x_1 + x_3^2 \end{pmatrix} =: f(x;\varepsilon) \tag{5.6}$$

where $0 < \varepsilon \ll 1$ is a timescale parameter, $a, b, c \in \mathbb{R}$, and $(0,0,0)$ is the canard point. In system (5.6), we refer to x_1, x_2 as slow variables and x_3 as a fast variable. As a two-timescale system, (5.6) has a critical manifold, given by the set $\mathcal{M} = \{x_1 = -x_3^2\}$ where $\dot{x}_3 = 0$, which can be decomposed into stable and unstable branches and the fold set given by $\mathcal{M}_S = \{x_1 = -x_3^2 | x_3 < 0\}, \mathcal{M}_U = \{x_1 = -x_3^2 | x_3 > 0\}$ and $\mathcal{M}_F = \{x_1 = x_3 = 0\}$, respectively. Trajectories of interest to us begin near the stable branch of $\mathcal{M}$, approach the fold, and linger near the repelling sheet for some amount of time.

To begin, we will identify the confluences of system (5.6), which we describe in the following proposition.

Proposition 7. *If $c^2 - 8ab > 0$ and $b \neq 0$ then there are two branches of infinite-class confluences of system* (5.6)*, given by*

$$C^{\infty}_{\mathcal{Z},\pm} = \left\{ x_1 = -x_3^2 - \frac{\varepsilon}{4}(c \pm \omega), x_2 = -\frac{x_3}{2b}(c \mp \omega) \middle| \, x_3 \in \mathbb{R} \right\}$$

where $\omega := \sqrt{c^2 - 8ab}$. These branches are invariant in the truncated normal form.

Proof. Let

$$\Gamma_{\pm}(\eta) = \left(-\eta^2 - \frac{\varepsilon}{4}(c \pm \omega), -\frac{\eta}{2b}(c \mp \omega), \eta \right)$$

denote parameterizations of $C^{\infty}_{\mathcal{Z},\pm}$, respectively. First we will demonstrate that $C^{\infty}_{\mathcal{Z},\pm}$ is invariant under (5.6). Suppose we reparameterize $\Gamma_{\pm}$ by $\Gamma_{\pm} \circ \eta(t)$ for some unknown function η, then

$$\frac{d}{dt}\Gamma_{\pm} \circ \eta(t) = (-2\eta, -\frac{c \mp \omega}{2b}, 1)\dot{\eta}$$

and

$$f(\Gamma_{\pm} \circ \eta(t), \varepsilon) = \left(\frac{\varepsilon(c \pm \omega)}{2}\eta, \varepsilon a, -\frac{\epsilon(c \pm \omega)}{4} \right)$$

if we choose

$$\dot{\eta} = -\frac{\varepsilon(c \pm \omega)}{4} \tag{5.7}$$

then

$$\frac{d}{dt}\Gamma_{\pm} \circ \eta(t) = f(\Gamma_{\pm} \circ \eta(t), \varepsilon)$$

and hence $C^{\infty}_{\mathcal{Z},\pm}$ are invariant under (5.6). To conclude, we note that $\Gamma_{\pm}$ itself has identically zero curvature, i.e.

$$\det(\Gamma'_{\pm}(\eta), \Gamma''_{\pm}(\eta), \Gamma'''_{\pm}(\eta)) \equiv 0,$$

which will be preserved under reparameterization. Thus, the trajectories $\phi_{\pm}(t) := \Gamma_{\pm} \circ \eta(t)$ have identically zero curvature for all time, which implies that

$$\kappa_{\phi_{\pm}}(t) = \frac{d}{dt}\kappa_{\phi_{\pm}}(t) = \cdots = \frac{d^k}{dt^k}\kappa_{\phi_{\pm}}(t) = \cdots = 0 \qquad \forall k \in \mathbb{N}, t \in \mathbb{R}$$

and hence $\Gamma_{\pm}$ parameterize sets of infinite-class confluences. □

Corollary 13. *If $c^2 - 8ab > 0$ and $b \neq 0$ then*

$$\phi_\pm(t) = \left(-\alpha_\pm^2 t^2 - \frac{\varepsilon c}{4} \pm \varepsilon\omega, -\frac{\alpha_\pm c t}{2b} \pm \alpha_\pm \omega t, \alpha_\pm t \right) \tag{5.8}$$

are trajectories of (5.6)*, where* $\omega = \sqrt{c^2 - 8ab}, 4\alpha_\pm = -\varepsilon(c \pm \omega)$.

Proof. Solving (5.7) with initial condition $\eta(0) = 0$ yields the result. □

Corollary 14. *The trajectories defined by* (5.8) *are the maximal canards for* $\varepsilon \geq 0$.

Proof. Note that $\phi_{\pm,1}(t) + \phi_{\pm,3}^2(t)\alpha_\pm$; hence for all $t \in [0, \infty)$, $\phi_\pm(t)$ is $\mathcal{O}(\varepsilon)$ near the repelling branch of the critical manifold and for all $t \in (-\infty, 0]$, $\phi_\pm(t)$ is $\mathcal{O}(\varepsilon)$ close to the attracting branch of the critical manifold. □

Theorem 5.3.1. *The maximal canards of* (5.6) *are rivers of infinite order.*

Proof. The conditions $c^2 - 8ab > 0, b \neq 0$ is the same condition presented in [61] for the existence of canards, specifically it guarantees that the folded singularity is not a folded focus or a folded saddle-node. The previous proposition with its corollaries demonstrate the result. If $c^2 - 8ab \leq 0, b \neq 0$ the system (5.6) has nFo maximal canards, thus the result is vacuously true. □

Corollary 15. *If $b = 0$, the maximal canards of* (5.6) *are rivers of inifinite order.*

Proof. If $b = 0$, then the folded singularity in (5.6) is a folded saddle-node, in which case the base normal form without non-linear terms becomes [66]

$$\begin{pmatrix} \dot{x}_1 \\ \dot{x}_2 \\ \dot{x}_3 \end{pmatrix} = \begin{pmatrix} \varepsilon\left(\frac{\mu}{2}x_2 - (\mu+1)x_3\right) \\ \varepsilon \\ x_1 + x_3^2 \end{pmatrix} \tag{5.9}$$

which, following the proof techniques of the previous results, has two invariant branches of infinite-class confluences, given by

$$C^\infty_{\mathcal{Z},i} = \left\{ x = -z^2 + \varepsilon\frac{1 + i(\mu-1)}{2}, y = \frac{2z}{1 + i(\mu-1)} \middle| z \in \mathbb{R} \right\}$$

for $i \in \{0, 1\}$. Replacing $C^\infty_{\mathcal{Z},\pm}$ with $C^\infty_{\mathcal{Z},i}$ in the previous proofs generates the result. □

5.3.2 Dynamics near the River-canard

We can use Local Orthogonal Rectification (LOR) to understand how trajectories behave near our infinite-class rivers and, in so doing, provide a novel analysis tool for canards.

We will choose our basecurve as one of the curves $\Gamma_\pm$ identified in the previous section. Note that, as we demonstrated in the proof of Prop.7, the curves $\Gamma_\pm$ are invariant under the flow of our normal form, and have $\kappa_2(\eta) \equiv 0$. Therefore we can simplify the LOR equations greatly, as $C(\eta) \equiv 0$, hence we have

$$\mathcal{L}_{\Gamma_\pm} f(\eta, \xi) = \begin{pmatrix} \frac{Tf(\eta,\xi)}{\|\gamma'(\eta)\|\,(1-\xi_1\kappa_1(\eta))} \\ Nf(\eta,\xi) \end{pmatrix}.$$

Furthermore, as $\Gamma_\pm$ are invariant, we know that $Nf(\eta, 0) = 0$ as $\{\xi = 0\}$ maps to the set $\{\Gamma(\eta) | \eta \in \mathbb{R}\}$ under Ψ, hence $\dot{\xi}|_{\xi=0} = 0$, thus to lowest order

$$\mathcal{L}_{\Gamma_\pm} f(\eta, \xi) = \begin{pmatrix} \frac{Tf(\eta,0)}{\|\gamma'(\eta)\|} + \mathcal{O}(\|\xi\|) \\ D_\xi Nf(\eta,0)\xi + \mathcal{O}(\|\xi\|^2) \end{pmatrix}. \tag{5.10}$$

We will use this approximate system to understand how trajectories near our river-canards are funnelled towards the canard point, linger near the fold, and are pushed away from the repelling manifold; specifically we will demonstrate that trajectories approach the fold along an *invariant angular manifold*, experience a short period of unconstrained rotation, and exit the neighborhood of the repelling manifold along a stable invariant angular manifold.

In order to expose the angular dynamics hidden in system (5.10), we will represent our ξ dynamics in polar coordinates, i.e. we let $\xi = (r\cos\theta, r\sin\theta)$ and compute the ODEs induced on r, θ, which are given by

$$\dot{\eta} = \frac{Tf(\eta, r\cos\theta, r\sin\theta)}{\|\gamma'(\eta)\|\,(1 - r\cos\theta\kappa_1(\eta))} \tag{5.11}$$

$$\dot{r} = \left\langle (\cos\theta, \sin\theta), \dot{\xi} \right\rangle$$

$$r\dot{\theta} = (\cos\theta, \sin\theta) \wedge \dot{\xi}. \tag{5.12}$$

This change of coordinates is functionally equivalent to blowing up the entirety of the river-canard trajectory; although we note that we can avoid using the unpleasant chart conventions, as we do not need to increase the dimension of our system.

At first glance, the third equation seems problematic, as we are interested in the region where $r \ll 1$, however note that

$$\lim_{r\to 0} \frac{z(\theta) \wedge Nf(\eta, rz(\theta))}{r} = \lim_{r\to 0} \frac{z(\theta) \wedge D_\xi Nf(\eta, rz(\theta))z(\theta)}{1} = z(\theta) \wedge D_\xi Nf(\eta, 0)z(\theta)$$

from L'Hopitals rule, as $Nf(\eta, 0) = 0$. Therefore our small r dynamics are given by

$$\begin{aligned}
\dot{\eta} &= Tf(\eta, 0) + \mathcal{O}(r) \\
\dot{r} &= \langle D_\xi Nf(\eta, 0)z(\theta), z(\theta)\rangle\, r + \mathcal{O}(r^2) \\
\dot{\theta} &= -D_\xi Nf(\eta, 0)z(\theta) \wedge z(\theta) + \mathcal{O}(r)
\end{aligned} \tag{5.13}$$

where $z(\theta) = (\cos\theta, \sin\theta)$. In effect, we have performed a geometric desingularization along the entirety of $\Gamma_\pm$, as the set $\{r = 0\}$ is invariant under the above, and we have uncovered non-trivial angular dynamics on the set $\{r = 0\}$, given by

$$\begin{aligned}
\dot{\eta} &= \frac{Tf(\eta, 0)}{\gamma'(\eta)} \\
\dot{\theta} &= -D_\xi Nf(\eta, 0)z(\theta) \wedge z(\theta)
\end{aligned} \tag{5.14}$$

which will be dominant in the region where $r \ll 1$, i.e. near the river-canards. Once we understand these dynamics, we can piece together a full picture of the dynamics by considering the $\dot{r}$ equation to leading order, to learn how trajectories are drawn to, or pushed away from, our river-canards.

First we will study the dynamics in the invariant subset $\{r = 0\}$. Let $D_\xi Nf(\eta, 0; \varepsilon) =: A(\eta; \varepsilon)$. Using the reparameterization described in Cor. 13, we have

$$\frac{Tf(\eta, 0)}{\gamma'(\eta)} = \frac{-\varepsilon(c \pm \omega)}{4}$$

therefore system (5.14) is a fast-slow system. Note that this system is invariant under the transformation $\theta \mapsto \theta + \pi$, hence if $(\eta(t), \theta(t))$ is a solution to the above, $(\eta(t), \theta(t) + \pi)$ will also be a solution. We have a critical manifold given by

$$\mathcal{M}_{ang} = \{A(\eta; 0)z(\theta) \wedge z(\theta) = 0\}$$

which will change shape based on the folded singularity, several examples of which are shown below.

Note that $x \wedge y = 0$ if and only if $x = cy$ for some scalar c, hence our critical manifold can be re-expressed as

$$\mathcal{M}_{ang} = \{(\eta, \theta) | \exists \lambda : A(\eta; 0) z(\theta) = \lambda z(\theta)\}$$

or stated more naturally, $(\eta, \theta) \in \mathcal{M}_{ang}$ if and only if $z(\theta)$ is an eigenvector of $A(\eta; 0)$, furthermore as $\|z(\theta)\| = 1$ the eigenvalue associated with $z(\theta)$ must be $\lambda = \langle A(\eta; 0) z(\theta), z(\theta) \rangle$. Note that $\langle A(\eta; 0) z(\theta), z(\theta) \rangle$ appears as the leading order coeffecient of r in (5.13), hence the radial stability is closely related to the angular manifolds. Furthermore, $\det A(\eta; 0) = 0$ for all η regardless of a, b, c, thus the eigenvalues of $A(\eta; 0)$ are $0, \mathrm{tr} A(\eta) = 2\eta$. We will label the two branches of the critical manifold:

$$\mathcal{M}_{ang,0} = \{(\eta, \theta) \in \mathcal{M}_{ang} | A(\eta; 0) z(\theta) = 0\}$$
$$\mathcal{M}_{ang,tr} = \{(\eta, \theta) \in \mathcal{M}_{ang} | A(\eta; 0) z(\theta) = 2\eta z(\theta)\}.$$

The stability and hyperbolicity of the critical manifold will be determined by the sign of $\partial \dot{\theta} / \partial \theta$, which can be computed using (5.14)

$$\frac{\partial \dot{\theta}}{\partial \theta} = -A(\eta; 0) z'(\eta) \wedge z(\theta) - A(\eta; 0) z(\eta) \wedge z'(\theta).$$

We make use of the following equalities

$$A(\eta; 0) z(\theta) \wedge z'(\theta) = \langle A(\eta; 0) z(\theta), z(\theta) \rangle$$
$$-A(\eta; 0) z'(\theta) \wedge z(\theta) + A(\eta; 0) z(\theta) \wedge z'(\theta) = \mathrm{tr} A(\eta)$$

to reduce

$$\frac{\partial \dot{\theta}}{\partial \theta} = \mathrm{tr} A(\eta; 0) - 2 \langle A(\eta; 0) z(\theta), z(\theta) \rangle .$$

Given what we have deduced about $\langle A(\eta; 0) z(\theta), z(\theta) \rangle$, namely that it is either 0 or 2η on $\mathcal{M}_{ang}$, we can reduce

$$\left. \frac{\partial \dot{\theta}}{\partial \theta} \right|_{\mathcal{M}_{ang,0}} = 2\eta \qquad \left. \frac{\partial \dot{\theta}}{\partial \theta} \right|_{\mathcal{M}_{ang,t}} = -2\eta$$

hence the branch of $\mathcal{M}_{ang}$ associated with the zero eigenvector will be stable for $\eta < 0$, lose hyperbolicity at $\eta = 0$, and become unstable for $\eta > 0$; the other eigenvector will have the opposite stability.

With this information, we can organize the $(\eta, \theta, 0)$ plane: trajectories having initial conditions with $\eta < 0$ will be attracted to the set $\{A(\eta; 0)z(\theta) = 0\}$ and travel along this set until $\eta(t) = \mathcal{O}(\varepsilon)$. Trajectories will rotate freely in the neighborhood of $\eta = 0$ until they are drawn to the set $\{A(\eta)z(\theta) = 2\eta z(\theta)\}$ and travel along this branch of the critical manifold indefinitely.

Now we want to add the radial dynamics into the mix. We compute that

$$\dot{r} = \langle A(\eta; 0)z(\theta), z(\theta)\rangle\, r + h(\eta, \theta)r^2 + \mathcal{O}(\varepsilon)$$

where $h(\eta, \theta)$ is a smooth function which satisfies $h(\eta, \theta + \pi) = -h(\eta, \theta)$. In the domain where r is non-zero but small, we can use our knowledge of the (η, θ) dynamics on $\{r = 0\}$ to approximate the r dynamics.

Suppose that $(\eta(t), r(t), \theta(t))$ is a solution to the system (5.11) with initial condition (η_0, r_0, θ_0). If r_0 is small, then $(\eta(t), \theta(t))$ will be well-approximated by (5.14). Denote by $(\tilde{\eta}(t), \tilde{\theta}(t))$ the solution to (5.14) with initial conditions $(\tilde{\eta}(0), \tilde{\theta}(0)) = (\eta_0, \theta_0)$. In order to approximate the radial dynamics we will consider the ODE

$$\dot{\tilde{r}} = \left\langle A(\tilde{\eta}; 0)z(\tilde{\theta}), z(\tilde{\theta})\right\rangle r + h(\tilde{\eta}, \tilde{\theta})r^2 \tag{5.15}$$

where $\tilde{\eta}, \tilde{\theta}$ are known functions of t, hence $\tilde{r}$ satisfies a Bernoulli equation, then $|r(t) - \tilde{r}(t)|$ should remain small for t near zero.

Furthermore, if $\eta_0 < 0$, our approximate angular solutions will rapidly evolve to $\mathcal{M}_{ang,0}$. Interestingly, the bilinear form in (5.15) will vanish along $\mathcal{M}_{ang,0}$, as $A(\tilde{\eta}; 0)z(\tilde{\theta}) = 0$, hence our $\tilde{r}$ dynamics will display quadratic approach behavior. It can be shown that

$$h(\eta, \theta)\Big|_{\mathcal{M}_{ang,0}} \neq 0$$

for all (η, θ), and, as $\mathcal{M}_{ang,0}$ contains 2 identical, π-shifted branches, which we will denote by $\mathcal{M}_{ang,0,S}, \mathcal{M}_{ang,0,R}$, we conclude

$$h(\eta,\theta)\Big|_{\mathcal{M}_{ang,0,S}} < 0 \qquad\qquad h(\eta,\theta)\Big|_{\mathcal{M}_{ang,0,U}} > 0.$$

Unpacking this expression, there is one branch of $\mathcal{M}_{ang,0}$ which will be *radially* stable and *angularly* stable, while the other branch of $\mathcal{M}_{ang,0}$ will be angularly stable and radially unstable. Therefore, our canard solution will only trap trajectories which approach from the right initial angles; this radial and angular analysis has demonstrated the existence of the canard funnel effect.

The trajectories which are trapped in the canard funnel, those whose angular approximations approach $\mathcal{M}_{ang,0,S}$, will have quadratically decreasing radial components; therefore our accuracy of our radial approximation will increase over time, as $r(t)$ will be approaching zero. Thus, we can use our approximation up to an $\mathcal{O}(\varepsilon)$ neighborhood of the fold $\{\eta = 0\}$, where the normal hyperbolicity of $\mathcal{M}_{ang,0,S}$ breaks down.

To conclude this section, we will show that we can easily extract the way-in way-out function for the system, using the LOR dynamics. Suppose that ϕ is a trajectory with initial conditions $\phi(0) = (\eta_0, r_0, \theta_0)$ which are in the funnel (namely $\eta_0 < 0$, θ_0 is near $\mathcal{M}_{ang,0,S}$, and $r_0 \ll 1$) will be drawn towards $r = 0$ until it reaches the fold, $\eta = 0$. As we have previously noted, the radial stability along the angularly-stable slow manifold changes as ϕ crosses the fold; after the fold ϕ will be repelled from $r = 0$. However, ϕ will not immediately escape the neighborhood of $r = 0$, indeed ϕ can be delayed for as long as $\mathcal{O}(1/\varepsilon)$ time. In order to explain this delay effect, we will construct the WIWO function.

Let $\phi(t) =: (\eta(t), r(t), \theta(t))$ and define

$$T(r_0, \eta_0) = \inf_{t>0}\{r(t) = r_0 | \eta(0) = \eta_0\}$$

which is, intuitively, the first time that $r(t)$ has returned to its initial value. As $r(t)$ will decrease until after η has crossed zero, we expect $T(r_0, \eta_0)$ to approximate the time at which $r(t)$ is escaping from zero. The WIWO function is the mapping

$$H(r_0, \eta_0) = \eta \circ T(r_0, \eta_0)$$

i.e. H measures the value of η at which r leaves a neighborhood of zero.

Note that we can numericaly integrate the solutions to the full, unapproximated system (5.11) and compute the WIWO function directly, which is shown in Fig. 34. However this is a mechanistically unsatisfactory solution, and we can better explain the cause of this delay by approximation the radial dynamics implicitly.

Following the derivation of (5.15), we suppose we can solve the η, θ dynamics for $r = 0$, which can be given by

$$\frac{d\theta_a}{d\eta} = -\frac{4}{\varepsilon\lambda_\pm} \langle A(\eta;\varepsilon)z(\theta_a), z(\theta_a)\rangle \qquad\qquad \theta_a(\eta_0) = \theta_0$$

where $\lambda_\pm = (c \pm \omega)/2$, which will be a reparameterized solution to (5.14). Then we approximate the r dynamics by solving

$$\frac{dr_a}{d\eta} = -\frac{4}{\varepsilon\lambda_\pm}\left(l(\eta)r_a + q(\eta)r_a^2\right)$$

where $l(\eta) = \langle A(\eta;\varepsilon)z(\theta_a(\eta)), z(\theta_a(\eta))\rangle$, $q(\eta) = h(\eta, \theta_a(\eta))$, recalling that $h(\eta, \eta)$ is the coeffecient multiplying the r^2 term in the expansion of the r dynamics. This ODE can be solved explicitly, but it is most useful to semi-solve as

$$\exp\left(-\frac{4}{\varepsilon\lambda_\pm}\int_{\eta_0}^{\eta} l(\sigma)\mathrm{d}\sigma\right)\frac{1}{r_a(\eta)} = \frac{1}{r_0} + \frac{4}{\varepsilon\lambda_\pm}\int_{\eta_0}^{\eta}\exp\left(-\frac{4}{\varepsilon\lambda_\pm}\int_{\eta_0}^{s} l(\sigma)\mathrm{d}\sigma\right)q(s)\mathrm{d}s.$$

We are interested in approximating the η at which $r_a(\eta) = r_0$, subsitituting and re-arranging

$$1 = \exp\left(\frac{4L(\eta)}{\varepsilon\lambda_\pm}\right)\left(1 + \frac{4r_0}{\varepsilon\lambda_\pm}\int_{\eta_0}^{\eta}\exp\left(-\frac{4L(s)}{\varepsilon\lambda_\pm}\right)q(s)\mathrm{d}s\right)$$

where $L(\eta) = \int_{\eta_0}^{\eta} l(\sigma)\mathrm{d}\sigma$. Hence

$$-\frac{4L(\eta)}{\varepsilon\lambda_\pm} = \ln\left(1 + \frac{4r_0}{\varepsilon\lambda_\pm}\int_{\eta_0}^{\eta}\exp\left(-\frac{4L(s)}{\varepsilon\lambda_\pm}\right)q(s)\mathrm{d}s\right).$$

Here we will apply what we know about $L(\eta)$, namely that

$$L(\eta) = \begin{cases} 0 & \eta < 0 \\ \eta^2 & \eta \geq 0 \end{cases}$$

as θ will approach the fold along $\mathcal{M}_{ang,0}$ hence $l(\eta)) = 0$ for $\eta < 0$ and after the fold θ will be attracted to $\mathcal{M}_{ang,t}$ and $l(\eta) = 2\eta$. Making use of $\ln(1+x) = x + \mathcal{O}(x^2)$ we find

$$-\eta^2 = r_0 \left(Q_0 + \int_0^\eta \exp\left(\frac{-4s^2}{\varepsilon\lambda_\pm}\right) q(s)\mathrm{d}s \right) + \mathcal{O}\left(r_0^2\right)$$

where $Q_0(\eta_0) = \int_{\eta_0}^0 q(s)\mathrm{d}s$, which we call the quadratic residual. Noting that $Q_0(\eta_0) < 0$ (as we have approched on the funnel side), we rearrange this into its final form,

$$\int_0^\eta \exp\left(-\frac{4s^2}{\varepsilon\lambda_\pm}\right) q(s)\mathrm{d}s + \frac{\eta^2}{r_0} = -Q_0(\eta_0) + \mathcal{O}(r_0).$$

Now our escape condition is (somewhat) understandable; in order to escape from the river-canard, our trajectory must overcome the quadratic residual term.

The integral on the left hand side of the above will diverge rapidly from zero, as $\exp(\frac{1}{\varepsilon^2})$ is exceedingly large. Note, however, that the integral need not be increasing after $\eta = 0$; indeed for $\eta \in [0, .31]$, $F(\eta)$ is decreasing in Fig. 35, as $q(\eta) < 0$ for those values.

Define

$$F(\eta) = \int_0^\eta \exp\left(-\frac{4s^2}{\varepsilon\lambda_\pm}\right) q(s)\mathrm{d}s + \frac{\eta^2}{r_0} \tag{5.16}$$

and note that

$$\begin{aligned} F\left(\frac{\sqrt{-\varepsilon\lambda_\pm}}{2}\right) &= \frac{\sqrt{-\varepsilon\lambda_\pm}}{2} \int_0^1 \exp(u^2) q\left(\frac{\sqrt{-\varepsilon\lambda_\pm}u}{2}\right) + \frac{\varepsilon|\lambda_\pm|}{4} \\ &\leq \frac{\sqrt{-\varepsilon\lambda_\pm}}{2} \int_0^1 q(0)\mathrm{d}u + \mathcal{O}(\varepsilon) \end{aligned}$$

and, as $q = \mathcal{O}(1)$, $F(\sqrt{-\varepsilon\lambda_\pm}/2) = \mathcal{O}(\sqrt{\varepsilon})$ and hence $H_a(r_0, \eta_0) > \sqrt{-\varepsilon\lambda_\pm}/2$ for r_0 sufficiently small. The curves $F(\eta), -Q_0(\eta_0)$ are shown in Fig. 35.

Note that the left-hand side of our escape condition is approach agnostic, changing η_0 will only affect $Q_0(\eta_0)$ on the right hand side. One of the more curious features of the WIWO function is the buffer point effect: a buffer point is a value η^* such that all trajectories will leave the river-canard before $\eta = \eta^*$, regardless of η_0. In some sense, the buffer point is the longest a solution can be delayed. In our LOR system, the buffer point phenomenon is easily understood; sending $\eta_0 \to -\infty$, we find

$$\lim_{\eta_0 \to -\infty} Q_0(\eta_0) = Q_0^*$$

i.e. $q(s)$ is integrable on $(-\infty, 0]$, hence our quadratic residual will always have finite size, and the rapidly diverging integral will always overcome Q_0^*, hence the buffer point solves $F(\eta^*) = -Q_0^*$.

The preceding analysis is summarized in the following proposition.

Proposition 8. *The way-in way-out function, $H(\eta_0, r_0)$ will satisfy*

$$-\frac{4L \circ H(\eta_0, r_0)}{\varepsilon\lambda_\pm} = \ln\left(1 + \frac{4r_0}{\varepsilon\lambda_\pm}\int_{\eta_0}^{H(\eta_0,r_0)} \exp\left(-\frac{4L(s)}{\varepsilon\lambda_\pm}\right) q(s)\,ds\right).$$

and will be approximated by the solution to

$$F \circ H(\eta_0, r_0) = -Q_0(\eta_0) + \mathcal{O}(r_0)$$

where

$$F(\eta) = \int_0^\eta \exp\left(-\frac{4s^2}{\varepsilon\lambda_\pm}\right) q(s)\,ds + \frac{\eta^2}{r_0}$$

and

$$Q_0(\eta_0) = \int_{\eta_0}^0 q(s)\,ds.$$

Trajectories in the funnel which have $r(0) = r_0 \ll 1$ must remain within a tube of radius r_0 around $\Gamma_\pm$ until $\eta > \sqrt{-\varepsilon\lambda_\pm}/2$, or for at least $2/\sqrt{-\varepsilon\lambda_\pm}$ time after crossing the fold. Let

$$Q_0^* = \lim_{\eta_0 \to -\infty} Q_0(\eta_0)$$

all trajectories in the funnel must exit a tube of radius r_0 around $\Gamma_\pm$ before η^* given by

$$F(\eta^*) = -Q_0^*.$$

The LOR frame has given us a new perspective on the dynamics near our river-canard solutions. Instead of tracking solutions through multiple blow-up charts, we can desingularize the dynamics along the entrie river-canard trajectory; instead of complexifying time to evaluate way-in way-out integrals along elliptical contours, we can approximate the radial dynamics explicitly. By viewing the normal-form flow from the perspective of the river-canards, we expose non-trivial dynamics in a geometric way. This approach also exposes the essential assymmetry in the way nearby trajectories appoach and depart from canards; trajectories in the funnel region, which itself is the product of quadratic stability, will be drawn to $r = 0$ algebraically yet will escape exponentially.

5.4 Transformations

5.4.1 Nearly Curvature Preserving Maps

In this section we consider the case $n = 3$ for fast-slow systems. First we will establish two computational lemmas. The crux of these results is understanding how certain transformations of a flow affect the curvature of the flow.

Definition 5.4.1. Suppose that $\dot{x} = f(x)$ induces a flow for $x \in \mathbb{R}^3$, and $H : \mathbb{R}^3 \to \mathbb{R}^3$ is a smooth diffeomorphism. Let $y = H(x)$, then we can induce the flow

$$\dot{y} = [D_x H(x)]\dot{x} = [D_x H \circ H^{-1}(y)] f \circ H^{-1}(y) =: g(y)$$

on y. We say that H is Δ_ℓ-preserving if $\Delta_\ell f(x) = 0$ if and only if $\Delta_\ell\ g \circ H(x) = 0$ for all $\ell \in \mathscr{L}$.

If $\dot{x} = f(x)$ is a fast-slow system with timescale parameter $0 < \varepsilon \ll 1$, we say that H is nearly Δ_ℓ-preserving to order k if there exists a smooth, positive definite, $\mathcal{O}(1)$ map $C(x)$ such that

$$C(x)\Delta_\ell f(x) - \Delta_\ell\ g \circ H(x) = \mathcal{O}(\varepsilon^k)$$

for all x in an $\mathcal{O}(\varepsilon)$ neighborhood of the critical manifold.

Note, as curvature is a geometric property, most non-linear maps are not ZCL preserving.

Lemma 5.4.2. *Non-degenerate linear mappings are Δ-preserving.*

Proof. Denote $H(x) = Ax$ where A is invertible, then it is simple to compute $y^{(i)} = Ax^{(i)}$ so $\Delta_\ell g \circ H(x) = \det(A)\Delta_\ell f(x)$. □

Lemma 5.4.3. *Given a 1-fast 2-slow system*

$$\dot{x} = \begin{pmatrix} \varepsilon g_1(x_1, x_2, x_3; \varepsilon) \\ \varepsilon g_2(x_1, x_2, x_3; \varepsilon) \\ F(x_1, x_2, x_3; \varepsilon) \end{pmatrix} =: f(x; \varepsilon) \tag{5.17}$$

then near identity transformations are nearly Δ_ℓ preserving to order $|\ell| + 1$.

Proof. We can write $H(x;\varepsilon) = x + \varepsilon h(x;\varepsilon)$, and inductively compute

$$y^{(i)} = \left(I_n + \varepsilon D_x h(x,\varepsilon)\right) x^{(i)} + \mathcal{O}(\varepsilon^{i+1})$$

when x is in an $\mathcal{O}(\varepsilon)$ neighborhood of the critical manifold. Here we have used the fact that, when x is $\mathcal{O}(\varepsilon)$ close to the critical manifold, $x^{(i)} = \mathcal{O}(\varepsilon^i)$. Computing the wedge products

$$\Delta_\ell \; g \circ H(x) = \det(I_n + \varepsilon D_x h(x;\varepsilon)) \Delta_\ell f(x) + \mathcal{O}\left(\varepsilon^{|\ell|+1}\right),$$

taking $C(x) = \det(I_n + \varepsilon D_x h(x;\varepsilon)) = 1 + \mathcal{O}(\varepsilon)$ proves the result. □

Note that in a fast-slow system, when x is $\mathcal{O}(\varepsilon)$ close to the critical manifold, we expect $\Delta_\ell f(x;\varepsilon)$ to be $\mathcal{O}(\varepsilon^{|\ell|})$, which is to say it has the form

$$\Delta_\ell f(x;\varepsilon) = \frac{\partial^{|\ell|}}{\partial \varepsilon^{|\ell|}} \Delta_\ell f(x;0) \frac{\varepsilon^{|\ell|}}{|\ell|!} + \mathcal{O}\left(\varepsilon^{|\ell|+1}\right)$$

from Taylor's equation.

Definition 5.4.4. The set of class k near-confluences, denoted by $C^k_{\mathcal{Z},\varepsilon}$, is given by

$$C^k_{\mathcal{Z},\varepsilon} = \bigcap_{i=0}^{k} \left\{ x \in B(\mathcal{M}, \mathcal{O}(\varepsilon)) \,\middle|\, \sum_{\ell \in \mathscr{L}_i} \frac{\partial^{|\ell|}}{\partial \varepsilon^{|\ell|}} \Delta_\ell f(x;0) = 0 \right\}$$

5.4.2 On the Nonexistence of Terrestrial Canards

Combining this definition with Lemmas 5.4.2, 5.4.3 and Theorem 5.3.1 yields the following result.

Theorem 5.4.5. *Given a 1-fast 2-slow system of the form* (5.17) *which satisfies the sufficient conditions for a canard point, then the canard solutions to* (5.17) *lie* $\mathcal{O}(\varepsilon)$ *close to the set* $C^3_{\mathcal{Z},\varepsilon}$.

Proof. As (5.17) satisfies the sufficient conditions for a canard point, there are a sequence of linear and near-identity transformations which convert (5.17) to the canard point normal form (5.6). We have already demonstrated the existance of river-canard solutions to the truncated normal form in Theorem 5.3.1. Applying the inverse linear and near-identity transformations (which are themselves linear and near-identity transformations, respectively), we can track the set $C^3_{\mathcal{Z}}$ using Lemmas 5.4.2, 5.4.3; namely they will be mapped to the set $C^3_{\mathcal{Z},\varepsilon}$. Finally, we note that under the inverse linear and near-identity transformations the canard solution of the normal form (5.6) must remain $\mathcal{O}(\varepsilon)$ close to the image of $C^3_{\mathcal{Z}}$. □

As the set $C^3_{\mathcal{Z},\varepsilon}$ can be computed, with the aid of numerical or symbolic computational tools, we can use $C^3_{\mathcal{Z},\varepsilon}$ to find the canard solutions of any system in which they exist. More details on the exact nature of this approximation are given in the following section, however the outline of the process is quite simple: given the system (5.17) we identify $C^3_{\mathcal{Z},\varepsilon}$ by computing series expansions of $\Delta_{1,2,3}, \Delta_{1,2,4}, \Delta_{1,2,5} + \Delta_{1,3,4}$ in ε, then we use this set as a pool of initial conditions, the trajectories through $C^3_{\mathcal{Z},\varepsilon}$ will be $\mathcal{O}(\varepsilon)$ close to the canard solution we desire. Indeed, canards must stay close to weak rivers.

5.5 The Autocatalator System

In this final section of this chapter, we present a well-known example of a system which displays canard solutions, the autocatalator system.

We will study the dynamics given by

$$\begin{aligned}\dot{a} &= \varepsilon\left(\mu\left(\frac{5}{2}+c\right)-ab^2-a\right)\\ \dot{b} &= ab^2+a-b\\ \dot{c} &= \varepsilon(b-c)\end{aligned} \tag{5.18}$$

where $0 < \varepsilon \ll 1, \mu > 0$ are parameters. The system represents the dynamics of a chemical reaction involving three reactants, the concentrations of which are proportional to a, b, c. In this reaction schema, reactant B slowly bolsters the concentration of reactant C, which, in the presence of reactant A, produces more of itself and reactant B. The fact that reactant B begets more of itself is the source of the name of the system.

In the singular limit, we find $\mathcal{M} = \{a = b/(1+b^2)\}$ to be the critical manifold of the system, with

$$\begin{aligned}\mathcal{M}_S &= \left\{a = \frac{b}{1+b^2}, |b| < 1\right\}\\ \mathcal{M}_U &= \left\{a = \frac{b}{1+b^2}, |b| > 1\right\}\\ \mathcal{M}_F &= \left\{a = \frac{b}{1+b^2}, |b| = 1\right\}\end{aligned}$$

where $\mathcal{M}_S, \mathcal{M}_U, \mathcal{M}_F$ are the stable, unstable portions of $\mathcal{M}$. As a, b, c are unitless proxies for concentrations, we only consider the dynamics in the first octant.

It is known that the system has a canard point at $a = 1/2, b = 1, c = 1$, indeed the canard trajectories of the system influence the shape of the attractor of the system, which is a mixed-mode oscillation. The attractor of the sytem is shown in Fig. 36. Note that the system exhibits a large-scale oscillation which is modulated by smaller amplitude oscillations.

5.5.1 Finding Canards in the Autocalator System

We will verify that the canard solutions of (5.18) lie near weak rivers. Recall that weak rivers must lie $\mathcal{O}(\varepsilon)$ close to the critical manifold, thus we numerically search for weak-confluences in a tube around the manfiold, i.e. we minimize $|\Delta_{1,2,3}f|, |\Delta_{1,2,4}f|, |\Delta_{1,2,5}f + \Delta_{1,3,4}f|$ on the set $B(\mathcal{M}, \varepsilon)$. Interestingly, we find an actual confluence point (i.e. $\Delta_{1,2,3}f = 0, \Delta_{1,2,4}f = 0, \Delta_{1,2,5}f + \Delta_{1,3,4}f = 0$) at $(a, b, c) \approx (0.498, 1.06, 1.06)$ which is not guaranteed by our theory, but is a nice proof of concept.

Using a symbolic computation engine (Wolfram Mathematica) we find a set of weak confluences of order 2, i.e. $C^2_{\mathcal{Z},\varepsilon}$ near the fold, which is shown in Fig. 37. To find the canard solution, we minimize $|\Delta_{1,2,5}f + \Delta_{1,3,4}f|$ along the relevant branch of $C^2_{\mathcal{Z},\varepsilon}$; in fact, we find that the minimum occurs at $(a^*, b^*, c^*) \approx (0.495, 1.07, 1.04)$ which is almost on top of the previously mentioned confluence point and the canard point. We find that $|\Delta_{1,2,5}f(a^*, b^*, c^*) + \Delta_{1,3,4}f(a^*, b^*, c^*)| \approx \varepsilon^{7.42}$ which places it reasonably close to the desired ε^8, as $|\ell| = 8$.

Denote by $\phi(t)$ the trajectory through our minimum (a^*, b^*, c^*), we claim that this trajectory has all of the hallmark characteristics of a canard solution. The right portion of Fig. 37 shows that ϕ lingers near the canard point for an $\mathcal{O}(1/\varepsilon)$ amount of time, and upon its exit from the canard point exhibits small scale ocsillations which grow rapidly.

To conclude this chapter, we demonstrate how we can use the weak confluence set $C^2_{\mathcal{Z},\varepsilon}$ to approximate the perturbed slow manifold. It is well known that the perturbed slow manifolds near a canard point will exhibit a complicated twisted shape due to the rotational influence of the canard solution [61, 66]. To approximate these twisting manifolds, we flow the points of $C^2_{\mathcal{Z},\varepsilon}$ forward in time; as the canard solution must lie near $C^3_{\mathcal{Z},\varepsilon} \subset C^2_{\mathcal{Z},\varepsilon}$ and as the canard solution must lie on $\mathcal{M}_{S,\varepsilon}$, the trajectories which flow from $C^2_{\mathcal{Z},\varepsilon}$ will be a good approximation of $\mathcal{M}_{S,\varepsilon}$. Two views of this continuum of trajectories are shown in Fig. 38.

In the standard numerical approach, one starts by numerically approximating the perturbed slow manifolds $\mathcal{M}_{S,\varepsilon}, \mathcal{M}_{U,\varepsilon}$, usually using a boundary value problem formulation [66]. The canard solution is found by computing the intersection $\mathcal{M}_{S,\varepsilon} \cap \mathcal{M}_{U,\varepsilon}$, as the canard solution begins on $\mathcal{M}_{S,\varepsilon}$ and crossed into $\mathcal{M}_{U,\varepsilon}$ [61, 66]. In our formulation of this computation,

we first identify the canard solution and use the results of that computation to identify the perturbed slow manifold. However, there is no obvious way to identify the secondary canards using curvature methods.

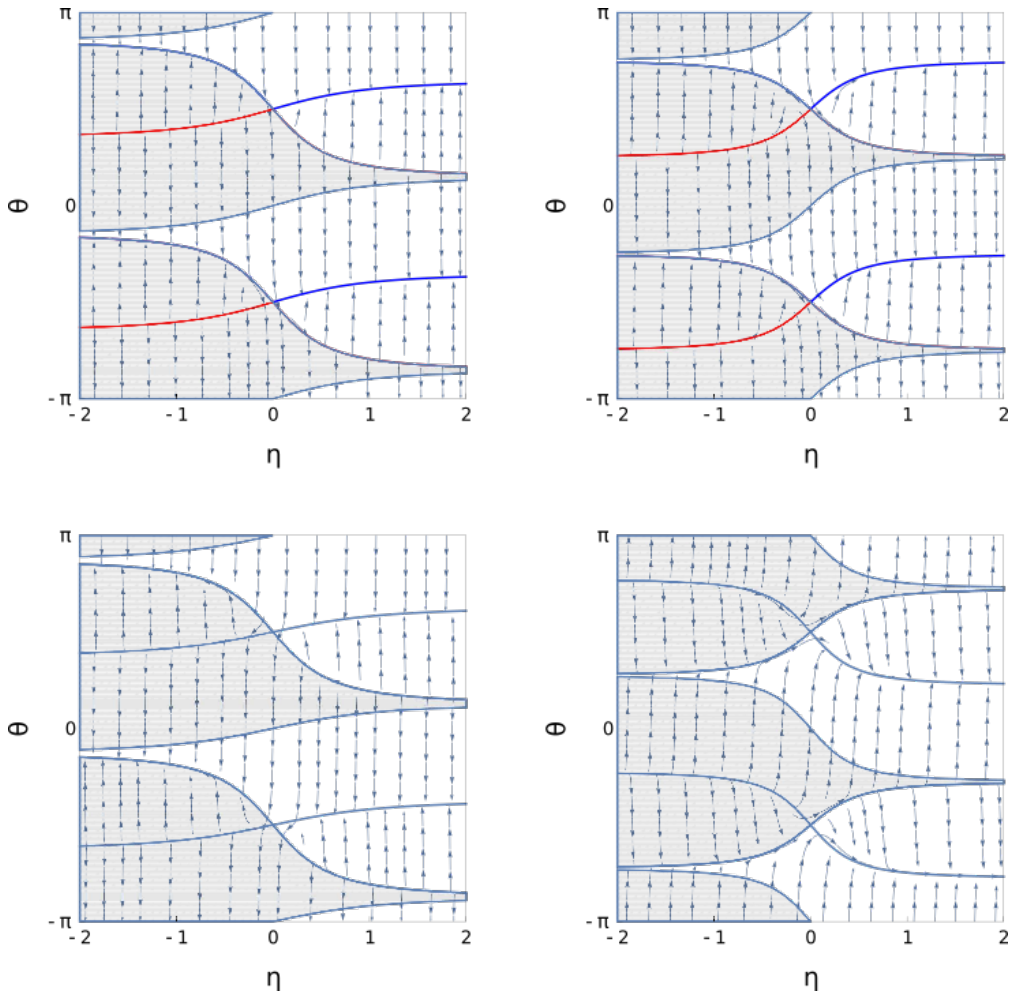

Figure 31: Four configurations of the angular dynamics (Upper Left) A phase plot for the node ($a = b = 1, c = -3$) case with $\varepsilon = .01$ for the river-canard Γ_+. The colored curves are the slow manifolds of the system, the stable manifolds are shown in blue and purple, and the unstable manifolds are shown in red. The gray region is where $\langle A(\eta; 0)z(\theta), z(\theta)\rangle < 0$, which is the region of linear radial stability. (Upper Right) The same parameter configuration as (a) for Γ_-. (Lower Left) The angular dynamics of the folded saddle ($-a = b = 2, c = -3$), again with $\varepsilon = .01$ for Γ_+; note that $\dot{\eta} < 0$, hence Γ_+ is a faux canard. (Lower Right) The same parameter configuration as (Lower Left) for Γ_-, which is the true canard for the folded-saddle system.

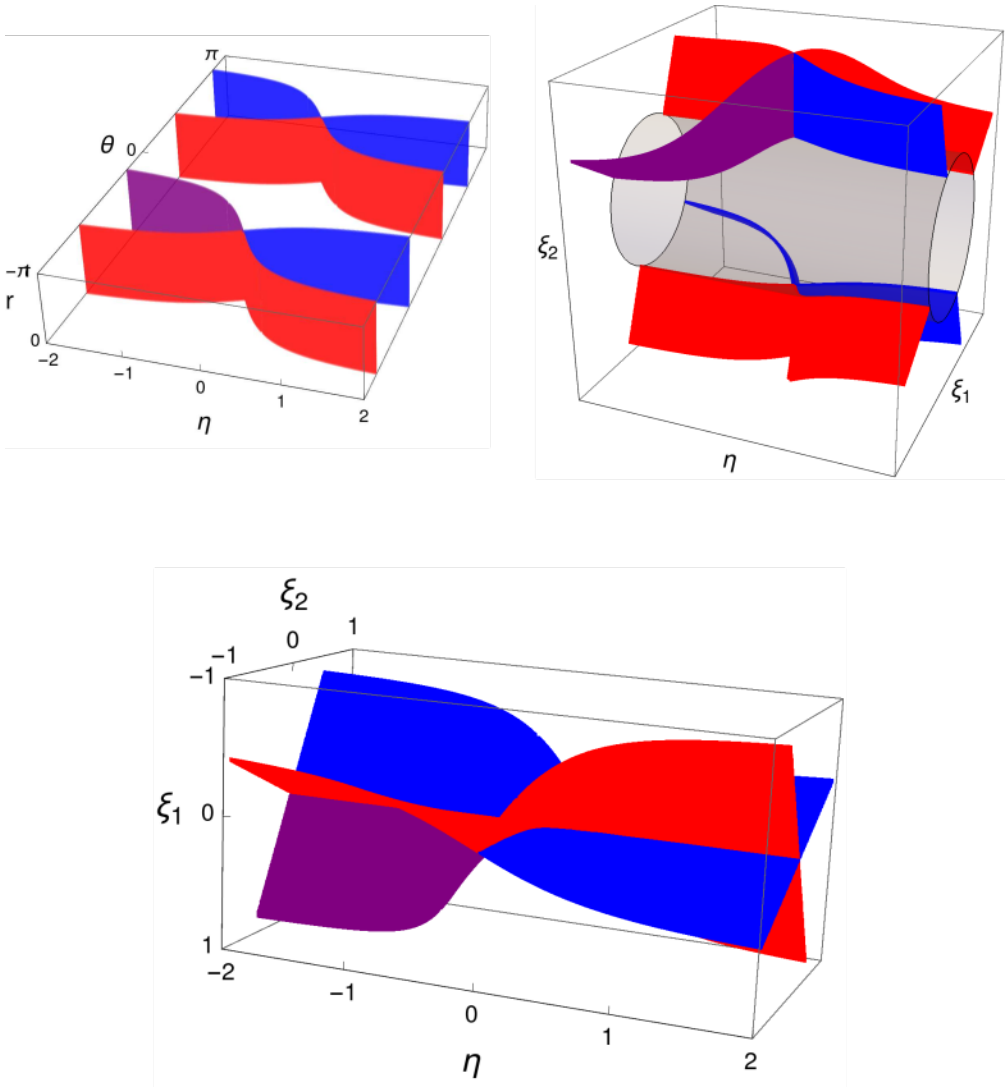

Figure 32: Organizing angular manifolds (a) A sketch of the angular manifolds for the (η, θ, r) system; for small r_0, the (η, θ) dynamics will quickly approach their slow limit, and be drawn to the plotted manifolds. The stable manifolds are plotted in blue and purple, and the unstable manifolds are shown in red; the purple manifold corresponds to the funnel branch of the stale manifold. (b) The angular manfiolds shown in a "blow-up" cartoon, the manifolds from (a) are wrapped around the "cylinder" $\|\xi\| = 0$. (c) The angular manifolds in the original LOR coordinates.

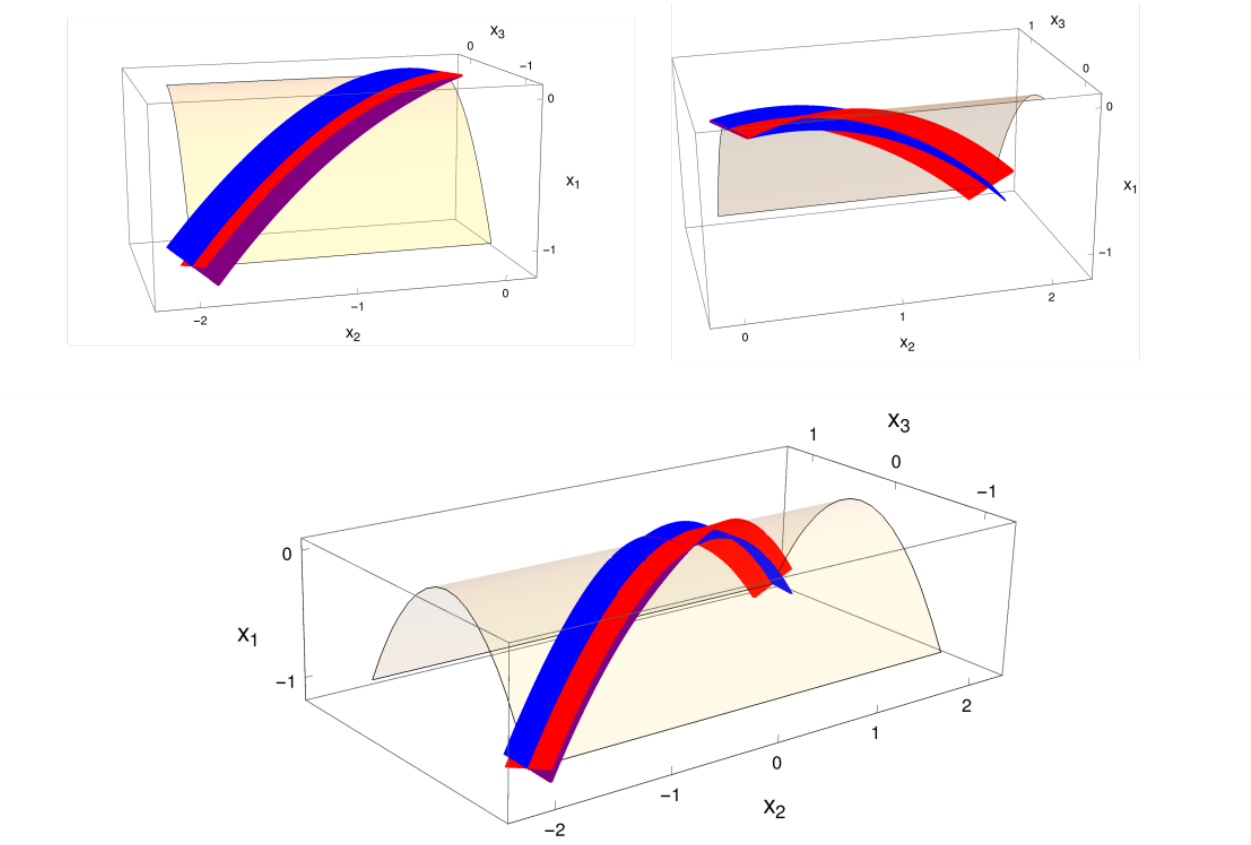

Figure 33: Organizing angular manifolds in (x_1, x_2, x_3)-space. (a) The angular manifolds mapped back to (x_1, x_2, x_3) space on the funnel side. Note how the blue and purple stable angular manifolds align with the original slow manifold, shown in yellow, while the unstable angular manifolds, which here serve as funnel separatrices, intersect the original slow manifold tranversely. (b) The exit side of the slow manifold, $x_3 > 0$. Note that here, the unstable angular manifolds in red lie along the original slow manifold, and the blue stable manifolds intersect transversely. (c) The full view of the angular manifolds.

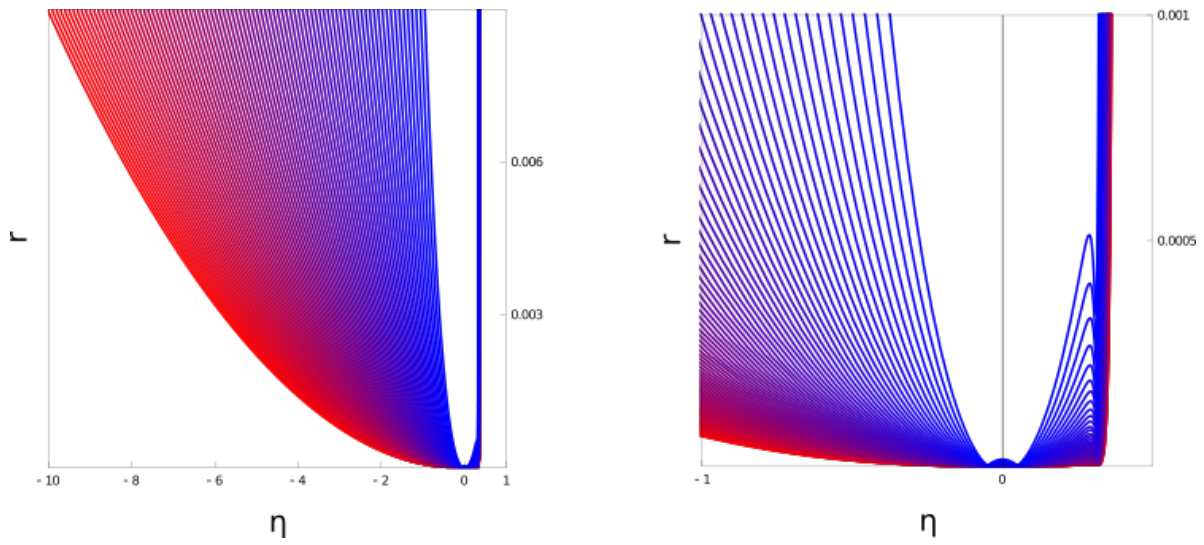

Figure 34: The radial dynamics near the fold (a) Plots of $(\eta(t), r(t))$ for trajectories in the funnel for various η_0 values. Plots in redder colors have more negative η_0 values, while bluer colors have η_0 values closer to the fold. (b) A zoom near the fold which displays small radial oscillations in the exiting trajectories.

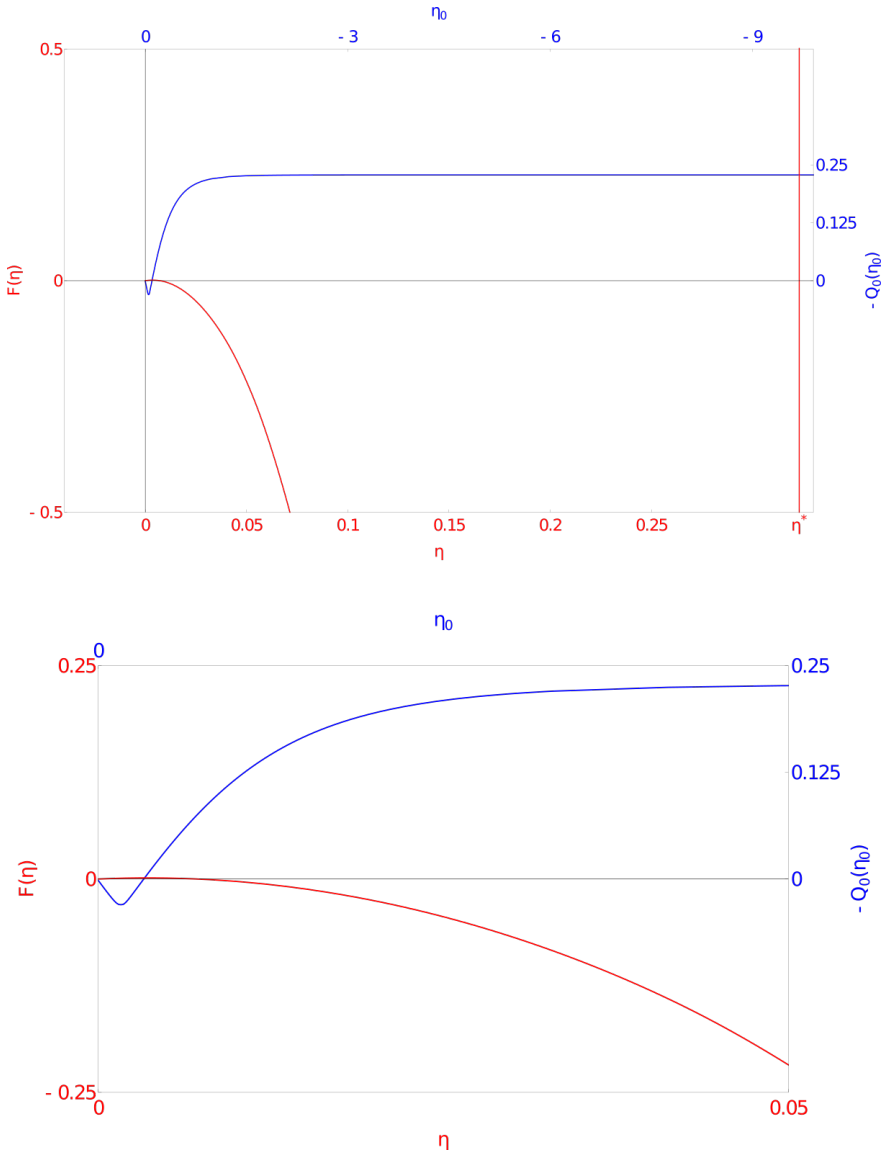

Figure 35: An approximate way-in way-out sliderule. (Top) In red, we plot the function $F(\eta)$ defined by (5.16) against its indepenedent variable η in red on the bottom axis. In blue, we plot $-Q_0(\eta_0)$ against its independent variable η_0 in blue on the top axis. Given an input η_0, to visualize the escape η, find the η value where $-Q_0(\eta_0)$ is equal to $F(\eta)$. Note that $-Q_0(\eta_0)$ aymptotically approaches $-Q_0^* \approx .21$ hence all solutions must jump before $\eta* \approx .323$. This matches well with the radial dynamics we observe in Fig. 34, where all solutions jump near $\eta \approx .32$. Note that the right portion of the red curve is not vertical, however near $F'(\eta^*) \approx 10^{11}$, so F is growing extremely quickly. We use $a = b = 1, c = -3, \varepsilon = 0.01$ for these plots, placing us in the folded-node regime. (Bottom) A zoom near $\eta = 0$, showing that some solutions escape almost immediately.

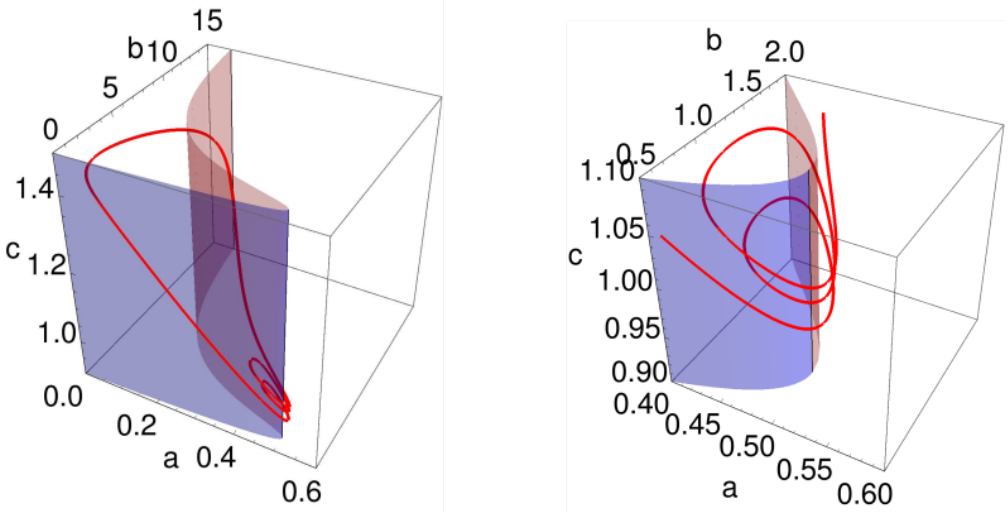

Figure 36: The attractor of the autocalator system. (Left) The attractor of system (5.18) shown for $\varepsilon = 0.013, \mu = 0.299$. The stable branch of the critical manifold $\mathcal{M}_S$ is shown in light blue, and the unstable branch of the critical manifold $\mathcal{M}_U$ is shown in light red. (Right) A zoom on the attractor near the canard point $(1/2, 1, 1)$, note that the attractor exhibits multi-scale oscillations.

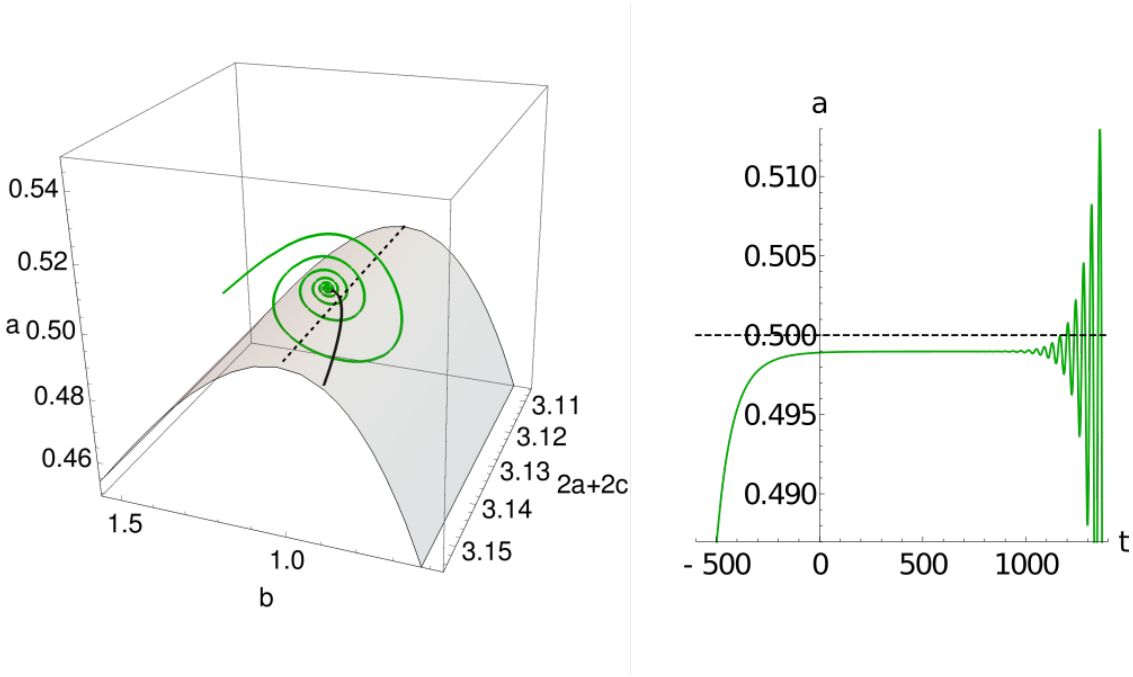

Figure 37: The weak confluences $C^2_{\mathcal{Z},2}$ leading to the canard point. (Left) In gray we show the critical manifold near the fold, which is shown in dashed black; note that the axes here are $a, b, 2a+2c$, we chose to plot $2a+2c$ in order to make the following manifold plots more digestable. The solid black curve which crosses the fold is the weak confluence set $C^2_{\mathcal{Z},2}$. The green curve is the trajectory through the point on $C^2_{\mathcal{Z},2}$ which has minimal $|\Delta_{1,2,5}f + \Delta_{1,3,4}f|$ along $C^2_{\mathcal{Z},2}$; we contend this is the canard solution. (Right) A plot of $a(t)$ along the canard solution; note the long delay near $a = 1/2$ followed by the onset of growing, small scale oscillations.

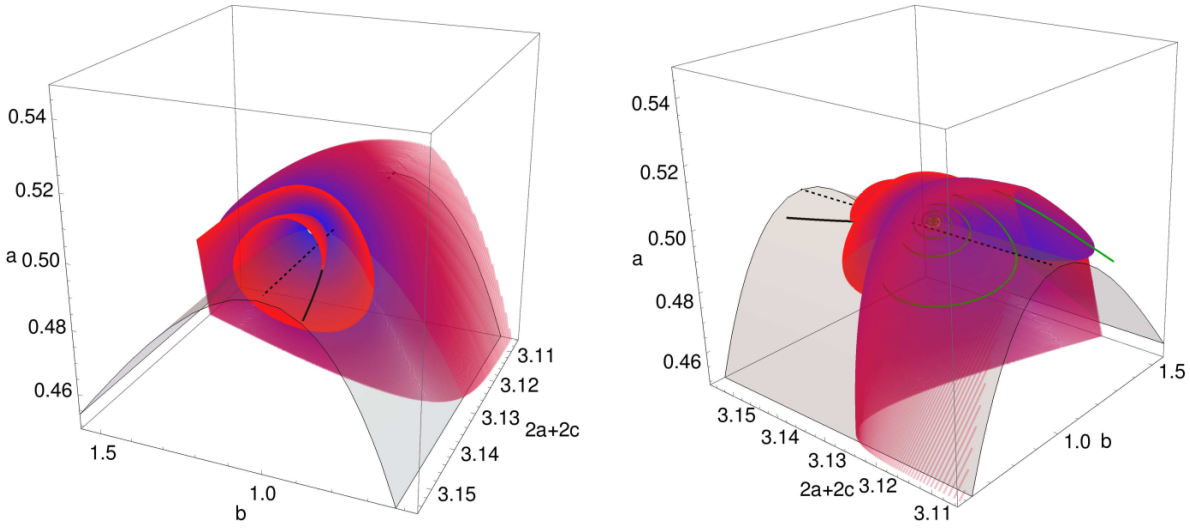

Figure 38: Approximations of $\mathcal{M}_{S,\varepsilon}$. We overlay the trajectories with initial conditions in $C^2_{\mathcal{Z},\varepsilon}$ near the fold. Trajectories with initial conditions further from the fold are colored in red, while trajectories with initial conditions nearer to the fold are colored bluer. The set $C^2_{\mathcal{Z},\varepsilon}$ is shown in solid black, the fold in dashed black, and the canard solution (only visible in the right panel) in green. Note that we again plot $2a + 2c$ in place of c.

6.0 Conclusions

LOR provides a general approach to deriving a natural coordinate frame, based on a geometric representation, that is well suited to study dynamics relative to any manifold embedded in the flow of an ODE of arbitrary dimensions. LOR is advantageous because, to our knowledge, it is the unique approach with a full range of desirable properties: it is not based on linearization, it is not limited to scenarios involving periodic orbits, it generally extends well beyond the local neighborhood of the base manifold used to define it, and it applies naturally in arbitrary dimensions. LOR leads to LOR equations describing the evolution of trajectories in the LOR frame, which encode the geometry of the flow. These equations do not depend on the choice of normal frame used in their derivation, which allows a specific frame to be chosen to simplify associated calculations. An additional blow-up transformation of the LOR equations provides an especially convenient decomposition for studying transient aspects of the behavior of trajectories near structures in a phase space.

We have used LOR to present a rigorous definition for rivers, a class of attracting or repelling trajectories that had previously been identified in the literature but had not been defined precisely with any degree of generality. Our approach harnesses the LOR frame and associated quantities, such as a measure of invariance, and links them with curvature, or specifically with the *zero-cuvature locus*. Using the LOR frame to study the near-invariance of the zero-curvature locus allows us to locate rivers and to avoid the "ghosts" that have been previously identified by curvature-based techniques for identifying significant structures in two-timescale systems [1]. Our definition of rivers does not encompass all attracting structures that are "river-like"; however, we note that it unifies a variety of previously unexplained or poorly understood phenomena. In a phase plane, our results provide a useful new way to explain behavior of trajectories, both special trajectories that we identify and other trajectories that approach attracting structures in the flow.

Also using the LOR frame, we can identify and compute continuations of periodic trajectories, study local stability of these orbits, construct novel invariant manifolds associated with these orbits (of particular utility in $\mathbb{R}^3$), and compute the asymptotic phases of trajecto-

ries in the neighborhood of each orbit in a computationally synergistic way. The key insight underlying the approach is that we can tailor our phase space geometry to the problem at hand by considering curvilinear geometries.

While there is an initial computational cost to computing Frenet frames and curvatures of curves, we note that there is a significant return on investment in using the LOR frame for local analysis. For identification of periodic orbits, LOR allows us to solve a single BVP that does not require the computation of the period itself. Although the cost of LOR increases when we study stability and local dynamics near a periodic orbit by computing a second LOR frame using the identified periodic orbit itself as the basecurve, there is no need to solve a second time, and this second LOR transformation provides a computationally efficient LOR frame for our subsequent analysis and directly allows for the derivation of invariant angular manifolds, which are not accessible with traditional geometric approaches.

We plan to make all of the code for this thesis available on GitHub to facilitate future use of the methods we have discussed, and we note that symbolic computation software is well-suited to these differential-geometric computations. The ability to use the same computed trajectories in multiple ways yields significant return on investment from these startup computational costs; the benefit grows in applications involving continuation of periodic orbits, in that the same LOR frame, based on the first periodic orbit found, can be used repeatedly. Furthermore, LOR techniques can be used to quickly identify canards solutions and avoid the complexification of time used in way-in way-out computations.

In the final chapter we generalized the definition of rivers beyond the plane, and demonstrate that canard solutions must lie in an $\mathcal{O}(\varepsilon)$ neighborhood of weak rivers. Furthermore, we can use this characterization of canards to perform detailed analysis of the dynamics near these river-canards, specifically we can explain the onset of small scale oscillations and approximate the way-in way-out function.

Bibliography

[1] E Benoît, M Brons, M Desroches, and M Krupa. Extending the zero-derivative principle for slow-fast dynamical systems. *Z. angew. Math. Phys.*, 99, 2015.

[2] R Bertam and J E Rubin. Multi-timescale systems and fast-slow analysis. *Mathematical Biosciences*, 287:105–121, 2017.

[3] R. Bertram and A. Sherman. A calcium-based phantom bursting model for pancreatic islets. *B. Math. Biol.*, 66:1313–1344, 2004.

[4] C Börgers. *An introduction to modeling neuronal dynamics*. Texts in Applied Mathematics. springer, 1 edition, 2017.

[5] C Börgers and N Kopell. Synchronization in networks of excitatory and inhibitory neurons with sparse, random connectivity. *Neural Computation*, 15:509–538, 2003.

[6] C Börgers and N Kopell. Effects of noisy drive on rhythms in networks of excitatory and inhibitory neurons. *Neural Computation*, 17:557–608, 2005.

[7] J W Bruce and P J Giblin. *Curves and Singularities*. Cambridge University Press, 1984.

[8] John Charles Butcher. *Numerical methods for ordinary differential equations*. John Wiley & Sons, 2016.

[9] Oriol Castejón, Antoni Guillamon, and Gemma Huguet. Phase-amplitude response functions for transient-state stimuli. *The Journal of Mathematical Neuroscience*, 3(1):13, 2013.

[10] F. Clément and J.-P. Françoise. Mathematical modeling of the gnrh pulse and surge generator. *SIAM J. Appl. Dyn. Syst.*, 6:441–456, 2007.

[11] Charles Conley. *Isolated Invariant Sets and the Morse Index*. Number 38 in Regional Conference Series in Mathematics. AMS, 1978.

[12] Z Denkowska and R Roussarie. A method of desingularization for analytic two-dimensional vector field families. *Bol. Soc. Bras. Math.*, 22:93–126, 1991.

[13] M Desroches and M Jeffrey. Canards and curvature: the 'smallness of ϵ' in slow-fast dynamics. *Proc. Math. Phys. and Engin. Sciences*, 467(2132):2404–2421, 2011.

[14] Casey O Diekman and Amitabha Bose. Reentrainment of the circadian pacemaker during jet lag: East-west asymmetry and the effects of north-south travel. *Journal of theoretical biology*, 437:261–285, 2018.

[15] Francine Diener. Proprietes asymptotiques des fleuves. *C. R. Acad. Sc. Paris*, 302(2):55–58, 1986.

[16] Marc Diener. Determination et exitsence des fleuves en dimension deux. *C. R. Acad. Sc. Paris*, 301(20):899–914, 1985.

[17] Eusebius J Doedel, Thomas F Fairgrieve, Björn Sandstede, Alan R Champneys, Yuri A Kuznetsov, and Xianjun Wang. Auto-07p: Continuation and bifurcation software for ordinary differential equations, 2007.

[18] Richard C Dorf and James A Svoboda. *Introduction to electric circuits*. John Wiley & Sons, 2010.

[19] Bard Ermentrout. Type i membranes, phase resetting curves, and synchrony. *Neural computation*, 8(5):979–1001, 1996.

[20] G B Ermentrout and D H Terman. *Mathematical foundations of Neuroscience*, volume 35. Springer, 2010.

[21] N Fenichel. Geometric singular perturbation theory for ordinary differential equations. *J. Diff. Eq.*, 31:53–98, 1979.

[22] N Fenichel. Geometric singular perturbation theory for ordinary differential equations. *J. of Diff. Eqs.*, 31, 1979.

[23] Daniel B Forger. *Biological clocks, rhythms, and oscillations: the theory of biological timekeeping*. MIT Press, 2017.

[24] Emilio Friere, Armengol Gasull, and Antoni Guillamon. Limit cycles and lie symmetries. *Bull. Sci. Math*, 131, 2007.

[25] R. A. Garcia, A Gasull, and A Guillamon. Geometric conditions for the stability of orbits in planar systems. *Math. Proc. Camb. Phil. Soc.*, 120, 1996.

[26] J Ginoux, B Rossetto, and Leon Chua. Slow invariant manifolds as curvature of the flow of dynamical systems. *Inter. Jour. of Bifur. and Chaos*, 18(11):3409–3430, 2007.

[27] Brian C Goodwin. Oscillatory behavior in enzymatic control processes. *Advances in Enzyme Regulation*, 3:425–437, 1965.

[28] J Guckenheimer and P Holmes. *Nonlinear Oscillations, Dynamical Systems, and Bifurcations of Vector Fields*. Springer-Verlag New York Inc., 1983.

[29] E. Harvey, V. Kirk, M. Wechselberger, and J. Sneyd. Multiple timescales, mixed mode oscillations and canards in models of intracellular calcium dynamics. *J. Nonlinear Sci.*, 21(5):639–683, 2011.

[30] Frank C Hoppensteadt and Eugene M Izhikevich. *Weakly connected neural networks*, volume 126. Springer Science & Business Media, 2012.

[31] A. Huber and P. Szmolyan. Geometric singular perturbation analysis of the yamada model. *SIAM J. Appl. Dyn. Syst.*, 4(3):607–648, 2005.

[32] Brian P Ingalls. *Mathematical modeling in systems biology: an introduction*. MIT press, 2013.

[33] Carl Hirschie Johnson. Phase response curves: what can they tell us about circadian clocks. *Circadian clocks from cell to human*, pages 209–249, 1992.

[34] C K R T Jones. *Dynamical Systems*, chapter Geometric Singular Perturbation Theory, pages 44–120. Lecture Notes in Mathematics. Springer, 1995.

[35] Bernd Krauskopf and Hinke Osinga. Growing 1d and quasi 2d unstable manifolds of maps. *J. of Comp. Physics*, 146(1):404–419, 1998.

[36] M. Krupa, A. Vidal, M. Desroches, and F. Clément. Mixed-mode oscillations in a multiple time scale phantom bursting system. *SIAM J. Appl .Dyn. Syst.*, 11(4):1458–1498, 2012.

[37] Martin Krupa, Nikola Popović, Nancy Kopell, and Horacio G Rotstein. Mixed-mode oscillations in a three time-scale model for the dopaminergic neuron. *Chaos*, 18(015106):19, 2008.

[38] Martin Krupa and Peter Szmolyan. Extending geometric singular perturbation theory to nonhyperbolic points – fold and canard points in two dimensions. *SIAM J. Math. Anal.*, 33(2):286–314, 2001.

[39] Martin Krupa and Martin Wechselberger. Local analysis near a folded saddle-node singularity. *J. Differ. Equations*, 248(12):2841–2888, 2010.

[40] W Kühnel. *Differential geometry: curves, surfaces, manfiolds*. Student Mathematical Library. AMS, 2 edition, 2005.

[41] W Kühnel. *Differential Geometry: Curves, Surfaces, Manifolds*. AMS, 2013.

[42] Yoshiki Kuramoto. *Chemical oscillations, waves, and turbulence*. Courier Corporation, 2003.

[43] Yuri A Kuznetsov. *Elements of applied bifurcation theory*, volume 112. Springer Science & Business Media, 2013.

[44] Peter Lax. *Linear Algebra and Its Applications*. Wiley, 2007.

[45] Benjamin Letson and Jonathan E Rubin. A new frame for an old (phase) portrait: Finding rivers and other flow features in the plane. *SIAM Journal on Applied Dynamical Systems*, 17(4):2414–2445, 2018.

[46] Benjamin Letson and Jonathan E Rubin. Local orthogonal rectication: deriving natural coordinates to study flows relative to manifolds, 2019. accepted.

[47] Benjamin Letson and Jonathan E Rubin. Lor for analysis of periodic orbits: A one-stop shop approach, 2019. accepted.

[48] T B Luke, E Barreto, and P So. Complete classification of the macroscopic behavior of a heterogeneous network of theta neurons. *Neural Computation*, 25:3207–3234, 2013.

[49] A Mauroy, I Mezic, and J Moehlis. Isostables, isoschrons, and koopman spectrum for the action-angle representation of stable fixed point dynamics. *Physica D*, 261, 2013.

[50] James Munkres. *Topology.* Pearson, 2000.

[51] Gary Nave Jr. and Shane Ross. Trajectory-free calculation of attracting and repelling manifolds, 2017. arXiv preprint arXiv:1705.07949.

[52] C. A. Del Negro, C.-F. Hsiao, and S. H. Chandler. Outward currents influencing bursting dynamics in a guinea pig trigeminal motoneurons. *J. Neurophysiol.*, 81:1478–1485, 1999.

[53] Hinke Osinga. Nonorientable manifolds of three-dimensional vector fields. *Int. J. Bifurcation and Chaos*, 13(3):553–570, 2003.

[54] Lawrence Perko. *Differential equations and dynamical systems.* Springer Texts in Applied Mathematics, 2000.

[55] V Petrov, S K Scott, and K. Showalter. Mixed-mode oscillations in chemical systems. *J. Chem. Phys.*, 97:6191–6198, 1992.

[56] S Revzen and J Guckenheimer. Estimating the phase of synchronized oscillators. *Phys. Rev. E*, 78, 2008.

[57] Nathan W Schultheiss, Astrid A Prinz, and Robert J Butera. *Phase response curves in neuroscience: theory, experiment, and analysis.* Springer Science & Business Media, 2011.

[58] M. Sekikawa, N. Inaba, T. Yoshinaga, and T. Hikihara. Period-doubling cascades of canards from the extended bonhoeffer-van der pol oscillator. *Phys. Lett. A*, 374(36):3745–3751, 2010.

[59] Sho Shirasaka, Wataru Kurebayashi, and Hiroya Nakao. Phase-amplitude reduction of transient dynamics far from attractors for limit-cycling systems. *Chaos: An Interdisciplinary Journal of Nonlinear Science*, 27(2):023119, 2017.

[60] S. S. Stojilkovic, H. Zemkova, and F. Van Goor. Biophysical basis of pituitary cell type-specific ca^{2+} signaling-secretion coupling. *Trends Endocrinol. Metab.*, 16:152–159, 2005.

[61] P Szmolyan and M Wechselberger. Canards in $\mathbb{R}^3$. *J. of Diff. Eqs.*, 177, 2001.

[62] D Terman, J E Rubin, and C O Diekman. Irregular activity arises as a natural consequence of synaptic inhibition. *Chaos*, 23, 2013.

[63] Gerald Teschl. *Ordinary differential equations and dynamical systems*, volume 140. American Mathematical Soc., 2012.

[64] Fred W Turek. Pharmacological probes of the mammalian circadian clock: use of the phase response curve approach. *Trends in Pharmacological Sciences*, 8(6):212–217, 1987.

[65] J A Vano, J C Wildenberg, M B Anderson, J K Noel, and J C Sprott. Chaos in low-dimensional lotka-volterra models of competition. *Nonlinearity*, 19:2391–2404, 2006.

[66] Theodore Vo and Martin Wechselberger. Canards of folded saddle-node type I. *SIAM Journal on Mathematical Analysis*, 47(4):3235–3283, 2015.

[67] Kyle CA Wedgwood, Kevin K Lin, Ruediger Thul, and Stephen Coombes. Phase-amplitude descriptions of neural oscillator models. *The Journal of Mathematical Neuroscience*, 3(1):2, 2013.

[68] Stephen Wiggins. *Normally hyperbolic invariant manifolds in dynamical systems*. Springer-Verlag, 1994.

[69] D Wilson and J Moehlis. Isostable reduction with applications to time-dependent partial differential equations. *Phys. Rev. E*, 94, 2016.

[70] D Wilson and J Moehlis. Isostable reduction with applications to time-dependent partial differential equations. *Phys. Rev. E*, 94, 2016.